



# Optimization of railway network using smart-grid solutions

Sarah Nasr

## ► To cite this version:

Sarah Nasr. Optimization of railway network using smart-grid solutions. Electric power. Université Paris Saclay (COMUE), 2016. English. NNT : 2016SACLC026 . tel-02100502

**HAL Id: tel-02100502**

**<https://theses.hal.science/tel-02100502>**

Submitted on 16 Apr 2019

**HAL** is a multi-disciplinary open access archive for the deposit and dissemination of scientific research documents, whether they are published or not. The documents may come from teaching and research institutions in France or abroad, or from public or private research centers.

L'archive ouverte pluridisciplinaire **HAL**, est destinée au dépôt et à la diffusion de documents scientifiques de niveau recherche, publiés ou non, émanant des établissements d'enseignement et de recherche français ou étrangers, des laboratoires publics ou privés.

NNT : 2016SACLC026

THESE DE DOCTORAT  
DE  
L'UNIVERSITE PARIS-SACLAY  
PREPAREE A  
CENTRALESUPELEC

ECOLE DOCTORALE N° 575  
Electrical, optical, bio-physics and engineering  
(Physique et ingénierie : Electrons, Photons, Sciences du vivant)

Spécialité de doctorat (Génie électrique)

Par

**Mme Sarah NASR**

Optimisation d'un réseau ferroviaire à l'aide de solutions smart-grids

**Thèse présentée et soutenue à Gif-sur-Yvette, le 23 mars 2016 :**

**Composition du Jury :**

Mr. Demba DIALLO	Professeur, Université Paris-sud	Président
Mr. Bruno FRANCOIS	Professeur, Ecole Centrale de Lille	Rapporteur
Mr. Luc LORON	Professeur, Polytech Nantes	Rapporteur
Mr. Pierre LEFRANC	Maître de conférences, INP Grenoble	Examineur
Mme Florence OSSART	Professeur, UPMC University Pierre et Marie Curie-Paris 6	Examinatrice
Mr. Marc PETIT	Professeur adjoint, CentraleSupélec	Co-encadrant
Mr. Marius IORDACHE	Expert, Alstom Transport	Co-encadrant
Mr. Olivier LANGLOIS	Expert, Alstom Transport	Invité

**Titre :** Optimisation d'un réseau ferroviaire à l'aide de solutions smart-grids

**Mots clés :** efficacité énergétique, ferroviaire, freinage électrique, grille-horaire, DC micro-grid

**Résumé :** L'amélioration de l'efficacité énergétique est devenue aujourd'hui une nécessité dans tous les domaines techniques. La réduction de la consommation, et donc du bilan carbone, est placée parmi les priorités mondiales tel que le paquet énergie-climat 2020 de l'Union Européenne. Les systèmes ferroviaires font partie des plus grands consommateurs d'énergie. Des solutions électriques sont développées pour réduire les pertes dans ces systèmes, optimiser la consommation et donc réduire la facture énergétique globale. Étant donné la diversité de ces systèmes, deux catégories principales sont considérées. La première regroupe les lignes urbaines caractérisées par une électrification en mode DC et un trafic relativement dense. Dans ce cas, l'énergie de freinage brûlée dans les rhéostats des trains constitue une perte considérable. La solution proposée consiste à récupérer cette énergie à l'aide d'un DC micro-grid installé dans une station passager. Elle permettra une interaction avec son environnement non-ferroviaire comme par exemple réutiliser cette énergie pour charger des bus électriques hybrides stationnant à proximité. Ce micro-grid contient un premier convertisseur DC/DC qui récupère l'excès d'énergie de freinage d'un train et l'injecte dans un DC busbar. Un deuxième convertisseur DC/DC va ensuite la stocker dans un système de stockage hybride pour que le bus électrique puisse se charger une fois branché au DC busbar.

Le micro-grid est relié au réseau par un onduleur réversible AC/DC de faible puissance. L'ensemble est géré localement par un système gestion de puissance. Une évaluation énergétique montre que cette solution est intéressante lorsqu'un investissement, station de charge, est nécessaire pour charger les bus. En plus, dans le cas du DC micro-grid, aucun contrat avec le fournisseur d'électricité n'est nécessaire. La stabilité du système est aussi étudiée et une commande de stabilisation, le backstepping, est appliquée. Ce nouveau concept d'une future station intelligente permettra au système ferroviaire de communiquer avec son environnement qui est en pleine évolution. La deuxième catégorie est constituée par les lignes régionales et les lignes à grandes vitesses fonctionnant en mode AC. Contrairement au cas précédent, l'excès d'énergie de freinage est renvoyé à travers les sous-stations d'alimentation. Par conséquence, une deuxième solution propose la réduction de la consommation totale par l'optimisation du profil de vitesse de chaque train et la synchronisation de la grille horaire. Ceci est réalisé à l'aide d'un algorithme d'évolution différentielle. Chaque profil de vitesse est découpé en zones auxquelles sont attribuées des paramètres de conduite. L'optimisation de ces derniers permet de générer un nouveau profil de conduite optimal. Les résultats montrent la possibilité de faire des économies d'énergie tout en respectant la ponctualité des trains.

**Title :** Optimization of railway network using smart-grid solutions

**Keywords :** energy efficiency, railway, electric braking, timetable, DC micro-grid

**Abstract :** Increasing energy efficiency is nowadays a requirement in all technical fields. The reduction of global consumption, thus carbon footprint, has become the world's priority, as for example, the climate and energy package of the European Union. Railways' share of energy consumption is one of the highest. Electrical solutions are developed in order to reduce these systems' losses, optimize their consumption and reduce global energy bill. Given their diversity, two main categories are considered in this study. The first one consists of urban lines that are characterized by a DC electrification and a relatively dense traffic. In this case, braking energy burned in trains' rheostats represents the main share of losses. The proposed solution is to recuperate this energy using a DC micro-grid implemented in a passengers' station. It allows an interaction with the non-railway electrical environment, for example, re-using this energy in charging electric hybrid buses parked nearby. The excess of braking energy is recuperated using a DC/DC converter and injected into a DC busbar. A second DC/DC converter will store it in a hybrid storage system. It will then serve to charge the buses connected to the DC busbar.

The micro-grid is also connected to the grid using a low power AC/DC converter. A power management system ensures optimizing power flow between different components. An energy evaluation showed that this solution is a good investment especially because no contract is needed with the energy provider. The system's stability is studied and a stabilizing command, the backstepping, is applied. This new smart station allows railways to communicate, energetically, with its evolving environment. The second category is suburban and high speed lines that are AC electrified. Contrarily to the previous case, braking energy is reinjected to the upper grid through substations. Therefore, a second solution is to reduce global energy consumption by optimizing trains' speed profiles and timetable's synchronization. It is done using a differential evolution algorithm. Each speed profile is divided into zones to which are associated driving parameters. The optimization of the latter allowed generating new optimal speed profiles and a less-consuming timetable. Simulation results showed that it is possible to make important energy savings while respecting train's punctuality.

## REMERCIEMENT

---

Maintenant que cette aventure est achevée, je tiens à remercier des personnes sans lesquels je n'aurais pas pu y arriver car malgré le fait qu'une thèse de doctorat est préparée par une personne, c'est tout un groupe qui est derrière.

D'abord, côté professionnel, je remercie mon encadrant Marius IORDACHE qui m'a donné l'opportunité de développer mes compétences au sein d'Alstom Transport et de vivre une expérience unique en participant à plusieurs projets européens. Ensuite, je remercie mes collègues Olivier LANGLOIS, Julien ROQUES, Laurent NOTTE et Tao LIU qui sont devenus rapidement des amis et étaient un vrai support pour moi. Leur expérience ainsi que leur humour constituaient un package qui me motivait à aller travailler à Saint-Ouen, malgré les 3 heures de route, au lieu d'aller au laboratoire. Ensuite, côté laboratoire, je remercie aussi mon encadrant Marc PETIT et les autres professeurs : Mr. Amir ARZANDE pour avoir été toujours à l'écoute et prêt à m'aider et Mr. Charif KARIMI pour son support technique. Je remercie aussi mes camarades, surtout Jad TAKI, pour la belle ambiance. Je remercie aussi tous les professeurs et les doctorants des autres départements qui m'ont aidé avec leurs compétences multiples et variées.

Je remercie surtout ma famille, mon père Riad, ma mère Siham et mon frère Jad qui m'ont accompagné pendant cette période et ont été des murs porteurs.

Enfin, un très grand « MERCI » à mon mari, Samer, qui est toujours à mon côté dans toutes les épreuves. C'est surtout grâce à lui que j'ai pu résister jusqu'à la fin. Il est ma source de patience, mon inspiration et mon courage.

Pour mon pays LIBAN...pour qu'un jour on retrouve la même voie...

# **FRENCH ABSTRACT**

De nos jours, le monde fait face à des enjeux écologiques et économiques majeurs. La réduction de la pollution ainsi que l'optimisation de la consommation des ressources énergétiques épuisables s'avèrent une urgence. Etant donné que les systèmes ferroviaires font partie des plus grands consommateurs d'énergie, leur optimisation demeure pertinente. De point de vue émission du CO<sub>2</sub> en Europe, la part du ferroviaire est négligeable par rapport aux autres moyens de transport tel que l'aérien et le routier. Ceci peut être expliqué par le fait qu'aujourd'hui la plupart des lignes sont électrifiées. Cependant, la production de l'énergie électrique consommée par le ferroviaire est souvent polluante (exemple : charbon, fuel..) et les sources renouvelables ne constituent qu'une petite partie. D'où l'importance d'améliorer l'efficacité de ces systèmes. Dans ce contexte, l'Union Européenne a adopté en 2007 le plan 20-20-20 qui vise d'ici 2020 d'atteindre :

- 20% de réduction des émissions de gaz à effet de serre par rapport à l'année 1990
- 20% d'augmentation de la part des énergies renouvelables
- 20% d'augmentation de l'efficacité énergétique globale

Par conséquent, l'UE a lancé depuis 2007 plusieurs projets européens pour améliorer les différents secteurs dont le ferroviaire. Cette thèse s'inscrit dans le cadre de deux projets européens : d'une part, OSIRIS pour les réseaux ferroviaires urbains, d'autre part, MERLIN pour les lignes à grande vitesse. Les deux ont pour objectif commun la proposition de nouvelles solutions technologiques, pour l'amélioration de l'efficacité énergétique de ces systèmes.

Ce rapport est donc divisé en trois parties principales. D'abord, afin de mieux comprendre ses particularités et ses contraintes, une première section A, expliquera de point de vue historique l'évolution du secteur ferroviaire à travers le siècle dernier. Elle présentera les différentes décisions, politiques et techniques, qui ont abouti au système actuel. Un 'focus' sera fait sur les sous-systèmes principaux impactant la consommation d'énergie. Les technologies de traction électrique seront présentées ainsi que leurs caractéristiques (tension, stations d'alimentation, caténaire et 3<sup>ème</sup> rail...). Ensuite, les statistiques montreront l'impact du ferroviaire sur l'environnement et son évolution à travers les dernières décennies suite à l'augmentation du taux d'électrification des lignes. Après ce résumé d'histoire, le système de freinage sera détaillé vue son impact sur le bilan énergétique. Aujourd'hui, la plupart des trains sont équipés de deux types de freinage : électrique et mécanique. Le premier, le freinage régénératif, utilise les moteurs électriques de traction pour freiner en inversant le sens du champ tournant à l'intérieur de la machine. Ce dernier, en s'opposant au mouvement mécanique, permet de ralentir la vitesse en convertissant la différence d'énergie cinétique en énergie électrique. Dans les systèmes AC, comme les lignes à grandes vitesses, cette énergie est soit consommée par un autre train qui accélère à proximité soit réinjectée vers le réseau à travers les stations d'alimentation. Dans les systèmes DC, et selon la réceptivité de la ligne, cette énergie est soit échangée avec un autre train soit brûlée dans les rhéostats du train et donc perdue. La quantité de



cette perte d'énergie dépend directement de la ligne étudiée (métro, tramway) et de la fréquence des trains. Dans certains cas défavorables, cette énergie peut atteindre 40% de l'énergie totale consommée. Face à l'augmentation des prix de l'énergie, les opérateurs commencent à s'intéresser à la réduction de leur consommation et donc de leur facture énergétique. Plusieurs solutions existent aujourd'hui. Certaines sont déjà commercialisées alors que d'autres sont encore en phase de développement. Ces solutions peuvent être séparées en deux catégories ; la première regroupe les solutions 'intrusives' qui viennent modifier le système existant en remplaçant des équipements tandis que la deuxième, les 'non-intrusives', vient simplement se connecter au système tel que les systèmes de stockage et les onduleurs. Ces différentes solutions sont listées dans cette section. Malgré le fait qu'elles soient efficaces, ces solutions sont destinées à être utilisées en 'interne' dans un système ferroviaire. Autrement dit, le système reste isolé de son environnement énergétique. Ce choix est justifié par le fait que, dans certains pays, les opérateurs n'ont pas le droit d'être un fournisseur d'énergie. Par contre, dans le cas contraire, et lorsque le prix de revente de l'énergie est supérieur à celui de son achat, il est intéressant de proposer des solutions pour qu'au sein d'une ville, un système ferroviaire devient aussi une source d'énergie électrique.

La deuxième partie, section B, présente un nouveau concept, la station DC intelligente, qui permet de réduire les pertes en récupérant l'énergie de freinage des trains. Cette solution s'inspire des systèmes de transport multimodaux, dans lesquels le flux de passagers évolue entre le système ferré (métro, tramway...) et le système routier (bus, voitures...). La question qui se pose la suivante : pourquoi ne pas permettre à ces systèmes d'interagir énergétiquement ? Aujourd'hui, les voitures et les bus électriques sont de plus en plus nombreux dans les zones urbaines denses. Ceci permet de réduire le taux de pollution dans les grandes villes. Par exemple, à Paris, la RATP est entrain de remplacer ses bus diesel par des bus électriques hybrides dans une phase intermédiaire vers un transport 100% électrique [RTP00]. En plus, les stations modernes donnent de plus en plus d'importance au confort des passagers. Des charges comme les escalators, ascenseurs... se trouvent aujourd'hui dans presque toutes les gares urbaines. Ces charges particulières sont capables de régénérer de l'énergie en freinant. Cette énergie est actuellement brûlée dans des résistances. Par conséquence, en parallèle à ces évolutions, cette section propose une station DC intelligente permettant l'échange énergétique entre les différents sous-systèmes d'une gare (trains, bus et voitures électriques, escalators...). Elle est constituée d'un 'DC micro-grid' permettant un flux énergétique bidirectionnel entre les différents composants à travers un 'DC busbar' auquel sont raccordés des convertisseurs DC/DC. Le concept sera détaillé dans le chapitre V. Le chapitre VI étudiera la stabilité de ce système et proposera une commande de stabilisation, le backstepping. A la fin de cette section, et après avoir détaillé chaque sous-système, des recommandations techniques seront données pour un éventuel développement futur.

Après l'étude de la solution urbaine, une troisième section C proposera une solution software pour les lignes à grande vitesse où des consignes de vitesse permettront d'optimiser énergétiquement une grille horaire. En fait, pendant que l'énergie de freinage constitue l'élément clé pour une optimisation énergétique d'un système urbain DC, les lignes AC à grandes vitesses sont impactées par leurs profiles de vitesse et leur synchronisation. Par exemple, des trains accélérant simultanément sur une même zone électrique impliquent un pic de puissance au niveau de la station d'alimentation qui pourrait dépasser le maximum de puissance souscrite. Ce problème sera donc détaillé et un algorithme d'optimisation sera développé dans cette section. Il sera constitué de deux étapes successives : la première consiste à optimiser, à l'aide d'un algorithme d'évolution différentiel, le profil de vitesse de chaque train dans une grille horaire donnée. Le résultat est un train consommant moins d'énergie tout en respectant les contraintes de temps. La deuxième étape consistera à améliorer la synchronisation de ces trains afin de réduire le pic de puissance au niveau des stations d'alimentation. Elle agira sur le temps d'arrêt des trains dans les gares.

Pour résumer, l'objectif de cette thèse est donc d'améliorer l'efficacité énergétique des différents systèmes ferroviaires électrifiés, AC et DC. Les particularités de chacun de ces systèmes imposent l'étude de deux solutions différentes adaptées à chaque cas. La première propose une solution hardware, la station DC intelligente, qui permet de récupérer l'énergie de freinage des trains et l'utiliser dans des applications non-ferroviaires, dans notre cas il s'agit des bus hybrides électriques. Ceci permet de faire un pont énergétique entre une ligne ferrée et son environnement. Cette solution entre dans le cadre de l'évolution des grandes villes et permet de réduire les pertes d'énergie. La deuxième propose une solution pour les lignes à grandes vitesses. Elle optimise d'abord le profil de vitesse de chaque train individuellement puis réajuste les temps d'arrêt dans les stations pour optimiser leur synchronisation. Cette stratégie permettra de réduire à la fois le bilan énergétique global ainsi que l'appel de puissance au niveau des sous-stations.

## Station DC intelligente : une solution urbaine

Un réseau ferroviaire urbain est un système largement distribué. Dans les grandes villes denses, l'étude de ces lignes constitue une tâche complexe vu le grand nombre d'interconnexions et d'échanges énergétiques sous différentes formes. Par conséquent, au lieu de chercher à optimiser le système complet, une solution 'locale' est proposée. Elle peut être multipliée tout au long d'une ligne pour augmenter l'efficacité énergétique globale. D'autre part, la consommation d'énergie d'un système ferroviaire est caractérisée par un grand nombre de paramètres interdépendants au niveau de la transmission, de l'utilisation et de l'échange énergétique sous ses différentes formes (mécanique, électrique, thermique). Dans cette étude, on s'intéresse à l'aspect électrique. De plus, vu que le freinage/accélération est très fréquent et que les stations sont proches, la quantité d'énergie de freinage pouvant être récupérée dans un système urbain est beaucoup plus importante que dans les lignes à grande vitesse. Enfin, pour optimiser la consommation d'énergie dans un système urbain DC, l'action principale est la réduction des pertes en énergie de freinage qui constituent une part importante du bilan énergétique globale.

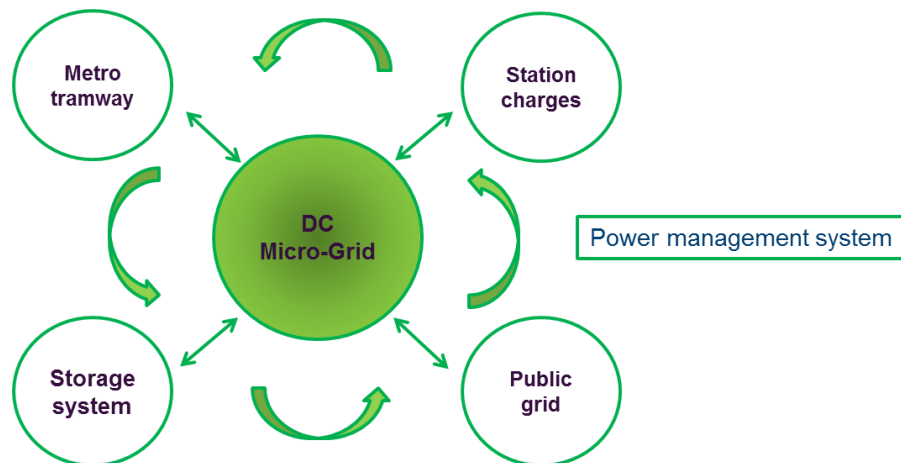


Figure I. Le concept général du DC micro-grid

La solution ainsi proposée est d'utiliser un DC micro-grid pour connecter le métro/tramway, les stations de charge des bus électriques et le réseau public avec ses différents consommateurs (Figure I). Le flux d'énergie sera optimisé à l'aide d'un gestionnaire de puissance. Un système de stockage introduira de la flexibilité au micro-grid.

La Figure II présente l'architecture du DC micro-grid et son principe de fonctionnement. Lorsqu'un train freine, il converti son énergie mécanique en électrique et la tension au niveau de son pantographe augmente. Si un autre train accélère à proximité, l'énergie sera échangée naturellement entre les deux trains. Dans le cas contraire, cette énergie est brûlée dans des résistances embarquées pour empêcher d'avoir des surtensions au niveau de la caténaire (ou 3<sup>ème</sup> rail). Au lieu

de perdre cette énergie, la solution consiste à installer un DC micro-grid dans une station de passagers. L'excès d'énergie de freinage sera donc récupérer par un convertisseur DC/DC qui va l'injecter sur un busbar DC. Elle est ensuite stockée dans un système de stockage hybride. Lorsqu'un bus électrique vient se brancher sur le DC busbar, elle sera restituée pour le charger. Le DC busbar est relié au réseau interne de la station à l'aide d'un convertisseur AC/DC bidirectionnel qui va garder la tension du busbar autour de 900V. L'ensemble est géré par un PMS (Power Management System).

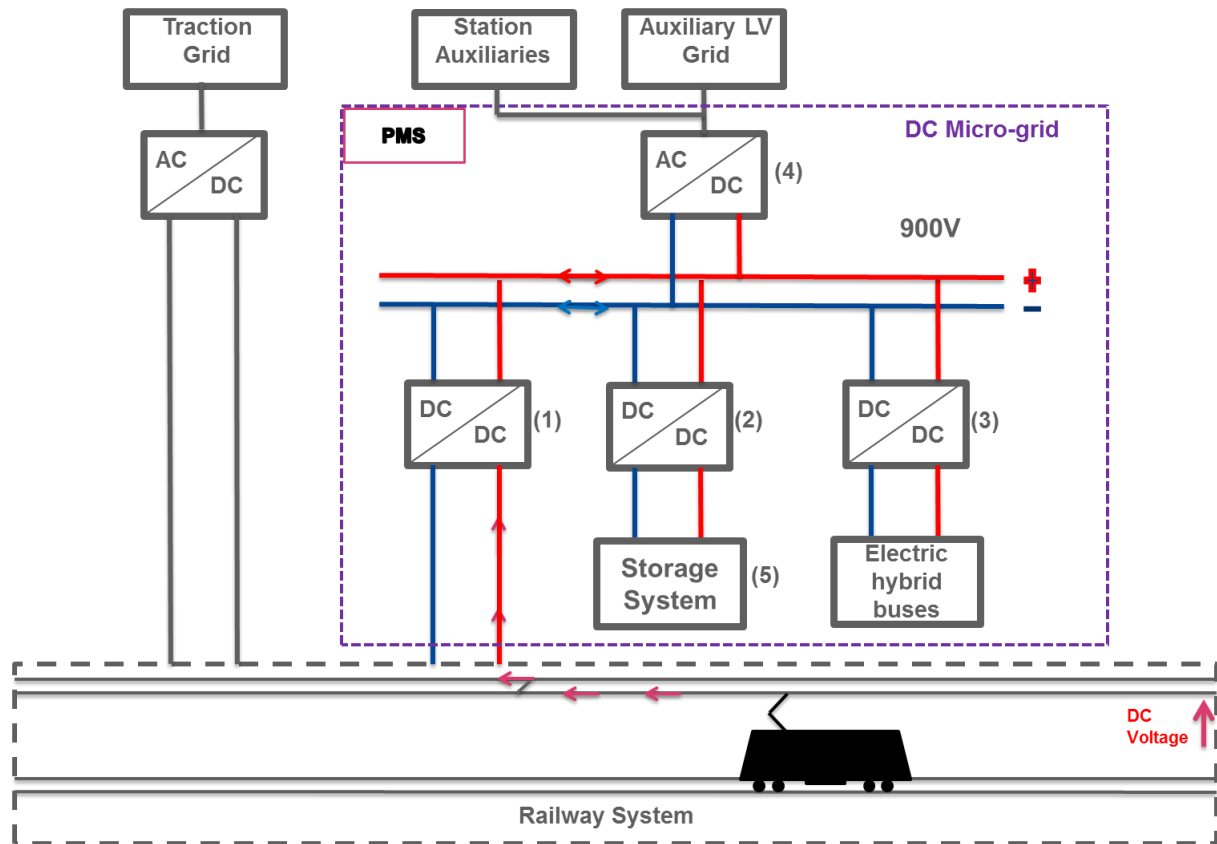


Figure II. Architecture du DC micro-grid

### 1. Modélisation des sous-systèmes

Dans cette étude, deux milieux différents doivent être étudiés : d'une part, le système ferroviaire avec ses contraintes électriques, mécaniques, trafic... et d'autre part le DC micro-grid avec ses convertisseurs et leurs boucles de régulation. Par conséquent, deux outils de simulation sont nécessaires. Pour simuler une ligne de métro, nous utiliserons Elbas Sinanet, simulateur multi-train destiné au dimensionnement de l'infrastructure électrique. Le reste sera modélisé et simulé dans Matlab-Simulink et plus précisément, Matlab sera utilisé pour l'approche énergétique, Simulink pour la modélisation des composants du DC micro-grid et enfin, Matlab-Simulink pour l'étude de stabilité. Malheureusement, aucun lien ne peut être établi entre Sinanet et Matlab-Simulink ce qui empêche toute co-simulation. Par conséquent, les courbes de puissance seront extraites de Sinanet sous forme de fichier csv et injectées dans les modèles Matlab-Simulink.

- Convertisseur DC/DC côté ferroviaire

La connexion avec le réseau ferroviaire se fait par un convertisseur DC/DC bidirectionnel. La figure ci-dessous montre l'architecture de ce module. T1 représente un train qui freine et donc injecte de l'énergie de freinage, quant à T2 un train à proximité qui commence à accélérer à  $t=0,4s$ . La résistance 'R' représente la caténaire/3<sup>ème</sup> rail séparant les deux trains. La station d'alimentation est représentée par une source de tension idéale et une diode indiquant le flux de puissance unidirectionnel.

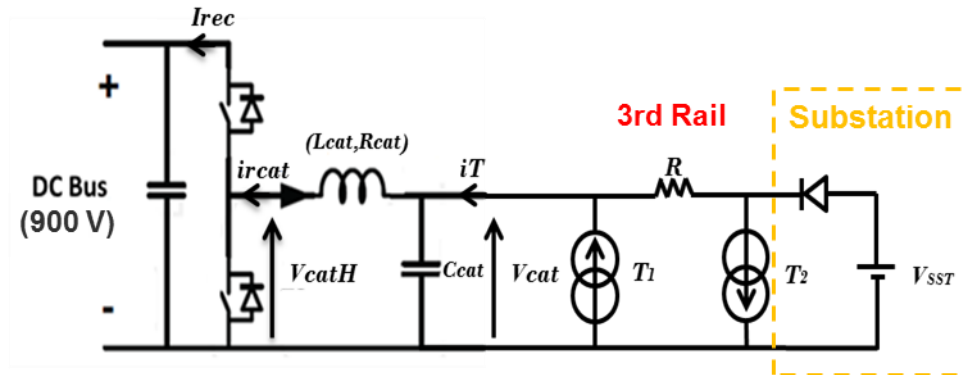


Figure III. Convertisseur DC/DC raccordé au réseau ferroviaire

Le convertisseur DC/DC va récupérer l'énergie de freinage, en fonctionnant comme boost, et l'injecter sur le DC busbar de 900V. Il doit respecter l'échange entre les trains et ne récupérer que l'excès d'énergie. La figure ci-dessous montre les courants de T1 (en bleu) et T2 (en violet).

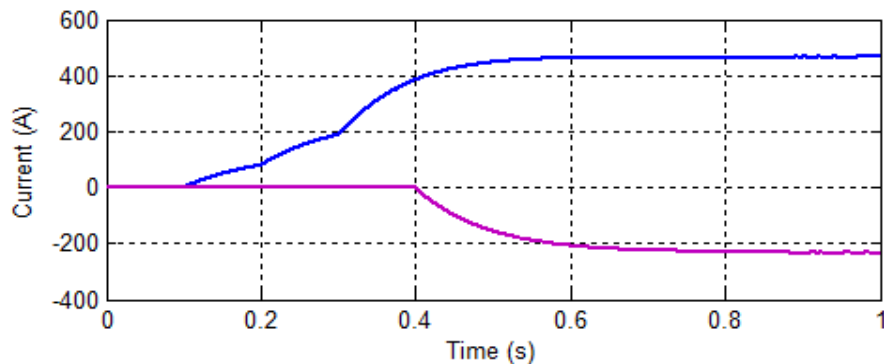


Figure IV. Profils des courants de T1 et T2

Lorsque la tension  $V_{cat}$  du convertisseur est régulée à une valeur constante, le courant mesuré dans la diode est non nul et donc l'échange entre trains n'est pas respecté.

La régulation ci-dessous permet de respecter cet échange. Elle consiste à varier la tension de référence  $V_{cat}$  en fonction de la variation de courant mesuré dans  $L_{cat}$ . Si ce dernier augmente, le convertisseur va baisser la tension  $V_{cat}$  pour augmenter l'appel de puissance et inversement.

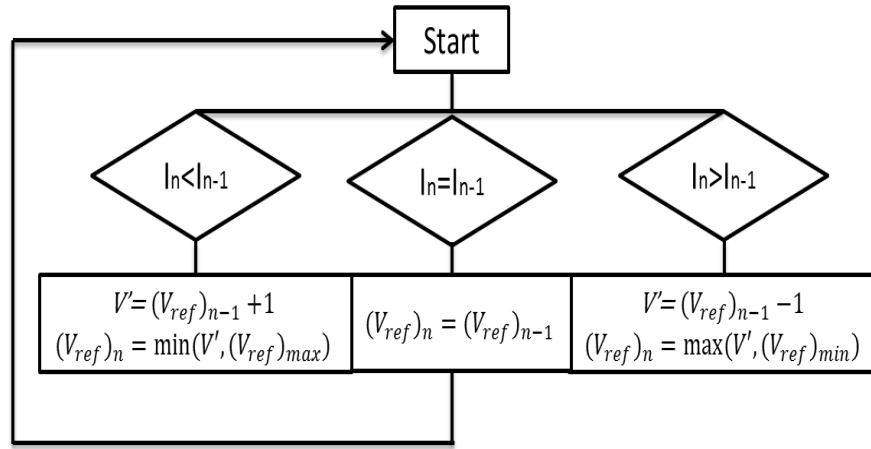


Figure V. Variation de la tension de référence du convertisseur DC/DC côté ferroviaire

- Module de stockage

La puissance de freinage à récupérer est constituée de pics de puissance qui peuvent dépasser les 3 MW en quelques secondes. Afin de pouvoir l'absorber, on a besoin d'un système hybride contenant à la fois un module avec une densité de puissance élevée et un module de stockage d'énergie. Par conséquent, on propose d'utiliser des supercapacités (SCs) et des batteries Li-ion montés en cascade selon la figure VI. Un premier convertisseur DC/DC va récupérer l'énergie de freinage du busbar DC et la stocker dans des SCs.

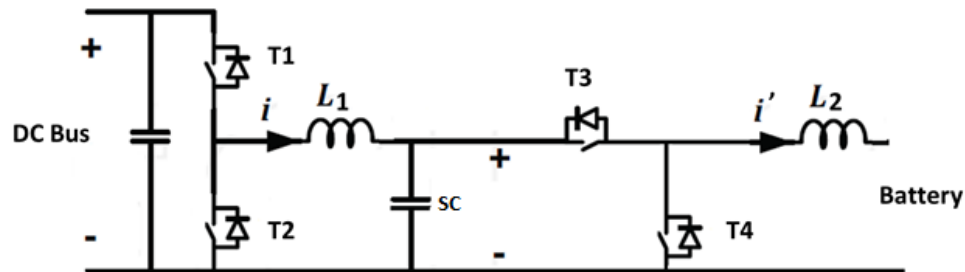


Figure VI. Architecture du module de stockage hybride

Ensuite, les batteries vont essayer de garder l'état de charge des SCs autour de 50%. Lorsque ce dernier dépasse ce seuil, la batterie va consommer de l'énergie fournie par la SC. Inversement, lorsqu'il chute au-dessous de 50%, la batterie va injecter du courant dans les SCs.

- Convertisseur AC/DC côté réseau public

Le micro-grid est relié au réseau de la station par un convertisseur AC/DC bidirectionnel qui garde la tension du DC busbar autour de 900V. C'est un onduleur à deux niveaux contrôlé par une boucle de tension suivie d'une boucle de courant. La régulation du courant  $i_q$  (et donc de la puissance réactive) à une valeur nulle permet l'utilisation de l'onduleur en question comme un correcteur de facteur de puissance.

La tension du busbar n'est pas réglée à une valeur fixe de 900V. La figure ci-dessous montre le principe de fonctionnement de ce convertisseur. Lorsque la tension dépasse 940V, il va agir en tant qu'onduleur et donc ramener la tension jusqu'à 920V en injectant de la puissance au réseau. Inversement, lorsque la tension chute en dessous de 860V, il va agir comme redresseur et donc consommer de la puissance du réseau pour ramener la tension à 880V. Une zone morte de 40V est imposée pour donner la priorité au module de stockage pour qu'il absorbe l'énergie injectée sur le busbar.

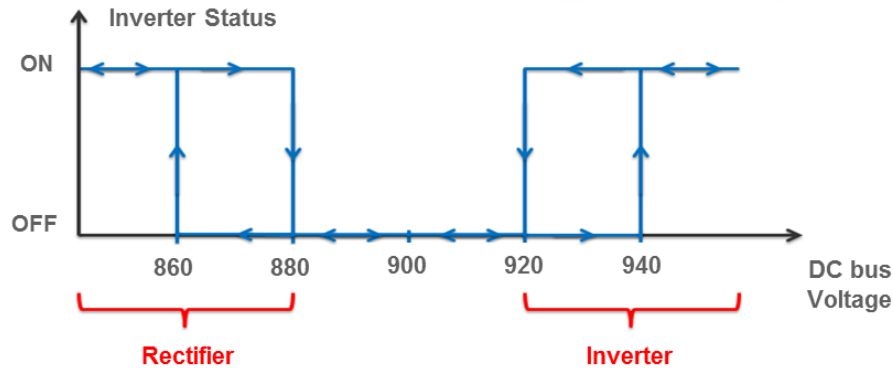


Figure VII. Principe de fonctionnement du convertisseur AC/DC

- Système de gestion du flux de puissance

Afin d'optimiser le flux énergétique entre les différents composants, un gestionnaire de puissance communique avec ces derniers selon des scénarios préprogrammés. Le tableau suivant montre la logique à suivre pour les cas fonctionnels principaux.

OM	Railway	SC	Battery	Hybrid buses	Auxiliary Loads	Inverter
RM 1	Braking energy available	SOE (SC) < 1 (Charging) P1	SOE (Bat) ≤ 1 (Charging ) P2	Not connected	Connected (consuming) P3	Feeding power to the AC grid P4
RM 2	Braking energy available	SOE (SC) = 1 (fully charged)	SOE (Bat) = 1 (fully charged)	Not connected	Connected (consuming) P1	Feeding power to the AC grid P2
RM 3	Braking energy available	SOE (SC) = 1 (fully charged)	SOE (Bat) = 1 (fully charged)	Not connected	Not connected	Feeding power to the AC grid P1
RM 4	Braking energy available	SOE (SC) < 1 (charging ) P2	SOE (Bat) ≤ 1 (charging) P3	Connected (Charging) P1	Connected (consuming) P4	Feeding power to the AC grid P5
SM	No braking energy	Standby	Standby	Not connected	Not connected	Standby
FM	No braking energy	SOE (SC) > 25% (discharging) P1	SOE > 30% (discharging) P2	Connected (charging) P1	To be disconnected	Consuming power from the AC grid P3
EM	Fault case*	SOE > 25% (discharging) P1	SOE > 30% (discharging) P2	To be disconnected	To be disconnected	Consuming power from the AC grid P3

Les quatre modes de récupération (RM) correspondent à des cas où l'énergie de freinage est récupérée du réseau ferroviaire et injectée dans le micro-grid. Selon la disponibilité du système de stockage et le raccordement ou non des bus hybride, le gestionnaire va donner des ordres de priorité aux différents sous-systèmes. Le mode 'SM' est le 'Standby Mode' pour lequel il n'y a pas de flux de puissance dans le système. Le mode 'FM', ou Feeding Mode, permet de charger des bus hybrides connectés au micro-grid alors qu'il n'y a pas d'énergie de freinage disponible et donc l'énergie nécessaire vient uniquement du système de stockage. Enfin, étant donné qu'un grand module de stockage sera installé dans une station passager, le mode 'EM', ou 'Emergency Mode', sert en cas de défaut électrique côté ferroviaire, à alimenter un train pour qu'il puisse évacuer les passagers en toute sécurité.

## 2. Application : ligne 13 du métro parisien

Etant donné que la RATP était partenaire d'Alstom dans le projet européen Osiris, la ligne 13 de paris est choisie pour tester le système et évaluer énergétiquement son efficacité. Cette ligne est modélisée et simulée dans Elbas. Un convertisseur est placé à la station « Porte de Saint-Ouen » pour récupérer l'énergie de freinage des trains. La courbe de puissance résultante est ensuite injectée dans Matlab.



Figure VIII. Ligne 13 de Paris simulée

Les résultats d'énergie montre que plus l'intervalle entre les trains augmente plus il y a d'énergie à récupérer. Ceci peut être expliqué par le fait que lorsque les trains sont proches, la plupart de l'énergie de freinage est échangée entre les trains et il n'en reste pas beaucoup à récupérer.

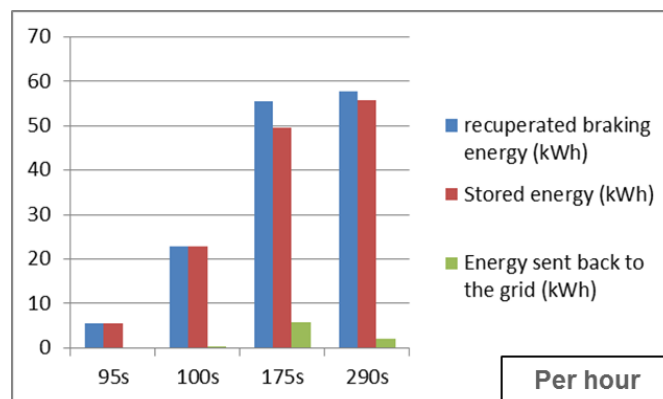


Figure IX. Energie de freinage récupérée par le DC micro-grid



La quantité d'énergie qui peut être récupérée sur une année est de 300 MWh tandis que l'énergie nécessaire pour charger un bus hybride électrique chaque heure (cas d'usage étudié dans notre cas) est de 160 MWh.

En conclusion, le DC miro-grid est capable de récupérer l'énergie de freinage des trains malgré le fait qu'elle est aléatoire et constituée de pics de puissance de grande amplitude et courte durée.

### 3. Etude de stabilité du DC micro-grid

Un circuit résonnant, contenant donc au moins un élément inductif et un autre capacitif, devient instable s'il présente une charge de puissance constante. En effet, son modèle linéaire se comporte comme une résistance négative et donc amplifie les variations dynamiques du circuit. Dans le cas du DC micro-grid, le circuit résonnant est constitué des filtres des différents convertisseurs raccordés au même busbar DC. L'amplification de leurs régimes dynamiques par une consommation constante de puissance (par exemple les bus hybrides qui se chargent à 200 kW) peut entraîner l'instabilité du système. Afin d'éviter ce problème, une commande de stabilisation, basé sur le concept du « Backstepping », peut être ajoutée à la commande du module du stockage. Cette stratégie est testée sur un modèle simplifié (figure X) où les convertisseurs sont remplacés par des sources/charges de courant/tension idéales.

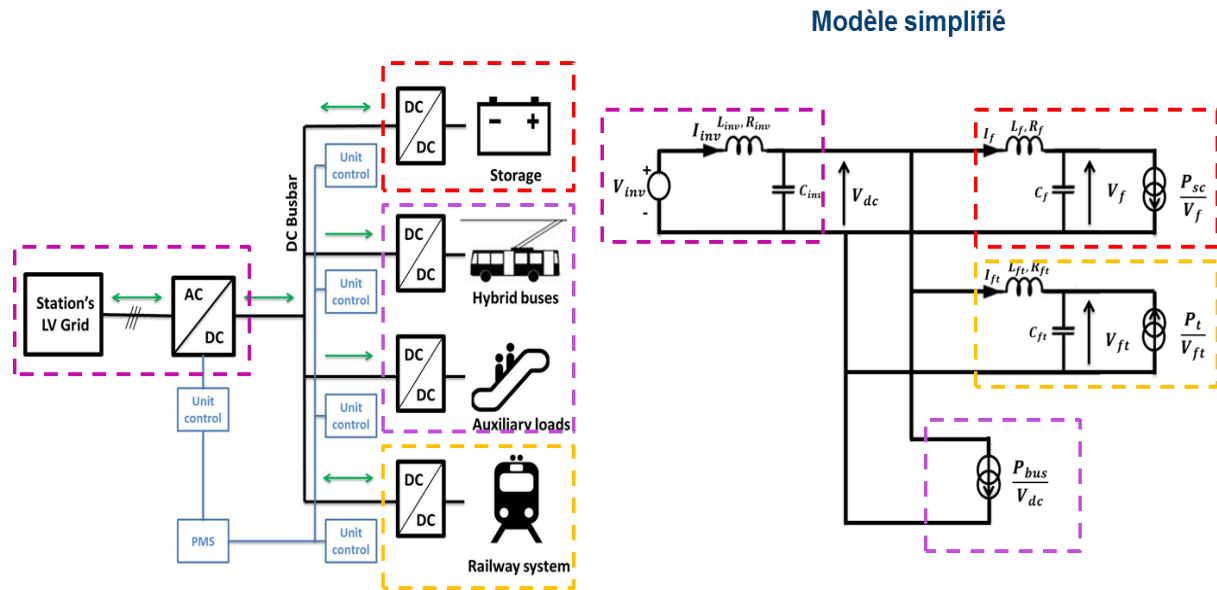


**Figure X. Modèle simplifié pour l'étude de stabilité**

Le principe du backstepping est de modéliser le système de 'N' variables, grâce à un changement de variable, sous forme de 'N' équations en cascade c.à.d. la sortie de l'une est l'entrée de l'autre. Cette approche permet de diviser un système complexe en des sous-systèmes de façon à ce que la stabilisation de chacun par la sortie du précédent amène à la stabilisation du système complet. Il faut noter que cette méthode nécessite une linéarisation autour d'un point de

fonctionnement. Etant donné que dans notre application le système n'a pas de mode nominal vue la variation de la puissance de freinage, cette étape doit être faite en dynamique et donc elle suivra l'évolution du flux énergétique. Dans notre cas, la méthode de Newton-Raphson est utilisée. La figure ci-dessous présente la mise en équation et le changement de variables qui a été fait pour aboutir à la commande backstepping 'u'.

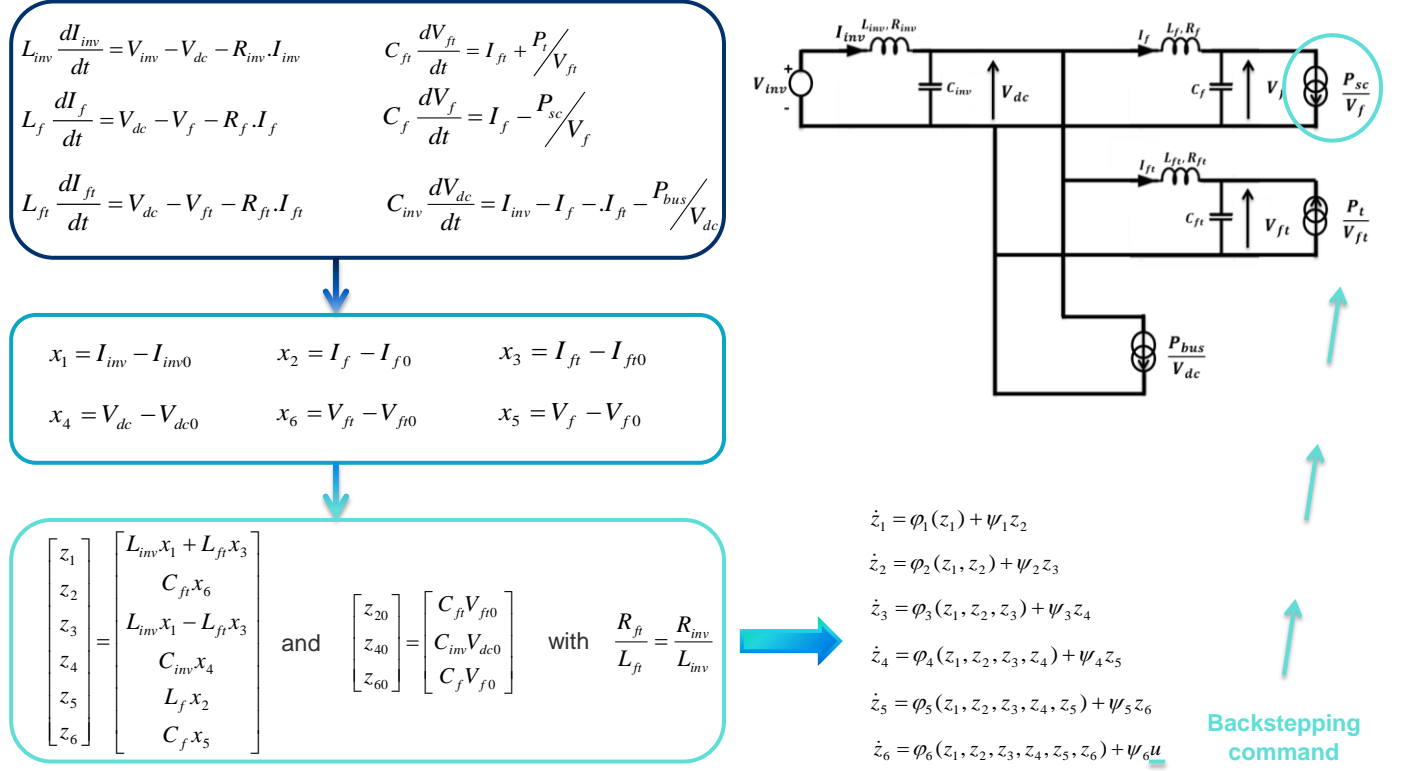
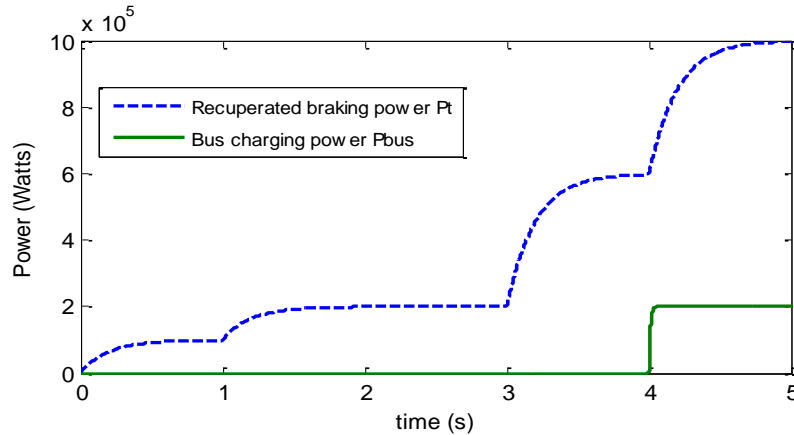


Figure XI. Calcul de la commande du backstepping

Le scénario suivant est simulé. Pendant que le micro-grid récupère l'énergie de freinage et à  $t=4s$ , un bus se branche au DC busbar et consomme 200 kW. Avant l'introduction de la commande de stabilisation 'u', la tension du bus est instable. En ajoutant 'u' à la puissance de référence du module de stockage, la tension du busbar reste stable.



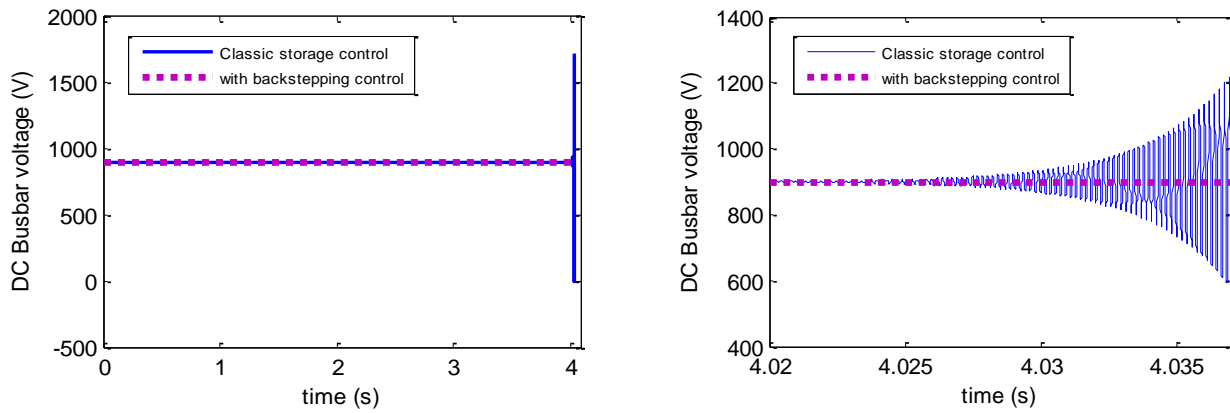


Figure XII. Simulation de l'approche Backstepping

#### 4. Conclusion sur la station DC intelligente

Cette thèse présente une solution pour l'amélioration de l'efficacité énergétique des systèmes ferroviaires urbains. Elle consiste à intégrer dans une station de passagers un DC micro-grid pour récupérer l'énergie de freinage des trains qui est aujourd'hui brûlée dans les rhéostats des trains. Un système de stockage hybride a permis d'absorber les pics de puissance renvoyés par les trains. De plus, grâce à une régulation évolutive, le convertisseur côté ferroviaire a respecté les échanges entre les trains. D'autre part, aucune perturbation n'est constatée côté réseau public. Enfin, la quantité d'énergie stockée était suffisante pour charger plusieurs bus électriques hybrides toutes les heures.

## Optimisation énergétique de la grille horaire: Solution pour les grandes vitesses

---

Dans cette partie, il s'agit d'une solution pour les lignes à grandes vitesses. Ces dernières étant électrifiées en mode AC, ne présentent pas de pertes d'énergie de freinage électrique qui est renvoyée à travers les sous-stations. En plus, elles sont divisées en zones électriques alimentées chacune par une phase électrique différente pour ne pas déstabiliser le réseau public. Par conséquent, l'optimisation énergétique doit être faite pour chaque zone séparément tout en prenant en compte l'influence de l'une sur l'autre.

Il faut aussi prendre en compte le fait que ces lignes ne sont pas automatiques et donc, toute solution qui consiste à communiquer des consignes au conducteur doit prendre en compte son temps de réflexe et son imprécision. Autrement dit, il ne faut pas chercher à descendre au-dessous de 5s entre deux consignes consécutives ou à calculer un profil de vitesse très précis. L'idée est d'envoyer des consignes faciles à interpréter.

En plus les lignes à grande vitesse s'étendent sur des longues distances avec un petit nombre de stations. Ceci ajoute plus de flexibilité au profil de vitesse à optimiser. Cependant, pour chaque mission, il existe des points opérationnels auxquels il faut passer à des temps précis (à la minute près). Ces contraintes seront prises en compte lors de l'optimisation.

Afin de pouvoir optimiser une grille horaire, deux étapes sont nécessaires. D'abord, chaque train (ou mission) doit être étudié seul indépendamment des autres. Cela consiste à lui calculer le profil de vitesse qui consomme le moins d'énergie tout en respectant les différentes contraintes (d'exploitation, électriques, mécaniques...). Cette étape d'optimisation est une approche énergétique. Mais optimiser la grille énergétiquement ne suffit pas car la puissance totale consommée est un élément très important vu l'amplitude des pics qui peuvent dépasser le maximum de puissance souscrite. Par conséquent, après avoir optimisé chaque train indépendamment, une deuxième étape consiste à réduire le pic de puissance des sous-stations en agissant sur le temps d'arrêt des trains dans les gares.

### 5. Optimisation du profil de vitesse

En général, le profil de vitesse d'un train est constitué de quatre types différents de conduite : la phase de traction (1) qui utilise les moteurs des trains pour accélérer, la phase de 'maintien de vitesse' (2) pendant laquelle le conducteur va accélérer/freiner pour garder sa vitesse constante, la phase de la 'marche sur l'erre' où l'alimentation est coupée et le train avance par inertie, et enfin la phase de freinage où le train réduit sa vitesse à l'aide du freinage mécanique ou électrique.

Il faut aussi noter que dans une grille horaire, le temps accordé à une mission contient une détente ou marge ajoutée au temps de parcours minimal possible. Cette marge rend la mission plus flexible et permet par exemple au conducteur de rattraper son retard en cas de perturbations et donc arriver à temps. En plus du temps d'arrivée, les points opérationnels sont définis pour chaque mission et auxquels un train doit passer à une heure bien précise (à la minute près). Dans cette étude, une mission est découpée en zones de vitesse qui prennent en compte ces points opérationnels et les changements des vitesses limites. Une mission est donc caractérisée par les paramètres suivants définis pour chaque zone de vitesse :

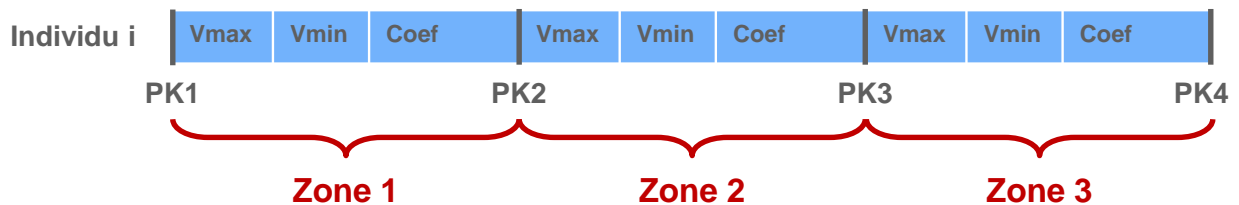
- $V_{max}$  : la vitesse maximale à partir de laquelle la marche sur l'erre est activée
- $V_{min}$  : la vitesse minimale à partir de laquelle le train accélère
- $Coef$  : le coefficient de traction maximal. Il représente les performances mécaniques maximales du moteur.

Les contraintes suivant sont appliquées dans chaque zone de vitesse :

- $\frac{V_{limit}(z)}{2} \leq V_{max}(z) \leq V_{limit}(z)$
- $\frac{V_{max}(z)}{2} \leq V_{min}(z) \leq V_{max}(z)$
- $0.5 \leq Coef \leq 1$

$V_{max}$  doit être inférieure à la vitesse limite et supérieure à la moitié de cette dernière.  $V_{min}$  ne doit pas dépasser  $V_{max}$  et doit être supérieure à  $V_{max}/2$ .  $Coef$  est compris entre 1 et 0.5. Les limites inférieures des trois paramètres permettent d'éviter des retards considérables.

L'algorithme d'optimisation est basé sur le principe de l'évolution différentielle où un individu correspond à une mission :



Le concept est le suivant : la population initiale est générée aléatoirement tout en respectant les contraintes de chaque paramètre ainsi que les contraintes de temps. Ensuite, deux opérations, la mutation puis le croisement, sont appliquées sur chaque individu afin d'obtenir une nouvelle génération provisoire. Chaque individu de cette dernière est comparé à son correspondant de la génération initiale en utilisant une fonction 'fitness' qui prend en compte les différentes contraintes et la consommation de l'énergie. La nouvelle génération contiendra les meilleurs individus. Ce processus est répété jusqu'à la convergence. La fonction fitness utilisée est la suivante :

$$f(x) = w_e \frac{E(x) + \Delta E_{kinetic}}{E_{flat-out}} + \sum_{\substack{op=1 \\ T \leq T_{target}}}^{Nb_{OP}-1} w_t(op) \left( \frac{T_{target}(op)}{T(x,op)} \right)^2 + \sum_{\substack{op=1 \\ T \geq T_{target}}}^{Nb_{OP}-1} w_t(op) \left( \frac{T(x,op)}{T_{target}(op)} \right)^2$$

Où :

- la partie jaune pénalise la consommation des trains
- la partie bleue pénalise les trains en avance à chaque point opérationnel
- la partie rouge pénalise les trains en retard à chaque point opérationnel.

## 6. Application de l'algorithme d'optimisation du profil de vitesse

Pour tester l'algorithme, et étant donné que la SNCF était le partenaire d'Alstom dans le projet européen MERLIN, la ligne à grande vitesse entre Paris et Lyon (la LGV1) est choisie pour cette application. Elle est modélisée et simulée dans un simulateur de mouvement de train développé en interne chez Alstom. Les caractéristiques principales suivantes sont donc prises en compte lors de la simulation :

- Caractéristiques de la ligne : topologie, limitations de vitesses...
- Caractéristiques du train : courbes de traction et de freinage, masse, longueur, résistance à l'avancement...
- Caractéristiques de la conduite : les arrêts marqués, le temps d'arrêt en station, la marche sur l'erre...

La grille horaire à optimiser est celle du vendredi 21/02/2014 entre 16h et 18h. Elle correspond à un jour de départ en vacances de ski avec 34 trains allant de Paris à Lyon et 10 missions différentes. Voici les résultats d'optimisation de la mission la plus longue allant de Crisenoy à Montanay, contenant 11 zones de vitesses et donc 33 paramètres à optimiser. L'algorithme a convergé au bout de 580 générations.

Vmax1	Vmin1	Coef1	Vmax2	Vmin2	Coef2	...	Conso	E_kinetic	Tps1	Tps2	Tps3	Tps4	Tps5	Tps6	Fitness	E / E_flat_out	Exit speed
254	138	1.0	279	276	0.6	...	6418	0	0	44	-9	-12	7	21	0.97082055	0.61652257	160
247	152	0.9	283	279	0.5	...	6536	0	-3	13	-3	-7	16	34	0.97020185	0.62785783	160
269	166	0.9	277	277	0.6	...	6631	0	3	25	3	-1	4	13	0.969733	0.63698367	160
268	174	1.0	278	276	0.6	...	6614	0	3	15	1	-2	14	24	0.96989852	0.63535062	160
270	145	1.0	281	278	0.5	...	6488	0	5	27	-4	-8	7	23	0.97024912	0.62324688	160
221	148	0.9	282	277	0.5	...	6535	0	5	18	-10	-14	-2	15	0.96990001	0.62776177	160
173	164	1.0	285	278	0.5	...	6521	0	-5	12	-13	-17	4	32	0.97077948	0.62641691	160
250	158	1.0	285	277	0.5	...	6495	0	-3	27	3	-1	19	37	0.97103816	0.62391931	160

Paramètres des 8  
Individus de la génération finale

Consommation  
d'énergie

Ecart de temps à chaque  
point opérationnel

Le tableau suivant résume ces résultats. La solution optimale est la troisième (en rouge). Elle permet d'économiser 36% d'énergie par rapport à une marche tendue tout en respectant la ponctualité à  $\pm 30$ s.

Energy savings (%)	$\Delta T 1$	$\Delta T 2$	$\Delta T 3$	$\Delta T 4$	$\Delta T 5$	$\Delta T 6$
38	0	44	-9	-12	7	21
37	-3	13	-3	-7	16	34
36	3	25	3	-1	4	13
36	3	15	1	-2	14	24
38	5	27	-4	-8	7	23
37	5	18	-10	-14	-2	15
37	-5	12	-13	-17	4	32
38	-3	27	3	-1	19	37

## 7. Optimisation de la synchronisation des trains

Après avoir optimisé chaque mission de la grille horaire indépendamment, cette étape consiste à améliorer la synchronisation des trains (phases d'accélération et de freinage) pour réduire le pic de puissance dans les sous-stations. Le concept général est présenté dans la figure ci-dessous. Elle montre que le décalage d'un train peut réduire la consommation de puissance en favorisant l'échange entre trains. En plus de cet échange, l'optimisation peut consister à désynchroniser deux accélérations simultanées.

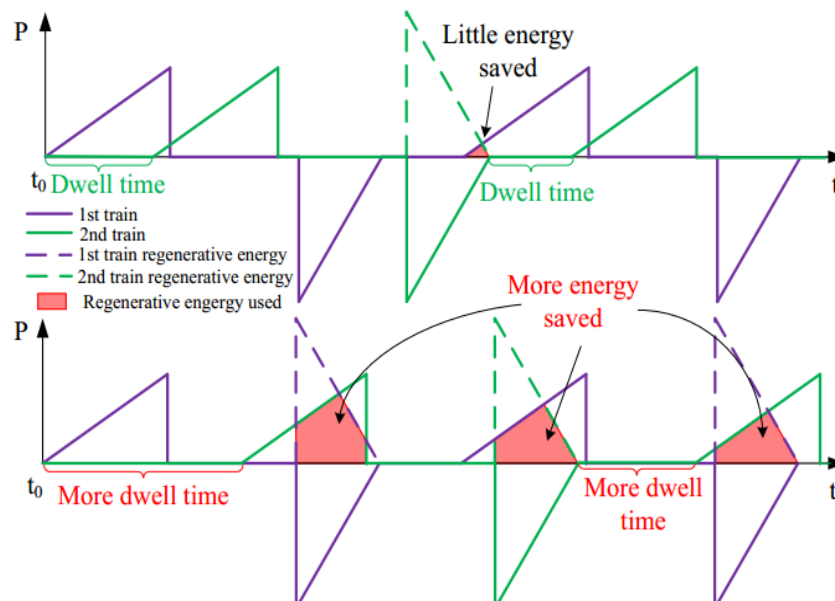


Figure XIII. Modification du temps d'arrêt et son impact sur l'échange énergétique entre trains [CHE14]

Vu que dans cette étape on étudie l'interaction entre les trains, il faut prendre en compte la particularité du réseau électrique ferroviaire AC. Ce dernier étant découpé en zones électriques

séparées par des zones neutres et alimentées par des sous-stations différentes, la consommation en puissance de la mission de chaque train doit être distribuée sur les différentes zones. De plus, cette étape doit prendre en compte les écarts du temps de passage aux points opérationnels déjà introduits par la première optimisation pour ne pas dépasser les  $\pm 30s$ . Ceci a un grand impact sur la marge d'optimisation restant. A noter que dans cette phase, un train peut toujours être retardé mais ne peut pas être avancé.

Les étapes de cet algorithme sont les suivantes :

1. Sélectionner une sous-stations non-optimisée avec le plus haute puissance moyenne sur 10 minutes.
2. Sélectionner le train qui consomme le plus aux extrémités de cette fenêtre de 10 minutes.
3. Décaler le train avec un pas de 5s tant que :
  - La puissance moyenne de la sous-stations n'augmente pas
  - La puissance moyenne des autres sous-stations déjà optimisées n'augmente pas
  - Le retard maximal n'est pas dépassé

Une fois terminé, le train optimisé ne peut plus être décalé dans la prochaine étape. L'optimisation se termine lorsqu'il n'y a plus de trains qui peuvent être décalés.

#### 8. Application de l'algorithme de synchronisation des trains

L'algorithme est appliqué sur la même grille horaire que l'étape précédente. Afin de voir l'impact de la marge d'optimisation, deux cas sont simulés pour 30s puis 45s de retard maximal. Les résultats sont les suivants :

Maximal Average Power (MW)					
SST Name	Before optimisation	ShiftMax=30		ShiftMax=45	
MOISENAY	8.047	7.81	-2.9%	7.81	-2.9%
LA VOULZIE	26.205	26.175	-0.1%	26.145	-0.2%
VILLECHETIVE	31.4	31.059	-1.1%	30.843	-1.8%
CARISEY	23.93	23.001	-3.9%	22.521	-5.9%
SARRY	35.952	35.155	-2.2%	35.128	-2.3%
COMMUNE	35.593	35.77	0.5%	34.929	-1.9%
CURTIL	21.057	21.053	0.0%	20.855	-1.0%
MACON	12.851	12.605	-1.9%	11.935	-7.1%
LES MEUNIERES	11.111	11.199	0.8%	11.199	0.8%

Les sous-stations les plus chargées sont marquées en gris. Pour un retard maximal de 45s, une réduction moyenne de 2% des pics de puissance est obtenue. Par contre pour 30s, l'amélioration de la situation de la sous-station de SARRY a dégradé celle de COMMUNE. Mais dans ce cas, un retard de plus que 10 s était introduit par la première optimisation.

#### 9. Conclusion sur l'optimisation énergétique de la grille horaire

L'optimisation énergétique de la grille horaire permet de réduire grâce à ses deux étapes, le bilan énergétique ainsi que les pics de puissance à l'aide de consignes de conduite transmises au conducteur. Cette optimisation respecte la ponctualité des trains à  $\pm 30s$ . Enfin, ces deux étapes



optimisent une grille horaire 'offline' d'où l'intérêt d'ajouter une troisième étape qui a pour but de réduire l'écart entre les grilles réelles et celles théoriques à travers des consignes de vitesses transitoires.

Cette thèse a pour but l'amélioration de l'efficacité énergétique des systèmes ferroviaires urbains et à grande vitesse. La première partie a proposé une solution 'hardware' qui peut être intégrée dans une gare. Cette station intelligente a permis de récupérer l'énergie de freinage des trains et de la stocker dans un système de stockage hybride pour l'utiliser après dans des applications « non-ferroviaire ». Dans cette étude, le cas d'usage étudié était la recharge des bus électriques hybrides chaque heure. La simulation énergétique de la ligne 13 du métro de Paris a montré qu'il y avait assez d'énergie pour charger plusieurs bus par heure. La stabilité du système a été ensuite étudiée et une commande de stabilisation basée sur l'approche du Backstepping a été détaillée. De point de vue technique, cette solution utilise des technologies qui sont aujourd'hui suffisamment matures. Par contre, de point de vue économique, il faudrait attendre encore pour que le prix des convertisseurs DC/DC et des batteries diminue. Ceci est très probable vu l'augmentation considérable de la demande ces dernières années.

La deuxième partie est consacrée aux lignes à grandes vitesses. Contrairement au cas urbain, c'est une solution 'software' qui est proposée. Elle consiste à réduire la consommation, en énergie et en puissance, d'une grille horaire. Un algorithme basé sur l'évolution différentielle a été détaillé. Il est constitué de deux phases : la première optimise chaque mission à part en calculant des paramètres caractérisant la conduite sur différentes zones de vitesses. Une réduction moyenne de 35% est obtenue par rapport à une marche tendue tout en respectant la ponctualité des trains à  $\pm 30$ s. La deuxième étape optimise l'interaction entre trains afin de diminuer les pics de puissance des sous-stations. Cette seconde étape prend en compte les retards/avances déjà introduites par la première. Ceci a limité la marge d'optimisation restante. Des meilleurs résultats sont obtenus pour un retard max de 45s. Enfin, contrairement au cas urbain, cette solution nécessite moins d'investissement et peut être facilement appliquée.

Pour plus d'information sur ces sujets, un rapport détaillé en anglais suivra ce résumé.

## **INDEX**

<b>GENERAL INTRODUCTION</b>	<b>32</b>
<b>SECTION A: OVERVIEW ON RAILWAY SYSTEMS</b>	<b>36</b>
I – Historical railway evolution .....	37
II – Railway electric traction systems .....	41
III – Environmental impact and existing solutions .....	45
III.a. Environmental impact .....	45
III.b. Train braking system .....	47
III.c. Solutions for reducing energy consumption .....	51
IV – Conclusion .....	56
<b>SECTION B: SMART DC STATION FOR URBAN SYSTEMS</b>	<b>57</b>
V – DC Micro-grid integration in railway system .....	58
V.a. Introduction .....	58
V.b. Context and Concept .....	59
V.c. Smart grid reference architecture .....	62
V.d. Storage system technologies .....	66
V.e. Power converters .....	71
V.f. Power management system .....	95
V.g. Use case: Application On Paris metro line 13 .....	97
VI – Stability of DC Micro-grid .....	109
VI.a. Instability of low damped systems .....	110
VI.b. Small signal stability of the DC Micro-grid .....	111
VI.c. Backstepping approach .....	123
VII - Technical recommendations .....	130
VII.a. Inverter's specifications .....	130

VII.b. Storage converter's specifications .....	132
VII.c. Railway converter specification.....	133
<b>SECTION C: ENERGY OPTIMIZATION FOR SUBURBAN AND HIGH SPEED LINES</b>	<b>136</b>
VIII - Introduction .....	137
IX - Speed profile and energy optimization .....	140
IX.a. Introduction.....	140
IX.b. Methodology general specifications .....	141
IX.c. Definition of the algorithm .....	147
IX.d. Conclusion.....	156
X - Trains synchronization .....	158
X.a. Dwell times modification .....	159
X.b. Delay compensation .....	162
XI - Simulations: Application on Paris-Lyon high speed line.....	166
XI.a. Context.....	167
XI.b. Results of speed profile optmization .....	169
XI.c. Results of substations power optimization .....	174
<b>CONCLUSION AND PERSPECTIVES</b>	<b>176</b>
<b>REFERENCES</b>	<b>182</b>
<b>APPENDICES</b>	<b>187</b>
<b>A- OSIRIS PROJECT</b>	<b>188</b>
<b>B- MERLIN PROJECT</b>	<b>191</b>
<b>C- ELBAS SOFTWARE USED FOR ENERGY SIMULATIONS</b>	<b>194</b>
<b>D- TIMETABLE OF PARIS-LYON HIGH SPEED LINE</b>	<b>196</b>

## **LIST OF FIGURES**

FIGURE 1. RAILWAY EVOLUTION IN FRANCE .....	37
FIGURE 2. SIEMENS & HALSKE FIRST ELECTRICAL TRAMWAY IN BERLIN .....	38
FIGURE 3. FIRST FRENCH ELECTRICAL TRAIN « BOITE A SEL » .....	38
FIGURE 4. THREE-PHASE RAILCAR “A” OF SIEMENS AND AEG .....	39
FIGURE 5. OLD PANTOGRAPH (LEFT) VS NEW PANTOGRAPH (RIGHT) .....	41
FIGURE 6. DIFFERENT TYPES OF 3 <sup>RD</sup> RAIL CURRENT COLLECTION [NET00] .....	42
FIGURE 7. 2x25 kV ELECTRIFICATION SYSTEM.....	43
FIGURE 8. DC ELECTRIFICATION SYSTEM.....	43
FIGURE 9. CO <sub>2</sub> GAS EMISSION OF DIFFERENT SECTORS IN 2011 [SUS11] .....	45
FIGURE 10. TRANSPORT SECTOR CO <sub>2</sub> EMISSIONS BY MODE, 1990-2011 .....	46
FIGURE 11. PASSENGER AND FREIGHT RAILWAY ACTIVITY (TRAIN-KM), 2005 INSIDE – 2011 OUTSIDE [IEA14] .....	46
FIGURE 12. EU27 RAILWAY ENERGY SOURCES MIX EVOLUTION, 1990-2011 .....	47
FIGURE 13. SHOE BRAKING VS DISC BRAKING [EUR01] [NET01] .....	48
FIGURE 14. ENERGY FLOW DIAGRAM FOR A PASSENGER TRAIN WITH REGENERATIVE BRAKING (SOURCE: IZT).....	49
FIGURE 15. ON-BOARD ELECTRICAL CIRCUIT.....	49
FIGURE 16. POWER CIRCUIT SCHEMATIC REPRESENTATION OF HESOP 750LP .....	52
FIGURE 17. POWER CIRCUIT SCHEMATIC REPRESENTATION OF HESOP 1500HP.....	53
FIGURE 18. ABB’S ENVILINE-ERS REVERSIBLE SUBSTATION [ABB00].....	53
FIGURE 19. BRAKING POWER AT A REVERSIBLE TRACTION SUBSTATION .....	60
FIGURE 20. PRE-FABRICATED CHARGING STATION ARCHITECTURE.....	60
FIGURE 21. SMART DC MICRO-GRID ARCHITECTURE .....	61
FIGURE 22. RAILWAY MICRO-GRID INTEGRATION IN SGAM.....	62
FIGURE 23. INTEROPERABILITY CATEGORIES DEFINED BY GWAC (2008) [CEN00] .....	63
FIGURE 24. INTEROPERABILITY LAYERS [CEN00] .....	63
FIGURE 25. MAPPING OF COMMUNICATION NETWORKS ON SGAM COMMUNICATION LAYER [CEN00] .....	65
FIGURE 26. HYBRID STORAGE SYSTEM [MAX00].....	67
FIGURE 27. CLASSIFICATION OF ELECTRICAL ENERGY STORAGE SYSTEMS ACCORDING TO ENERGY FORM [ELC11] .....	67
FIGURE 28. ENERGY DENSITY OF DIFFERENT TYPES OF BATTERIES [TAR01] .....	68
FIGURE 29. CAPITAL COST PER CYCLE FOR STORAGE SYSTEMS (SOURCE: ESA) .....	69
FIGURE 30. STORAGE TECHNOLOGIES COMPARISON (SOURCE : CEA).....	70
FIGURE 31. CAPITAL COST VS. RUNTIME FOR ENERGY STORAGE SYSTEMS [APC65].....	71
FIGURE 32. HYBRID STORAGE SYSTEM’S ARCHITECTURE.....	72
FIGURE 33. SUPERCAPACITOR CONTROL LOOP .....	72
FIGURE 34. SYSTEM’S LINEAR CONTROL LOOP .....	73
FIGURE 35. BODE DIAGRAM OF THE SC CONVERTER’S OPEN-LOOP REGULATION.....	74
FIGURE 36. BATTERY’S CONTROL LOOP .....	75

FIGURE 37. REFERENCE POWER TO BE ABSORBED BY THE STORAGE SYSTEM.....	77
FIGURE 38. REFERENCE CURRENT (DASHED BLUE LINE) AND MEASURED CURRENT (CONTINUOUS RED LINE) IN THE SC'S CONVERTER .....	78
FIGURE 39. BATTERY'S INPUT CURRENT AND SC'S SOE.....	78
FIGURE 40. CHARGING POWER LIMITATION .....	79
FIGURE 41. DISCHARGING POWER LIMITATION .....	79
FIGURE 42. TEST OF SC'S POWER PROTECTION.....	80
FIGURE 43. PULSE WIDTH INTESECTIVE MODULATION .....	81
FIGURE 44. 2-LEVEL AC/DC BIDIRECTIONAL CONVERTER.....	81
FIGURE 45. BIDIRECTIONAL INVERTER ON/OFF COMMAND .....	82
FIGURE 46. INVERTER CONTROL LOOP.....	82
FIGURE 47. ROTATION ANGLE EXTRACTION USING DSOGI-QSG-PLL.....	84
FIGURE 48. DSOGI-QSG FILTER .....	84
FIGURE 49. SRF-PLL CONCEPT .....	85
FIGURE 50. CURRENT CONTROL LOOPS OF THE AC/DC CONVERTER CONNECTED TO THE GRID .....	87
FIGURE 51. SIMPLIFIED CURRENT CONTROL LOOP .....	87
FIGURE 52. BODE DIAGRAM OF THE CURRENT CONTROL OPEN LOOP .....	88
FIGURE 53. THE SIMPLIFIED CONTROL LOOP OF THE AC/DC CONVERTER CONNECTED TO THE GRID.....	88
FIGURE 54. BODE DIAGRAM OF THE SYSTEM'S OPEN LOOP .....	89
FIGURE 55. DC OUTPUT VOLTAGE OF THE AC/DC CONVERTER IN RECTIFIER MODE.....	90
FIGURE 56. ZOOM ON AC VOLTAGE AND CURRENT IN RECTIFIER MODE.....	90
FIGURE 57. DC OUTPUT VOLTAGE OF THE AC/DC CONVERTER IN INVERTER MODE.....	91
FIGURE 58. ZOOM ON AC VOLTAGE AND CURRENT IN INVERTER MODE .....	91
FIGURE 59. DC/DC CONVERTER CONNECTED TO RAILWAY.....	92
FIGURE 60. REGULATION LOOP OF THE DC/DC CONVERTER CONNECTED TO RAILWAY.....	92
FIGURE 61. DC/DC CONVERTER CONNECTED TO TRAINS AND A SST.....	92
FIGURE 62. BRAKING CURRENT INJECTED BY T1 (BLUE) AND TRACTION CURRENT ABSORBED BY T2 (PINK).....	93
FIGURE 63. CURRENT CONSUMED FROM THE SUBSTATION .....	93
FIGURE 64. DC/DC CONVERTER OUTPUT VOLTAGE $V_{CAT}$ AT RAILWAY SIDE.....	93
FIGURE 65. REFERENCE VOLTAGE CALCULATION .....	94
FIGURE 66. CURRENT CONSUMED FROM THE SUBSTATION .....	94
FIGURE 67. DC/DC CONVERTER OUTPUT VOLTAGE AT RAILWAY SIDE.....	94
FIGURE 68. DECENTRALIZED CONTROL OF THE DC MICRO-GRID .....	95
FIGURE 69. PARIS METRO LINE 13 SIMULATED IN ELBAS .....	98
FIGURE 70. EXTRACT OF CONVERTER'S TIME FUNCTION POWER CURVE CALCULATED BY ELBAS FOR 95S HEADWAY.....	98
FIGURE 71. BRAKING POWER INJECTED INTO THE MICRO-GRID THROUGH RAILWAY DC/DC CONVERTER .....	99
FIGURE 72. REFERENCE AND MEASURED CURRENTS OF SC'S DC/DC CONVERTER.....	99
FIGURE 73. MEASURED CURRENT AT AC SIDE AND DC BUSBAR VOLTAGE .....	100
FIGURE 74. FFT OF CURRENT INJECTED INTO AC GRID DURING CONVERTER'S OPERATIONAL PERIOD .....	100

FIGURE 75. ZOOM ON AC CURRENT AND VOLTAGE .....	101
FIGURE 76. AVERAGE MODEL'S FLOW CHART .....	102
FIGURE 77. ENERGY STORED IN THE BATTERY (A) AND THE ENERGY SENT BACK TO THE GRID (B) FOR DIFFERENT HEADWAYS .....	103
FIGURE 78. MAXIMAL SUBSCRIBED POWER VARIATION FOR AN A5 BASE CONTRACT WITH EDF .....	106
FIGURE 79. BRAKING ENERGY DISTRIBUTION PER HOUR .....	107
FIGURE 80. SYSTEM'S STABILITY ILLUSTRATION .....	110
FIGURE 81. LINEAR MODEL OF A CONSTANT POWER LOAD: (A) DC ELECTRICAL NETWORK WITH CPL/CPS AND (B) NEGATIVE AND POSITIVE IMPEDANCE OF CPL/CPS [HAM00] .....	111
FIGURE 82. ARCHITECTURE OF DC MICRO-GRID .....	112
FIGURE 83. SC'S DC/DC CONVERTER .....	112
FIGURE 84. CONTROL LOOP OF THE SC'S DC/DC CONVERTER .....	113
FIGURE 85. BATTERY'S DC/DC CONVERTER .....	114
FIGURE 86. BATTERY'S CONTROL LOOP .....	114
FIGURE 87. AC/DC CONVERTER.....	115
FIGURE 88. ILQ REGULATION LOOP .....	116
FIGURE 89. ILD REGULATION LOOP.....	116
FIGURE 90. DC VOLTAGE REGULATION LOOP.....	117
FIGURE 91. RAILWAY DC/DC CONVERTER .....	118
FIGURE 92. RAILWAY VOLTAGE'S REGULATION LOOP .....	119
FIGURE 93. DAMPING RATIO $\xi$ OF A SECOND-ORDER SYSTEM'S POLE.....	121
FIGURE 94. SIMULATED POWER FLOW SCENARIO FOR OPERATIONAL POINTS EXTRACTION .....	122
FIGURE 95. BACKSTEPPING STABILIZING PROCESS.....	124
FIGURE 96. SIMPLIFIED MODEL ON WHICH BACKSTEPPING CONTROL IS TESTED.....	128
FIGURE 97. RECOVERED POWER AND BUS CHARGING POWER SIMULATED PROFILE .....	129
FIGURE 98. DC BUSBAR VOLTAGES FOR CLASSIC AND BACKSTEPPING CONTROLS .....	129
FIGURE 99. RAILWAY CONVERTER MAXIMUM RMS POWER OVER INCREASING TIME WINDOW .....	133
FIGURE 100. ENERGY AND TRAFFIC REGULATION FLOW CHART .....	138
FIGURE 101: RUN TIME-ENERGY CONSUMPTION AND PARETO CURVE [CUC12] .....	140
FIGURE 102: THE FOUR DIFFERENT MODES FOR A TRAIN'S RUN.....	142
FIGURE 103. SLACK-TIME REPRESENTATION.....	142
FIGURE 104. DESCRIPTION OF MUTATION. PARAMETERS ARE CHANGED RANDOMLY .....	143
FIGURE 105. DIFFERENTIAL MUTATION: THE WEIGHTED DIFFERENTIAL, $Fscaling(xr1 - xr2)$ , IS ADDED TO THE BASE VECTOR $xr0$ TO CREATE THE MUTANT $vi$ [PRI00].....	144
FIGURE 106. Crossover OF TWO INDIVIDUALS.....	144
FIGURE 107: PSEUDO C-CODE OF THE DIFFERENTIAL EVOLUTION ALGORITHM [PRI00] .....	146
FIGURE 108: FLOW CHART OF THE DIFFERENTIAL EVOLUTION ALGORITHM [PRI00] .....	146
FIGURE 109: FLOW CHART OF THE HANDLING OF THE CONSTRAINTS FOR $V_{min}$ .....	149
FIGURE 110. COMPARISON BETWEEN TWO SOLUTIONS WITH DIFFERENT EXIT SPEEDS.....	155

FIGURE 111: ENERGY OPTIMIZATION FLOWCHART .....	159
FIGURE 112: DWELL TIME MODIFICATION AND BRAKING ENERGY EXCHANGE [CHE14] .....	160
FIGURE 113. DIFFERENT DELAYS INTRODUCED BY THE TWO-STEP OPTIMIZATION .....	162
FIGURE 114. DIFFERENT SPEED PROFILE VARIATIONS DEPENDING ON SPEED LIMITATIONS .....	163
FIGURE 115: SPEED PROFILE CONTAINING THE 4 DRIVING PHASES .....	164
FIGURE 116: DELAY COMPENSATION FLOW CHART.....	165
FIGURE 117. MAP OF RTE POWER GRID ON THE LEFT (400kV IN RED, 250kV IN GREEN) AND MAP OF THE HIGH-SPEED LINE BETWEEN PARIS AND LYON ON THE RIGHT (LINE IN WHITE AND BLUE) [RTE00][TGV00].....	166
FIGURE 118: TOPOLOGY OF THE LGV1 LINE PARIS-LYON .....	168
FIGURE 119. FINAL POPULATION AND ASSOCIATED VALUES AFTER 580 GENERATIONS FOR THE TRAIN A5135 .....	169
FIGURE 120. SPEED PROFILE OF THE OPTIMAL SOLUTION .....	170
FIGURE 121: SPEED PROFILE OF THE OPTIMAL SOLUTION FOR TRAIN A6759 .....	171
FIGURE 122. SPEED PROFILE OF THE OPTIMAL SOLUTION FOR A6621 .....	172
FIGURE 123. ENERGY CONSUMPTION VS FINAL RUNNING TIME FOR ALL THE INDIVIDUALS SIMULATED BY THE ALGORITHM AND PARETO CURVE ...	173
FIGURE 124. ENERGY CONSUMPTION VS FINAL RUNNING TIME FOR ALL THE INDIVIDUALS SIMULATED BY THE ALGORITHM (BLUE) AND SOLUTIONS OF THE FINAL POPULATION (IN RED) FOR THE TRAIN A6759 .....	173
FIGURE 125. ENERGY CONSUMPTION VS FINAL RUNNING TIME FOR ALL THE INDIVIDUALS SIMULATED BY THE ALGORITHM (BLUE) AND SOLUTIONS OF THE FINAL POPULATION (IN RED) FOR ALL THE TRAINS GOING FROM CRISENOY (P) TO PASILLY (P) .....	174
FIGURE 126. OSIRIS ORGANIZATION.....	189
FIGURE 127. INTERFACE DIAGRAM.....	192
FIGURE 128. PROJECT STRUCTURE.....	193
FIGURE 129: ELBAS PROGRAM STRUCTURE .....	195



## **GENERAL INTRODUCTION**

Today, our world is facing crucial problems: water, food and energy security is raised by UNESCO because they form a complex web of inter-linkages. Energy is now an essential factor for ensuring the continuance of human life. For example, agriculture is an energy consumer with 70% of global water use and 6% of global energy use [UNE00]. On the other hand, fighting climate change becomes a universal concern. Unfortunately, pollution has considerably increased in the last century due to greenhouse gas emissions and deforestation. In addition, energy resources such as fossil fuels (oil, coal, gas and nuclear) have various impacts on water quantity (for cooling) and quality (water acidification). Therefore, with continuous population increase, energy's price is expected to increase dramatically in next decades. European Union (EU), same as other unions and countries, launched series of projects to improve energy efficiency and reduce environmental impact. In particular, in 2007, EU leaders set three key targets to be enacted in legislation in 2009. They are known as 20-20-20 plan: reducing by 20% greenhouse gas emissions from 1990 levels, increasing by 20% renewables energy share and improving by 20% EU's energy efficiency. This plan covers several areas (energy production, transportation, waste, agriculture...). EU set many Framework Programs for Research (FP). For example, FP7 includes all projects launched between 2007 and 2013. It is followed by Horizon 2020, EU's biggest Research and Innovation program ever with nearly 80 billion euros of funding available over 7 years (2014 to 2020) [EUR01].

Given the fact that transport sector represents an important share when coming to gas emissions and energy consumption, EU gives particular attention to railway sector, one of the biggest energy consumers. In fact, with overall demographic increase and population shift to urban areas, electric railways (tramways, metros, trolleybus) become a solution reducing pollution peaks in large cities. The work presented in this thesis is done in the framework of two FP7 European projects, OSIRIS and MERLIN (Appendices A and B). Both projects' aim is to make railways more efficient by introducing new energy solutions (storage, heat pumps, hybrid substations...) and more intelligence to the system (on-board and wayside energy management, passengers and trains fluidity...). While OSIRIS focused on urban systems, MERLIN was more dedicated for suburban and high speed lines (HSL). They are collaborative projects; companies from around Europe, sometimes even competitors, are working together with universities and research institutes. The common objective is to study new concepts and evaluate their results from different angles (operators, constructors, universities...). European collaborative projects consist an opportunity to remove barriers (competitiveness, confidentiality, multi-culture...) and work together for global interest.

In order to better understand their particularities and challenges, **Section A** will be dedicated to railway systems. An historical overview will show the evolution of this sector over the last century because it is important to understand different decisions, political and technical, which led to today's systems' variety. Nevertheless, a focus will be done on different subsystems that impact energy

consumption since it is the subject of this study. Electric traction technologies are detailed starting from current collectors to voltage levels and types. AC and DC electrification systems are presented showing each one's characteristics (voltage, substations, catenary and 3<sup>rd</sup> rails). Then, some statistics will explain concretely railways' impact on environment and its changing during last decade due to increasing number of electrified lines. After going through this historic survey, a closer look to the train and how it interacts with its entourage will be done. More precisely, braking system will be detailed because it represents the main share of energy losses. In fact, almost all trains today include two kinds of brakes: electrical and mechanical. The first one, also called regenerative braking, uses electric traction machines to brake by reversing the direction of their rotating electro-magnetic field. This allows converting mechanical power into electrical power. In AC systems, this power is either used by other trains accelerating nearby or reinjected to the upper grid through substations. In DC systems and depending on the receptivity of the line, this power may be either exchanged with other trains or burned in on-board resistors. In the latter case, the energy is lost into heat. Its quantity depends on the line (metro, tramway...) and trains' frequency. In some cases, it could even reach 40% of the total energy consumption. With increasing energy prices, operators start to get interested in saving this energy and reducing their electricity bill. Thus, many solutions already exist on the market and some are still being developed. Some solutions are intrusive and requires replacing old equipment (mainly wayside) or installing new ones on-board the train. Others will be only connected to the catenary/3<sup>rd</sup> rail, this is the case of wayside storage systems and inverters. These different technologies will be also detailed in Section A. Even though they are efficient, most of these solutions are designed to be used internally in railways. In other words, the sector is kept isolated from its environment and the energy is reused internally. This choice is politically correct especially when, in some countries, operators are not allowed to sell energy directly to consumers. The only seller should be the energy provider. Thus, if re-selling energy price is lower than purchase price, it is more interesting to re-use braking energy internally.

For DC railway systems, **Section B** presents the "smart DC station", a new concept connecting railway to its environment. It is inspired from multimodal transport: passengers flow between railway (metro, tram...) and road transportation (buses, cars...). Yet, why not also make these two sectors interact energetically? As a matter of fact, electric buses and cars are more and more numerous especially in big cities where pollution rate is higher. For example, in Paris, RATP is replacing its diesel buses with electric hybrid buses as an intermediary step towards 100% electric transportation [RTP00]. In addition, more comfort is now requested in passengers' stations. Specific loads such as escalators and lifts are capable of braking electrically and regenerating energy that is today simply burned in resistors. Thus, with the evolution of all these surrounding systems, from simple energy consumers to possible producers (also called prosumers), future stations should allow electrical

interaction between them (trains, electric buses and cars, escalators...). The smart DC station is a DC Micro-grid with bidirectional energy flow connecting different components with a common DC busbar through DC/DC converters. The concept will be detailed in paragraph V. Then, chapter VI will study the stability of the system and a stabilization command will be described. At the end of this section, after going through each detail, technical recommendations will be given for eventual future development.

After studying micro-grid solution for DC urban railways, **Section C** is dedicated to HSL. In fact, both systems are quite different in terms of energy. While DC powered systems' main key is braking power saving, AC systems are more impacted by the timetable and trains synchronization. For example, one of unfavorable cases is when many trains are accelerating simultaneously on an electric zone, fed by one substation, because it generates power peaks that may exceed maximum subscribed power. This problem will be detailed in this section and an energy optimization algorithm will be developed. It is divided into two main parts: Chapter IX will present an algorithm based on differential evolution. Its objective is to optimize, according to a theoretical predefined timetable, the speed profile of each train separately so they consume less energy while respecting time constraints. After this step is done, in chapter X, a more macro optimization should be done including results of the previous one. A full timetable will be studied and power peaks at substation will be reduced by shifting trains within a certain margin. At the end, simulation results will be presented to evaluate both steps' efficiency.

To summarize, the thesis aim is to enhance energy efficiency of railways, both AC and DC electrified lines. Particularities and challenges of this sector will be presented, starting from the first beginning of railways till today. Then, because of the difference between urban and HSL, the study is divided into two main parts. The first one will propose a hardware solution, the "DC smart station", to recover braking energy and reuse it for non-railway applications (in our case electric hybrid buses) making by that a bridge between a sector, historically energetically isolated, with its environment. This solution meets tomorrow's big cities evolution in terms of reducing pollution and energy losses. The second part is dedicated to HSL with a software solution due to their large scale and AC powered infrastructure. Thus, an optimization algorithm will act on trains' speed profile to reduce energy consumption and then on their synchronization in order to avoid power peaks at substations' level. This software solution is more adapted to HSL's case due to their flexibility, when compared to urban lines, and their need for wide area coverage solution.

## **SECTION A: OVERVIEW ON RAILWAY SYSTEMS**

## I – Historical railway evolution

Railways invention goes back well before steam engine's discovery. The need to carry heavy loads gave the idea of creating a guided transport system. It was pulled by horses or humans on wooden then iron tracks. This system was mainly developed in mining environment. In Europe, during middle age, it was noticed that heavy carts were easier to move on rails which reduced friction resistance. In 1738, with the development of metallurgy, the English coal mining of Whitehaven was the first to cover wooden rails with cast-iron plates in order to reduce premature wear. In 1765, James Watt built the first steam machine with separate condensation chamber. In 1769, Nicolas Cugnot built the first three wheeled steam-driven vehicle. Then, for the first time in the world, a steam train ran on the 21<sup>st</sup> of February 1804, in Pen-y-Darren, a mining region in Wales, next to Merthyr Tydfil. The locomotive was designed by the engineer Richard Trevithick, a passionate about steam motorization. It carried 10 tons of iron, 5 wagons and 70 men on the full distance of 16 km in 4 hours and 5 minutes with an average speed of approximately 2.4 mph (3.9 km/h) [RAT04]. Then, in 1828, Marc Seguin invented the tubular boiler [COM91]. This new invention was applied directly on railway locomotives that ran, since 1831, on the first French railway line between Saint-Etienne and Andrézieux. Finally, steam trains started to be developed and in 1838, Schneider factory in Creusot built the first series of steam locomotives "Gironde" for the line connecting Paris to Versailles. In the same period, the company Koechlin in Mulhouse built the "Napoléon" for the line of Thann. After that, the world witnessed fast railway progress. Private investors and public support helped developing these new means of transportation. The figure below shows railways evolution in France:

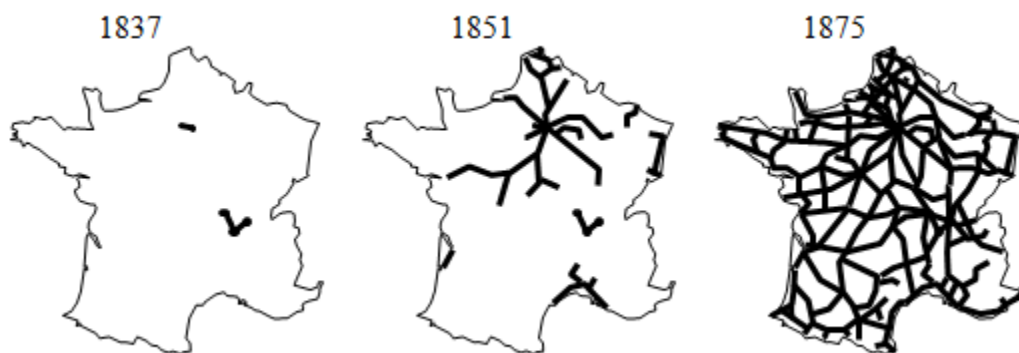


Figure 14. Railway evolution in France

We had to wait till 1879 to introduce electrical motorization in railway systems. That's when Siemens & Halske built a small electrical train which was presented at the industrial exposition in Berlin. Later in 1881, the first electrical tramway was installed in the same city (Figure 15).



**Figure 15. Siemens & Halske first electrical tramway in Berlin**

Urban railway systems were electrified well before high speed lines (HSL) due to many reasons. In fact, at that time, transportation was mainly based on animal-drawn sledges and carts (horses, donkeys, dogs...) which caused hygiene problems. In addition, electronics existed only for low power applications while steam engines were capable of attending high speeds with important traction efforts. The first metropolitan line in Paris was inaugurated the 19<sup>th</sup> of July 1900 [PAR00]. In the same year, the line Paris-Austerlitz/Paris-Orsay was electrified using a 3<sup>rd</sup> rail of 600 volts, same technology as metros. It was run by the first French electrical train E1 nicknamed “Boîte à sel” or box of salt due to its physical shape (figure 3). Its maximum speed was 70 km/h. It started to get removed from service in 1970 [CIT00].



**Figure 16. first French electrical train « Boîte à sel »**

The first high speed achievement came from Germany. In 1903, a three-phase express railcar from Siemens and AEG attained a sensational maximum speed of 206.7 km/h on the Marienfelde-Zossen test route near Berlin. The operating voltage was set at 14 kV with a frequency of 50 Hz [UIC12]. The three-phase technology was used because, at that time, there was still no powerful DC motors. Therefore three-phase AC asynchronous motor had to be used and supplied directly from contact wires (Figure 17).

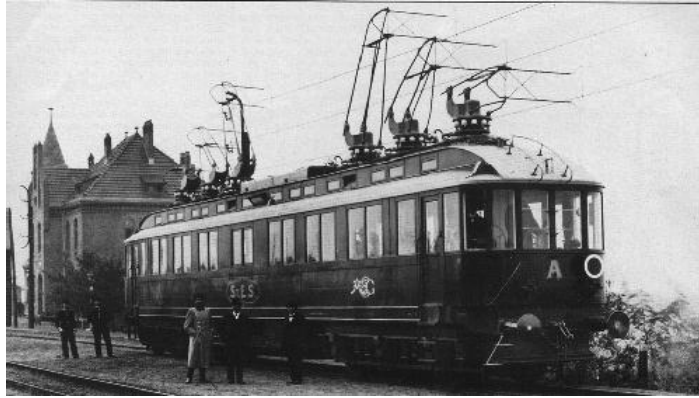


**Figure 17. Three-phase railcar “A” of Siemens and AEG**

The 750 V-AC electrification system, with a lowered frequency of 40 Hz, constituted the first true AC railway electrification system. It was first used in Switzerland then converted to 15 kV  $\sim 16\frac{2}{3}$  Hz in 1933. The reason of using this frequency was to protect the universal motor used at that time from the electric arc generated at the collector's level. In northern Italy, the three-phase electrification at 3 kV or 3.6 kV  $\sim 16\frac{2}{3}$  Hz spread until 1976. But with two contact wires above each track (the third phase was then connected to the rails), this technology required expensive investment and was complicated to install due to voltage and frequency conversion stage because the railway network could not be directly connected to the public grid. Therefore, this system was replaced later by single-phase AC systems and high voltage DC systems.

In France, electrical traction progressed quickly after the end of World War two. The first high speed line Paris-Lyon was inaugurated in 1952 with 1500 V DC electrification [CIT01]. Then came the usage of single-phase 25 kV  $\sim 50$  Hz (beginning with the line of Valenciennes Thionville) with increasing commercial speeds. Two speed records were achieved: the first in February 1954 with 243 km/h between Dijon and Beaune using the CC7121, the second in March 1955 with 331 km/h on the line of Landes using the CC7107 and BB9004. Since then, many speed records were reached. The last one was in April 2007 when Rail speed record of 574.8 km/h was reached by Alstom, SNCF and RFF with a test train on the East-European high-speed line [ALS00]. Recently, a new technology tested in Japan, the magnetic levitation train, is starting to attract the world's attention. In April 2015, it has broken the world speed record, hitting 603km/h (374mph) in a test run near Mount Fuji [BBC15].

In summary, railway can be divided into three main categories:

- Urban and suburban lines

During the 20<sup>th</sup> century, urban (metro/tramway) and suburban lines were extended and modernized to meet the increasing demand. For example, Paris metro has 214 km of lines, used by almost 1.4 billion travelers every year [FRA00].

- High speed lines

Since high-speed lines were introduced, the number of passengers opting for this mode



of transport has constantly increased. The number of passengers on all French, German, Belgian, Spanish, Italian and British lines increased from 15.2 billion passenger-kilometers in 1990 to 92.33 billion in 2008 [EUR09].

- Freight lines

Unlike other categories, freight lines weren't subject to strong development. In fact, road transport occupies the largest part due to its flexibility and door-to-door services. Nevertheless, freight lines remain more punctual (no traffic), cause less pollution and are more secured. In addition, many European projects try to improve this sector such as e-freight [FRE00].

## II – Railway electric traction systems

---

Today, there are no unified electric traction systems. A large variety can be listed due to historical, security and safety reasons. Nevertheless, in Europe, there is a growing trend towards a single European rail area with trains easily crossing state borders. This will increase the competitiveness, the robustness and the interoperability of European railways.

In this chapter, we will focus on the most popular traction power supply systems used in the world. Historically, as seen in chapter I, railways were built progressively in the last century while different technologies were evolving very quickly. This explains the variety we have today because each line was based on the newest technology available at its time. Some solutions were abandoned (e.g. aerotrain), other were progressively replaced (e.g. three-phase power supply) and some are still being used (e.g. 750 VDC). In addition to technological reason, the voltage choice for high speed lines was also political. Changing the type of traction power supply from one country to another helped also protecting from potential offensive attacks.

To begin, electric trains need a power supply system available during whole operation period. Its main characteristics are: safety, reliability and sustainability. It could be through an AC or DC overhead contact line (catenary), or through a rail at ground level (3<sup>rd</sup> rail supply, 4<sup>th</sup> rail supply, ground-level power supply). The latter can only be supplied in DC mode for safety reasons. The contact with overhead lines requires a current collector called “pantograph” due to its initial shape used until 30 years ago.



Figure 18. Old pantograph (left) vs new pantograph (right)

When supplied through rails, the train collects the current using a “shoe”. There are a variety of designs for the 3<sup>rd</sup> rail current collection. The figure below shows the different modes of 3<sup>rd</sup> rails. The simplest one is the “top contact” where the shoe slides upon the rail. Unfortunately, this mode has many drawbacks because the contact rail is not protected which on one hand raises safety issues (human contact) and on the other hand exposes the rail to weather degradations (ice, snow...). Side contact is less exposed but is not the most efficient. The best mode is the bottom contact where the contact rail is more protected.

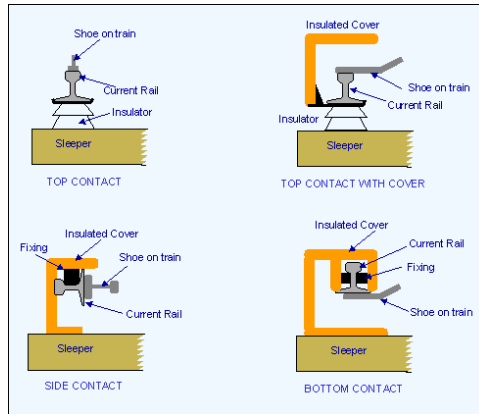


**Figure 19. Different types of 3<sup>rd</sup> rail current collection [NET00]**

For all traction power systems, except the 4<sup>th</sup> rail power supply, the return current goes through the rails using wheels, made of steel. In the 4<sup>th</sup> rail's case, as in London, the 3<sup>rd</sup> rail is subject to electric positive voltage (+420 VDC) and the 4<sup>th</sup> rail, placed in the center between rails, is subject to electric negative voltage (-210 VDC) which makes a difference of 630 V DC.

Nowadays, the most common electrification voltages are:

- In DC mode (urban/suburban):
  - 600V and 750 V usually used for tramways and metros
  - 1500V and 3000V usually used for suburban lines
- In AC mode (mainlines):
  - 15 kV ~ 16 $\frac{2}{3}$  Hz that is still used in many countries such as Germany, Switzerland, Austria...
  - 25 kV ~ 50 Hz is now considered as a standard for high speed lines around the world, it is used in France, Denmark, UK...
  - 2x25 kV ~ 50 Hz that helps boosting the voltage and by that reducing the number of substations. In this case, the supply current is distributed between the 25 kV contact line and a feeder of 25 kV with a 180° phase shift due to auto-transformers (see Figure 20).

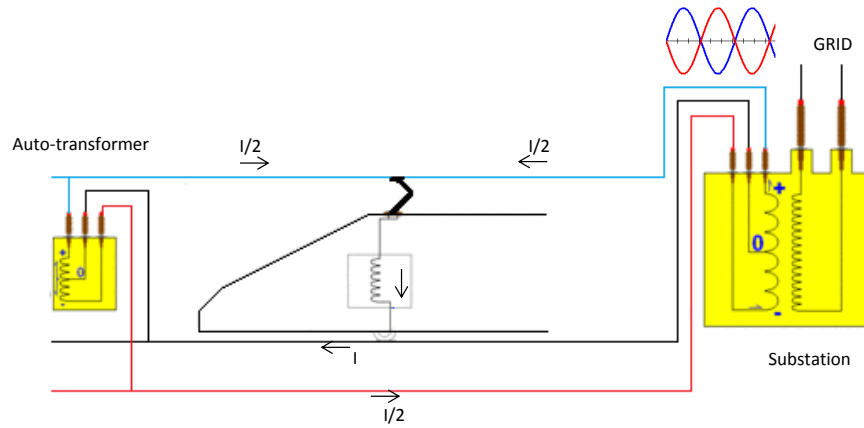


Figure 20. 2x25 kV electrification system

A classic DC traction power supply station, also called substation, consists of a wye-delta /wye-wye (Y- $\Delta$ /Y-Y) transformer followed by two three-phase diode rectifiers connected in series (Figure 21). This type of transformers helps reducing harmonic currents on grid's side. This architecture imposes unidirectional power flow (from public grid to the catenary).

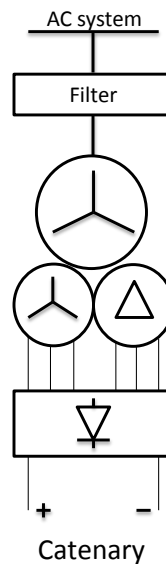


Figure 21. DC electrification system

In AC mode, the substation consists of a single-phase transformer which allows a bidirectional power flow. Yet, in order to maintain three-phase equilibrium, a phase alternation is done from one substation to another. The catenary is then divided in electrical zones. Each zone is connected to a different phase and separated from the others by neutral zones that are sufficiently long (30 meters in general) to avoid short-circuits through the pantograph. When a train crosses these zones, its power should be cut by opening the circuit breaker. In addition, the train should enter this zone with a minimum speed to be able to cross it with its mechanical inertia. Therefore, no power exchange is possible between two trains running in different electrical zones.

Due to heterogeneity of railway electrification system, some lines require trains operating on more than one type of current, voltage and collector. In cities such as London, New York City and Boston, trains are equipped with pantograph and 3<sup>rd</sup> rail current collector so they can run under overhead wires on one part of the line and use the 3<sup>rd</sup> rail on the remaining part. In Europe, some locomotives can operate under four voltages: 25 kV AC, 15 kV AC, 3000 V DC and 1500 V DC. This is nowadays possible due to power electronics and specific control strategies. Same as in AC mode, neutral zones separate these different types of power supply (60 meters long in general).

### III – Environmental impact and existing solutions

#### III.a. ENVIRONMENTAL IMPACT

Despite their diversity, railways common objective is to transport passengers and goods. Safety, punctuality and fluidity remain their essential targets. But recently, due to increasing energy prices and environmental impact of electricity production, many studies aim to improve the efficiency of electrical systems by reducing energy losses.

In March 2007, the European Union fixed what is known as “20-20-20” targets which are expected to be achieved by 2020. The first target is to reduce by 20% EU greenhouse gas emissions from 1990 levels. The second one is to raise the share of EU energy consumption produced from renewable resources to 20%. The third is to improve EU’s energy efficiency by 20%. For the 2030 horizon, the EU has agreed on a more ambitious target which is attending 40% reduction of greenhouse gas emissions, 27% increase of renewable’s share and 27% increase of energy efficiency. In particular, the EU launched many projects in railway sector because it is one of the largest energy consumers. Their aim is to improve the efficiency at different levels (trains, substations, catenary...) and for all types of lines (urban, suburban, HSL...).

The figure below shows the share of CO<sub>2</sub> emissions from fuel combustion by sector in 2011. Emissions from rail electrical traction are reallocated from electricity, heat and other energy industries to the transport sector.

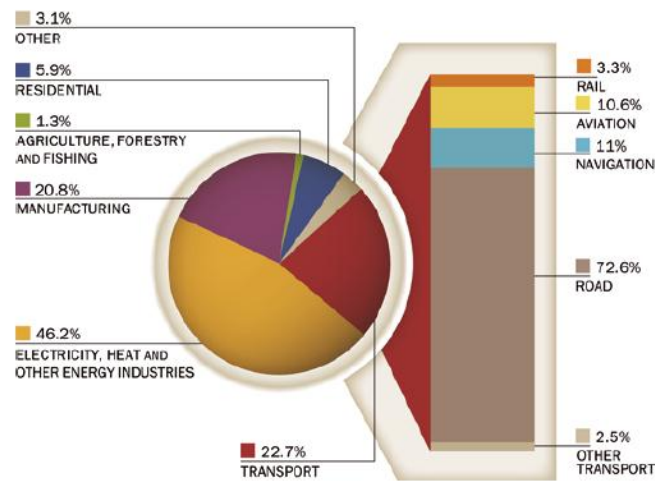


Figure 22. CO<sub>2</sub> gas emission of different sectors in 2011 [SUS11]

The transport sector was responsible for 22.7% of the total energy-related CO<sub>2</sub> emissions, of which 3.3% was due to rail activity. Railways therefore generated less than 1% of total energy-related CO<sub>2</sub> emissions (Figure 22). At the same time, railways transported more than 9% of the world’s passengers and freight activity [IEA14]. In Europe, total transport emissions increased by 25% between 1990 and 2011, while rail emissions dropped by 42% (Figure 23).

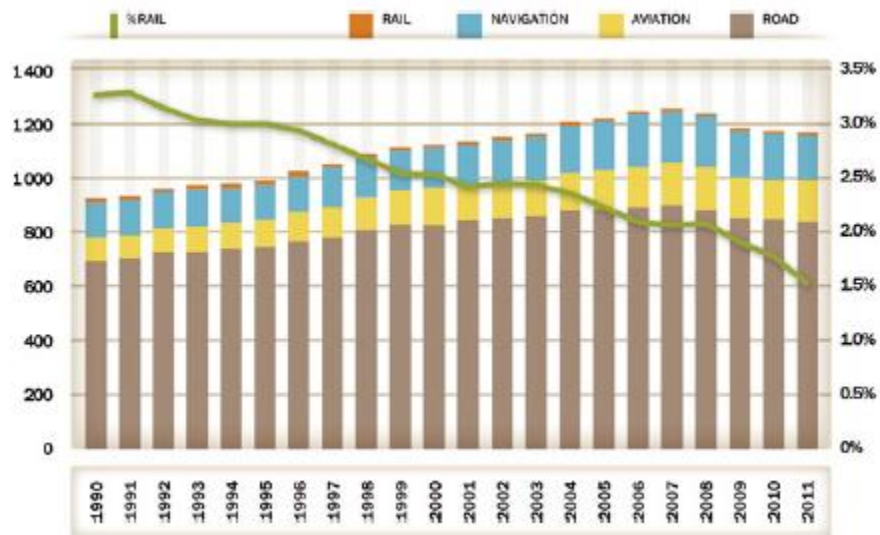


Figure 23. Transport sector CO2 emissions by mode, 1990-2011

(left: million tCO2, right: share of rail over total)

In Europe, the share of rail electric traction increased to 86% of train-km for freight and 81% for passenger service between 2005 and 2011 (Figure 24). The European rail was back then responsible only of 0.6% of the total energy consumed [IEA14].

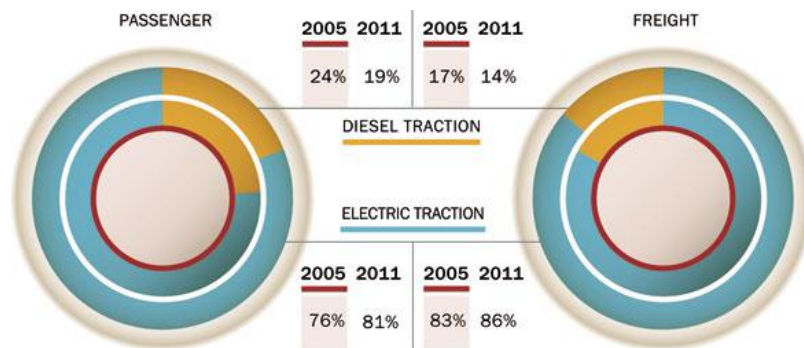


Figure 24. Passenger and freight railway activity (train-km), 2005 inside – 2011 outside [IEA14]

In addition, in 2011, 14% of railways energy sources, for electric and diesel tractions, came from renewable sources [IEA14] meaning that railways have already met the 2020 EU target for transport sector (10% share of renewables) [EUR00].

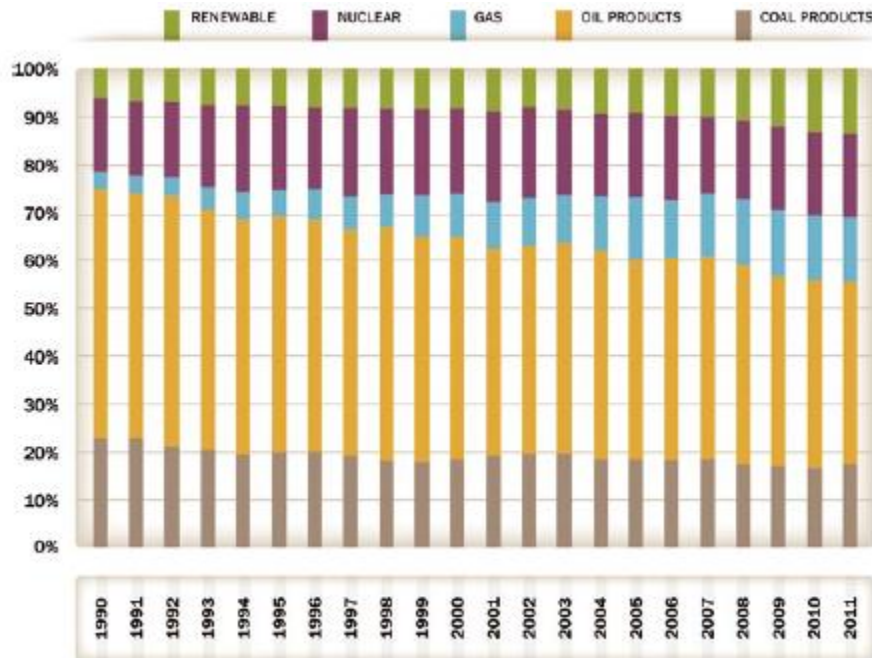


Figure 25. EU27 railway energy sources mix evolution, 1990-2011

### III.b. TRAIN BRAKING SYSTEM

Braking is reducing train's kinetic energy in order to:

- maintain speed when descending a slope
- reduce running speed
- stop or held stopping

The train's braking system is designed to:

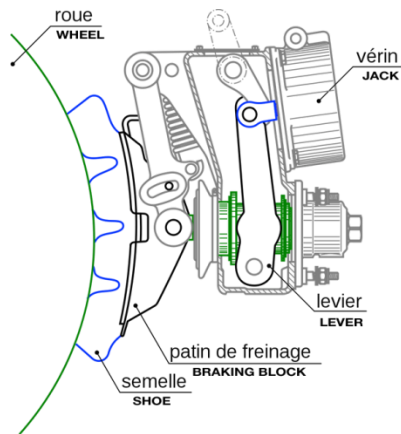
- respect the stopping distance indicated by the signalization and the distance between two successive trains
- respect passengers' comfort (acceptable deceleration:  $1.3 \text{ m/s}^2$ )
- respect train's materials: most braking systems produce heat (due to friction for mechanical braking and energy burned in resistors for electrical braking). Excessive heating can cause materials degradation.

Trains, railways first pro-consumers, consume energy when accelerating and regenerate energy when braking. In fact, braking process is divided into electrical and mechanical braking. The latter is used for low speeds to ensure stopping at the station's platform. It is also used for emergency braking that can be employed for safety reasons. In general, we can consider two main types of braking: friction braking and dynamic braking.

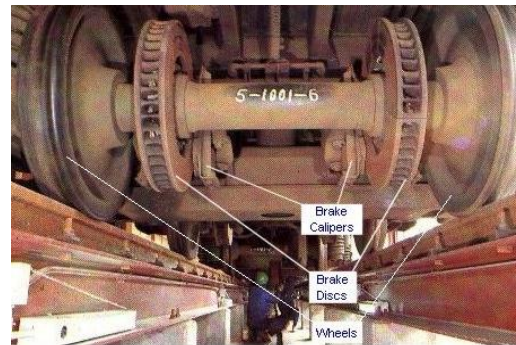


### III.b.1. Friction braking

Friction braking is the oldest and most common system. It can be applied to all kinds of vehicles (motorized and trailer cars). The principal ones are shoe brake and disc brake (Figure 26).



(a)



View Under Train Showing Wheelset fitted with Brake Discs.  
Each disc has two faces joined by vanes to assist cooling

(b)

**Figure 26. Shoe braking vs disc braking [EUR01] [NET01]**

The pneumatic brake was invented by George Westinghouse. As soon as the driver transmits the braking order, it is executed thanks to brake shoes (Figure 26.a) acting directly on the wheels. Brake shoes are made in a variety of materials (cast iron, composite, sintered), all of which have their own drawbacks (hard on the wheels, a low friction coefficient, cost...).

The disk brake (Figure 26.b) appeared in the 60's – 70's with the speed increase. It became then necessary to find ways to improve thermal dissipation. It is similar to the one used on road vehicles but may take the form of a pair of discs mounted on either side of the wheel web or a double-sided self-ventilating disc mounted on the axle. Very high speed trains, such as the French TGV, have up to four sets of double discs per axle. The design and number of discs is critical to train safety as they must be capable of dissipating the maximum amount of heat generated during emergency brake application from the highest speed attainable by the train [NET01].

### III.b.2. Dynamic braking

The dynamic braking does not rely on friction. Alternative resistant efforts are generated by the system itself. There are two types of dynamic braking: the hydrodynamic brake and the electrodynamic brake.

The hydrodynamic brake is applied when engines use a hydraulic transmission box, also called a torque convertor (e.g. the diesel-electric locomotive BB 67400). The particularity of these machines is that they can use the transmission to brake, a sort of engine braking.

The electrodynamic brake is possible due to reversible electrical motors. Figure 27 shows the energy flow in the passenger electric train with regenerative braking. When the train brakes, motors

become generators and convert the kinetic energy into electric energy. When the latter is burned in on-board resistors, it is called rheostatic braking. In this case, the motors are disconnected from the power line and connected to one or several air cooled resistors, generally placed at the top of the train. The regulation of the resistive torque is done by changing the resistors' value. When the braking power is injected to the catenary/ $3^{\text{rd}}$  rail, it is called recuperative braking. In this case, the injected power causes voltage increase. If another train is accelerating nearby, the power is exchanged else, it is burned in on-board resistors in order to avoid over-voltages and consequent damages.

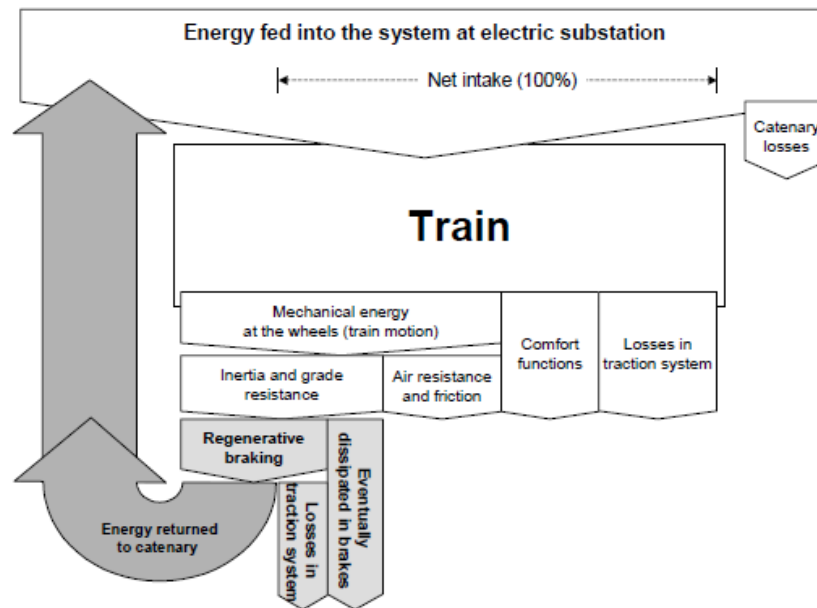


Figure 27. Energy flow diagram for a passenger train with regenerative braking (source: IZT)

The figure below shows the on-board electrical circuit in both DC and AC power supply:

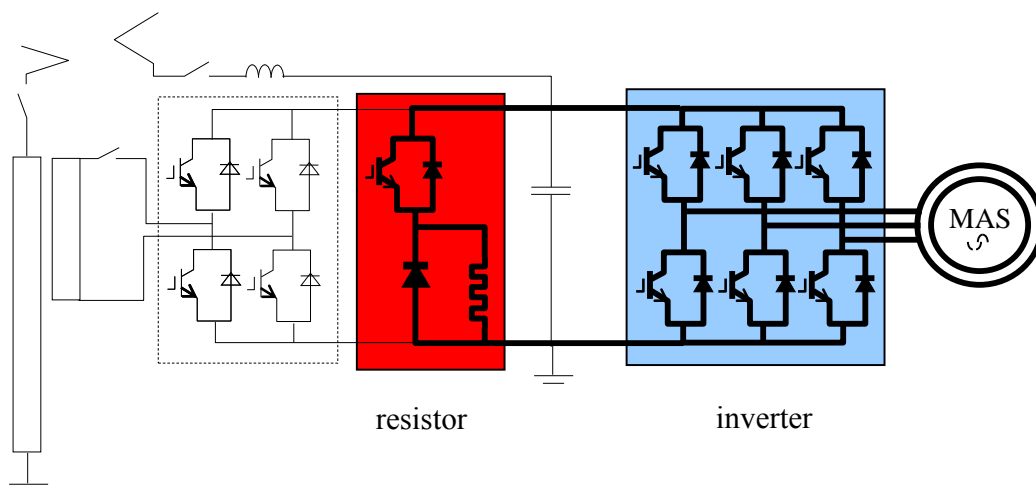


Figure 28. On-board electrical circuit

In addition to the DC electric chain, the AC chain contains a transformer, connected to the pantograph through a breaker, followed by a bidirectional converter (rectifier in traction phase and inverter in recuperative braking phase). When the train brakes electrically, the motor becomes generator and injects power through the bidirectional inverter operating as rectifier. This will increase the voltage in the capacitor. In AC mode, the braking energy will be fed directly through the converter and the transformer into the catenary even if no other train is accelerating in the same electric zone due to substations' reversibility. In DC mode, in case no power exchange is possible with another train, the capacitor's voltage will increase until a certain threshold (e.g. 900 V for 750 VDC, 1800 V for 1500 VDC). Once the voltage limit is reached, the energy will be dissipated in the resistor through a chopper that will regulate the voltage to its maximum value and prevent over-voltages and material damage.

The share of recoverable energy in railway system depends on one hand on trains' speed profiles (traction and braking frequency, effort, duration...) and on the other hand on the timetable and trains' synchronization. The list below shows the typical values of recovery rates for different DC rail systems [RAI00]:

- Main lines: 15%
- Regional lines: 35 %
- Suburban lines: 45%
- Freight lines: 20%

Note that these recovery rates are limited first by the efficiency of the traction chain (~ 90%), second, in the case of DC power supply, by the receptivity of the catenary that is directly related to the timetable (no receptivity when no other train is close enough to use braking energy) and third, by the braking power that sometimes is not sufficient requiring a simultaneous usage of mechanical brakes (especially in freight operation). The Table 1 below gives some estimated recovery rates for DC system. Since the main obstacle is limited receptivity of catenary, the table gives the theoretical potential, the potential to be exploited with new technologies such as reversible substation, storage and optimized automatic train operation, and the potential to be exploited without these technologies:

	Theoretical potential	Correction due to traction efficiency	Correction due to blended braking	Potential if additional technologies are used	Correction due to non-receptive catenary	Potential without additional technology
Main lines	15%	0,9	0,8	11%	0,2	2%
Regional lines	35%	0,9	0,8	25%	0,4	10%

<b>Local lines</b>	<b>45%</b>	<b>0,9</b>	<b>0,8</b>	<b>32%</b>	<b>0,5</b>	<b>16%</b>
<b>Freight lines</b>	<b>20%</b>	<b>0,9</b>	<b>0,5</b>	<b>14%</b>	<b>0,2</b>	<b>3%</b>

**Table 1. Potential recovery rates for different types of DC lines [RAI00]**

### III.b.3. Other braking systems

The electromagnetic brake consists of large electromagnets fixed under the vehicle at a short distance from the rail. When there's a braking order, a current passes through electromagnets which induces a strong electromagnetic force and the attraction with the rail will stop the vehicle. The electromagnetic brake, also called track brake, is generally used for emergency braking. There's also the parking brake that is intended to block the movement of an unpowered vehicle. It is a manually applied friction brake (also called handbrake) applied to the wheel tread or disc.

## III.c. SOLUTIONS FOR REDUCING ENERGY CONSUMPTION

Today, different solutions are developed for reducing rail energy consumption and increasing system's efficiency. We find software and hardware solutions that operate at various levels: infrastructure, traction chain, on-board auxiliaries...

### III.c.1. Software solutions:

Software solutions are cheap when compared to heavy hardware solutions that require high investment. Here are some solutions that are already employed:

- Optimization of energy purchase: when the infrastructure manager has access to the energy market, energy price is more flexible and could be optimized by adjusting the pre-estimated power consumption and selling/buying energy. For example, SNCF, National Society of French rails, created in 2012 a subsidiary called "SNCF Energie" that is in charge of optimizing energy purchase for traction and buildings (stations, administrative office...).
- Eco-driving: energy consumption could be reduced through speed instructions implemented in the control algorithm of automatic trains or suggested to the driver for classic trains. This part will be detailed in Section C.

### III.c.2. Hardware solutions:

Today, lots of works have been done to increase the traction chain's efficiency. Improvements were achieved in electronics as well as motors. For example, in new trains, thyristors and GTOs (Gate Turn-Off thyristor) are replaced by IGBTs (Insulated Gate Bipolar Transistor) that are voltage controlled. Therefore, unlike thyristors, they don't need high currents to turn off. In fact, until very recently, IGBTs were capable of handling only low currents and were used in low power applications.

Nowadays, they can handle high currents up to thousands of amps which make it possible to integrate these new components in traction converters. The main benefit of using IGBTs is that they are much faster than GTOs. This reduces heat losses and gives lighter units (e.g. passive filters, DC capacitor...).

New technologies also appeared in order to reduce energy losses in DC railway systems. They focused mostly on braking energy that is burned in resistors. In most lines, this energy's share is important and could sometimes reach 30% of consumed energy.

### 1. Inverters:

A power inverter is an electronic device that converts Direct Current (DC) to Alternative Current (AC). It can be based on IGBT, GTOs or Thyristor technologies. In a DC railway system, train's braking energy is burned when there's no other train powering close enough. When an inverter is connected to the power line (catenary/3<sup>rd</sup> rail), it can recuperate the excess of braking energy and that will stop voltage increase and on-board resistors activation. The energy will be then injected into the upper grid. The inverter could be placed in a substation, in passengers' station or sometimes, it could be connected at a specific point along the line. A substation that is capable of feeding power from the catenary to the grid is called "reversible substation". Different architectures are proposed by companies. HESOP, Alstom Transport's reversible substation consists of a bidirectional IGBT inverter. HESOP optimizes the power required for traction and captures more than 99% of recoverable energy during braking mode which can be re-injected into the electricity network [ALS01]. Furthermore, the optimization of energy usage in traction mode means that the distance between each sub-station can be increased and their number decreased by 20%, so limiting infrastructure costs (equipment, civil engineering and urban real estate) [ALS01]. Today, Alstom provides two products; HESOP 750LP and HESOP 1500HP. Figure 29-17 show HESOPs architectures.

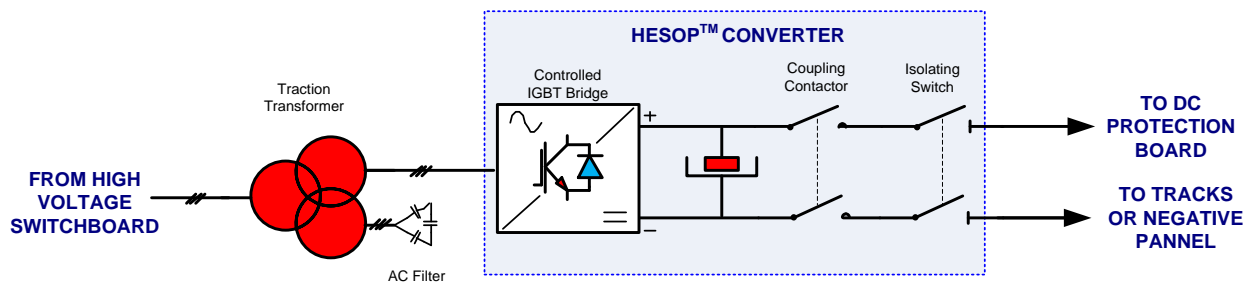


Figure 29. Power Circuit Schematic representation of HESOP 750LP

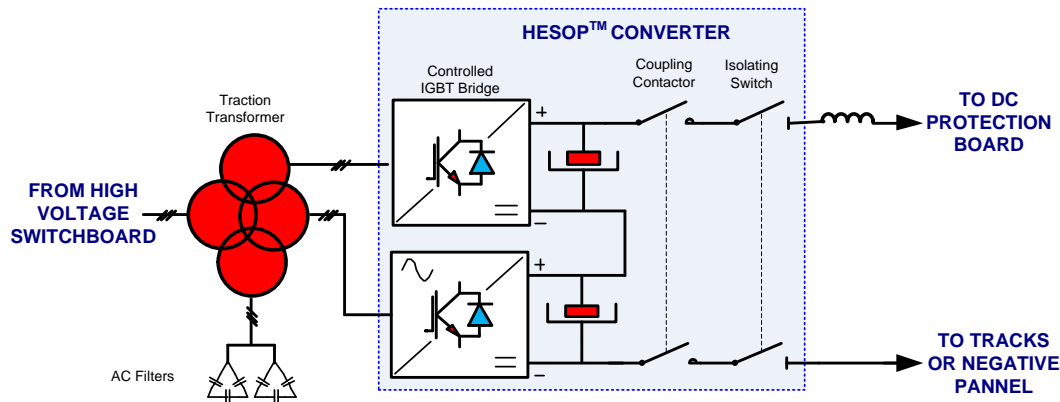


Figure 30. Power Circuit Schematic representation of HESOP 1500HP

Another constructor, ABB, suggests connecting an inverter in parallel to the classic diode rectifier substation. The solution is called ENVILINE-ERS. The main benefit of this architecture is that it can be applied on both existing and new substations. Figure 31 represents ABB's solution:

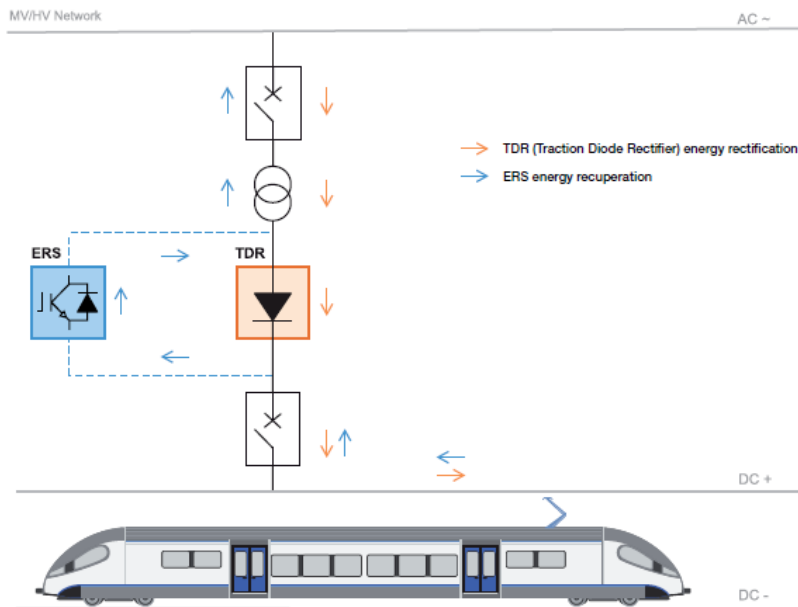


Figure 31. ABB's ENVILINE-ERS reversible substation [ABB00]

The same architecture was also adopted by ADIF (Spanish administrator of railway infrastructure) who has developed the first 3kV DC reversible substation in its conventional network. A prototype was installed in Substation La Comba, Málaga – Fuengirola suburban Line [ADF00]. Note that this new technology, the reversible substation, is still at R&D level for other constructors such as CAF (Spanish railway constructor). However, recuperating trains braking energy through an inverter directly up to the public grid has also some drawbacks. In fact, auxiliary station's power supply is usually independent of the traction network. Therefore, in the majority of cases, the only solution is to sell the energy to the grid operator. But, there is no obligation for the electricity provider to buy back the intermittent braking energy (few MWs in seconds). Moreover, in weak grid areas, injecting

instantaneous power peaks causes grid's perturbation which will force some electricity providers to refuse connecting such power sources to their network. Therefore, other solutions are to recuperate braking energy in storage systems.

## 2. Storage system:

An alternative is to store trains' braking power. In order to absorb high power peaks in few seconds, technologies with high power density are employed such as supercapacitors and flywheels. Batteries, with high energy density, may be used but in a second step. Storage systems can be divided into two types: on-board storage and wayside storage.

The advantage of on-board storage devices is that they can detect easier the braking phase and then recuperate directly braking power with less energy losses (e.g. heat losses in the catenary). It also can provide autonomy (catenary-free zones). However, all trains should be equipped instead of aggregating the energy along the line. In addition, on-board storage means also on-board additional weight which will increase traction power consumption. Based on supercapacitor technology, Alstom developed in conjunction with the RATP the "Citadis Ecopack system". It allows a tram to operate without overhead catenary lines and increase tramway systems energy efficiency. It consists of independent supercapacitors installed on the roof of the tram that are recharged in 20 seconds during tram station stops and with regenerated energy during braking. Siemens also proposes a range of storage systems that consist of Sitras modules [SIE00]. Concerning on-board flywheels, Alstom has teamed up with Williams Hybrid Power to try its composite MLC flywheel energy storage technology which will save braking energy and re-use it to add more power to the tram while reducing energy use and CO2 emissions [ALS02].

On the other hand, wayside energy storage becomes more interesting when it comes to specific applications: the stored energy can be used for regulating the catenary's voltage or reinforce a substation. It could be also used to regulate frequency which is a good deal in some countries. Some drawbacks although exist: location especially in dense urban areas, power losses in catenary and the difficulty of respecting power exchange between trains. Different types of batteries are employed today for braking energy storage. For example, Hitachi developed B-CHOP, a wayside storage system based on lithium-ion batteries technology that stores trains braking energy. Two devices were installed in November 2015 on two lines in HONG KONG and will start operation after February 2016. On the other hand, Toshiba proposes a Traction Energy Storage System with SciB (lithium-titanate batteries). Supercapacitors are also used as a wayside storage, for example, NeoGreen by ADETEL, ESS by Sécheron, Sitras SES by Siemens, EnerGstor by Bombardier and Envistore by ABB. Concerning flywheels, Alstom Transport, in cooperation with INFRABEL and other Belgian companies, is developing a new wayside high power flywheel solution (3 MW) dedicated to DC railway applications. Other flywheels with lower power rate already exist on the market, for example: Powerbridge by Piller (1 MW), blueprint's flywheel (120 kW), VYCON's REGEN (500 kW).

### 3. Renewable energy sources:

Distributed energy resources (DERs) are also a possible solution for reducing total energy consumption. Local electricity production, especially when coupled with a storage system, could help smoothing power demand's profile. Some operators are studying the benefit of a hybrid substation integrating renewables such as wind turbines, PVs and even hydraulic power generation. For example, SNCF developed a tool called "CONIFER" to study and design a hybrid railway power substation including electric network connection, storage system and production system. This concept is particularly interesting when a substation should be installed in an area where there is no grid connection (e.g. near a forest in the case of high speed rail) [CON00]. DERs could also be implemented at stations' level. For example, in India, Delhi Metro Rail Corporation Ltd. (DMRC) installed 500 kW of solar energy on the roof of Dwarka Sector-21 metro Station. DMRC is willing to replicate similar projects up to 10 MW of capacity on other stations and buildings.



Rail sector was well developed through the three last centuries. It was first developed in mining environment then, due to the discovery of steam machine, the first steam-driven train was designed. Seventy years after, electrical motorization was introduced into railways. Many technologies were tested. Some have been directly eliminated at prototype level, other were employed during a limited period and few are still being used until today (e.g. 750 VDC power supply). This fast evolution resulted in a large diversity worldwide and even at regional scale. This section has presented the different electric traction systems that existed and a focus was done on the ones being used today (AC and DC power supply). Then, the environmental impact of transportation, especially railways, was detailed by giving the latest statistics done worldwide and in Europe. It was showed that this transportation mode is becoming greener by reducing its CO<sub>2</sub> emissions and using more renewable energy. Furthermore, trains' braking system was detailed because it represents the main source of energy losses. The difference between mechanical and electrical braking was explained and some braking energy-related solutions were listed.

In conclusion, electric railways remain an eco-friendly means of transportation. Many ideas for enhancing the energy efficiency are being studied and some solutions already exist on the market such as reversible substation, energy storage devices... The European commission is particularly interested in improving this sector in order to meet its 20-20-20 plan. Therefore, several European projects were dedicated to the improvement of rail's energy efficiency: RailEnergy, OSIRIS, MERLIN, In2Rail... The following sections present two studies that were done in the scope of OSIRIS and MERLIN which aim is to increase the energy efficiency of respectively urban and high speed lines.

## **SECTION B: SMART DC STATION FOR URBAN SYSTEMS**

### V.a. INTRODUCTION

In 2011, the transport sector's share of the total energy-related CO<sub>2</sub> emissions was 22.7%. Particular attention has been drawn to urban areas where 80 % of European citizens live and where 40 % of all transport related GHG emissions are produced. A new target was then fixed: decarbonize transport sector and increase its efficiency. One of the possible solutions is to develop public electric transportation. Statistics show that in London, in 2006, the energy cost of buses was 32 kWh per 100 pkm (passenger km) and the total energy cost of underground trains (traction and auxiliaries) was 15 kWh per 100 pkm which is four times better than a fuel car average consumption (6 liters – 60 kWh– per 100 km). In addition, in London, a passenger emits 151 g of GHG per km if travelling by car, 102.8 g of GHG per km if travelling by bus and 83.3 g of GHG per km if travelling by metro. Yet by 2025, the number of daily trips made in urban areas worldwide is expected to rise by 50 % compared to 2005. The associated energy consumption already represents a high share of the total national consumption. In France for example, the transport sector consumes 31 % of the total national energy consumption. The energy price is expected to rise by 100 % in 10 years which make the improvement of transport's energy efficiency an essential need.

In DC railway systems used in almost all urban transportation systems, there are relatively low energy conversion losses, no gas emission in urban areas (emissions depend on electricity generation mix) and the capability to regenerate braking energy and to exchange it between trains. But due to unidirectional power flow of diode DC substations, there is no energy exchange with surrounding energy network and little possibility to integrate smart energy management systems. Besides, with the emergence of smart grid concept, it became imminent to also introduce innovations in railway sector. It is unlikely to stay away from the technological development observed worldwide in different fields such as communication, information, electronics... Smart railway electrification can provide energy savings by accommodating all distributed generations (braking trains, renewable energy...) and storage systems (batteries, supercapacitors, flywheel...). It dynamically optimizes the total power consumption and enhances power quality and system's efficiency. Railway system will no longer be a passive load consuming energy from the grid. It will be part of a larger smart grid and communicate with "non-railway" systems such as smart buildings, electrical vehicles charging station, distributed energy resources... In addition, operators encounter daily service disruption due to various failures, especially electrical equipment breakdowns. This can be avoided by integrating Smart Grid technologies with its self-healing property. It can anticipate system failures by performing continuous self-assessments to detect possible disturbances and take corrective actions. Its intelligence consists in handling problems too large and too fast for human intervention. To achieve its goals, the smart grid's structure is based on the following components:

- Smart sensing and metering technologies: nowadays, information transmitted to the control room is basically related to signaling and train operation. No real-time data is collected in order to optimize energy signature of the global system. It is now possible to receive the dynamic state of the energy system thanks to communicating measurement tools, some could be integrated in the trains (speed, real position, regenerated power...) and other could be distributed along the infrastructure (voltage and current measurement...).
- Two-way standardized communication infrastructure: a fast and reliable connection should be established between different railway components including trains, metering equipment, electronics... The control center should be able to reach each point of the system.
- Robust software able to control critical situations quickly and efficiently: it should also be configured to operate in a self-healing manner. It will then perform system's diagnosis and take suitable decisions autonomously.
- Flexible and controllable infrastructure: a smart grid is before anything else a flexible grid. Therefore, it is important to ensure that the system is able to control operations from distance. Instantaneous modification of the electrical equipment's status is thus possible. The railway infrastructure and especially converters should also be bidirectional allowing bidirectional power flow.

In this section, an innovative solution is proposed. It is a first step towards the future smart station that is capable of interacting with its surroundings. It allows reducing braking energy losses by reusing this energy in an eco-friendly application by charging electric hybrid buses.

## **V.b. CONTEXT AND CONCEPT**

Nowadays, cities are encouraging green transportation (electric and hybrid vehicles, bikes and electric bikes...) in order to reduce pollution in dense urban zones. Yet, a charging station for electric hybrid buses is a critical load consuming high powers (200 kW in our case) in a short period of time (4-5 minutes). It requires a particular subscription contract in order to be connected to the grid and tariffs will be probably expensive. Therefore, given the fact that buses' stops usually coincide with metro stations, the braking energy wasted in the metros rheostats could be used to charge these buses. However, the braking energy is an unpredictable and discontinuous source of power with large instantaneous peaks (Figure 32) which make it difficult to use it directly without local storage implementation to overcome the intermittency of braking energy and time mismatch between production (braking energy recuperation) and consumption (electric buses charging). Additional energy can be sold back to the grid depending on the status and capacity of the energy storage unit.

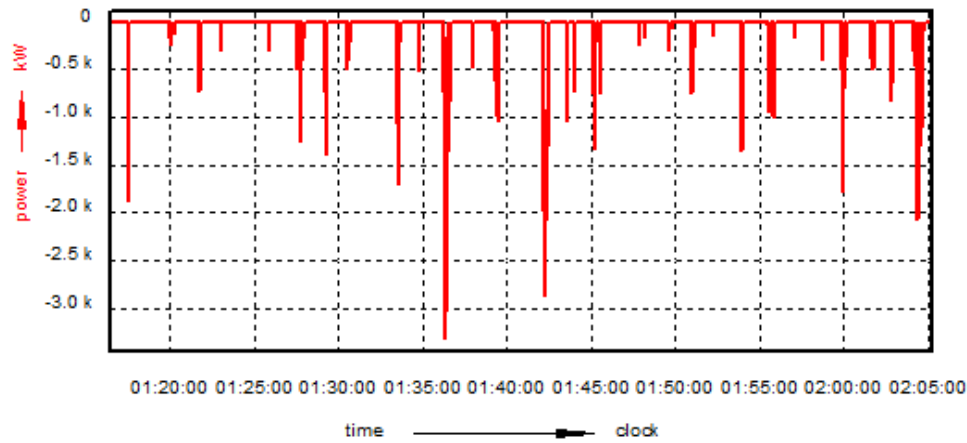


**Figure 32. Braking power at a reversible traction substation**

The use case is defined in cooperation with RATP, partner in OSIRIS project. It considers an electric hybrid bus which terminal stop will be close to “Porte de Saint-Ouen” station on metro line 13. Therefore, a fast charging station is needed. The classic solution is to buy a pre-fabricated HV/LV charging station containing:

- a 20 kV/400 V transformer
- one stage rectifier (400 V AC/ 700 V DC)
- filters
- a chopper for limiting short-circuit current

The station output voltage is 700 V DC connected to the catenary. The charging power is 200 kW. The figure below represents the conventional charger’s architecture:

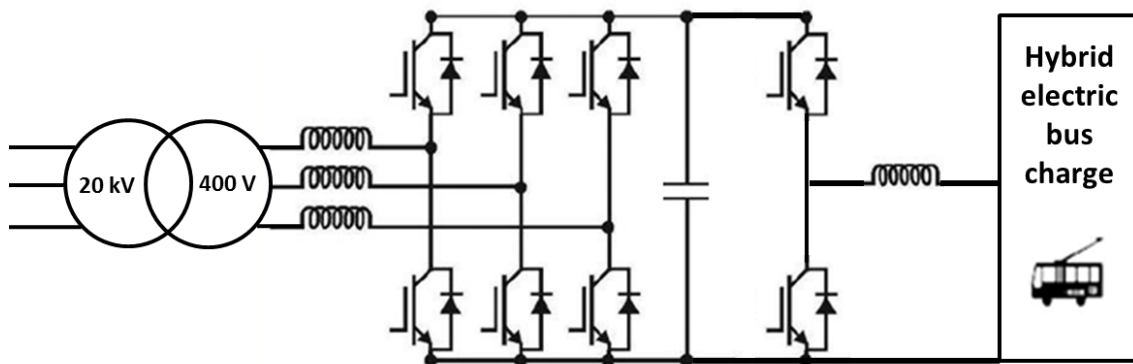


**Figure 33. Pre-fabricated charging station architecture**

The bus’s round-trip is 10 km (5 km going and 5 km returning) and the duration is estimated to 54 minutes. The charging frequency is then 1 bus/hour and the charging time duration is 4 minutes. The expected energy subscription for this type of charging stations is a regulated tariff known as “vert A5 courtes utilisations” with a maximum power of 750 kW.

Instead of consuming more energy, the braking power of metros can be used to charge the electric hybrid buses. Trains, buses and energy storage devices can be connected using a **Smart Micro-grid** that will manage the energy flow. It is a DC based concept where the main focus is set on achieving better power quality by aggregating sources and loads and connecting them through a DC busbar to the grid through a DC/AC converter. Because both loads and sources can interface to a common DC busbar with fewer redundant stages of power conversion, the result is less wasted heat and potentially lower cost than the pre-fabricated charging station. In addition, a “smart energy management system” will accommodate both intermittent generations as well as loads and optimize power flow between different terminals. It will allow saving metro’s wasted energy and make it available for charging the electric hybrid buses parked at a metro station. As the energy is mainly managed locally, a small amount of power is solicited from the grid and thus, less harmonic currents are injected on the AC side. In this case, transformerless operation and usage of a two-level inverter (as considered here) are possible in spite of the highly intermittent nature of the metro braking energy and the electric bus charging.

Moreover, no additional contract with the electricity provider needs to be signed for the bus charging station because it uses a low power AC/DC inverter. In fact, the power exchange between the railway system and the loads is done through the storage system. The AC/DC inverter serves only to regulate the DC bus bar voltage to avoid over or under voltages. For example, it could be connected directly to the LV power supply grid already existing in the metro station. The proposed architecture of the Smart DC Micro-grid is shown in Figure 34.

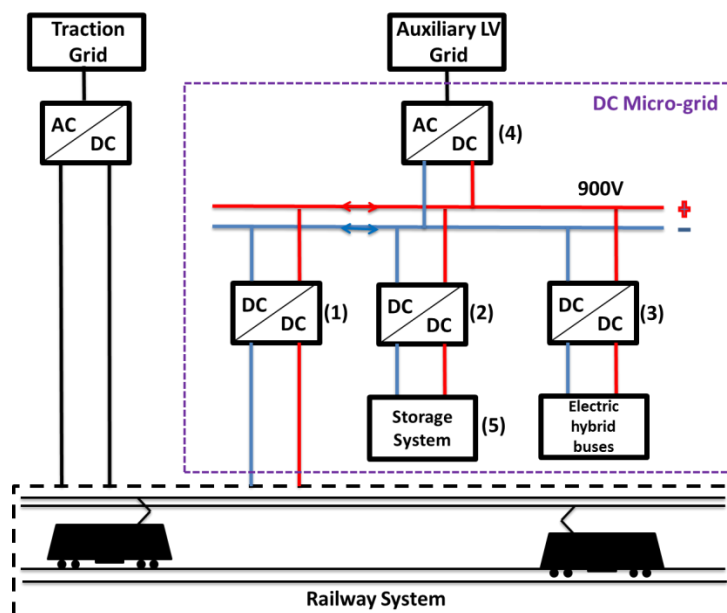


Figure 34. Smart DC micro-grid architecture

The DC micro-grid architecture consists of the following components:

- 900V DC Busbar

- DC/DC converters connecting the railway system (1), the energy storage (2) and the hybrid buses (3) to the common DC Busbar
- Two-level bidirectional inverter (4) connected to the LV power supply already available in the metro station
- Hybrid energy storage device (5) containing supercapacitors (SC) and batteries.

As shown in Figure 34, the DC micro-grid is connected to auxiliary low voltage grid. Therefore, a connection between both auxiliary and traction grids, usually separated for safety reasons, is possible through the DC micro-grid. When a train brakes, the catenary (or third rail) voltage increases. Once the voltage exceeds a specific threshold, the converter (1) will recuperate the braking energy and inject it into the DC bus. This converter should be regulated in a way that gives priority to energy exchanging between trains. In this study, the converter is regulated to 820V at railway side. The second DC/DC converter (2) will store the energy and reduce the DC bus voltage. The AC/DC bidirectional inverter is used to regulate the DC bus voltage to avoid voltage peaks or drops.

In the following, each component will be detailed then a stability study of the system will be done.

### V.c. SMART GRID REFERENCE ARCHITECTURE

Railway DC Micro-grid is a small scale smart grid. Thus, it should respect the Smart Grid Reference Architecture (SGAM) specified by “CEN-CENELEC-ETSI Smart Grid Coordination Group”. The use case’s components, functions, data flow and communication should be classified into layers, zones and domains to organize the system and ensure interoperability.

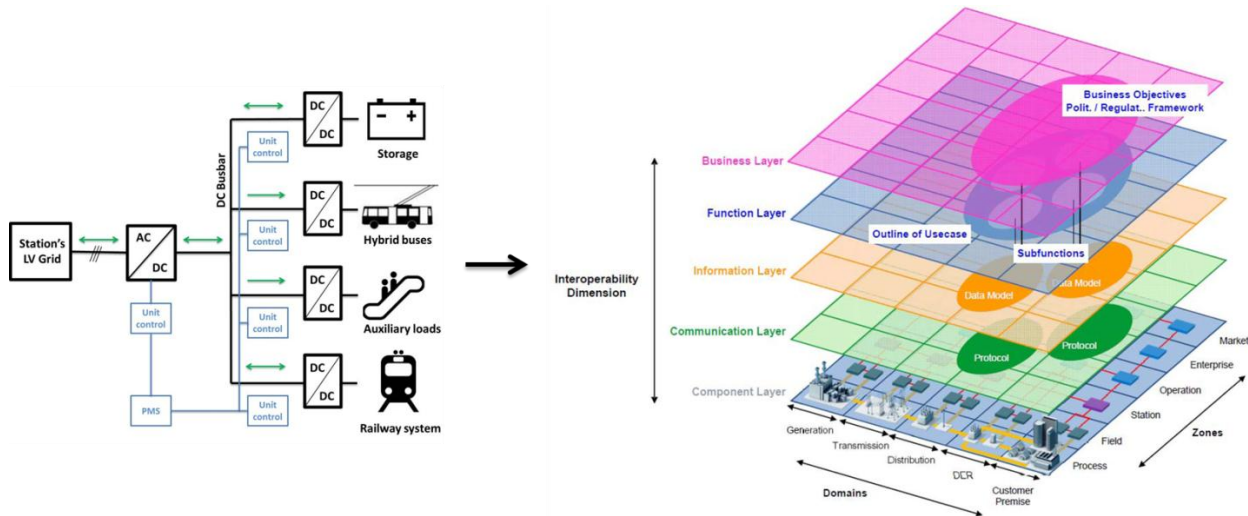


Figure 35. Railway micro-grid integration in SGAM

Interoperability is the main key of a smart micro-grid. According to IEC 61850-2010: “Interoperability refers to the ability of two or more devices from the same vendor, or different vendors, to exchange information and use that information for correct co-operation.”

Therefore, the GridWise Architecture Council (GWAC, 2008) defined interoperability categories describing requirement and methodology in order to achieve this mutual understanding within a micro-grid. For each interoperable function, all categories have to be covered, by means of standards or specifications.

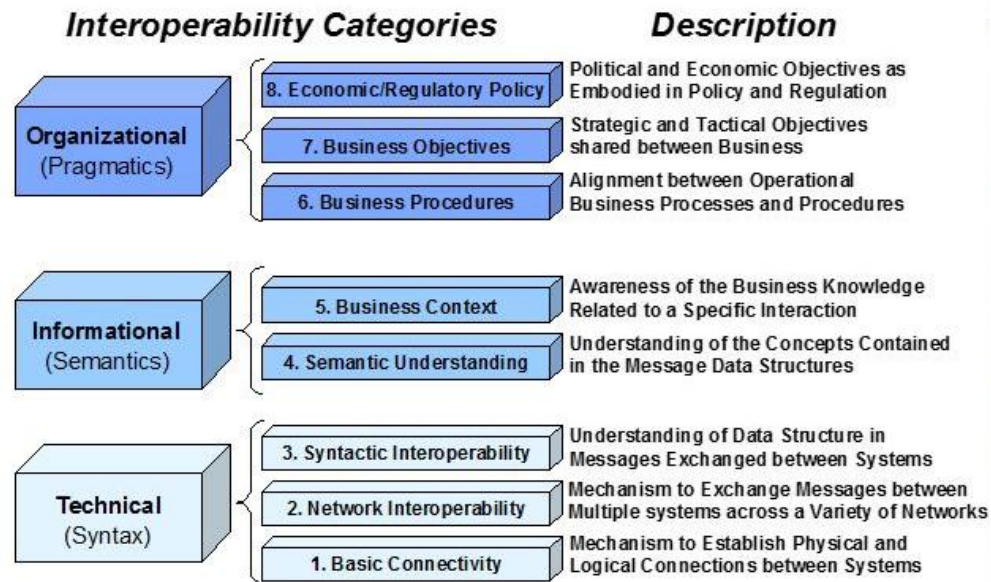


Figure 36. Interoperability categories defined by GWAC (2008) [CEN00]

To simplify the task, the interoperability categories were aggregated into five abstract layers: Business, Function, Information, Communication and Component [CEN00]. They are presented in Figure 37.

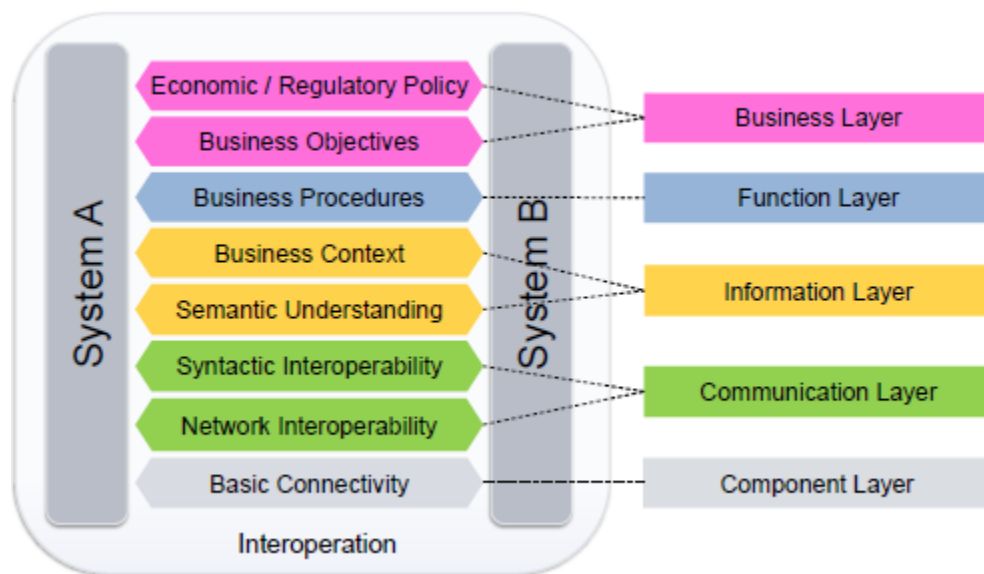


Figure 37. Interoperability layers [CEN00]



According to the Smart DC micro-grid architecture, the PMS should be able to communicate with the distributed control units. Therefore, it should contain more or less the five layers listed in Figure 37.

#### V.c.1. Business Layer

The business layer defines the objectives of the system based on a specific business model. It's where policies are decided. It includes the business processes, services and organizations that are related to the defined use case.

In this use case, the railway DC Micro-grid is mainly intended to:

- Recuperate trains' braking energy
- Charge electrical hybrid buses

#### V.c.2. Function Layer

The Function layer describes functions needed to fulfil objectives and roles defined by the business layer. Functions and their relationships are independent of the physical implementation of the system (applied technology or assigned actor). They represent the use case functionality. In the DC Micro-grid, the PMS main functions are to:

- recuperate the trains braking energy while respecting power exchange between trains,
- store the maximum of trains braking power in the hybrid storage system,
- regulate the DC Busbar voltage to avoid over or under voltages.

#### V.c.3. Information Layer

The information layer describes the information that is being used and exchanged between functions, services and components [CEN00]. In this use case, information is mainly exchanged between the PMS and the control units.

Below some examples on the information that could be exchanged:

- Authorisation to the AC/DC inverter unit control to interfere and regulate the DC busbar voltage.
- The power to be absorbed/delivered by the storage system based on its SOE.
- Authorization to the railway DC/DC converter unit control to inject power into DC busbar voltage.

The information is transferred according to a data model. It's an abstract model that documents and organizes data communication between different actors. Annex 6.2 of the JWG-SG Report on Smart Grid Standardization provides a thorough overview on the most important data models which have to be seen in context with the smart grid standardization [CEN00].

#### V.c.4. Communication Layer

This layer defines communication protocols within the smart micro-grid. In order to choose the type of communication, it is first required to define what type of networks will be used in this application. Figure 38 shows an example of different communication networks in communication layer.

The micro-grid mainly covers from the Process domain up to the Operation domain. Therefore, the selected networks should also cover these domains and be able to communicate (same communication technologies). For example, based on Table 2, the “Low-end intra substation” and the “field area” networks could be chosen.

It is recommended to use the IP for the communication because it is a well-known open standard that fits smart grid’s new requirements. It also offers migration path for some non-IP protocols and implementations like DNP, Modbus and KNX.

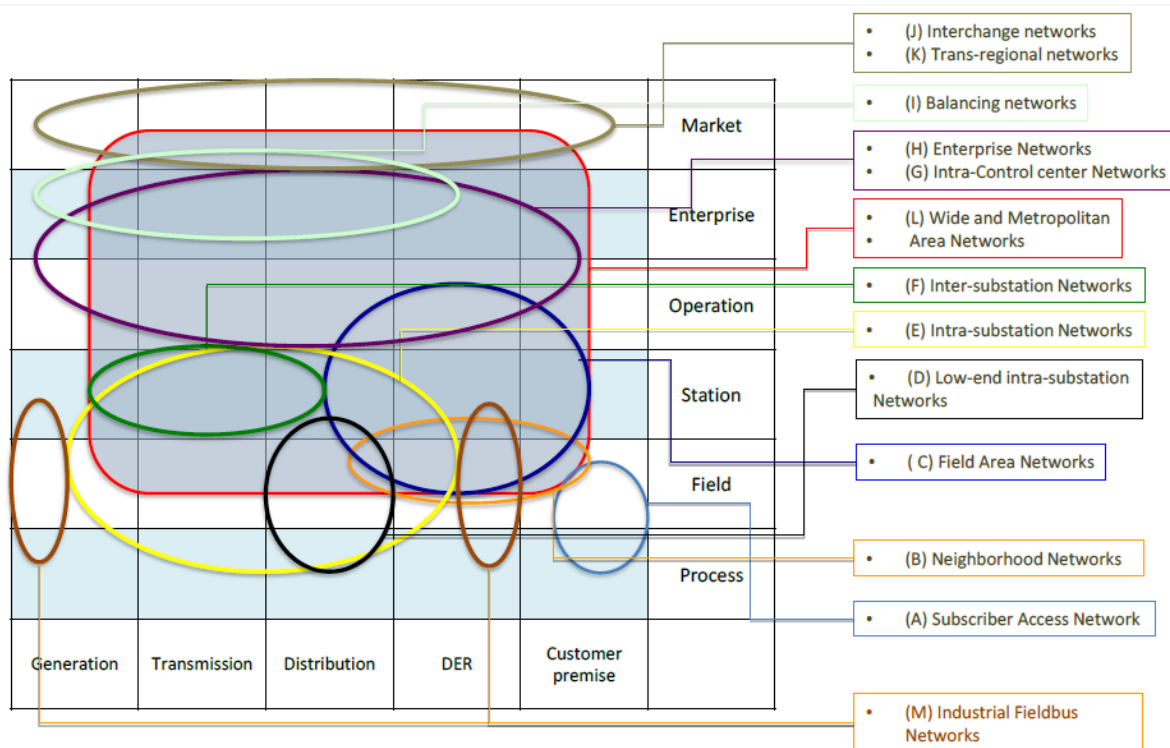


Figure 38. Mapping of communication networks on SGAM Communication Layer [CEN00]

	Subscriber access network	Neighbourhood Network	Field area	Low-end intra substation	Intra-substation	Inter-substation	Intra control centre	Intra data centre	Enterprise	Balancing	Interchange	Trans regional	Trans national	WAN	Industrial Fieldbus
	A	B	C	D	E	F	G	H	I	J	K	L	M		
Narrow band PLC (Medium and Low voltage)	x	x	x												
Narrow band PLC (High and very High voltage)					x	x									
Broadband PLC	x	x													
IEEE 802.15.4	x	x	x												
IEEE 802.11	x	x		x	x										
IEEE 802.3/1				x	x		x	x	x						x
IEEE 802.16	x	x	x												
ETSI TS 102 887		x	x												
IPv4	x	x	x	x	x	x	x	x	x	x	x	x	x	x	
IPv6	x	x	x	x	x	x	x	x	x	x	x	x	x	x	
RPL / 6LowPan	x	x	x												
IEC 61850		x	x	x	x	x								x	
IEC 60870-5				x	x	x								x	
GSM / GPRS / EDGE	x	x													x
3G / WCDMA / UMTS / HSPA	x	x					x	x	x	x	x	x	x	x	
LTE/LTE-A	x	x	x	x		x	x	x	x	x	x	x	x	x	
SDH/OTN	x	x	x	x	x	x	x	x	x	x	x	x	x	x	
IP MPLS / MPLS TP	x	x	x	x	x	x	x	x	x	x	x	x	x	x	
EN 13757		x													
DSL/PON	x	x				x								x	

**Table 2. Applicability statement of the communication technologies to the smart grid sub-networks [CEN00]**

#### V.c.5. Component Layer

It consists of the physical components of the smart micro-grid. This includes measurement devices, power system equipment (converters, storage...), protection and remote-control devices (programmable logic controllers, network infrastructure (wired / wireless communication connections, routers, switches, servers) and any kind of computers (in case there is an interface). For IP communication technologies, Ethernet or Wi-Fi could be used because the micro-grid is considered as a small area network.

#### V.d. STORAGE SYSTEM TECHNOLOGIES

As Katie Fehrenbacher said, “a next-generation smart grid without energy storage is like a computer without a hard drive: severely limited” [ENS02]. Therefore, the DC Micro-grid should contain a storage system to ensure flexibility and better energy management. A hybrid storage system stores the braking energy coming from the railway network. Primary energy sources, such as batteries, are usually used as a continuous source of low power. However, they cannot efficiently handle peak power demands because of their charging/discharging low power density. Power sources are needed to complement these energy sources in order to meet today’s applications. They consist together a hybrid storage system providing both high power and energy density (Figure 39).

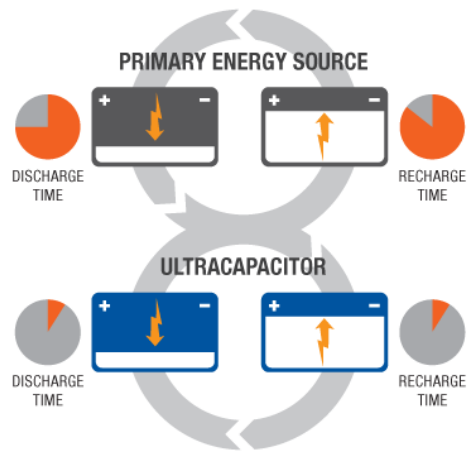


Figure 39. Hybrid storage system [MAX00]

There are many types of storage systems. Figure 40 below shows their classification based on their physical characteristics:

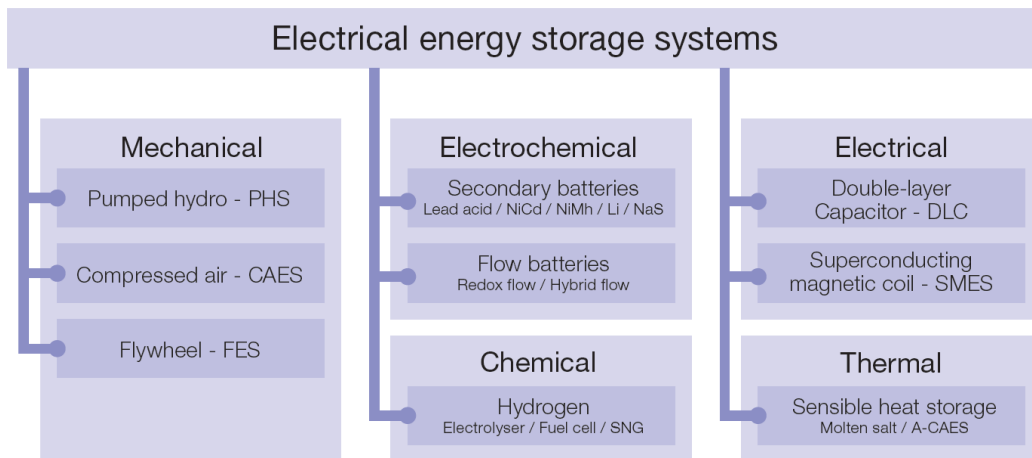


Figure 40. Classification of electrical energy storage systems according to energy form [ELC11]

Pumped hydroelectric storage facilities (PHS) store energy by pumping water from a lower reservoir to an upper reservoir. Power is then restored by releasing stored water through turbines the same as a conventional hydropower plant. The energy's round-trip efficiency (pumping/generating) is greater than 80%. However, this technology requires a large volume which is not compatible with urban applications. Compressed air energy storage (CAES) is an alternative to PHS but instead of pumping water, ambient air is compressed and stored under pressure in an underground cavern. When electricity is required, the pressurized air is heated and expanded in an expansion turbine driving a generator for power production [ENS00]. It can be employed in small-scale on-site energy storage solutions as well as in a very large storage with big energy reserve. CAES power-to-power efficiency varies between 40% (Diabatic Method) and 70% (Adiabatic Method). Thermal storage presents three main categories: Pumped heat electrical storage (PHES), hydrogen energy storage

(HES) and liquid air energy storage (LAES). PHES stores energy by pumping heat from the “cold store” to the “hot store” like in a refrigerator. To restore this energy, the engine takes heat from the hot store, delivers waste heat to the cold store and produces mechanical work which will drive an electric generator. The expected AC to AC around trip efficiency is 75-80% [ENS01]. HES is where electricity is converted to hydrogen by electrolysis. The produced hydrogen can be stored and burned later to produce electricity. Unfortunately, HES’s efficiency today is low (30-40%) but the interest in this technology is growing due to its storage capacity that is much higher than batteries (small scale) or PHS and CAES (large scale). LAES uses electricity to cool air until it liquefies. The liquid is then stored in a tank. Energy production is done by bringing back the air to its gaseous state using ambient air or waste heat from industrial process. The gas turns the turbines driving electric generators. This technology is usually used for large-scale and long duration energy storage.

Concerning batteries, they can be classified in two categories: solid state batteries (conventional batteries) and flow batteries. Conventional batteries consist of electrochemical cells that convert stored chemical energy into electrical energy. Each cell contains a positive terminal (cathode) and a negative terminal (anode). Ions move between terminals through electrolytes. New technologies such as electrochemical supercapacitors can be charged and discharged instantly and provide almost “unlimited” life cycles (commercially up to 1 Million cycles). The most common rechargeable batteries are: lead-acid battery the oldest, Nickel Cadmium (Ni-Cd) battery and lithium-ion (Li-ion) battery. The latter is the most promising battery chemistry. It is replacing the others in many applications. A flow battery is an electrical storage device that is a cross between a conventional battery and a fuel cell. Mechanically activated by pumps, flow batteries perform best at a size above 20kWh which make them suitable for bulk energy storage. For example, a flow battery for frequency regulation is being installed in Japan that will deliver a whopping 60MWh. The figure below compares the energy density of main battery technologies:

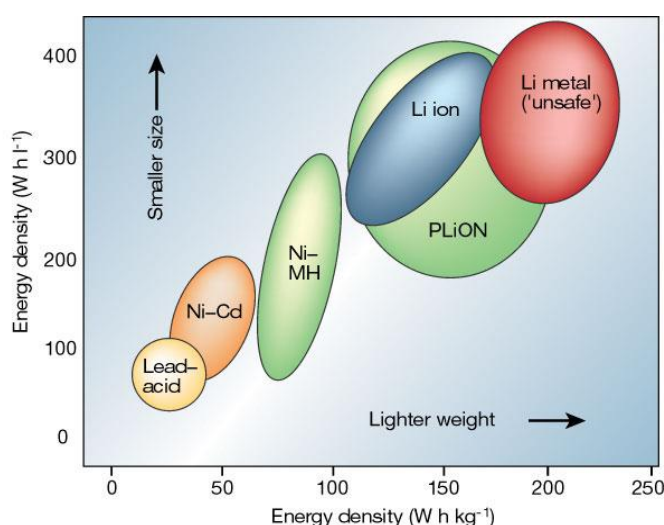


Figure 41. Energy density of different types of batteries [TAR01]

Lithium-ion batteries represent higher energy density than Lead-acid and Nickel based batteries. Yet, they have higher capital cost (see Figure 44) but also high number of cycles and low maintenance. This will reduce the cost per cycle which can become lower than lead batteries (Figure 42). In addition, their price is expected to drop with the increasing demand for Electric Vehicles (EV). The figure below shows the capital cost per cycle of different types of storage systems:

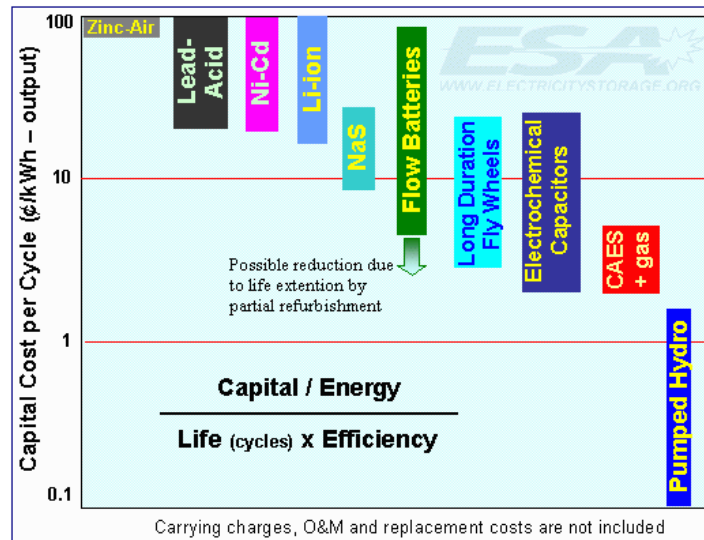


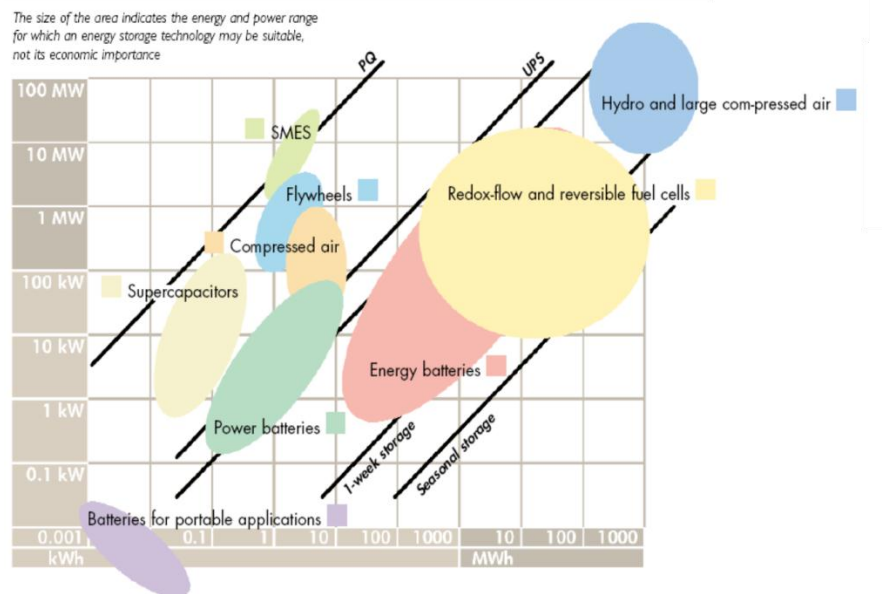
Figure 42. Capital cost per cycle for storage systems (source: ESA)

The table below lists the advantages/drawbacks of the batteries mentioned above:

	Lead-Acid batteries	Nickel based batteries	Lithium-ion batteries
<b>Advantages</b>	<ul style="list-style-type: none"> <li>High maturity</li> <li>Adequacy to all applications</li> <li>Low cost</li> <li>Recycling at 95%</li> <li>Safety</li> <li>Medium to high efficiency</li> </ul>	<ul style="list-style-type: none"> <li>Long life cycle</li> <li>High power density</li> <li>No maintenance</li> </ul>	<ul style="list-style-type: none"> <li>Long life cycle</li> <li>High power density</li> <li>High efficiency</li> <li>No maintenance</li> <li>Adapted to all applications</li> </ul>
<b>Drawbacks</b>	<ul style="list-style-type: none"> <li>Environmental impact of lead</li> <li>Sensitive to operating conditions</li> <li>Sensitive to management strategy</li> <li>Difficult prediction of state of charge, state of health and failure</li> </ul>	<ul style="list-style-type: none"> <li>Cost</li> <li>Environmental impact of Cadmium</li> <li>« Memory effect » of Ni-Cd</li> <li>Self-discharge</li> <li>Poor energy efficiency</li> </ul>	<ul style="list-style-type: none"> <li>Safety</li> <li>Cost (decreasing)</li> <li>Recycling</li> <li>Need of single cell monitoring</li> <li>Need of power and thermal management</li> </ul>

Table 3. Batteries advantages and drawbacks

Flywheels and Supercapacitors (SCs) are mostly used for high power applications. They are comparable in terms of energy density and power density (see Figure 43). The supercapacitor, also known as ultracapacitor or double-layer capacitor, differs from a regular capacitor in that it has very high capacitance. A capacitor stores energy by means of a static charge instead of electrochemical reaction. SCs can be bought in cells or modules. Modules incorporate balancing, monitoring and thermal management capabilities to ensure industry-leading charge/discharge performance, high reliability and long operational life. As a result, modules are more expensive than the equivalent quantity of cells. Nevertheless, choosing to buy cells requires from the buyer having skills and experience in assembling and controlling storage systems. The final cost depends on the produced quantity.



Nevertheless, SCs are more reliable, require no maintenance (no moving parts nor chemical reaction), have a more predictable failure mechanism, and have lower capital cost (Figure 44). In addition, given the fact that the Micro-grid will be installed in the station, there's only a limited volume available and flywheels are larger than SCs. Therefore, it is recommended to use SCs in the DC micro-grid to store trains braking energy. Meanwhile, the battery should be able to discharge the supercapacitor as soon as possible to allow storing the next train's braking power peaks. Consequently, the technology used should have high power density: when charging the hybrid electric buses, the battery should be able to provide a 200 kW constant power during 4 minutes. In addition,

high efficiency and no “memory effect” are needed because of the incomplete charging/discharging cycles. It is then recommended, for this application, to use Lithium-ion technology.

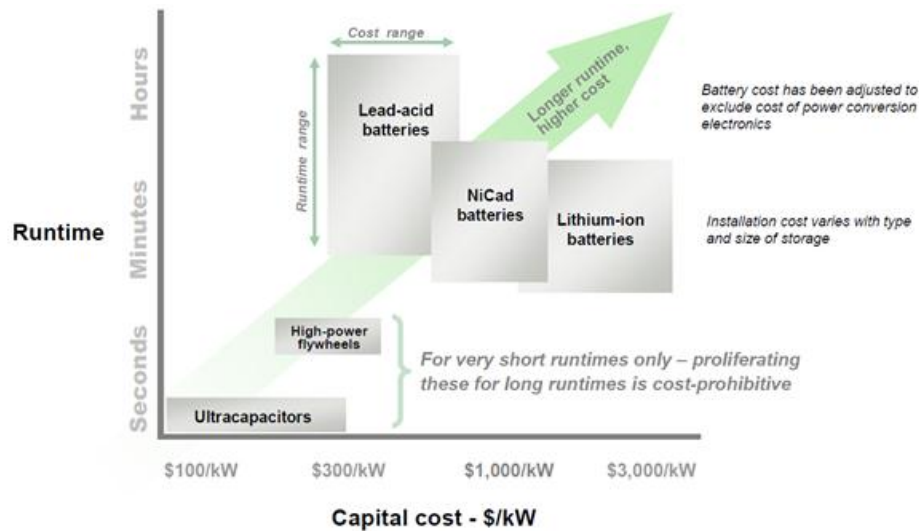


Figure 44. Capital cost vs. runtime for energy storage systems [APC65]

## V.e. POWER CONVERTERS

### V.e.1. Storage system's DC/DC converters

In order to adapt an unpredictable source of power to a short time constant charge, energy storage systems need to be integrated. Currently, the most commonly used device is the Lithium-ion battery. But even though it has high energy density, its power density is relatively low. Besides, its number of charging/discharging cycles is small and the battery's characteristics will degrade quickly over time. It is then unlikely to use only batteries to store braking energy. An intermediate storage system is needed to adapt the instantaneous braking power peaks to the battery's limited power. As mentioned before, supercapacitors are the most suitable for this application. They can last for a million of charge/discharge cycles without losing energy storage capability. Therefore, a hybrid storage system is used to store the braking energy. It consists of two cascaded stages. The first one (transistors T1 & T2) is a bidirectional converter controlled to charge the supercapacitor with the recuperated braking power and to discharge it when a hybrid bus is connected to the station. The second is also a bidirectional converter controlled to charge/discharge the battery with a constant current. The figure below shows the hybrid storage system modelled using Simulink:



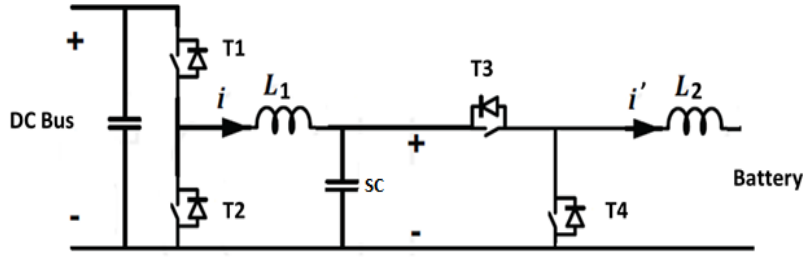


Figure 45. Hybrid storage system's architecture

This model is controlled with two control loops, one for each converter. The control signals of IGBTs T1 and T2 ensures that the power absorbed/delivered by the supercapacitor is equal to the reference power Pref (Table 4). Pref depends on the supercapacitor state of energy (SOE) calculated as follow:

$$SOE(\%) = \frac{V_{SC}^2}{V_{SC\_max}^2} \times 100 \quad (V-1)$$

Figure 46 shows the control loop of the SC's converter. It is a current regulation which reference is calculated based on the reference power in Table 4. To protect the supercapacitor, a current limitation is imposed when SOE exceeds 95% or goes under 30%. The discharging mode is stopped at 25%, that is when  $V_{sc} = V_{sc\_max}/2$ . In addition an anti-windup is added to the loop to avoid divergence. When a train brakes, T1 switches on and off in a manner that will make the current in L1 equal to the reference current. In this case, T2's diode is an anti-parallel diode. It is the buck mode. Contrarily, when power needs to be injected into the DC busbar, T2 switches on and stores energy in L1. When T2 turns off, this energy is fed into the Busbar through T1's diode. This is boost mode.

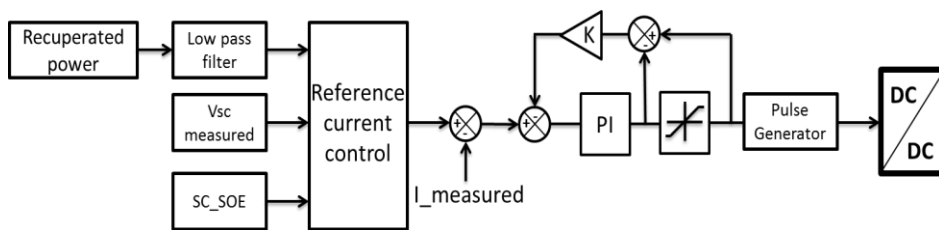


Figure 46. Supercapacitor control loop

The equivalent linear system of the SC's converter is represented in Figure 47.

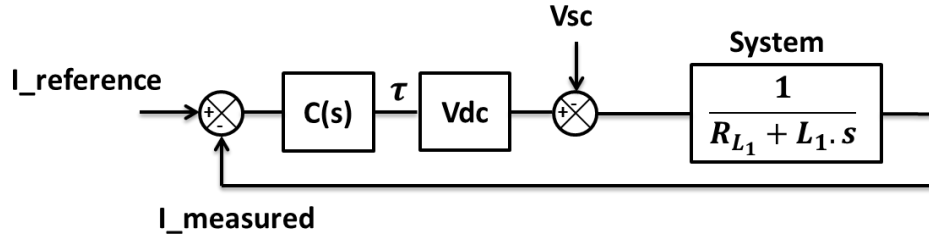


Figure 47. System's linear control loop

$C(s)$  is the corrector that will ensure that system's response meets the following specifications:

1. 10% step response overshoot
2. Rise time  $t_r=0.02$  ms
3. Cancellation of static error

The first specification is directly related to the damping ratio:

$$D_{\%} = 100e^{-\pi\xi/\sqrt{1-\xi^2}} \quad (V-2)$$

$$\rightarrow \xi = \frac{-\ln(D_{\%}/100)}{\sqrt{\pi^2 + (\ln(D_{\%}/100))^2}} = 0.59$$

The undamped natural frequency  $w_n$  can be calculated from the second specification:

$$t_r = \frac{1}{w_n\sqrt{1-\xi^2}}(\pi - \arccos(\xi)) \quad (V-3)$$

$$\rightarrow w_n = 1.3635 * 10^5 \text{ rad/s}$$

The third specification is already satisfied by the system's transfer function that contains an integrator.

A proportional correction will not be able to respect the three constraints. Therefore, we propose a first

order corrector:  $C(s) = \frac{k}{(1+\tau.s)}$

The system's open-loop transfer function is then:

$$H(p) = \frac{k.V_{dc}}{(1+\tau.s)(R_1 + L_1.s)} \quad (V-4)$$

The new closed-loop transfer function can be written in the standard form of a second-order system:

$$\frac{I_{measured}}{I_{reference}} = \frac{H(p)}{1+H(p)} = \frac{k.V_{dc}}{k.V_{dc} + R_1 + (\tau R_1 + L_1).s + \tau L_1.s^2} \quad (V-5)$$

$$\frac{I_{measured}}{I_{reference}} \equiv \frac{K}{1 + \frac{2\xi}{w_n}.s + \frac{1}{w_n^2}.s^2}, \text{ where}$$

$$\frac{1}{w_n^2} = \frac{\tau L_1}{(kV_{dc} + R_1)} \quad (V-6)$$

$$\frac{2\xi}{w_n} = \frac{\tau R_1 + L_1}{(kV_{dc} + R_1)} \quad (V-7)$$

(V-6) and (V-7) are two equations with two unknowns. By solving them, we obtain:

$$\tau = \frac{L_1}{2\xi w_n L_1 - R_1} \quad (V-8)$$

$$k = \frac{L_1 \tau w_n^2 - R_1}{V_{dc}} \quad (V-9)$$

The dimensioning of the converter's inductance depends on voltage and current variation amplitudes, of the switching frequency  $F_{sw}$  and the duty cycle.  $L_1$  can be calculated as follows:

$$L_1 = (V_{dc} - V_{sc})_{max} \times \left( \frac{D}{F_{sw} \Delta I_{L_1}} \right) \quad (V-10)$$

$$L_1 = 46.6 \mu H \rightarrow \tau = 6.215 \times 10^{-7}, \quad k = 0.0598$$

The Bode diagram of the SC converter's open-loop regulation is:

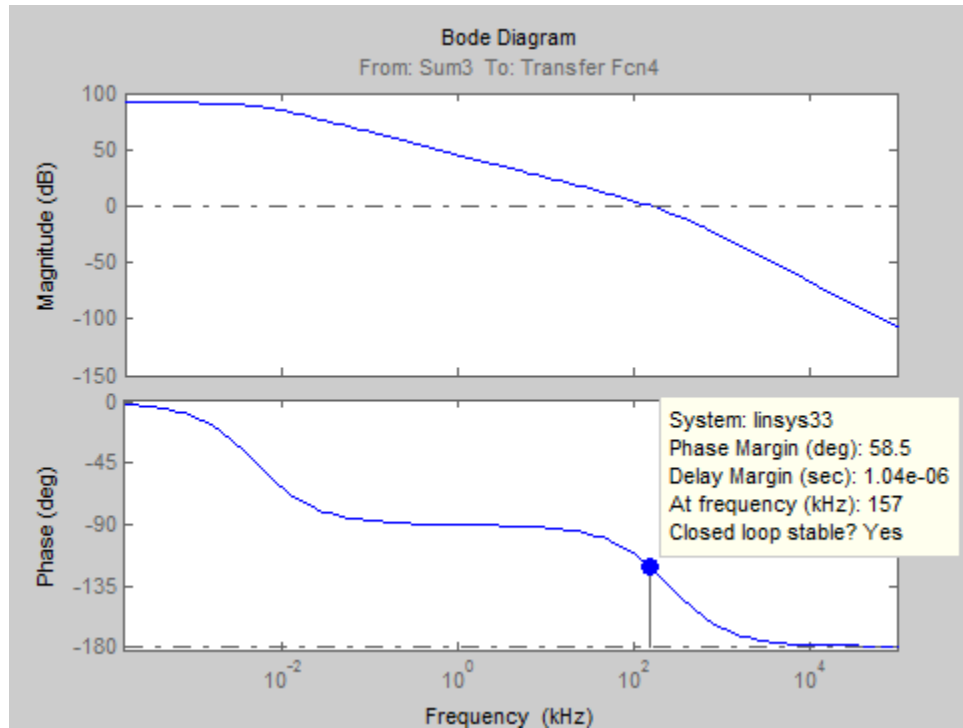


Figure 48. Bode diagram of the SC converter's open-loop regulation

The control loop below ensures that the battery is charged and discharged with a constant nominal current ( $I_{bat} = I_n$ ). The charging/discharging modes are shown in Table 4. The battery's reference current ( $I_{bat\_ref}$ ) depends on the SOE of the supercapacitor. Both modes attempt to bring

back the supercapacitor's SOE to 50%. In fact, if we consider that discharging and charging modes are equiprobable, the optimal case is to have around 50% of usable energy in the SC, which corresponds to a SOE of 62.5% (Table 4). But given the fact that braking energy is more frequent, the SOE will be set to 50% to give priority to the braking energy. Thus, the system will still be able to respond quickly to the operation mode selected by the PMS. Figure 49 shows the corresponding control loop. Same as the SC's control loop, an anti-windup is added to avoid unexpected divergence. The corrector's parameters were got by tuning:  $k_{pb} = 0.084$  and  $k_{ib} = 9.7$ .

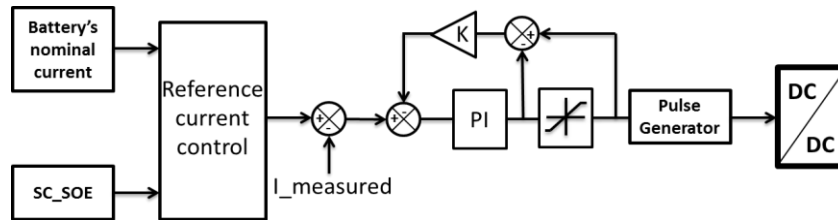


Figure 49. Battery's control loop

Table 4 represents how the PMS controls the hybrid storage system. Two modes can be distinguished: charging mode and discharging mode.

➤ Charging mode

When the SOE is below 50%, the supercapacitor absorbs all the recuperated braking power ( $P_{rec}$ ) injected into the DC busbar. The reference power ( $P_{ref}$ ), for calculating the reference current for the SC, is then equal to  $P_{rec}$ . However, the battery's reference current ( $I_{bat}$ ) is set to zero giving by that the priority to SC's charging.

When the SOE is between 50% and 95%,  $P_{ref}$  is kept equal to  $P_{rec}$  but the battery is allowed to charge.  $I_{bat}$  is then set equal to the battery's nominal current ( $I_n$ ).

When the SOE exceeds 95%, a power limitation is applied to  $P_{ref}$ . the battery keeps charging.

➤ Discharging mode

When the SOE is below 25% and one hybrid electric bus is connected to the DC Micro-grid, the power is provided by the battery.  $P_{ref}$  is then equal to the battery's maximum power ( $P_{bmax}$ ). In general, this case should be avoided in order to protect the SC.

When SOE is between 25% and 30%, a power limitation is introduced to protect the SC. The battery is also supporting the SC and  $I_{bat}$  is set to  $(-I_n)$ .

When SOE is between 30% and 50%,  $P_{ref}$  is equal to  $P_{dis}$  and the battery is also discharging with a nominal current.

When SOE is above 50%, the SC is discharging normally and the battery is in standby mode ( $I_{bat}=0$ ).

Charging mode		
Supercapacitor SOE	Supercapacitor Pref	Battery current
SOE < 50%	Pref=Prec*	I <sub>bat</sub> ** = 0
50% < SOE < 95%	Pref=Prec*	I <sub>bat</sub> ** = I <sub>n</sub>
95% < SOE < 100%	Pref = (-20*SOE+20).Prec*	I <sub>bat</sub> ** = I <sub>n</sub>
Discharging mode		
Supercapacitor SOE	Supercapacitor Pref	Battery current
SOE < 25%	Pref = P <sub>bmax</sub>	I <sub>bat</sub> = - I <sub>max</sub>
25% < SOE < 30%	Pref = (20*SOE-5).(P <sub>dis</sub> +P <sub>bmax</sub> )- P <sub>bmax</sub>	I <sub>bat</sub> = - I <sub>max</sub>
30% < SOE < 50%	Pref=P <sub>dis</sub>	I <sub>bat</sub> = - I <sub>n</sub>
50% < SOE < 100%	Pref=P <sub>dis</sub>	I <sub>bat</sub> = 0

\*Recuperated braking power absorbed by the SC

\*\* Battery's reference current

**Table 4. Hybrid storage power management**

- **Simulation**

The hybrid storage system model on Simulink is based on SC and battery products already existing on the market. The SC is based on Maxwell's 125V module. According to the product description, each module incorporates balancing, monitoring and thermal management capabilities to ensure industry-leading charge/discharge performance, high reliability and long operational life. In addition, the low equivalent series resistance provides the highest power capability required for heavy machinery such as trucks, light rail, mining... [MAX01]. Table 5 shows the main characteristics of Maxwell's 125 V modules.

Rated Capacitance	63 F	Usable Power	1700 W/kg
Rated voltage	125 V	Stored Energy	140 Wh
Absolute maximum voltage	136 V	Maximum ESR <sub>DC</sub>	18 mΩ
Absolute Maximum Current	1900 A	Weight	61 kg

**Table 5. Maxwell's 125 V module characteristics [MAX01]**

To recuperate trains' braking energy, seven parallel rows of 6 modules in series are used giving 735 kW of total continuous power and 9.46 MW of maximum total power.

The battery model is based on A123 systems' AMP20 energy module. It is a Nanophosphate lithium ion chemistry that has superior life cycle, high usable energy over a wide state of charge range and very low cost per watt-hour. It has high power density compared to other technologies. It is composed by three parallel rows of 28 cells in series. For our use case, we considered three parallel rows of three AMP20 modules in series. In Table 6, the main specifications of AMP20 Cell are listed.

Nominal Energy Content	65 Wh	Standard Charge Current	20 A
Nominal Voltage (50% SOC)	3.3 V	Maximum Charge Current	100 A
Minimum Cell Capacity	20 Ah	Pulse 10s Charge Current	200 A
Nominal Specific Power	2400 W/kg	Maximum Discharge continuous Current	200 A
Cell Weight	496 g	Pulse 10s Discharge Current	600 A

Table 6. A123's AMP20 module characteristics [AMP00]

Note that it is normal that the Specific Power of a cell is higher than Maxwell's 12 V module because a module includes also power electronics, ventilations, case, etc... which increase notably the module's total weight. To avoid batteries' fast deterioration, in normal mode, the batteries are charged / discharged with their standard low charging current ( $\approx 720\text{A}$ ).

In order to test previous regulations, a constant voltage source is connected to the DC/DC converter from the busbar's side and a varying power profile is injected to the SC's current regulation loop. This power, first positive then negative, is divided by the SC's voltage to give the reference current. The figure below shows the reference power of the control loop.

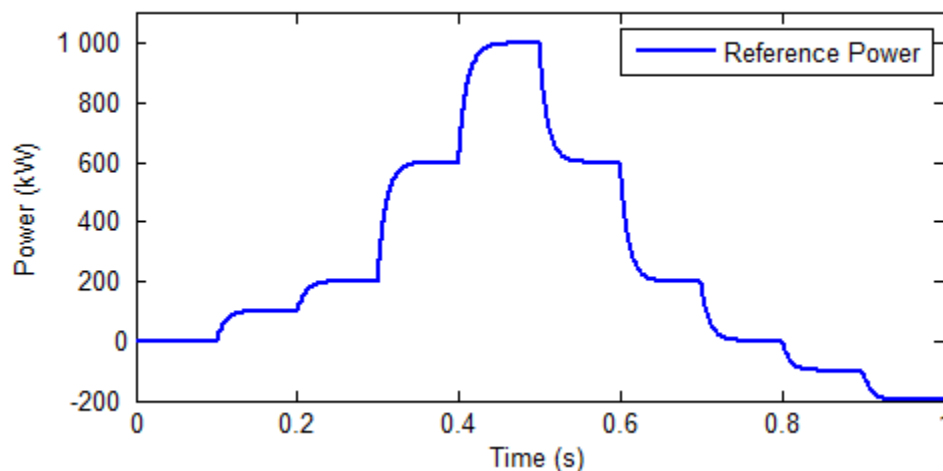


Figure 50. Reference Power to be absorbed by the storage system

The -200 kW corresponds to the power needed to charge the hybrid electric bus connected to the DC Micro-grid. Figure 51 shows reference and measured currents in the SC's corresponding inductance L1 (see Figure 45. Hybrid storage system's architecture). We can see that the currents almost overlap.

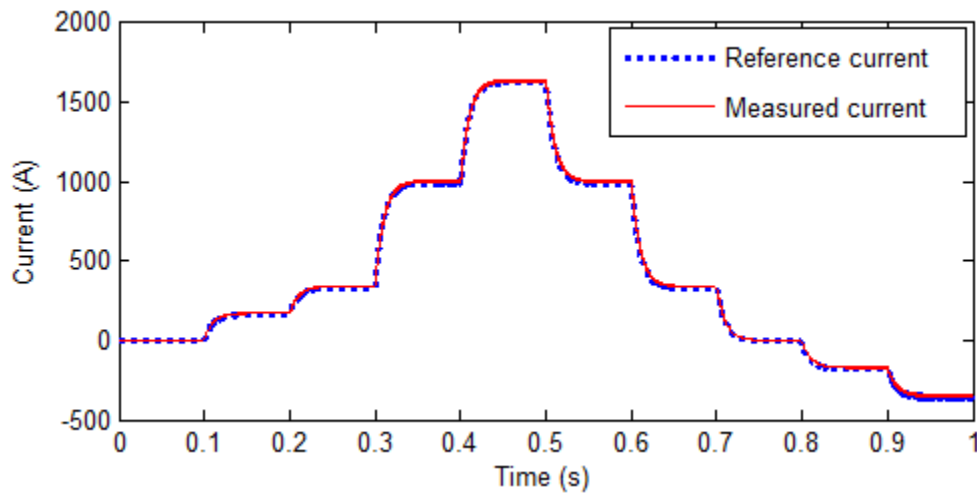


Figure 51. Reference current (dashed blue line) and measured current (continuous red line) in the SC's converter

Figure 52 shows the battery's input current evolving according to the SC's SOE. In order to avoid oscillating around SOE=50%, relays are introduced in the command. On one hand, the charging mode starts when SOE>53% and stops when SOE=51%. On the other hand, the discharging mode starts when SOE<47% and stops when SOE=49%.

The SOE represents ripples because of the SC's internal resistance.

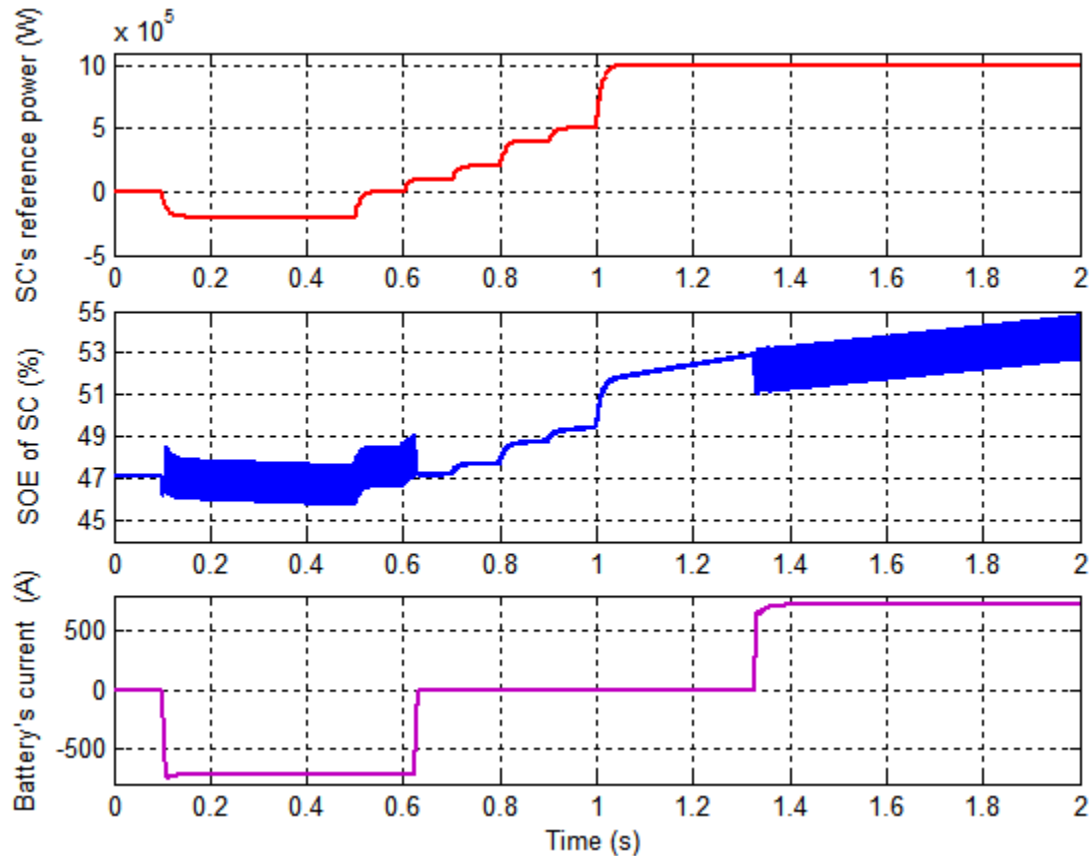


Figure 52. Battery's input current and SC's SOE

In Figure 53, the SC's initial SOE is set high enough that the reference power is limited. When the SOE exceeds 95%, a power limitation is applied according to Table 4. At time=0.8s, the power becomes negative. The storage system is discharging. No power limitation is then applied.

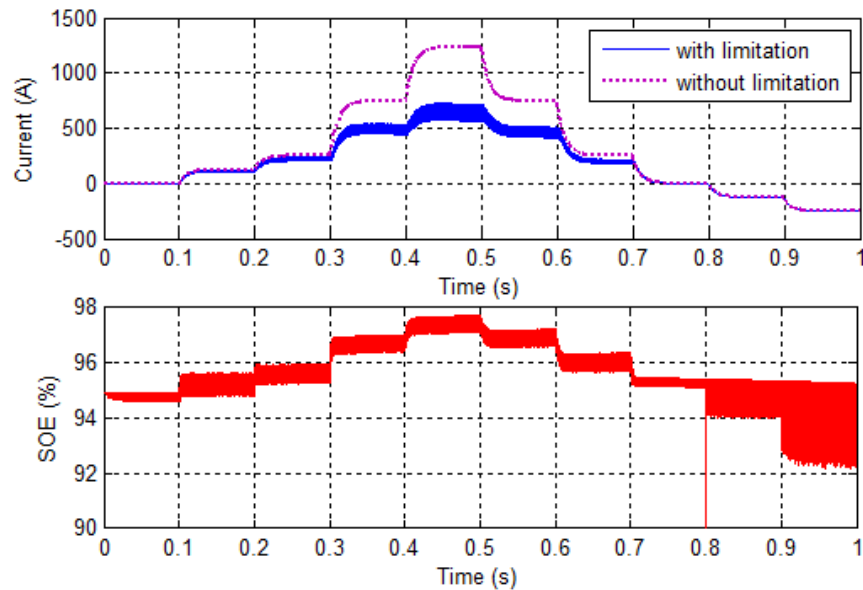


Figure 53. Charging power limitation

Contrarily to the previous case, in Figure 54, the SC's initial SOE is low enough to activate discharging power limitation. When the reference power is negative and the SOE is between 30% and 25%, the power is limited according to Table 4. But when the power is reversed (becomes positive) at  $t=5s$ , the charging mode begins and the power limitation is thus stopped.

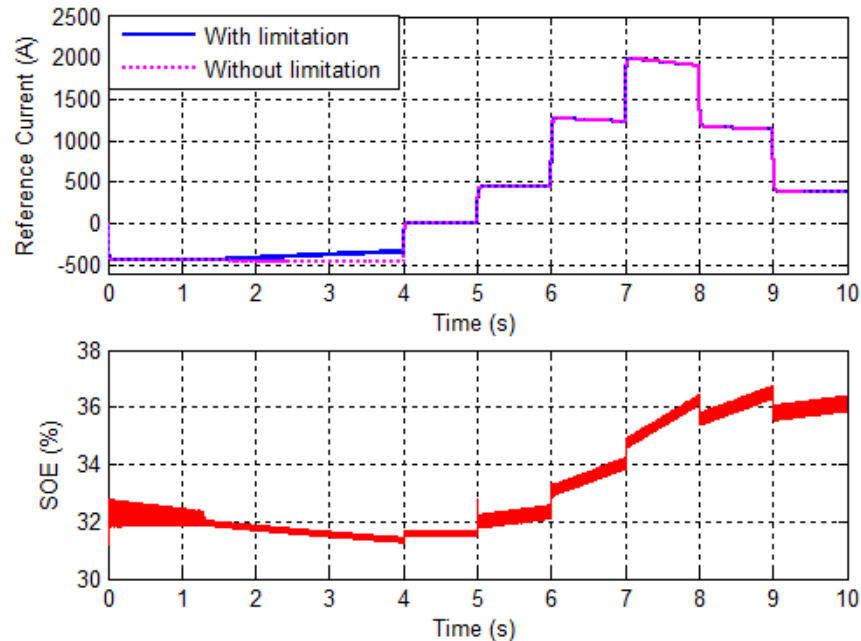


Figure 54. Discharging power limitation



To test the SC's protection through discharging power limitation, the initial SOE is set to 25% and a reference power of 200 kW is applied. Figure 55 shows that the reference current was reduced significantly to keep the SOE around 25%. The power is then delivered mainly by the battery.

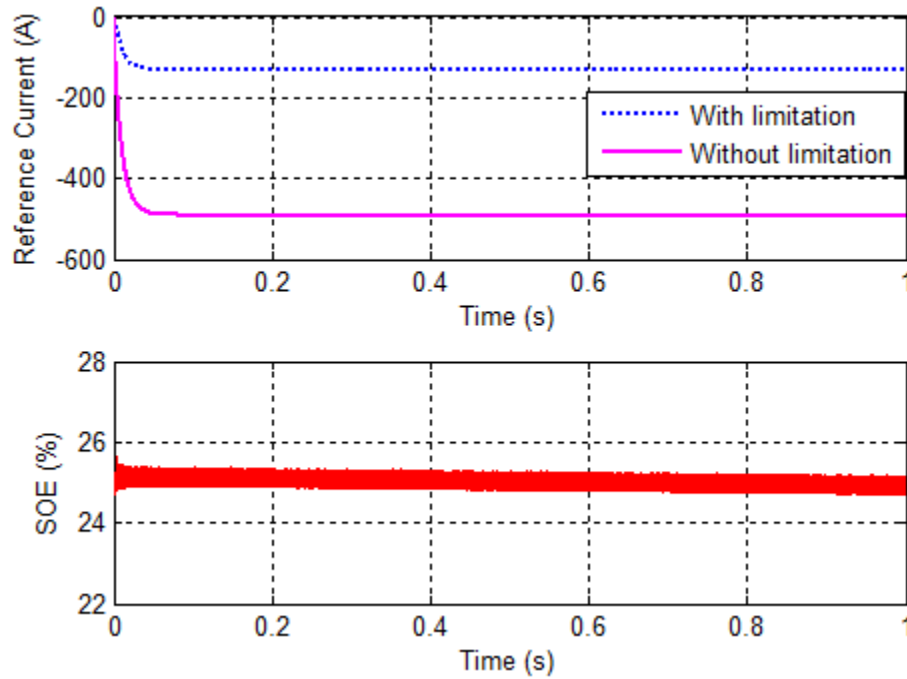


Figure 55. Test of SC's power protection

#### V.e.2. AC/DC bidirectional converter

An AC/DC bidirectional converter is a power electronic device that is able to transfer active power from AC side to DC side and conversely. It is based on IGBT technology which allows faster switching. Thus, harmonics with higher order are generated especially when applying Pulse Width Modulation (PWM). It is a modulation technique used to encode a message into a pulsing signal. These signals will then command the IGBTs. The simplest way to generate a PWM signal is the intersective method, which requires only a sawtooth or a triangle waveform (easily generated using a simple oscillator) and a comparator. When the value of the reference signal (the red sine wave in Figure 56) is more than the modulation waveform (blue), the PWM signal (magenta) is in the high state, otherwise it is in the low state. The PWM bloc can be considered as an amplifier of the modulated signal. The equation below can be applied in the case of under-modulation.

$$\hat{V}_{out} = \frac{V_{dc}}{2 \hat{V}_{triangle}} \times \hat{V}_{consigne} \quad \text{when} \quad \frac{V_{dc}}{2} \geq \frac{\sqrt{2}}{\sqrt{3}} V_{LL,RMS} \quad (V-11)$$

This well-known technique is not only used for controlling power electronics but also in other domains such as communication.

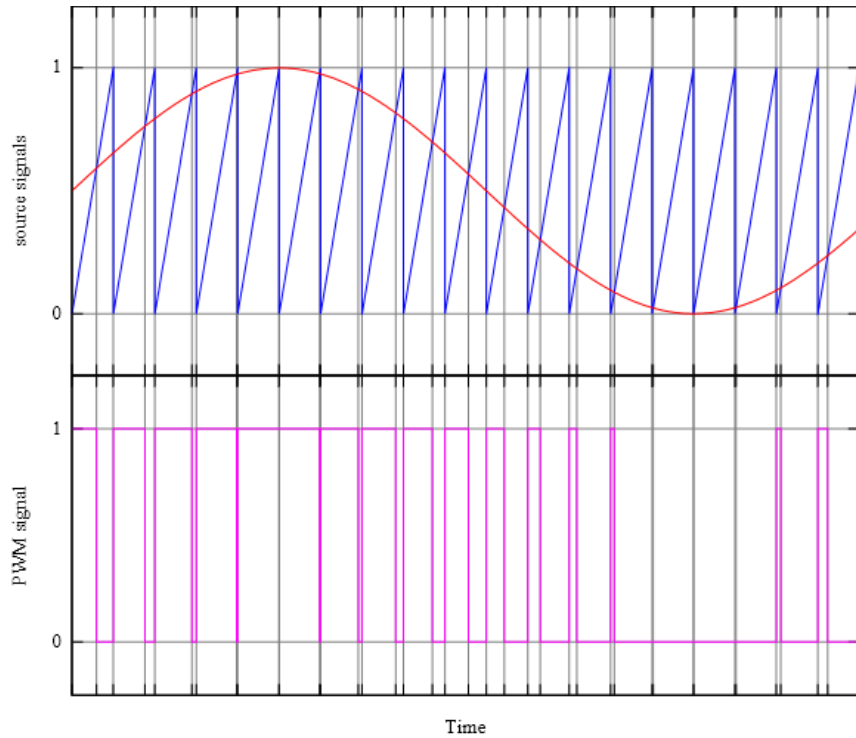


Figure 56. Pulse width modulated signals

In our case, the AC/DC converter is a classic two-level converter consisting of 6 switching IGBTs with anti-parallel diodes. Each branch is connected to a different phase through an inductance that serves as a filter connecting the converter's chopped voltage to the grid's sinusoidal low voltage. The three inductances are sized to reduce current ripples injected into the grid. The capacitor serves also as a filter. It is sized to reduce the DC Busbar voltage ripples.

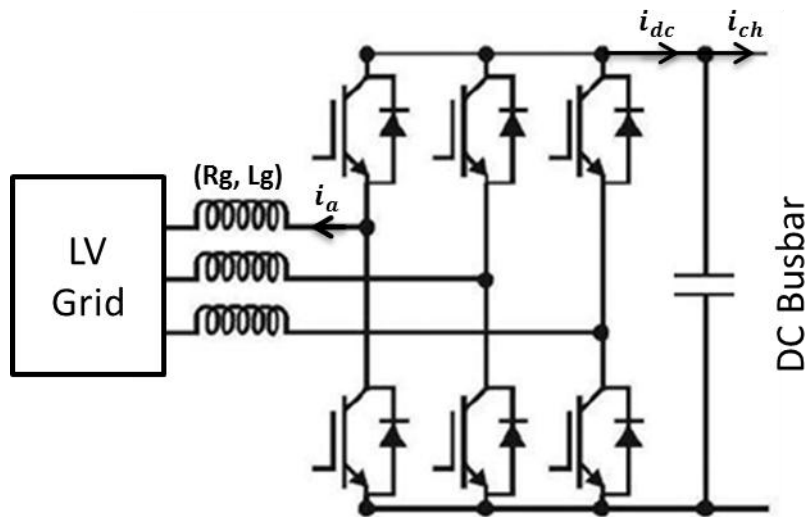


Figure 57. 2-level AC/DC bidirectional converter

The inverter is used to regulate the DC busbar voltage. Contrarily to classic regulations, the inverter's role is not to fix its output DC voltage. It rather operates in floating mode: it feeds back

The diagram illustrates the control system for a 6-pulse AC/DC converter. It features a Vdc reference block that receives Vdc measured and Status inputs. The Vdc reference is compared with Vd measured to generate an Id reference. This reference is then compared with Id measured to produce an error signal, which is processed by a PI controller. The output of this PI controller is compared with Iq measured (which is derived from a zero reference) to produce another error signal, processed by a second PI controller. The outputs of these two PI controllers are fed into an anti-saturation block. The outputs of the anti-saturation block are then transformed from the dq frame to the abc frame using a transformation block. Finally, the abc frame signals are processed by a PWM generator to produce the 6-pulse AC output, which is then converted to DC.

82 | P a g e

source converters) or with the current (e.g. used in current source converters). This transformation is referred to as Park transformation for Robert H. Park who first proposed it in 1929 [RHP29]. This transformation simplifies the regulation because simple PI correctors can be therefore used on DC quantities without worrying about regulators' additive phase-shift. It is although possible to do it with AC quantities but special correctors with zero-phase shift should be then used, such as resonant correctors. Park's transformation matrix is shown below:

$$C = \frac{2}{3} \begin{bmatrix} \cos(\theta) & \cos(\theta - \frac{2\pi}{3}) & \cos(\theta + \frac{2\pi}{3}) \\ -\sin(\theta) & -\sin(\theta - \frac{2\pi}{3}) & -\sin(\theta + \frac{2\pi}{3}) \\ \frac{1}{2} & \frac{1}{2} & \frac{1}{2} \end{bmatrix} \quad (V-10)$$

where  $\theta = \omega t + \delta_a$  is the angle between the rotating and fixed coordinate system at each time  $t$  and  $\delta_a$  is an initial phase shift of the voltage.

- **Phase Locked Loop**

In general, in order to connect a power electronic device to the grid, we need to have the exact position of grid's voltage vector at the coupling point. Sometimes, especially in industrial areas, the grid's 3-phase voltages are not perfectly balanced and present distortions. Therefore, different types of Phase Locked Loops (PLL) exist and are used depending on the particularity of each case [LIM00]. We list some of these solutions:

- Synchronous Reference Frame PLL (SFR-PLL): this technique is simple and is used for almost all classic three-phase systems.
- Double Synchronous Reference frame (DSRF-PLL): this technique is based on the separation of positive and negative sequences of the grid and is an optimal solution for unbalanced three-phase systems.
- Synchronous Reference Frame PLL with Positive Sequence Filter (PSF-PLL): this solution uses sinusoidal signal integrators (SSI) as a positive sequence filter.
- Synchronous Reference Frame PLL with Sinusoidal Signal Integrators (SSI-PLL): this solution uses different strategies of SSI filters to avoid distortions.
- Double Second Order Generalized Integrator PLL (DSOGI-PLL): this is another solution that also uses SSI filters for finding the fundamental of voltages' positive sequence.

In the following, the angle  $\theta$  is obtained using DSOGI-QSG-PLL shown in Figure 60 . This solution consists of two SOGI filters applied on the in-phase and quadrature signals. Its particularity is that it can be used independently of the perturbations that may occur on the grid's side.

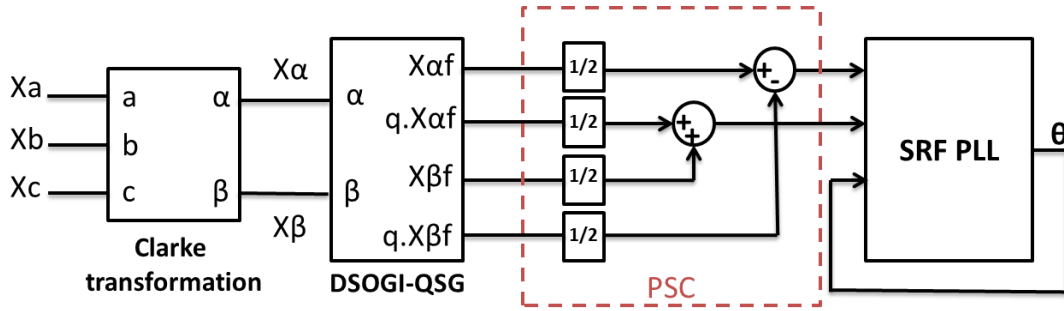


Figure 60. Rotation angle extraction using DSOGI-QSG-PLL

Clarke transform (or abc/αβ transform) allows the passage from a three-dimension system to a bi-dimension one.  $X_\alpha$  and  $X_\beta$  are also time variants with the same rotation angle as  $X_{abc}$ .  $X_\alpha$  and  $X_\beta$  are then filtered using the DSOGI-QSG filter. Figure 61 shows the details of this filter. It is a selective filter at  $w = w_0$  that gives in-phase and quadrature filtered signals.

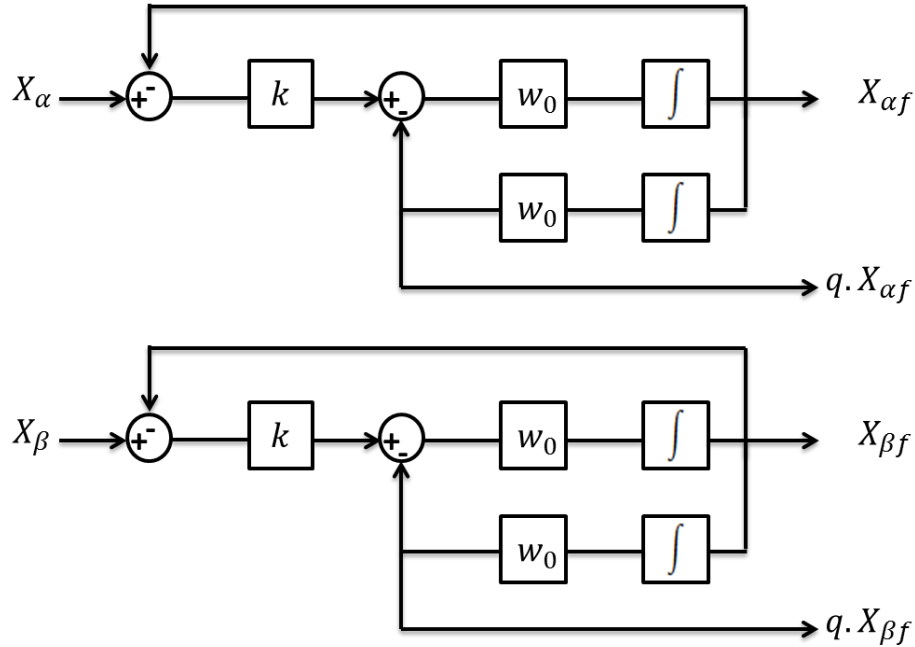


Figure 61. DSOGI-QSG filter

The equivalent transfer function of one filter loop:

$$T(s) = \frac{X_f(s)}{X(s)} = \frac{k \cdot w_0 \cdot s}{s^2 + k \cdot w_0 \cdot s + w_0^2} \quad (V-11)$$

For  $s = jw_0$ ,  $T(jw_0) = 1$ . Therefore, it is a selective filter that for  $w = w_0$  gives  $X_f(s) = X(s)$ .

In addition,

$$G(s) = \frac{q \cdot X_f(s)}{X(s)} = \frac{w_0}{s} T(s) = \frac{k \cdot w_0^2}{s^2 + k \cdot w_0 \cdot s + w_0^2} \quad (V-12)$$

For  $s = jw_0$ ,  $G(jw_0) = \frac{1}{j} = -j$ . Therefore, it is a selective filter that for  $w = w_0$  gives the in-quadrature signal  $q \cdot X_f(s) = -j \cdot X(s)$ .

The four output signals ( $X_{\alpha}, q, X_{\alpha}, q, X_{\beta}$ ) are the inputs of a Positive Sequence Calculation (PSC) in order to synchronize with the grid's positive sequence with the following equation:

$$\begin{bmatrix} X_{\alpha+} \\ X_{\beta+} \end{bmatrix} = \frac{1}{2} \begin{bmatrix} 1 & -q \\ q & 1 \end{bmatrix} \begin{bmatrix} X_{\alpha} \\ X_{\beta} \end{bmatrix} \quad \text{with } q = e^{-j\frac{\pi}{2}} \quad (\text{V-13})$$

The positive sequence calculated in (V-11) is then transformed in (d, q) frame. Only  $X_q$  is used in the SRF-PLL showed in the following block diagram:

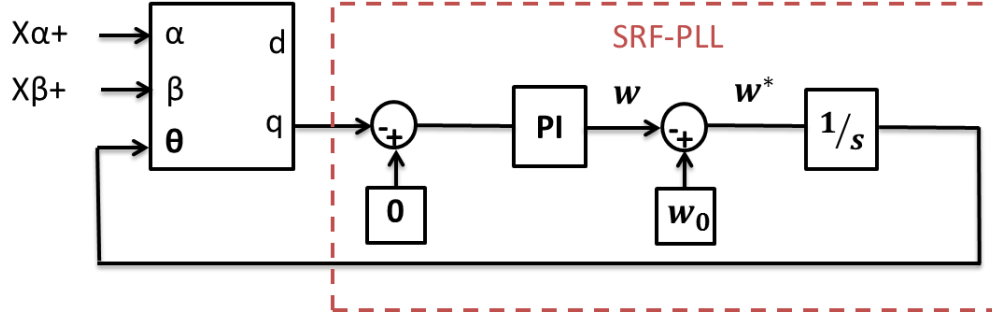


Figure 62. SRF-PLL concept

If we consider that the grid is well balanced and there's no distortion, we have the following:

$$\begin{bmatrix} V_a \\ V_b \\ V_c \end{bmatrix} = \begin{bmatrix} V \cos(\theta) \\ V \cos(\theta - 2\pi/3) \\ V \cos(\theta - 4\pi/3) \end{bmatrix} \quad (\text{V-14})$$

$$\begin{bmatrix} V_{\alpha} \\ V_{\beta} \end{bmatrix} = \frac{2}{3} \begin{bmatrix} 1 & -1/2 & -1/2 \\ 0 & \sqrt{3}/2 & -\sqrt{3}/2 \end{bmatrix} \begin{bmatrix} V_a \\ V_b \\ V_c \end{bmatrix} = \begin{bmatrix} V \cos(\theta) \\ V \sin(\theta) \end{bmatrix} \quad (\text{V-15})$$

$$\begin{bmatrix} V_d \\ V_q \end{bmatrix} = \begin{bmatrix} \cos(\theta)^* & -\sin(\theta)^* \\ \sin(\theta)^* & \cos(\theta)^* \end{bmatrix} \begin{bmatrix} V_{\alpha} \\ V_{\beta} \end{bmatrix} \quad \text{With } \theta^* \text{ the PLL's output} \quad (\text{V-16})$$

We then obtain:

$$\begin{bmatrix} V_d \\ V_q \end{bmatrix} = V \begin{bmatrix} \cos(\theta^* - \theta) \\ \sin(\theta^* - \theta) \end{bmatrix} = \begin{bmatrix} \cos(\Delta\theta) \\ \sin(\Delta\theta) \end{bmatrix} \quad (\text{V-17})$$

The SRF-PLL will cancel  $V_q$  and thus the phase error  $\Delta\theta$ . The PLL's output angle  $\theta^*$  will be then equal to the grid's rotation angle  $\theta$ .

Now that the rotation angle is calculated from the grid's three phase voltages, it is possible to apply Park transform to the measured three phase currents.  $I_d$  and  $I_q$  will be regulated using the current loops (see Figure 59). The reference value of  $I_d$  is the output of the voltage loop.  $I_d$  corresponds to the active power to be injected to or consumed from the grid. In fact, when the synchronous frame is aligned with voltage,  $V_q$  is equal to zero. The instantaneous active power can be calculated as follow:

$$P = V_d I_d + V_q I_q = V_d I_d \quad (V-18)$$

The reactive power is then determined by  $I_q$ . It can be calculated as follow:

$$Q = V_q I_d - V_d I_q = -V_d I_q \quad (V-19)$$

Depending on the application, the AC/DC converter can operate in leading mode (consuming reactive power from the grid) or in lagging mode (injecting reactive power to the grid). A third mode is possible it's when the converter is a power factor corrector with zero reactive power. It is then seen by the grid as a pure resistor. The latter case is considered in our use case.

- **Current Control Loop**

As mentioned before, the AC/DC converter is controlled using two cascaded regulations: an internal current control loop and an external voltage control loop. In this paragraph, a focus is done on the current regulation. As we can see in Figure 59, this loop operates in the rotating frame (d,q). The transfer function of the physical system can be calculated from the system's equations:

$$\begin{cases} V_d^* - V_{gd} = R_L I_{Ld} + L_g \frac{dI_{Ld}}{dt} - L_g \omega I_{Lq} \\ V_q^* - V_{gq} = R_L I_{Lq} + L_g \frac{dI_{Lq}}{dt} + L_g \omega I_{Ld} \end{cases} \quad (V-20)$$

where  $R_L$  and  $L_g$  represent the inductance connecting the AC/DC converter to the grid.

These equations show that the behaviour of in-phase and in-quadrature components is quite similar. Therefore, it is possible to apply the same corrector to both control loops. Thus, in the following, the study will be based on the in-phase current  $I_{Ld}$ .

The corrector's output is added to the grid's in-phase voltage  $V_{gd}$  and the inductance perturbation ( $-L_g \omega I_{Lq}$ ). The result is the voltage reference that is injected to the PWM generator. The latter can be considered as a signal amplifier with a time delay  $T_s = 1/(2f_s)$  with  $f_s$  the converter's switching frequency. The feedback measured current can be then calculated using equations (V-20).

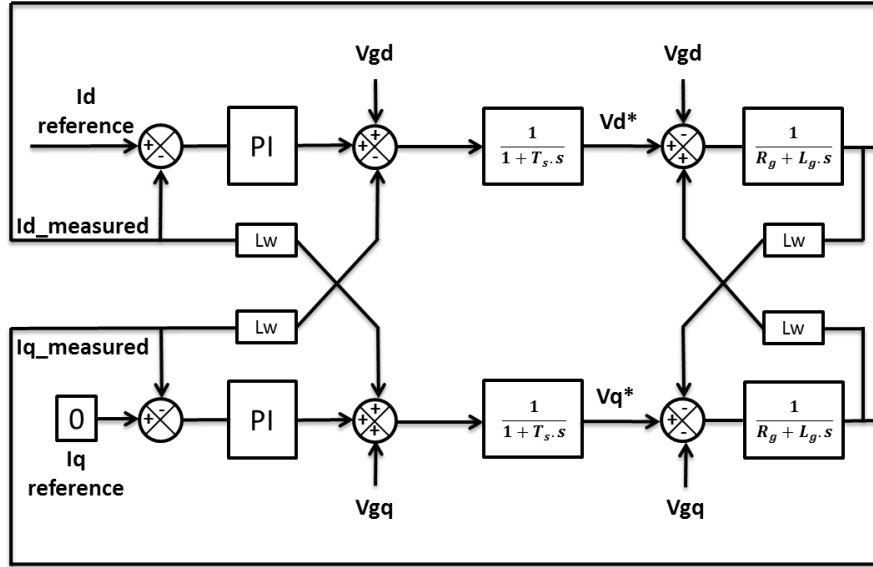


Figure 63. Current control loops of the AC/DC converter connected to the grid

To calculate the corrector's parameters, a simplified control loop is considered without perturbations. Using the tuning function in Simulink for a rise time  $t_r = 0.002s$  and a damping ratio  $\xi=0.87$ , we find:

$$C(s) = k_{pi} + k_{ii}/s \quad \text{with } k_{pi} = 37.68 \text{ and } k_{ii} = 685.7 \quad (V-21)$$

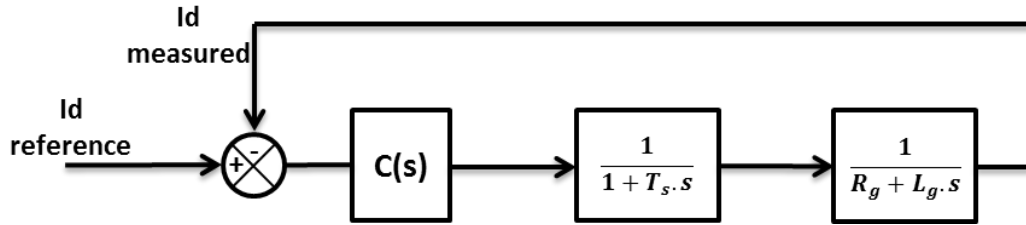


Figure 64. Simplified Current control loop

The system's Bode diagram is given in Figure 65.



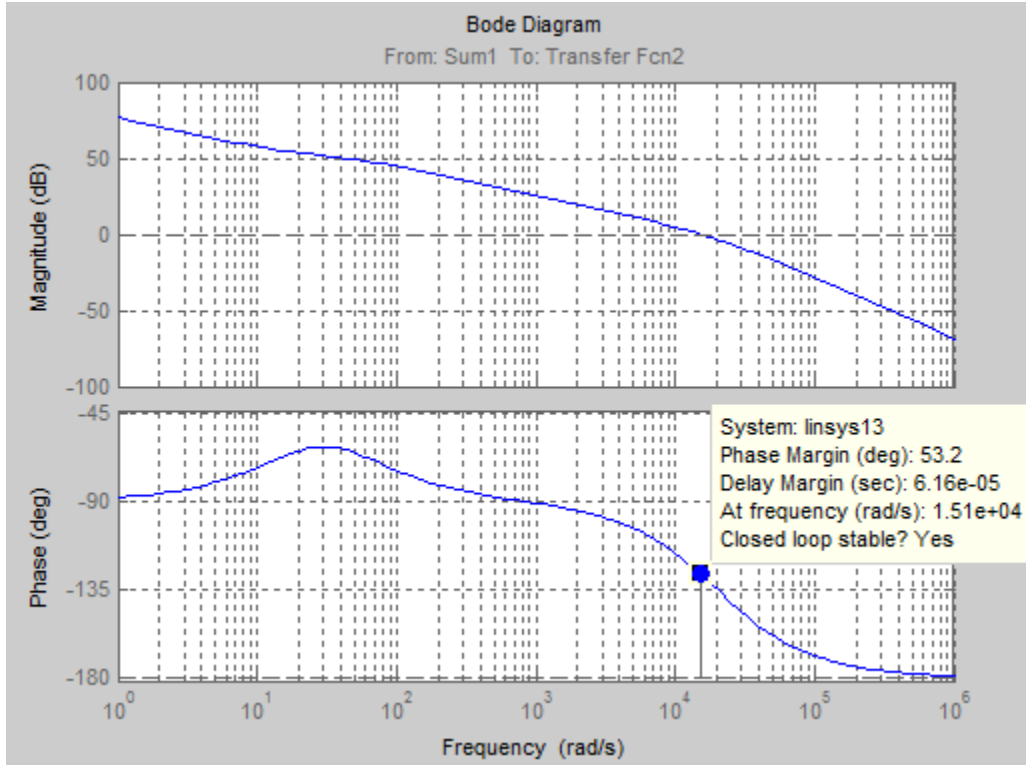


Figure 65. Bode diagram of the current control open loop

- **Voltage control loop**

The external voltage control loop should be at least 10 times slower than the inner current control loop. The output of the voltage corrector is the reference current that is injected in the current loop previously studied. The corresponding block diagram is shown in Figure 66.

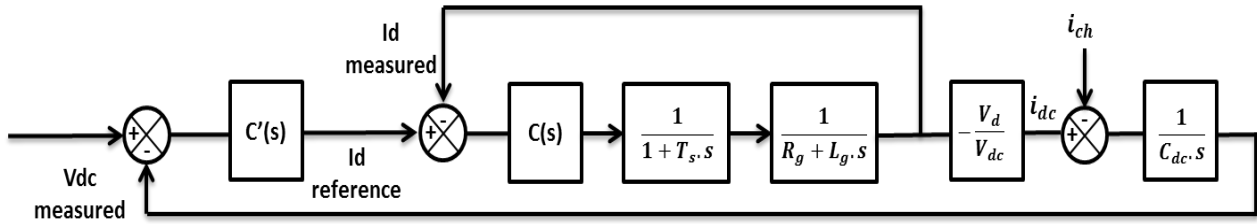


Figure 66. The simplified control loop of the AC/DC converter connected to the grid

We consider the currents' directions in Figure 57. The converter's output current on DC side is calculated using the current loop's output, the measured current, according to the law of power conservation:

$$P_{AC} = -P_{DC} \Rightarrow V_d I_d = -V_{dc} i_{dc}$$

$$i_{dc} = -\frac{V_d}{V_{dc}} \times I_d$$

(V-22)

Note that the corrector's tuning is done on a linearized system. Therefore,  $V_d$  and  $V_{dc}$  are considered as constants respectively equal to 320V and 900V. Once  $i_{dc}$  is calculated, the output DC voltage  $V_{dc}$  is obtained as follows:

$$C_{dc} \frac{dV_{dc}}{dt} = i_{dc} - i_{ch} \quad (V-23)$$

Using the tuning function in Simulink for a rise time  $t'_r = 0.01s$  and a damping ratio  $\xi' = 0.87$ , we find:

$$C'(s) = k_{pv} + k_{iv}/s \quad \text{with } k_{pv} = -0.517 \text{ and } k_{iv} = -1.83 \quad (V-21)$$

The Bode diagram of the global system is thereby presented in Figure 67.

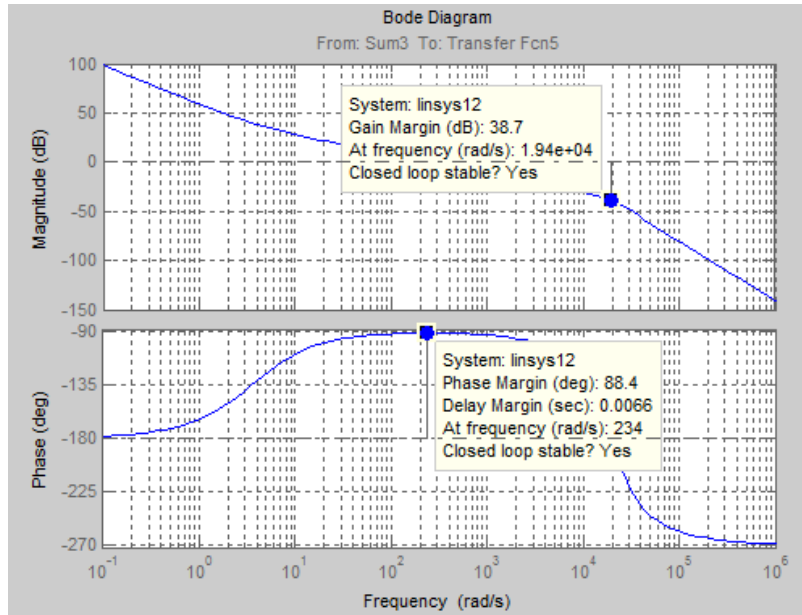


Figure 67. Bode Diagram of the system's open loop

- **Simulation**

To test the control loops calculated above, a constant current load is connected at converter's DC side. It starts consuming 5A (equivalent to 4.5 kW) at  $t = 0.15 s$ . Figure 68 shows the DC output voltage of the AC/DC converter when operating as a rectifier. It is regulated to 900V. The voltage drop at  $t = 0.15 s$  is due to the fact that the resistor is connected directly to the output capacitor through a breaker with a very short response time.

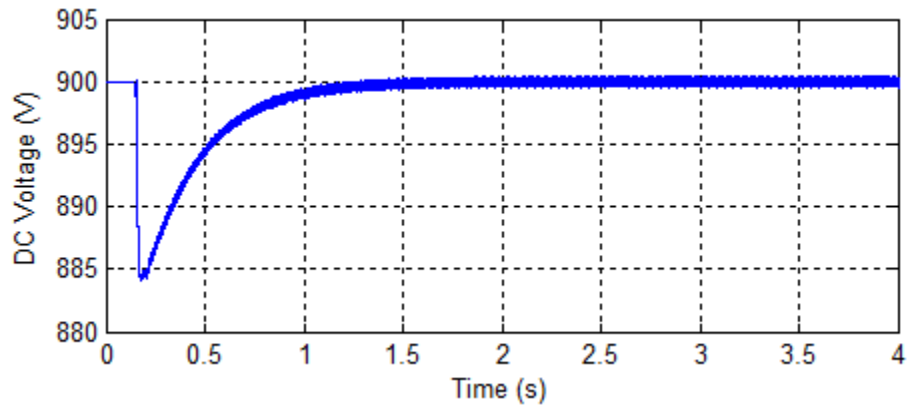


Figure 68. DC output voltage of the AC/DC converter in rectifier mode

In Figure 69, a zoom on the AC voltage and current of a single phase shows that PWM gives low distortion in rectifier mode. In addition, the converter acts as a power factor corrector because the current is in phase with the voltage. No reactive power is then injected or consumed from the grid.

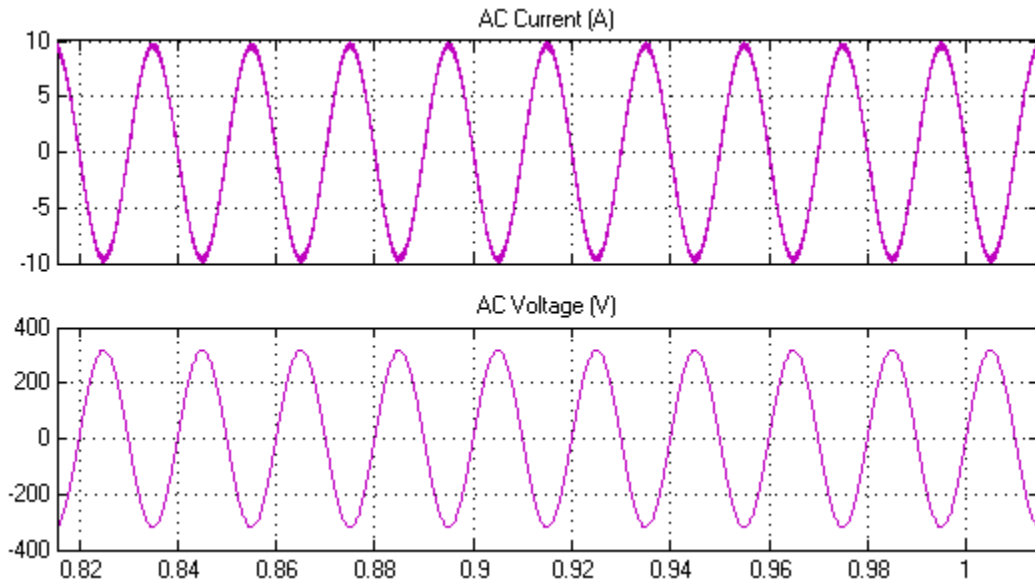


Figure 69. Zoom on AC Voltage and current in rectifier mode

As mentioned before, the AC/DC converter should be bidirectional. Therefore the same previous test is repeated but this time with a constant current source. The converter is thus in inverter mode. Figure 70 shows the DC output voltage regulated to 900V.

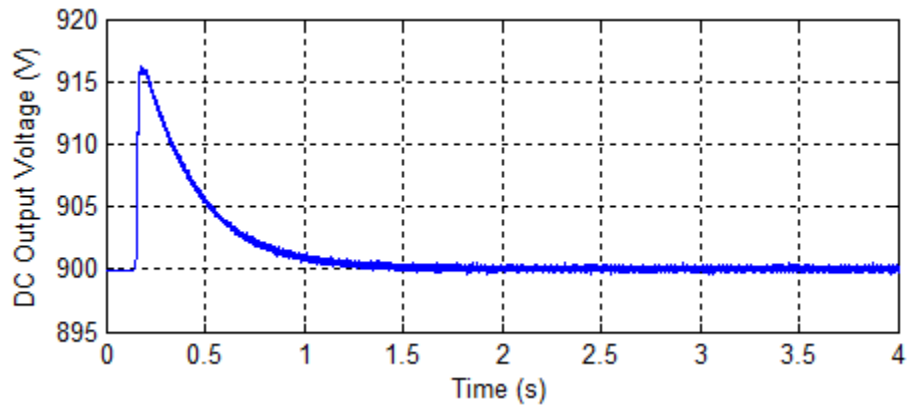


Figure 70. DC output voltage of the AC/DC converter in inverter mode

In Figure 71, a zoom on the AC voltage and current of a single phase shows that PWM also gives low distortion in rectifier mode and as before, the power factor is equal to 1.

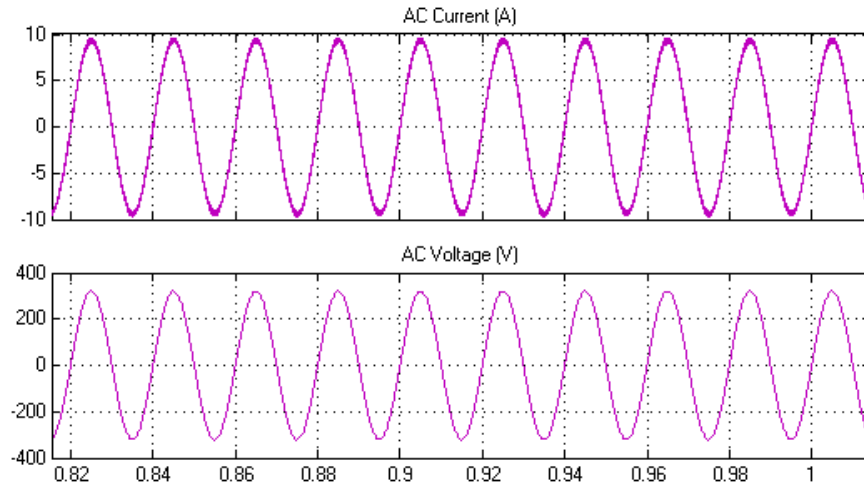


Figure 71. Zoom on AC Voltage and current in inverter mode

### V.e.3. Railway converter

The railway converter recuperates the braking energy from railway side and injects it into the DC busbar. Its control depends on the catenary/3<sup>rd</sup> rail's DC voltage. It should detect trains braking phase, recuperate its regenerated energy and stop when the braking phase ends or a close train starts consuming energy. That means power exchanging between trains should be respected or more power will be absorbed from substations and the energy bill will increase.

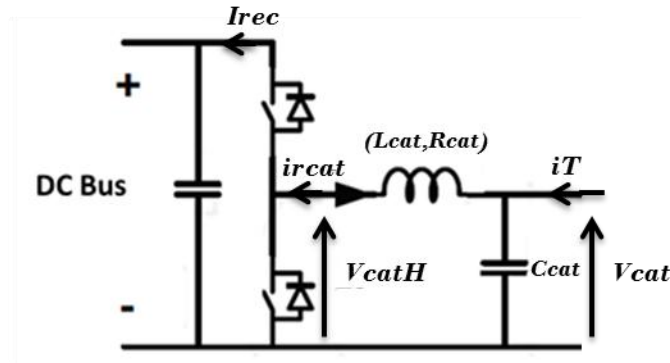


Figure 72. DC/DC converter connected to railway

A voltage loop is used to control the DC/DC converter. Figure 73 below shows the employed regulation. The voltage regulation at railway side should be fast enough to recuperate the braking energy before the activation of the rheostat braking.

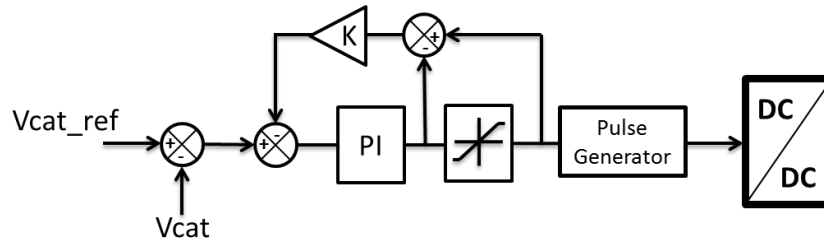


Figure 73. Regulation loop of the DC/DC converter connected to railway

The corrector's parameters were found by tuning:  $k_{pr} = -0.7$  and  $k_{ir} = -0.7$

When applying a constant reference voltage, there's a risk that if another train accelerates while the converter is recuperating the braking energy of the first train, the energy exchange between trains won't be respected. In this case, more energy will be absorbed from the substation nearby. Therefore, another strategy should be adopted. In Figure 74, the controlled current loads represent two trains T1 and T2. T1 starts braking at  $t=0.1s$  and T2 accelerates at  $t=0.4s$  (see Figure 75). The DC voltage source and its associated diode represent the diode rectifier substation (SST).  $V_{SST}$  is equal to SST's no-load voltage (780 V). The resistor "R" represents the catenary between T1 and T2.

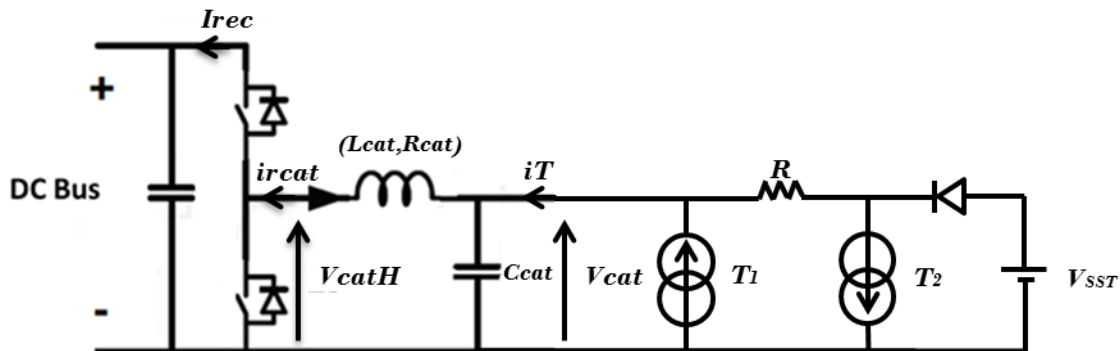


Figure 74. DC/DC converter connected to trains and a SST

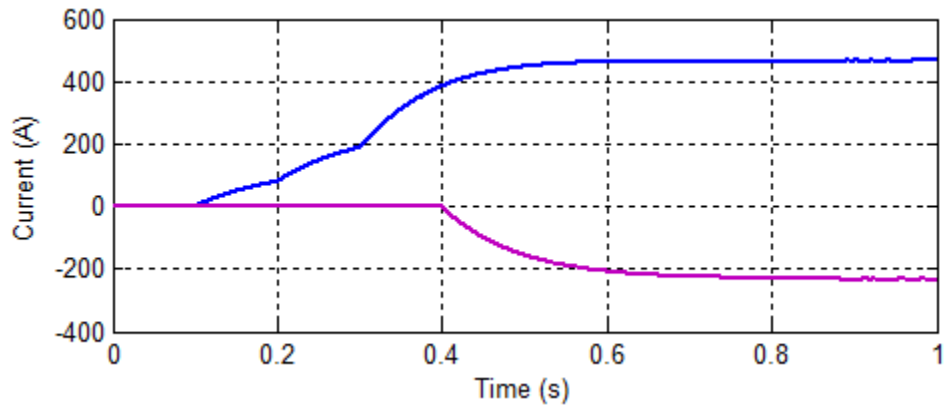


Figure 75. Braking current injected by T1 (Blue) and Traction current absorbed by T2 (Pink)

First, a constant reference voltage of 800V is injected in the voltage regulation loop. If power exchange is respected, no current should be absorbed from the SST because T1 is regenerating enough energy. The Figure 76 shows the current absorbed from the SST. It is not null therefore this solution is not effective. Figure 77 shows the regulated voltage at railway side.

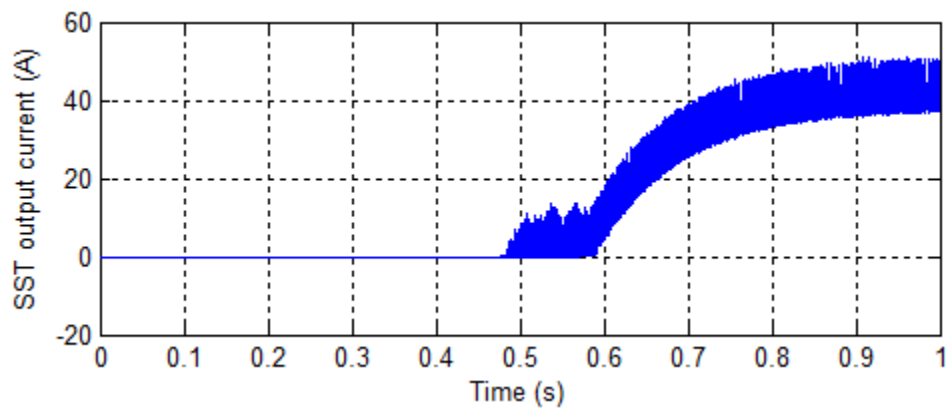


Figure 76. Current consumed from the Substation

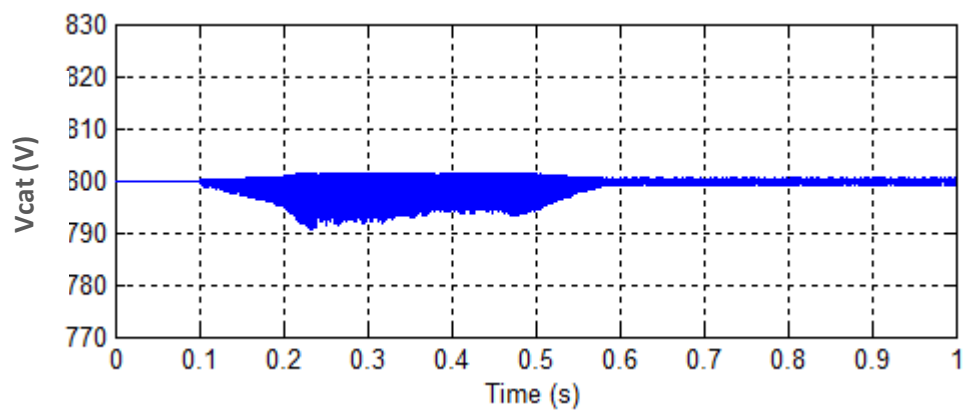


Figure 77. DC/DC converter output voltage  $V_{cat}$  at railway side

Now, another solution is based on the variation of the recuperated current. The flow chart in Figure 78 describes this strategy.

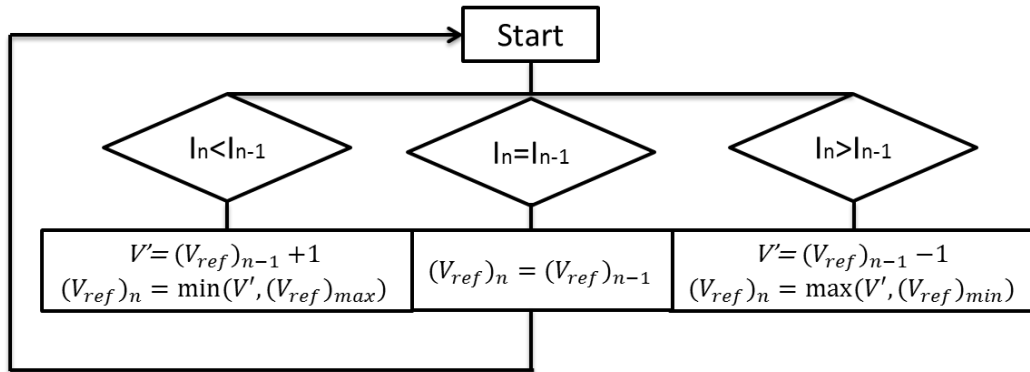


Figure 78. Reference voltage calculation

The same simulation is run with the new reference voltage calculation. Figure 79 shows that no current is consumed from the SST. The power exchange is thus respected. Figure 80 shows the regulated voltage variation at railway side.

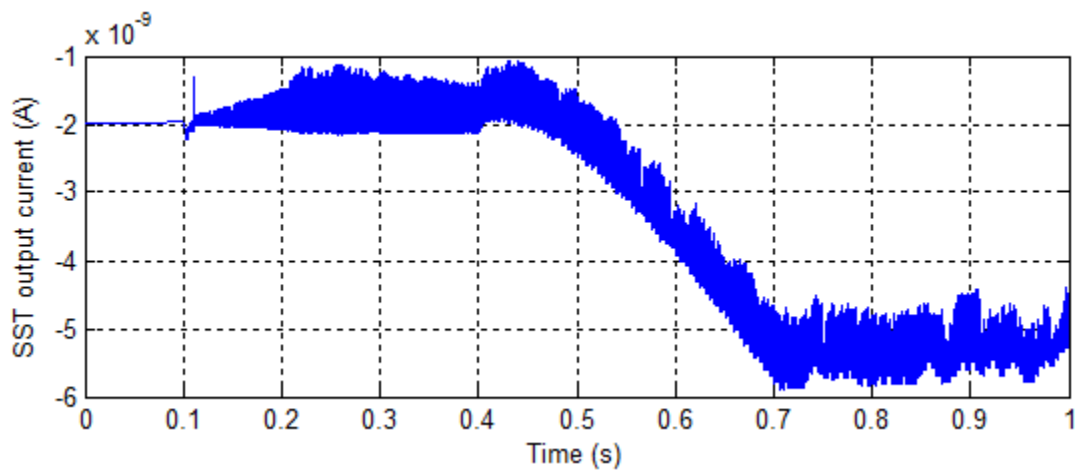


Figure 79. Current consumed from the Substation

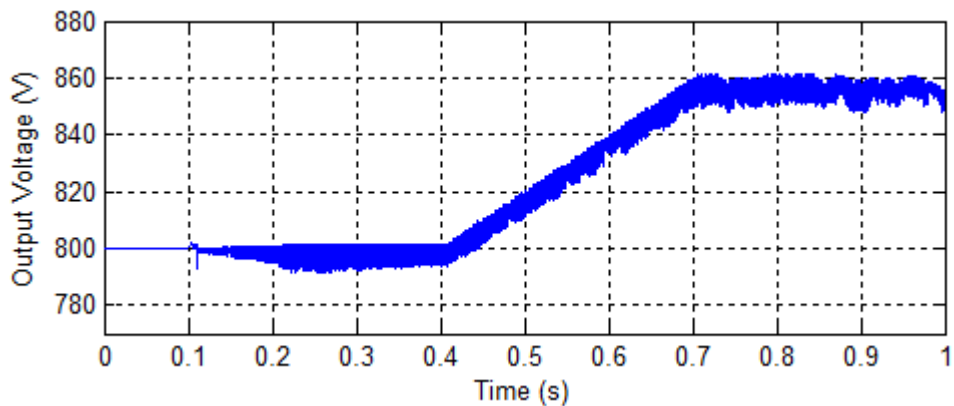


Figure 80. DC/DC converter output voltage at railway side

Note that the recuperated power is calculated in the converter's unit controller and is communicated instantaneously (response time between 500  $\mu$ s and 1 ms depending on employed controllers) to the PMS in order to send the necessary information to the Micro-grid's different components.

#### V.f. POWER MANAGEMENT SYSTEM

The Power Management system (PMS) is an energy router that manages the micro-grid by directing power flows. A decentralized control is applied for the micro-grid. Control units can be installed at subsystem's level. They are in charge of controlling locally each device. Their control functions consist of independent tasks that don't need to communicate with other devices nor have a global overview of the micro-grid such as voltage regulation. Controls units are then connected to a central unit, the PMS. It ensures coherence between subsystems' behavior and the scenario selected by the operator. It allows also respecting the micro-grid's constraints. For example, it supervises the storage's capacity and current limitations.

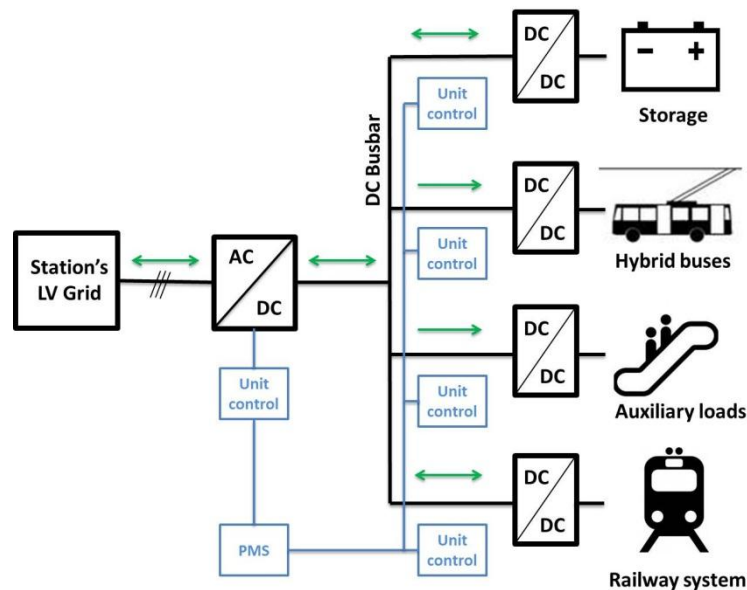


Figure 81. Decentralized control of the DC micro-grid

The system operates in four different modes: Recovery Mode (RM), Feeding Mode (FM), Standby Mode (SM) and emergency mode (EM). Table 7 describes the PMS behavior for each one of these modes selected depending on different possible scenarios. Functions are tagged with the letter "P" followed by a number that indicates the decreasing priority order (Top priority = 1).



OM	Railway	SC	Battery	Hybrid buses	Auxiliary Loads	Inverter
RM 1	Braking energy available	SOE (SC) < 1 (Charging) <b>P1</b>	SOE (Bat) ≤ 1 (Charging ) <b>P2</b>	Not connected	Connected (consuming) <b>P3</b>	Feeding power to the AC grid <b>P4</b>
RM 2	Braking energy available	SOE (SC) = 1 (fully charged)	SOE (Bat) = 1 (fully charged)	Not connected	Connected (consuming) <b>P1</b>	Feeding power to the AC grid <b>P2</b>
RM 3	Braking energy available	SOE (SC) = 1 (fully charged)	SOE (Bat) = 1 (fully charged)	Not connected	Not connected	Feeding power to the AC grid <b>P1</b>
RM 4	Braking energy available	SOE (SC) < 1 (charging ) <b>P2</b>	SOE (Bat) ≤ 1 (charging) <b>P3</b>	Connected (Charging) <b>P1</b>	Connected (consuming) <b>P4</b>	Feeding power to the AC grid <b>P5</b>
SM	No braking energy	Standby	Standby	Not connected	Not connected	Standby
FM	No braking energy	SOE (SC) > 25% (discharging) <b>P1</b>	SOE > 30% (discharging) <b>P2</b>	Connected (charging) <b>P1</b>	To be disconnected	Consuming power from the AC grid <b>P3</b>
EM	Fault case*	SOE > 25% (discharging) <b>P1</b>	SOE > 30% (discharging) <b>P2</b>	To be disconnected	To be disconnected	Consuming power from the AC grid <b>P3</b>

\* a need to feed power into the catenary or 3<sup>rd</sup> rail after fault detection in railway system

**Table 7. PMS different scenarios**

Four recovery modes are considered when braking energy is detected at railway side (see paragraph V.d.3) and injected into the Micro-grid. The energy is managed by the PMS according to the following:

- If no electric hybrid bus is connected to the Micro-grid: Priority P1 is given to supercapacitor (SC) while it is still not full (SOE (SC) < 1). Batteries come as a second priority (P2). They are charged with their nominal current (720A). In case auxiliary loads are connected, the excess of energy will serve to feed them as they are considered as a third priority (P3). The last one (P4) is given to injecting energy to AC grid; the inverter should operate only to ensure DC busbar's voltage stays in an acceptable ±40 V range.
- If an electric hybrid bus is connected to the Micro-grid: the highest priority (P1) is for charging the bus. If there's energy left, it will go for SC (P2) then batteries (P3). Auxiliary loads when connected and AC grid come with least priorities (P4 and P5).

Standby mode (SM) represents the case where there's no energy flow within the Micro-grid. Feeding mode (FM) represents the case where no braking energy is available and a bus is connected. The hybrid storage system should then provide needed energy. Power exchange happens in priority between the bus and SC (P1). Batteries (P2) step in when SC's SOE goes below 50% (see Table 4). As in previous modes, energy can be absorbed from the AC grid for stabilizing the busbar's voltage (P3). Last but not least, given the fact that a large storage system is installed in the station and that now, through the micro-grid, a power bridge exists between the station's grid and the traction grid, an additional mode, emergency mode (EM), can be configured. EM allows in traction fault cases injecting power into the catenary/3<sup>rd</sup> rail to help trains reaching the station and evacuating passengers. In addition, in every station, an emergency storage system exists to supply emergency exits, lights... It could be also replaced by the micro-grid storage system.

The micro-grid can also be connected to particular loads in the station (e.g. escalators, elevators...) that are also capable of regenerating electrical energy. In fact, when an escalators is going down in rush hours, the motor brakes to maintain its speed even with passenger's weight. Hence, instead of dissipating this braking energy into heat, it could be recuperated, stored and re-injected when needed. This is an interesting application especially in modern passengers' station with high energy consumption.

### **V.g. USE CASE: APPLICATION ON PARIS METRO LINE 13**

In order to demonstrate the efficiency of the DC micro-grid concept, separate simulations should be done using ELBAS, a multi-train simulator used by Alstom Transport (see Appendices-C), and Matlab-Simulink because it is not possible to create a direct link between ELBAS and Simulink allowing a simultaneous simulation. Therefore, the railway system is first simulated using ELBAS. The output of this simulation is the recuperated power as function of time. It is given in an Excel file format and then saved in Matlab variables to be used in the Simulink model.

#### **V.g.1. ELBAS simulation**

In this study, the simulation is based on RATP metro line 13 in Paris to evaluate the amount of braking energy that can be stored. It is considered that DC micro-grid with the hybrid buses charging station will be located in "Porte de Saint-Ouen" metro station (Figure 82). Only the left part, starting from "Invalides" station, was simulated because in normal mode, this part can be considered electrically independent from the right part. More precisely, braking energy recuperation at "Porte de Saint-Ouen" is not impacted by trains running on the right side of "Invalides". In addition, a power substation is connected at this station and thus, it separates electrically both sections.

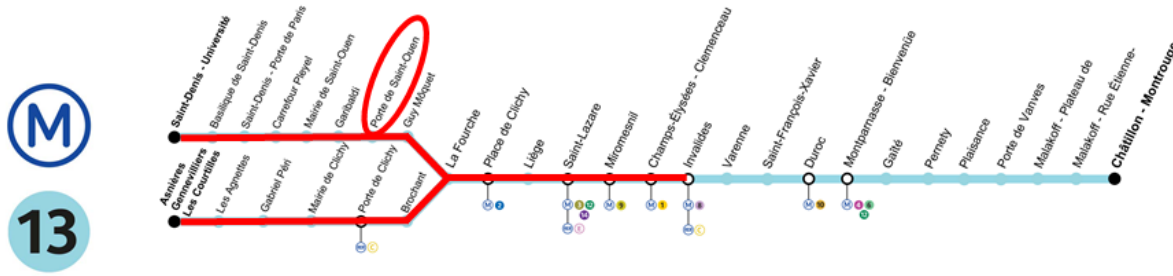


Figure 82. Paris metro line 13 simulated in ELBAS

Four scenarios have been simulated (Table 8), each one corresponding to a different headway (time delay between two consecutive trains). The simulated timetables were calculated in a way that takes into consideration all possible trains' crossings (worst case for power consumption):

Headway (s)	Simulation time
95	2 h 23 min
100	2 h 38 min
175	5 h 08 min
290	5 h 50 min

Table 8. Simulation time calculated for each headway

When trains brake, the line's voltage increases. To protect the line from over-voltages, the on-board rheostats are activated once the voltage reaches 900V. Therefore, the input voltage of the converter should be less than 900V and higher than the no load voltage of the nearest substation to avoid consuming energy from it. In this use case, the nearest substation has a 750V no-load voltage. The converter's input voltage was then set to a value of 820V. The simulations were done with a 1 second time step and a 10 meters KP (Kilometric point) step. ELBAS calculated the converter's recuperated power at each time step. Figure 83 shows the profile of the power recuperated by the DC/DC converter connected to the railway system. It is extracted in an Excel file to be used as an input to Matlab-Simulink model.

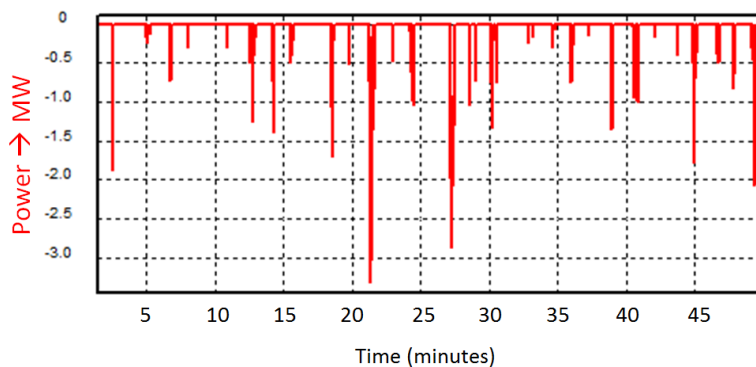


Figure 83. Extract of Converter's time function power curve calculated by ELBAS for 95s headway

The power pulses are intermittent and depend on trains speed profile and relative position. More power is recuperated when trains are braking at the same time closely enough to the DC/DC converter. The duration of these power peaks is generally shorter than ten seconds which justifies the usage of supercapacitors.

#### V.g.2. Simulink model simulation

All converters described earlier are now connected through a DC micro-grid (Figure 81). In addition, passive RLC filters are added to avoid interaction between chopped currents and cables' inductance. This could cause undesired voltage peaks that may cause equipment damage.

At  $t=0.1s$ , a train starts to brake. The railway DC/DC converter starts injecting into the DC busbar a power increasing gradually up to 400 kW. At  $t=0.4s$ , the bus consumes 200 kW with a 0.1s of rising time. Figure 84 shows the braking power injected into the system through the DC/DC railway converter.

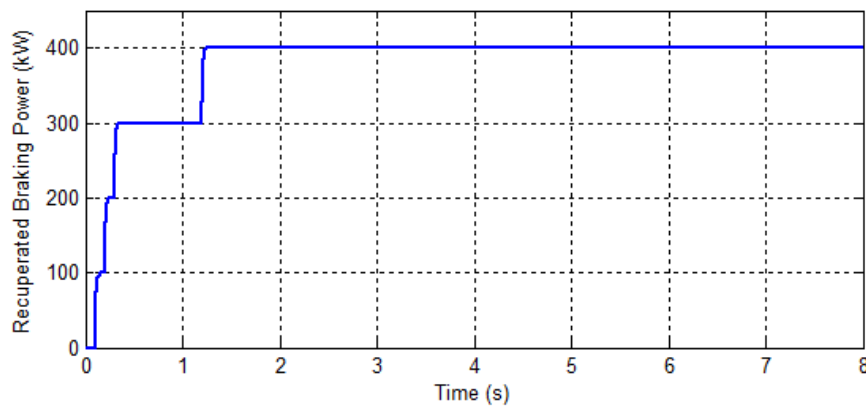


Figure 84. Braking power injected into the Micro-grid through railway DC/DC converter

This power is communicated to the PMS in order to calculate SC's reference current ( $I_{scL\_cons}$ ). Figure 85 shows how the SC's measured current follows its reference value. Reference current's drop at  $t=0.4s$  is due to charging the hybrid bus. This scenario was chosen because it requires all converters working at the same time.

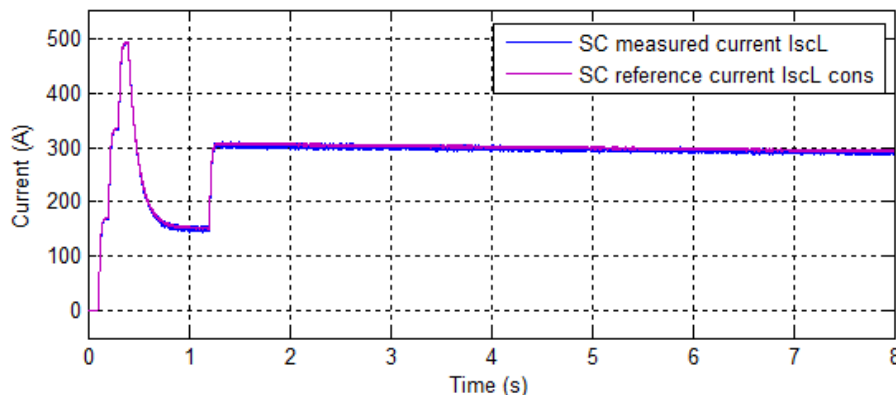


Figure 85. Reference and measured currents of SC's DC/DC converter

Figure 86 shows current at AC side variation according to DC busbar voltage. The AC/DC converter does not work permanently. It interferes according to the concept presented in Figure 58. When DC voltage reaches 940 V (as at  $t=0.31s$ ), the converter injects energy to the AC grid until it is reduced to 920 V. In the opposite case, when voltage drops to 860 V (as at  $t=6.55s$ ), the converter will consume energy from the AC grid to boost the voltage up to 880 V.

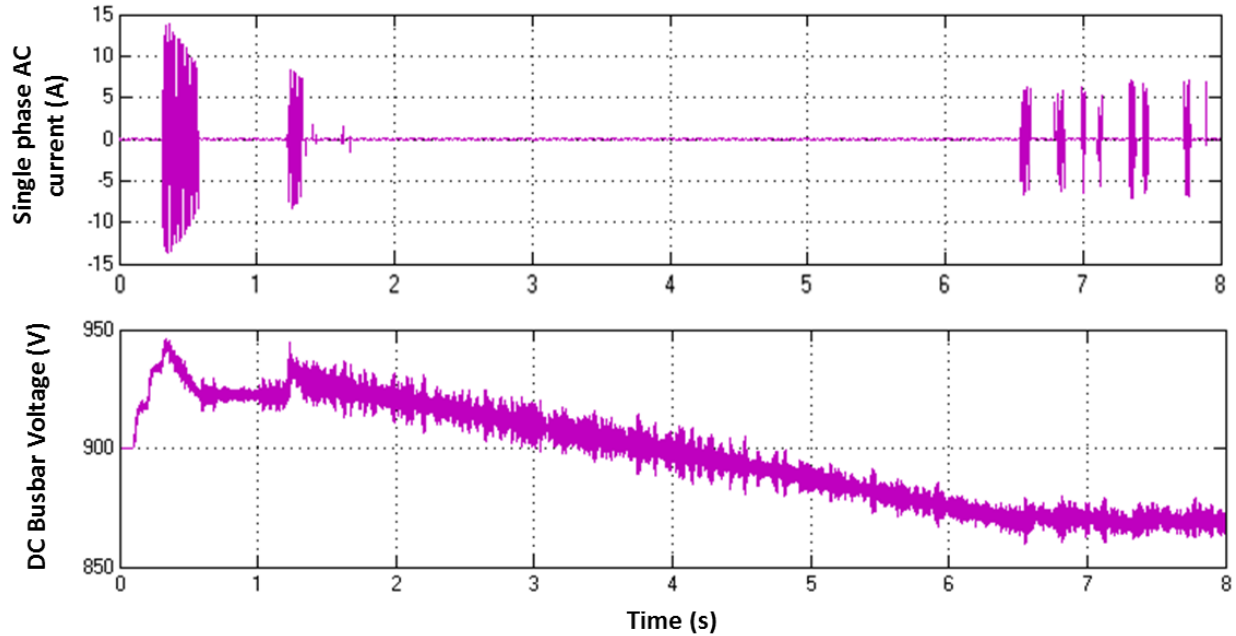


Figure 86. Measured current at AC side and DC busbar voltage

Even though the voltage is stable, 20V ripples (peak) are also measured. In order to see whether they impact current's quality at AC side, the FFT of a single phase current is done on an operational period of the converter. Figure 87 shows that harmonics are negligible.

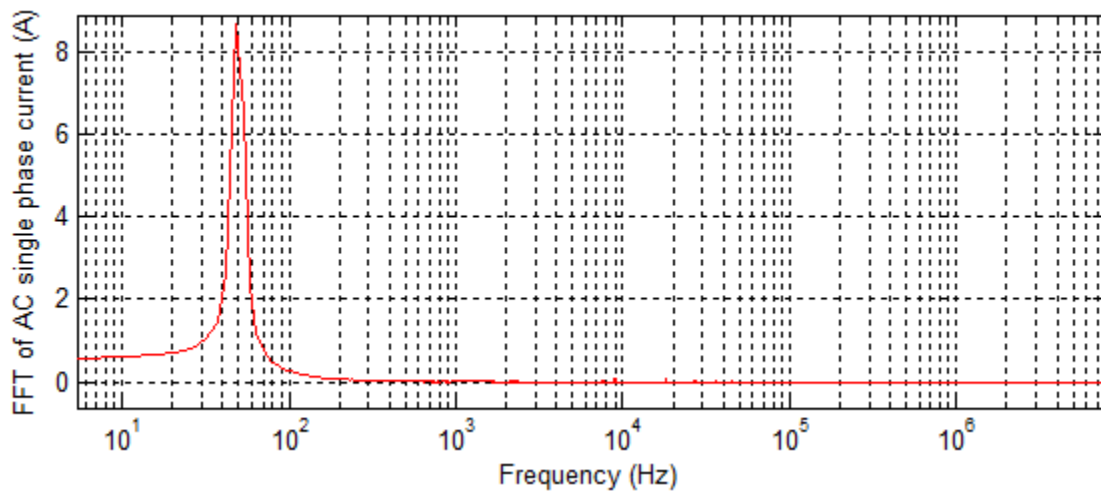


Figure 87. FFT of current injected into AC grid during converter's operational period

Figure 88 also shows that the current injected into the AC grid is in phase with the voltage which confirms the PFC function of the AC/DC converter.

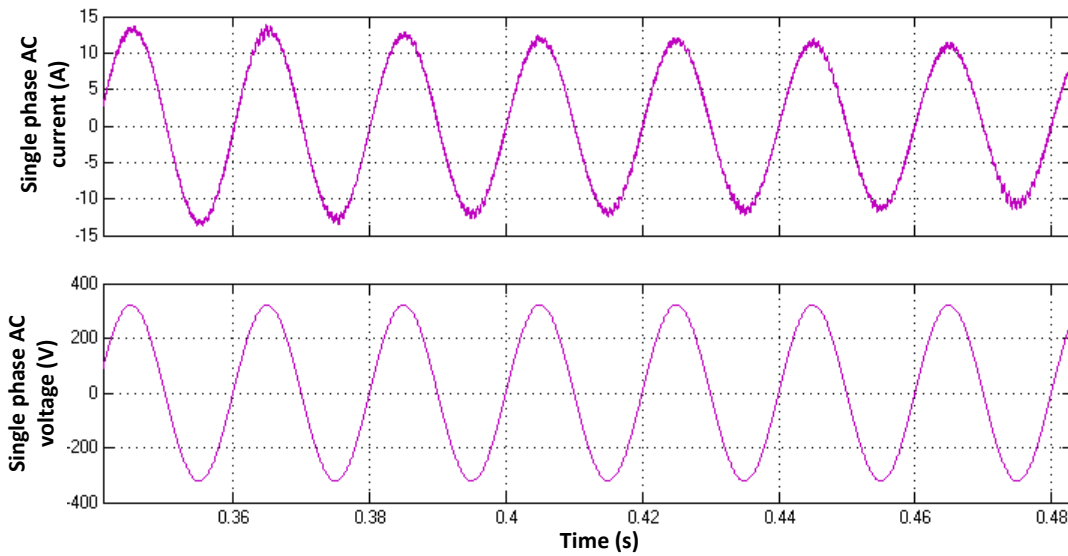


Figure 88. Zoom on AC current and voltage

### V.g.3. Simplified model simulation in Matlab

As mentioned before, 4 scenarios were simulated using ELBAS. Each scenario corresponds to a different headway. The simulation's timetable varies also from one scenario to another. It is calculated to include as many as possible different trains crossing positions. Given the fact that this duration is longer than an hour, simulating the electronic detailed model will be difficult because the time step of this simulation is too small and a very large memory is needed. Therefore, an energetic model was simulated in Matlab in order to evaluate the energy flow and thus a preliminary dimensioning. It is based on the flow chart showed in Figure 89. It is sufficient to evaluate the amount of braking energy that can be stored.

For each time step ( $T_s = 0.1s$ ), recuperated energy  $E_r$  is imported from ELBAS simulation's results. The next SC voltage ( $V_{sc\_next}$ ) needed to absorb this energy is calculated. If it's higher than SC's maximum voltage ( $V_{scmax}$ ), it is set equal to the latter. Duty cycle ' $\tau$ ' is then calculated. It represents the SC DC/DC converter's command. ' $\tau$ ' should be less or equal to 1. A higher value is not physically feasible during  $T_s$ . Thus,  $V_{sc\_next}$  should be recalculated to its realistic value. If its SOE is higher than 50%, the battery steps in and  $I_{bat}$  is set to the battery's nominal charging current ( $I_n$ ). The final value of  $V_{sc}$  can now be evaluated and the energy left from  $E_r$  will serve to calculate next busbar's voltage ( $V_{dc\_next}$ ). Based on AC/DC converter's control (see paragraph V.d.2), the energy sent to the grid is evaluated and  $V_{dc}$  is set to its new value. These steps are repeated every time step  $T_s$ .

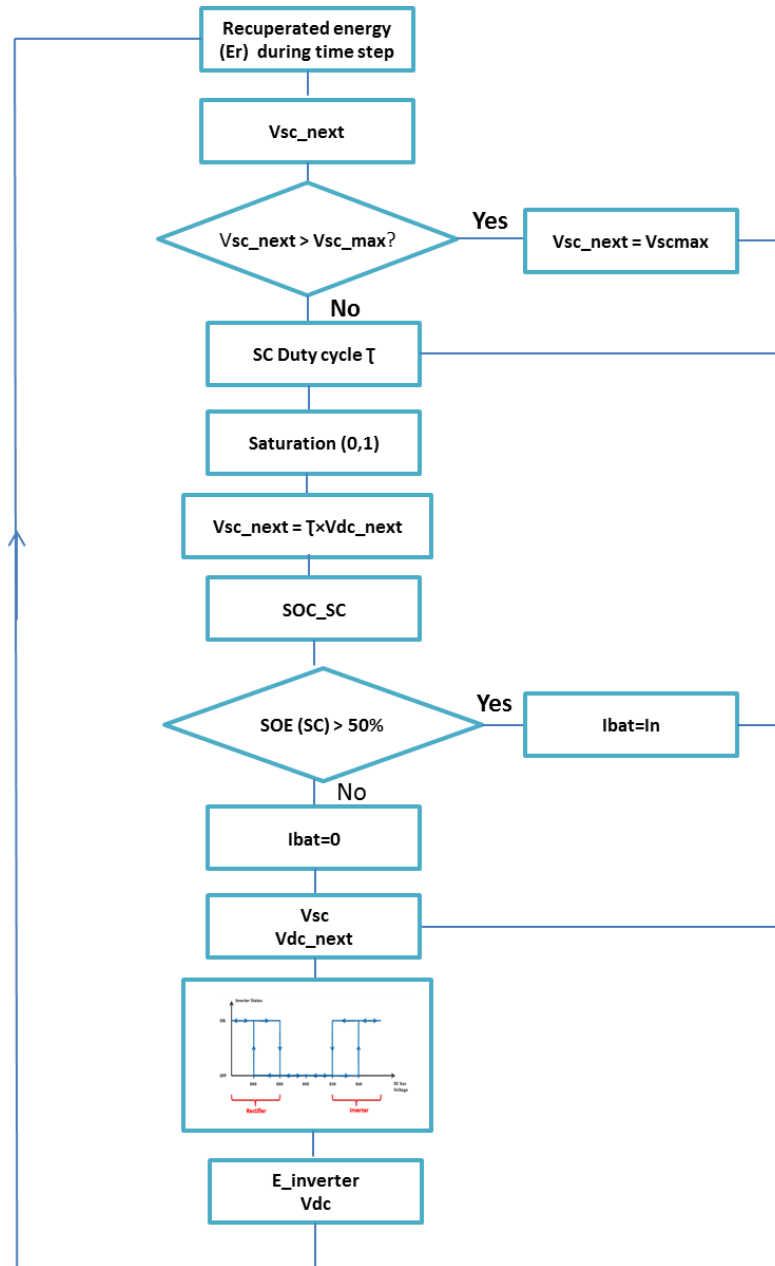


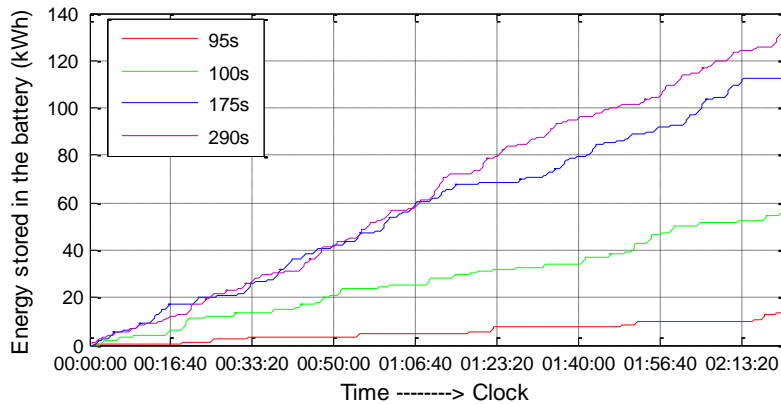
Figure 89. Average model's flow chart

Table 9 shows the amount of recuperated energy (input from ELBAS) and its distribution between the energy storage system and the grid. Note that the simplified model does not take into consideration energy losses. Therefore, it would be more realistic to multiply presented energy values by the system's energy efficiency. In addition, it is important to remind that the simulated timetable is not an extracted real timetable because there was no possibility to get it. Therefore we took a timetable, the must constraining energetically, that is normally used for infrastructure dimensioning. Thus, these energy values are theoretical. Real values cannot be predicted especially for Metro 13 which traffic is not automatic and depends directly on drivers' behavior.

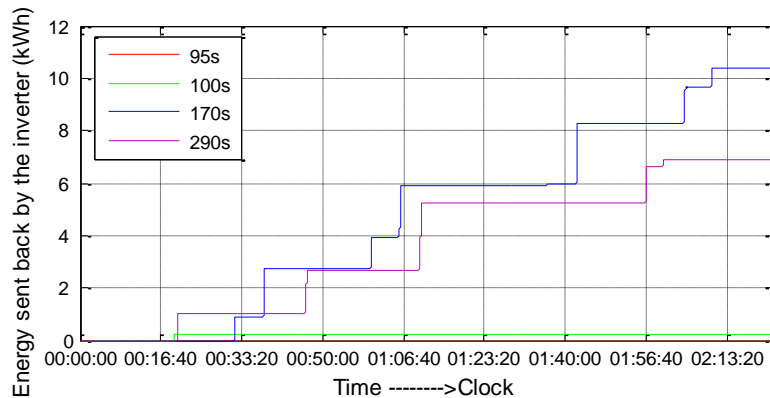
Headway (s)	Timetable duration	Recuperated braking energy (kWh)	Energy stored in the hybrid storage system (kWh)	Energy sent back to the grid (kWh)
95	2h 23min	13.4	13.4	0
100	2h 38min	60.33	60.1	0.23
175	5h 8min	284.7	254.46	30.29
290	5h 50min	336.4	324.3	12.1

**Table 9. Energy flow evaluation**

Figure 90 (a) and (b) show an extract of energies evolution stored in the battery and fed back to the AC LV grid during first two hours when no hybrid buses are connected. In the present case, the lowest energy is recuperated for the headway 95s corresponding to peak hours. In fact, trains are too close favoring energy exchange and reducing energy lost in on-board resistors. The more headway increases, the more trains are far from each other. Thus, more energy will be burned due to catenary's low receptivity. It is then recuperated by the DC/DC converter connected at railway side. The highest amount of energy is registered for headway 290s.



(a)



(b)

**Figure 90. Energy stored in the battery (a) and the energy sent back to the grid (b) for different headways**



As mentioned earlier, the defined use case, in collaboration with RATP, considers a hybrid electric bus charging every one hour. In order to calculate the total amount of energy per day, Table 10 presents the energy flow in the DC micro-grid brought back to one hour with the number of hours during which different headways are applied. For a 95s headway, trains are too close and the traffic is very dense. Therefore, the line's receptivity is efficiently high and the majority of braking energy is exchanged between trains. The more headways increase, the more trains are distant and the line's receptivity decreases. This explains the increasing recuperated energy when headway increases. In this case study, charging an electric hybrid bus needs 13.33 kWh (200kW during 4 minutes) available each hour. For 95s headway, the recuperated energy is not enough. But, just before this headway, there's two hours of 175s which allows storing 99 kWh. After charging three buses (at 5h30, 6h30 and 7h30), the excess of energy (59 kWh) will compensate the lack of next three hours with 95s headway.

Headway (s)	Recuperated braking energy per hour (kWh)	Energy stored in the hybrid storage system per hour (kWh)	Energy sent back to the grid per hour (kWh)	Time range	Total number of hours
95	5.62	5.62	0	7h30-10h30	3
100	22.91	22.82	0.09	16h30-19h30	3
175	55.46	49.57	5.9	5h30-7h30 10h30-16h30 19h30-21h30	10
290	57.67	55.59	2.07	21h30-1h00	3.5
Total per day	842.035	775.585	66.515		

Table 10. Energy flow per hour

#### V.g.4. Economic evaluation

RATP estimates the energy consumption for charging hybrid buses between 800 and 1000 hours a year with an average power of 200 kW. As mentioned before, the expected energy subscription is a regulated tariff known as "104ptimi vert A5 courte 104ptimizatio", or green tariff A5 short usage, with a maximum power of 750 kW. Table 11 shows EDF's tariff:

Version		Annual fix prime (€/kW)	Energy Price (c€/kWh)				
			Winter			Summer	
			Peak	Peak hours	Off-Peak hours	Peak hours	Off-Peak hours
	Very long usage	74,16	7,154	5,820	4,452	4,458	2,820
	Long usage	54,60	10,421	6,667	4,606	4,525	2,881
	Moderate usage	43,20	14,210	7,772	4,934	4,600	2,877
	Short usage	30,24	21,387	9,782	5,305	4,600	2,727
Reduced power coefficient	Very long usage		1,00	0,67	0,27	0,23	0,23
	Long usage		1,00	0,76	0,40	0,37	0,34
	Moderate usage		1,00	0,75	0,36	0,33	0,28
	Short usage		1,00	0,78	0,52	0,46	0,42
Overtaking computation	Count	Electronic	KN (PMAX-P)			K (PMAX-P)	
	(k <sub>3</sub> , k <sub>2</sub> , k <sub>1</sub> )	4,39 €/kW	1,46 €/kW			36,59 €/kW	
	Coefficients per poste		1,00	0,67	0,27	0,23	0,23

**Table 11. EDF tariff for an A5 base contract to be applied from 01/01/2014 [TAR02]**

Peak hours	Winter rush hours	Winter off-peak hours	Summer rush hours	Summer off-peak hours
N/10	7N/20	N/10	7N/20	N/10

**Table 12. Distribution of consumption hours (N)**

Considering the hours distribution in Table 12, the cost of the consumed energy is calculated below:

- For N=800 h:

$$\begin{aligned}
 \text{Cost} &= 200 \times 800 \times \left( \frac{1}{10} \times 21.387 + \frac{7}{20} \times 9.782 + \frac{1}{10} \times 5.305 + \frac{7}{20} \times 4.6 + \frac{1}{10} \times 2.727 \right) \\
 &= 1\,276\,096 \text{ c€} = 12\,760.96 \text{ €}
 \end{aligned}$$

- For N=1000 h:

$$\begin{aligned}
 \text{Cost} &= 200 \times 1000 \times \left( \frac{1}{10} \times 21.387 + \frac{7}{20} \times 9.782 + \frac{1}{10} \times 5.305 + \frac{7}{20} \times 4.6 + \frac{1}{10} \times 2.727 \right) \\
 &= 1\,595\,120 \text{ c€} = 15\,951.2 \text{ €}
 \end{aligned}$$

In addition to this cost, an annual fixed tax is added. It is calculated for a short usage based on reduced power coefficients (see Table 11). In fact, the maximum subscribed power depends on tariff periods. For example, in peak hours, it is better to reduce the maximum power because its coefficient is equal to 1 (it is most penalized). In general, maximum power increases when going from peak hours to summer's off-peak hours (see Figure 91).

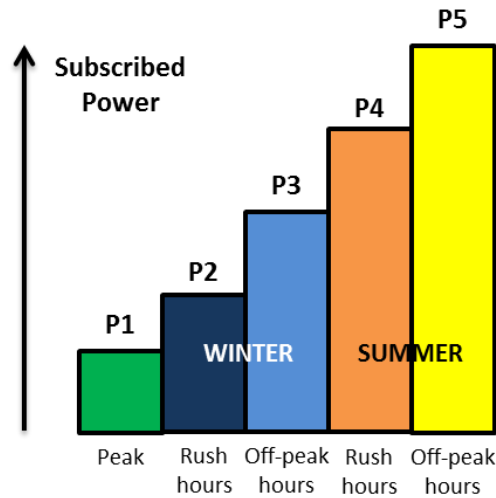


**Figure 91. Maximal subscribed power variation for an A5 base contract with EDF**

Based on Figure 91 and Table 11, the reduced annual fixed prime is calculated as follows:

$$Pr = P1 + 0.78 \times (P2 - P1) + 0.52 \times (P3 - P2) + 0.46 \times (P4 - P3) + 0.42 \times (P5 - P4) \quad (V-22)$$

In this use case, the information we had is that maximum power is 750 kW. No other indication on power variation was given. Therefore, in order to reduce the prime a little, we consider  $P1=250$  kW and  $P2=P3=P4=P5=750$  kW. Table 13 shows additional costs calculated based on previous assumptions.

	Annual fixed cost for 750 kW	TVA (19.6 % of total cost)	TICFE 0.5 c€/ kwh	CSPE 0.9 c€ / kWh
Short utilization (< 2000 h)	19021 €	800h: 6215 € 1000h: 6855 €	800h: 800 € 1000h: 1000 €	800h: 1440 € 1000h: 1800 €

**Table 13. Additional Costs**

Based on the tables above, the calculation of the annual energy bill shows that charging the electric hybrid buses from the national grid (EDF) will cost RATP between 40 237 € and 44 627€ without taking into consideration the cost of connection to the grid which costs more than 11 000 € and the price of the charging station (transformer, converters, filters, building...) which is estimated to 400 k€. Therefore, for 10 years, this solution costs between 800 k€ and 1 million euros.

Concerning the DC Micro-grid, the investment cost does not exceed 500 k€ (estimated cost based on the market). It remains less expensive than the alternative pre-fabricated solution because no energy contract is needed.

## V.g.5. Conclusion

The figure below represents the braking energy distribution per hour:

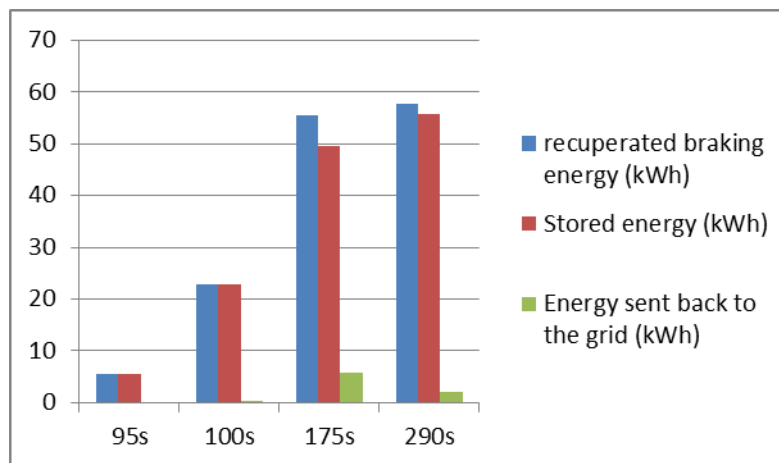


**Figure 92. Braking energy distribution per hour**

The hybrid storage system is capable to store a big amount of the recuperated energy. This energy is enough to charge every 1 hour a hybrid bus with a constant power of 200 kW during 4 minutes. For the headway 95s where the energy stored is relatively low, the excess of energy provided by the rest of headways will compensate the difference. In addition, the energy sent back to the grid will be used by the loads in the station (light, screens, escalators...) which will reduce the total energy bill.

The advantage of this solution is that the charging station will be connected at station's low voltage level (220 V-320 V). No additional contract is needed in contrary, the excess of braking energy will be used internally in the station. The table below compares the pre-fabricated charging station connected to MV grid and Alstom's solution using LV connection.

	Charging station connected to ERDF MV (20 kV)	Braking energy recuperation connected to RATP LV (220 V-320 V)
<b>Harmonics</b>	Penalty if RATP generates an harmonics rate exceeding the maximum rate	Due to the DC concept, less harmonics are generated.
<b>Connection Cost</b>	If ERDF's station is closer than a RATP HV branch, the solution can be more economical but ERDF power supply is more expensive.	RATP grid is distributed in almost all Paris, hence it is easy to connect. However, for sub-urban applications, more cost will be needed because of the cables brought from RATP's branches while there may exist closer

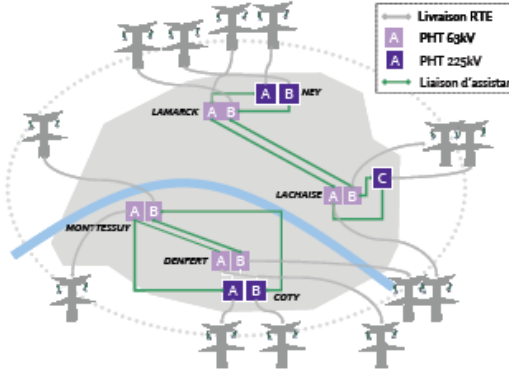
	<p>Alimentation des PHT par le RTE Schéma simplifié</p>  <p>ERDF stations.</p>	
<b>Operating Cost</b>	<p>The power consumption requests a regulated tariff called “108ptimi vert A5”. The market prices show that an ERDF supply with regulated tariff is better in summer (April to October). But these tariffs are likely to be stopped by 31<sup>st</sup> December 2015. In this case this comparison won't be valid. In addition, the tariffs “Bleu”, “Jaune” and “Vert” are regulated and increase each year in August (2 % to 8 % depending on the years and the contracts).</p>	<p>When using RATP's grid, the prices will be defined by the market (price not fixed in the contract). 1 MWh costs between 40 € and 80.90 €. Between 2007 and 2011, the average cost of 1 MWh paid by RATP for this kind of contracts has increased by 26 %.</p>
<b>Multiplication of delivery points</b>	<p>RATP can optimize these contracts by adjusting the choice of the subscribed power and by grouping the contracts. Yet by multiplying delivery points the cost may increase because of the subscription and the risk of power excess.</p>	

Table 14.Comparision between the common charging station and the DC micro-grid

In all sectors, a system should be stable in order to be used. Therefore, a stability study should always be done before system's physical implementation. Else, serious damages can be caused. For example, in robotics, an unstable robot can be dangerous and in chemistry, instability can cause unexpected reactions leading sometimes to explosions. The same problem exists in electricity. An AC grid stability is indicated by its frequency and its voltage. On one hand, frequency represents balance between power generation and demand. If production is higher than consumption, the frequency increases. The stability in this case is ensured by regulations implemented at power plants' level. For example, in steam power plant, power production can be reduced by closing valves to lower steam flow into turbines. In contrast, if production is lower than consumption, the grid's frequency decreases. The power plant will increase its generation until its maximum capacity. On the other hand, voltage stability of an AC or DC grid consists in keeping the voltage around its nominal value in spite of power flow variation (active and reactive powers for AC mode). Same as before, special regulations are implemented at power generation level. For example, when a voltage drop is detected, generators will switch to lagging mode and inject reactive power into the grid. In both cases, if the frequency or the voltage does not return to its nominal value, the grid is stable. Instability will cause materials damages and possible blackouts.

Nowadays, the electrical grid is facing fundamental changes. With the emergence of distributed energy resources such as renewable energy sources (wind, solar...), storage systems (fuel cells, batteries...) and active loads (electric vehicles, railway substations...) which are capable of producing and consuming electric power, the grid's stability becomes more complex and it will no longer be managed exclusively by power plants. This task is now responsibility of many actors. Today, studies are also investigating the advantage of using electric cars' batteries to help regulating frequency locally.

In railway DC micro-grid, the system's stability has some particularities. In classic non-isolated DC micro-grids, the main power supply remains the grid (or the power generator in case of isolated micro-grid). Therefore, the stability of the DC busbar is maintained by the AC/DC converter connected to the AC grid. In our case, the AC/DC converter is a low power device that is connected to the station's LV grid. Thus, its power capacity is rather limited. Another actor should be involved. As explained earlier, the AC grid's stability is maintained by power plants' generators and more precisely by their mechanical inertia. Hence, the latter can be replaced by a chemical inertia which is the storage system.

In the following, the instability risks in a DC micro-grid will be first described. Then, a small signal stability study is done on the system before filters' insertion. After that, a stabilization control

strategy is presented, the backstepping approach, which allows stabilizing the system using the hybrid storage system.

#### VI.a. INSTABILITY OF LOW DAMPED SYSTEMS

In general, a control system is stable, from automation point of view, if in absence of any disturbance or input, the output stays in the same state. This is called the absolute stability of the system's dynamic behavior. According to [OGA00], a linear time-invariant control system is:

- Stable or asymptotically stable if the output eventually comes back to its equilibrium state when the system is subjected to a small perturbation
- stable if the output is subject of a small deviation when a small perturbation is applied
- critically stable if oscillations of the output continue forever
- unstable if the output diverges without bound from its equilibrium state when the system is subjected to an initial condition

Figure 93 explains schematically when a system can be considered stable around a operational point.

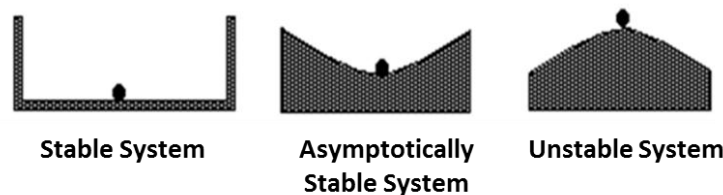
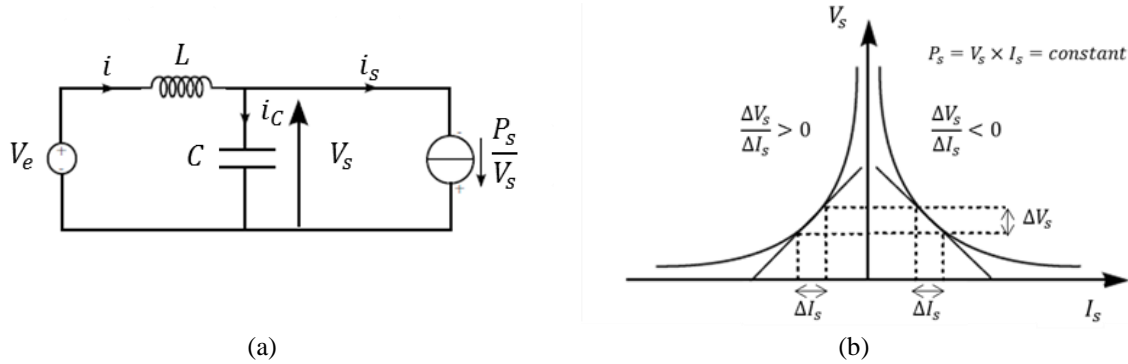


Figure 93. System's stability illustration

The most important thing in a dynamic behavior of a control system is its absolute stability which means whether the system is stable or not. A system is in an equilibrium position (or point) if it stays in the same state as long as no input or disturbance is applied. In practice, the transient response of a system often presents damped oscillations before reaching a steady state. In addition, when multi-sources and constant power loads (CPL) are connected to a DC Busbar, stability issues are faced. In the literature, this problem is usually analysed by small signal stability study which linearize the system around an operating point and makes it possible to use linear tools such as Bode and Nyquist diagrams, Routh-Hurwitz criterion [MID00], [REG00], [BAR05]. However, railway braking energy is in the shape of unpredictable power peaks that can go up to 3MW in few seconds which make it not possible to define only one operating point to the system. Therefore, it is necessary to study the Micro-grid in its non-linear form. On the other hand, some have chosen damping filters with passive elements [REG00], [ERI99]. This solution will increase the cost by over-sizing components (resistors, capacitors) which will also increase losses. In this study, trains' braking energy is stored and then used to charge the electric hybrid buses. These buses consume a constant power of 200 kW during 4-5 minutes. The problem of connecting a CPL is that its linear model behaves as a negative

resistance (Figure 94). It will then cause instability because it amplifies filters' dynamics in a resonant circuit. In the opposite case of constant power source (CPS), its linear model behaves as positive resistance. It will damp the system dynamics caused by the input filter. The figures below show the behaviour of CPL and CPS [HAM00].



**Figure 94. Linear model of a constant power load: (a) DC electrical network with CPL/CPS and (b) Negative and positive impedance of CPL/CPS [HAM00]**

#### VI.b. SMALL SIGNAL STABILITY OF THE DC MICRO-GRID

The micro-grid connects different converters that are non-linear systems. A first stability study consists in linearizing system's equations around an operational point  $X_0$ . A new equivalent linear model is then obtained. It represents the system's behavior around  $X_0$  when it's subject to small variations. If the linear model is stable, the non-linear system is stable around  $X_0$ . This method is called "small signal stability". Figure 95 shows the system's simplified architecture. In the following, the state-space representation will be done for each converter with its regulation. It is representing the physical model with a mathematical model consisting of a set of input (U), output (Y) and state variables (X) related by first-order differential equations. "State space" refers to the space which axes are the state variables. The state of the system can be then represented as a vector within that space with the following equations:

$$\dot{X} = A.X + B.U \quad (\text{VI-1})$$

$$Y = C.X + D.U \quad (\text{VI-2})$$

Where A is called "state matrix", B is called "input matrix", C is called "output matrix" and D is the "feedthrough (or feedforward) matrix". The eigenvalues of matrix A are the system's poles. If their real part is negative, the linear system is stable.



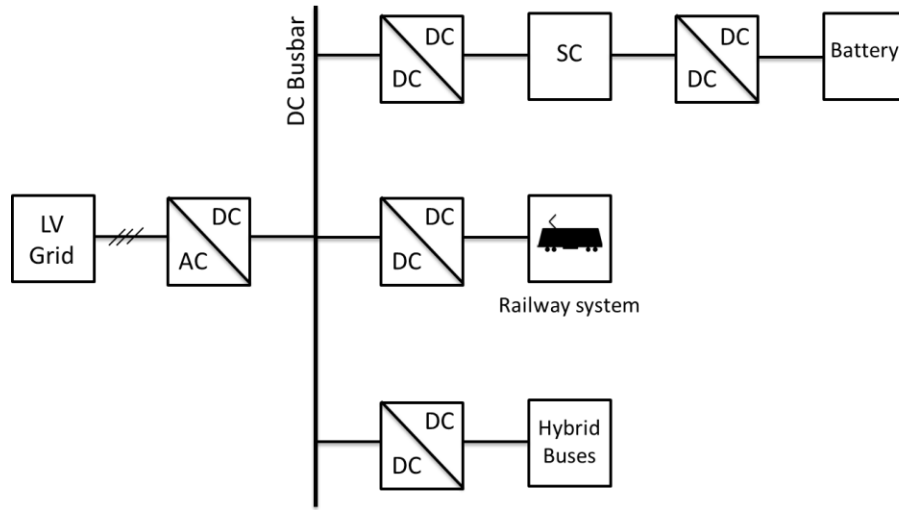


Figure 95. Architecture of DC Micro-Grid

#### VI.b.1. State-space representation of SC's DC/DC converter

First, the state-space representation of the SC's DC/DC converter is done. Then, the regulation loop is inserted in the representation to replace the control variable which is the loop's output.

- **Without regulation loop:**

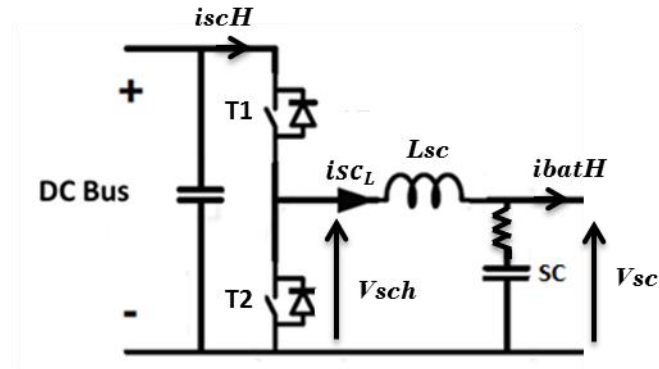


Figure 96. SC's DC/DC converter

The system's equations are presented below:

$$\left\{ \begin{array}{l} V_{scH} = V_{sc} + L_{sc} \times \frac{di_{scL}}{dt} + R_{sc} \times (i_{scL} - I_{batH}) \\ (i_{scL} - I_{batH}) = C_{sc} \times \frac{dV_{sc}}{dt} \end{array} \right. \quad \begin{array}{l} (VI-3) \\ (VI-4) \end{array}$$

The state-space representation of the SC's DC/DC converter is:

$$\begin{bmatrix} \frac{dV_{sc}}{dt} \\ \frac{disc_L}{dt} \end{bmatrix} = \begin{bmatrix} 0 & \frac{1}{C_{sc}} \\ -\frac{1}{L_{sc}} & -\frac{R_{sc}}{L_{sc}} \end{bmatrix} \begin{bmatrix} V_{sc} \\ isc_L \end{bmatrix} + \begin{bmatrix} 0 & -\frac{1}{C_{sc}} \\ \frac{1}{L_{sc}} & \frac{R_{sc}}{L_{sc}} \end{bmatrix} \begin{bmatrix} V_{scH} \\ I_{batH} \end{bmatrix} \quad (VI-5)$$

and the output is obtain by:

$$Y = \begin{bmatrix} V_{sc} \\ isc_L \end{bmatrix} = \begin{bmatrix} 1 & 0 \\ 0 & 1 \end{bmatrix} \begin{bmatrix} V_{sc} \\ isc_L \end{bmatrix} \quad (VI-6)$$

$V_{scH}$  and  $I_{batH}$  are un-measured values. They can be obtained respectively through the SC and battery regulation loop's output.

- **Insertion of SC current's regulation loop**

In converter's buck mode, T2 is always open and T1 is switching.  $V_{scH}$  is equal to  $V_{dc}$  when T1 is closed. When it opens, T2's flyback diode is active to ensure current's continuity.  $V_{scH}$  is then null. Thus,  $V_{scH}$ 's mean value over one switching period is equal to duty cycle  $x3 \times V_{dc}$ .

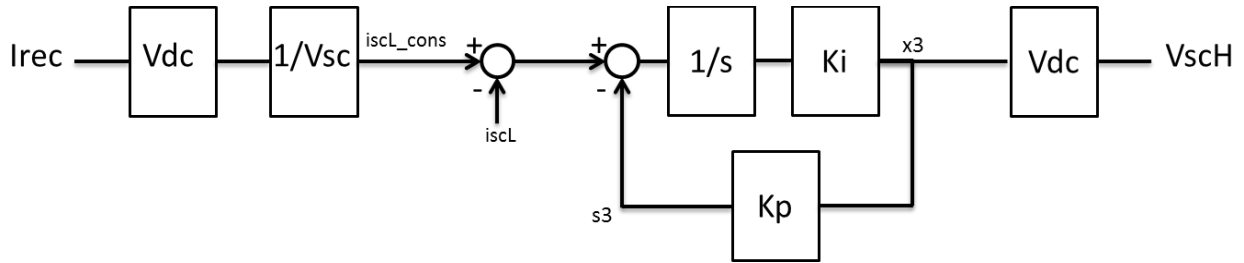


Figure 97. Control loop of the SC's DC/DC converter

$$\dot{x3} = Ki. (isc_{cons} - isc_L - kp.x3) \quad (VI-7)$$

$$V_{scH} = V_{dc} \times x3 \quad (VI-8)$$

After replacing  $V_{scH}$  in (VI-5), we obtain:

$$\begin{bmatrix} \frac{dV_{sc}}{dt} \\ \frac{disc_L}{dt} \\ \frac{dx_3}{dt} \end{bmatrix} = \begin{bmatrix} 0 & \frac{1}{C_{sc}} & 0 \\ -\frac{1}{L_{sc}} & -\frac{R_{sc}}{L_{sc}} & \frac{V_{dc}}{L_{sc}} \\ 0 & -ki & -ki.kp \end{bmatrix} \begin{bmatrix} V_{sc} \\ isc_L \\ x3 \end{bmatrix} + \begin{bmatrix} 0 & -\frac{1}{C_{sc}} \\ \frac{(ki.V_{dc}^2)}{L_{sc}V_{sc}} & \frac{R_{sc}}{L_{sc}} \\ ki.V_{dc}/V_{sc} & 0 \end{bmatrix} \begin{bmatrix} I_{rec} \\ I_{batH} \end{bmatrix} \quad (VI-9)$$

Hence, we obtain state-space representation of the DC/DC converter including its current's regulation loop. "irec", railway braking current, is an input value coming from PMS and  $I_{batH}$  can be obtained once the state-space representation of battery's DC/DC converter is done.

### VI.b.2. State-space representation of battery's DC/DC converter

The same thing is done for the battery's DC/DC converter. The state-space representation is done first for the converter in open-loop then the regulation is integrated.

- **Without regulation loop:**

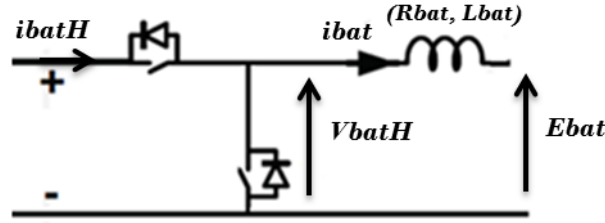


Figure 98. Battery's DC/DC converter

We consider that  $E_{bat}$  is approximately constant around an operational point. Therefore, the system can be represented by only one equation:

$$V_{batH} = R_{bat} \times i_{bat} + L_{bat} \frac{di_{bat}}{dt} + E_{bat} \quad (VI-10)$$

$$\dot{i}_{bat} = -\frac{R_{bat}}{L_{bat}} i_{bat} + \left[ \frac{1}{L_{bat}} \quad \frac{-1}{L_{bat}} \right] \begin{bmatrix} V_{batH} \\ E_{bat} \end{bmatrix} \quad (VI-11)$$

where  $V_{batH}$  can be obtained from the battery's current regulation loop.

- **With regulation loop:**

Figure 99 shows the battery's control loop. Its output ( $s4$ ) is the converter's duty cycle.

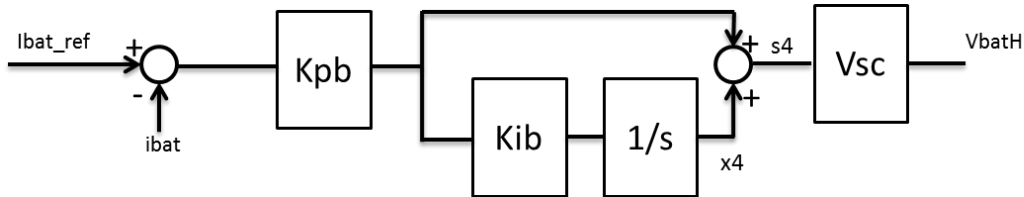


Figure 99. Battery's control loop

A new variable  $x4$  is added to the system due to the corrector's integrator:

$$\dot{x4} = K_{pb} \cdot K_{ib} (ibat_{ref} - ibat) \quad (VI-12)$$

$$V_{batH} = V_{sc} \times s4 = V_{sc} \times x4 + K_{pb} V_{sc} (ibat_{ref} - ibat) \quad (VI-13)$$

$$I_{batH} = ibat \times s4 = ibat \times x4 + K_{pb} ibat (ibat_{ref} - ibat) \quad (VI-14)$$

The state-space representation is then:

$$\begin{bmatrix} \frac{dibat}{dt} \\ \frac{dx^4}{dt} \end{bmatrix} = \begin{bmatrix} -\frac{Rbat}{Lbat} - \frac{K_{pb}V_{sc}}{Lbat} & \frac{V_{sc}}{Lbat} \\ -K_{pb}K_{ib} & 0 \end{bmatrix} \begin{bmatrix} ibat \\ x^4 \end{bmatrix} + \begin{bmatrix} \frac{K_{pb}V_{sc}}{Lbat} & -\frac{1}{Lbat} \\ K_{pb}K_{ib} & 0 \end{bmatrix} \begin{bmatrix} ibat_{ref} \\ Ebat \end{bmatrix} \quad (VI-15)$$

### VI.b.3. State-space representation of the AC/DC converter

- **Without regulation loop**

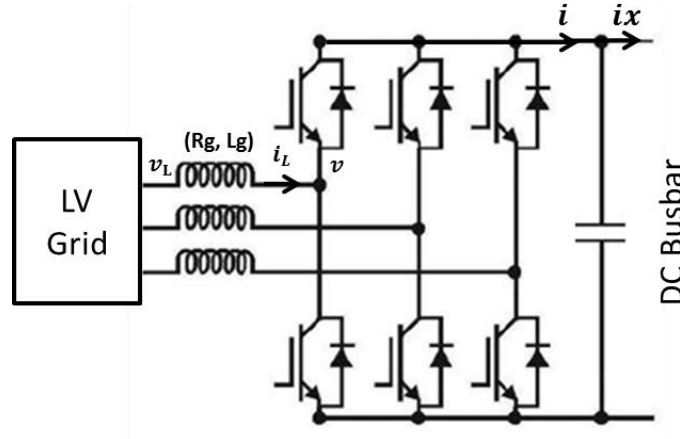


Figure 100. AC/DC converter

The AC/DC converter can be represented by the following three equations:

$$\left\{ \begin{array}{l} v_{Ld} - v_d = R_L i_{Ld} + L_g \frac{di_{Ld}}{dt} - L_g \omega i_{Lq} \\ v_{Lq} - v_q = R_L i_{Lq} + L_g \frac{di_{Lq}}{dt} + L_g \omega i_{Ld} \\ C_{dc} \frac{dV_{dc}}{dt} = i - ix \end{array} \right. \quad (VI-16)$$

(VI-16)

(VI-17)

(VI-18)

If we consider that the system is ideal and that the active power is conserved when going from AC side to DC side, the following equation allows the power to cross from the grid to the DC busbar:

$$P = V_{dc} \times i = (v_d i_{Ld} + v_q i_{Lq}) \rightarrow i = \frac{P}{V_{dc}} = \frac{1}{V_{dc}} (v_d i_{Ld} + v_q i_{Lq}) \quad (VI-19)$$

(VI-19)

$$\frac{dV_{dc}}{dt} = \frac{1}{C_{dc}} \left[ \frac{1}{V_{dc}} (v_d i_{Ld} + v_q i_{Lq}) - ix \right] \quad (VI-20)$$

(VI-20)

The system's state-space representation is then:

$$\begin{bmatrix} \dot{i}_{Ld} \\ \dot{i}_{Lq} \\ \dot{V}_{dc} \end{bmatrix} = \begin{bmatrix} -\frac{R_L}{L_g} & w & 0 \\ -w & -\frac{R_L}{L_g} & 0 \\ \frac{v_d}{C_{dc}V_{dc}} & \frac{v_q}{C_{dc}V_{dc}} & 0 \end{bmatrix} \begin{bmatrix} i_{Ld} \\ i_{Lq} \\ V_{dc} \end{bmatrix} + \begin{bmatrix} -\frac{1}{L_g} & 0 & 0 \\ 0 & -\frac{1}{L_g} & 0 \\ 0 & 0 & -\frac{1}{C_{dc}} \end{bmatrix} \begin{bmatrix} v_d \\ v_q \\ ix \end{bmatrix} + \begin{bmatrix} \frac{1}{L_g} & 0 \\ 0 & \frac{1}{L_g} \\ 0 & 0 \end{bmatrix} \begin{bmatrix} v_{Ld} \\ v_{Lq} \end{bmatrix} \quad (VI-21)$$

- **Insertion of  $i_{Lq}$  regulation loop:**

The input  $v_q$  is calculated from the output of the regulation loop of the in-quadrature current  $i_{Lq}$ . In this study, the AC/DC converter operates as a power factor corrector (PFC) by injecting only active power.  $i_{Lq\_ref}$  is then set to zero.

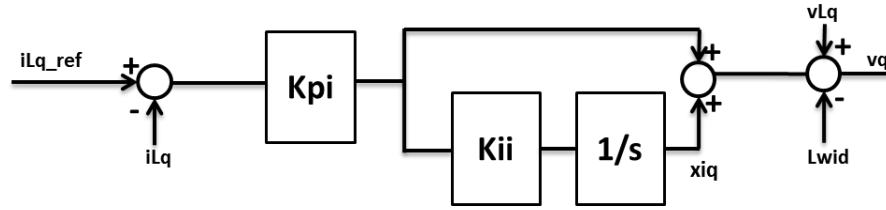


Figure 101.  $i_{Lq}$  regulation loop

$$x_{iq} = K_{ii} \cdot K_{pi}(i_{Lq\_ref} - i_{Lq}) \quad (VI-22)$$

$$v_q = x_{iq} + K_{pi}(i_{Lq\_ref} - i_{Lq}) + v_{Lq} - L_g w i_{Ld} \quad (VI-23)$$

After replacing  $v_q$  in (VI-20), we obtain:

$$\begin{bmatrix} \dot{i}_{Ld} \\ \dot{i}_{Lq} \\ \dot{V}_{dc} \\ \dot{x}_{iq} \end{bmatrix} = \begin{bmatrix} -\frac{R_L}{L_g} & w & 0 & 0 \\ 0 & \left(-\frac{R_L}{L_g} + \frac{K_{pi}}{L_g}\right) & 0 & -\frac{1}{L_g} \\ \frac{v_d}{C_{dc}V_{dc}} & \frac{v_q}{C_{dc}V_{dc}} & 0 & 0 \\ 0 & -K_{ii}K_{pi} & 0 & 0 \end{bmatrix} \begin{bmatrix} i_{Ld} \\ i_{Lq} \\ V_{dc} \\ x_{iq} \end{bmatrix} + \begin{bmatrix} -\frac{1}{L_g} & 0 & 0 \\ 0 & -\frac{K_{pi}}{L_g} & 0 \\ 0 & 0 & -\frac{1}{C_{dc}} \\ 0 & K_{ii}K_{pi} & 0 \end{bmatrix} \begin{bmatrix} v_d \\ i_{Lq\_ref} \\ ix \end{bmatrix} + \begin{bmatrix} \frac{1}{L_g} \\ \frac{1}{L_g} \\ 0 \\ 0 \end{bmatrix} \begin{bmatrix} v_{Ld} \\ v_{Lq} \end{bmatrix} \quad (VI-24)$$

- **Insertion of  $i_{Ld}$  regulation loop:**

The input  $v_d$  in (VI-21) is calculated from the output of the regulation loop of the in-quadrature current  $i_{Ld}$ . This current regulation is the inner loop of the voltage regulation. Thus,  $i_{Ld\_ref}$  is the output of DC voltage regulation (see Figure 103).

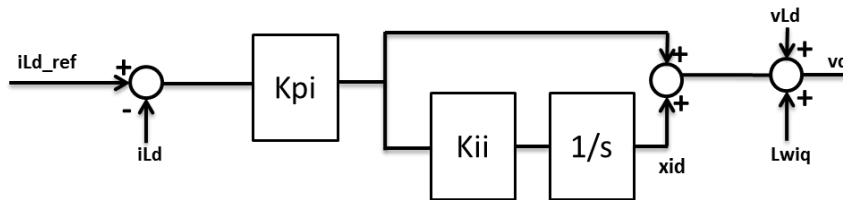


Figure 102.  $i_{Ld}$  regulation loop

$$\dot{x}_{id} = K_{ii}.K_{pi}(iLd_{ref} - iLd) \quad (VI-25)$$

$$vd = x_{id} + K_{pi}(iLd_{ref} - iLd) + vLd + L_g w i_{Lq} \quad (VI-26)$$

When replacing  $vd$  in (V-20), we obtain:

$$\begin{bmatrix} \dot{i}_{Ld} \\ \dot{i}_{Lq} \\ \dot{V}_{dc} \\ \dot{x}_{iq} \\ \dot{x}_{id} \end{bmatrix} = \begin{bmatrix} \left(-\frac{R_L}{L_g} + \frac{K_{pi}}{L_g}\right) & 0 & 0 & 0 & -\frac{1}{L_g} \\ 0 & \left(-\frac{R_L}{L_g} + \frac{K_{pi}}{L_g}\right) & 0 & -\frac{1}{L_g} & 0 \\ \frac{v_d}{C_{dc}V_{dc}} & \frac{v_q}{C_{dc}V_{dc}} & 0 & 0 & 0 \\ 0 & -K_{ii}K_{pi} & 0 & 0 & 0 \\ -K_{ii}K_{pi} & 0 & 0 & 0 & 0 \end{bmatrix} \begin{bmatrix} i_{Ld} \\ i_{Lq} \\ V_{dc} \\ x_{iq} \\ x_{id} \end{bmatrix} + \begin{bmatrix} -\frac{K_{pi}}{L_g} & 0 & 0 \\ 0 & -\frac{K_{pi}}{L_g} & 0 \\ 0 & 0 & -\frac{1}{C_{dc}} \\ 0 & K_{ii}K_{pi} & 0 \\ K_{ii}K_{pi} & 0 & 0 \end{bmatrix} \begin{bmatrix} iLd_{ref} \\ iLq_{ref} \\ ix \end{bmatrix} \quad (VI-27)$$

- **Insertion of the DC voltage's regulation loop:**

The replacement of  $vd$  by the expression given in (VI-26) introduced to the system a new unknown input  $iLd_{ref}$ . As explained in previous chapter, the AC/DC converter is controlled by two cascaded loops. Thus, the reference direct current  $iLd_{ref}$  is the output of the voltage loop (Figure 103).

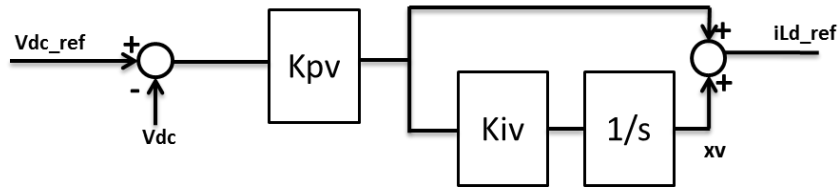


Figure 103. DC voltage regulation loop

$$\dot{x}_v = K_{iv}.K_{pv}(Vdc_{ref} - Vdc) \quad (VI-28)$$

$$iLd_{ref} = xv + K_{pv}(Vdc_{ref} - Vdc) \quad (VI-29)$$

When replacing  $iLd_{ref}$  in (VI-27), we obtain the state-space representation of the AC/DC converter where all the inputs are known.

$$\begin{aligned}
\begin{bmatrix} \dot{i}_{Ld} \\ \dot{i}_{Lq} \\ \dot{V}_{dc} \\ \dot{x}_{iq} \\ \dot{x}_{id} \\ \dot{x}_v \end{bmatrix} &= \begin{bmatrix} \left(-\frac{R_L}{L_g} + \frac{K_{pi}}{L_g}\right) & 0 & \frac{K_{pv} \cdot K_{pi}}{L_g} & 0 & -\frac{1}{L_g} & -\frac{K_{pi}}{L_g} \\ 0 & \left(-\frac{R_L}{L_g} + \frac{K_{pi}}{L_g}\right) & 0 & -\frac{1}{L_g} & 0 & 0 \\ \frac{v_d}{C_{dc} V_{dc}} & \frac{v_q}{C_{dc} V_{dc}} & 0 & 0 & 0 & 0 \\ 0 & -K_{ii} \cdot K_{pi} & 0 & 0 & 0 & 0 \\ -K_{ii} \cdot K_{pi} & 0 & -K_{ii} \cdot K_{pi} \cdot K_{pv} & 0 & 0 & K_{ii} \cdot K_{pi} \\ 0 & 0 & -K_{pv} \cdot K_{iv} & 0 & 0 & 0 \end{bmatrix} \begin{bmatrix} i_{Ld} \\ i_{Lq} \\ V_{dc} \\ x_{iq} \\ x_{id} \\ x_v \end{bmatrix} \\
&+ \begin{bmatrix} -\frac{K_{pi} \cdot K_{pv}}{L_g} & 0 & 0 \\ 0 & -\frac{K_{pi}}{L_g} & 0 \\ 0 & 0 & -\frac{1}{C_{dc}} \\ 0 & K_{ii} \cdot K_{pi} & 0 \\ K_{ii} \cdot K_{pi} \cdot K_{pv} & 0 & 0 \\ K_{iv} \cdot K_{pv} & 0 & 0 \end{bmatrix} \begin{bmatrix} V_{dc_{ref}} \\ i_{Lq_{ref}} \\ ix \end{bmatrix}
\end{aligned} \tag{VI-30}$$

With  $ix = isch - irec$ , where  $irec$  is the current injected from the railway's converter.

#### VI.b.4. State-space representation of the railway DC/DC converter

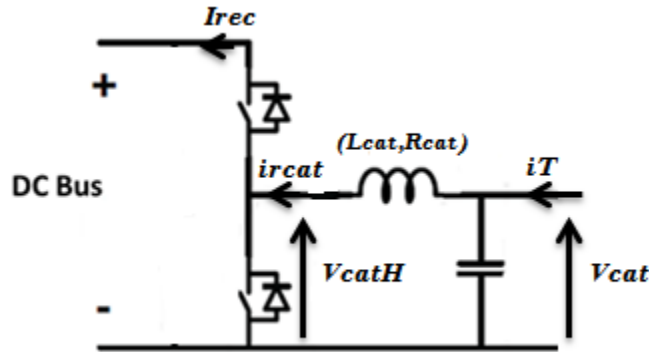


Figure 104. Railway DC/DC converter

$$V_{cat} - V_{catH} = L_{cat} \frac{di_{cat}}{dt} + R_{cat} \cdot i_{cat} \tag{VI-31}$$

$$\frac{di_{cat}}{dt} = \frac{1}{L_{cat}} V_{cat} - \frac{1}{L_{cat}} V_{catH} - \frac{R_{cat}}{L_{cat}} i_{cat} \tag{VI-32}$$

The input  $V_{catH}$  is obtained from the voltage regulation loop.  $V_{cat}$  is an input voltage measured at railway side.

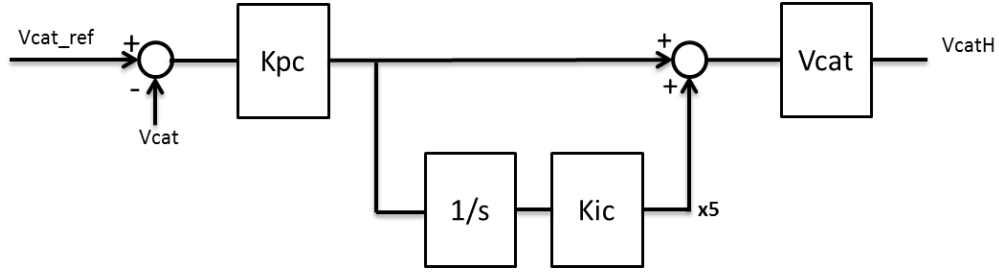


Figure 105. Railway voltage's regulation loop

From Figure 105, we obtain the following expression:

$$V_{catH} = [1 - ((V_{cat\ ref} - V_{cat}).K_{pc} + x5)].V_{out} \quad (VI-33)$$

$$\dot{x}5 = (V_{cat\ ref} - V_{cat}).K_{pc}.K_{ic} \quad (VI-34)$$

$$\dot{V}_{cat} = (iT - ircat)/C_{cat}, \text{ with } iT = P_{reg}/V_{cat} \quad (VI-35)$$

The state-space representation is then:

$$\begin{bmatrix} \dot{ircat} \\ \dot{x}5 \\ \dot{V}_{cat} \end{bmatrix} = \begin{bmatrix} -\frac{R_{cat}}{L_{cat}} & -\frac{1}{L_{cat}}V_{out} & \left(\frac{1}{L_{cat}} + \frac{K_{pc}}{L_{cat}}V_{out}\right) \\ 0 & 0 & -K_{pc}.K_{ic} \\ -1/C_{cat} & 0 & 0 \end{bmatrix} \begin{bmatrix} ircat \\ x5 \\ V_{cat} \end{bmatrix} + \begin{bmatrix} 0 & -\frac{K_{pc}}{L_{cat}}V_{out} & -\frac{1}{L_{cat}} \\ 0 & K_{pc}.K_{ic} & 0 \\ 1/C_{cat} & 0 & 0 \end{bmatrix} \begin{bmatrix} iT \\ V_{cat\ ref} \\ V_{out} \end{bmatrix} \quad (VI-36)$$

In (VI-22),  $ix$  is calculated as follows:

$$ix = isch - irec + ibus \quad (VI-37)$$

$$\text{With: } \begin{cases} irec = [(V_{cat\ ref} - V_{cat}).K_{pc} + x5].ircat \end{cases} \quad (VI-38)$$

$$\begin{cases} isch = isc_L \times x3 = isc_L.Ki.(isc_{cons} - isc_L - Kp.x3) \end{cases} \quad (VI-39)$$

$$\begin{cases} ibus = P_{bus}/V_{out} \end{cases} \quad (VI-40)$$

#### VI.b.5. Stability study of the DC micro-grid around an operational point without filters at DC side

The state-space representation of the DC micro-grid consists in regrouping previous matrixes into one equivalent system ( $\dot{X} = A.X + B.U$ ) with 12 state variables. As we can notice, the system is not linear because matrixes A and B contain state variables ( $A(X)$  and  $B(X)$ ). Therefore, a linearization process should be done around an operational point in order to calculate the system's poles. This



process is called small signals stability analysis. A small variation is thus introduced around the operational point  $(\bar{X}, \bar{U})$ . Using Taylor series limited to first order, we obtain:

$$\begin{cases} \dot{X}(t) = \dot{\bar{X}}(t) + \dot{x}(t) \approx f(\bar{X}, \bar{U}) + F_X \cdot x(t) + F_U \cdot u(t) \\ Y(t) = \bar{Y}(t) + y(t) \approx g(\bar{X}, \bar{U}) + G_X \cdot x(t) + G_U \cdot u(t) \end{cases} \quad (\text{VI-40})$$

The state-space linearized model for small variations around  $(\bar{X}, \bar{U})$  will be then:

$$\begin{cases} \dot{x}(t) = F_X \cdot x(t) + F_U \cdot u(t) \\ y(t) = G_X \cdot x(t) + G_U \cdot u(t) \end{cases} \quad (\text{VI-41})$$

Where  $F_X, F_U, G_X$ , and  $G_U$  are the Jacobian matrixes containing partial derivatives of  $f$  and  $g$  with respect to  $X$  and  $U$  respectively.

$$F_X = \begin{bmatrix} \frac{\partial f_1}{\partial x_1} & \dots & \frac{\partial f_1}{\partial x_n} \\ \vdots & & \vdots \\ \frac{\partial f_n}{\partial x_1} & \dots & \frac{\partial f_n}{\partial x_n} \end{bmatrix}_{(\bar{X}, \bar{U})} \quad F_U = \begin{bmatrix} \frac{\partial f_1}{\partial u_1} & \dots & \frac{\partial f_1}{\partial u_n} \\ \vdots & & \vdots \\ \frac{\partial f_n}{\partial u_1} & \dots & \frac{\partial f_n}{\partial u_n} \end{bmatrix}_{(\bar{X}, \bar{U})} \quad (\text{VI-42})$$

$$G_X = \begin{bmatrix} \frac{\partial g_1}{\partial x_1} & \dots & \frac{\partial g_1}{\partial x_n} \\ \vdots & & \vdots \\ \frac{\partial g_n}{\partial x_1} & \dots & \frac{\partial g_n}{\partial x_n} \end{bmatrix}_{(\bar{X}, \bar{U})} \quad G_U = \begin{bmatrix} \frac{\partial g_1}{\partial u_1} & \dots & \frac{\partial g_1}{\partial u_n} \\ \vdots & & \vdots \\ \frac{\partial g_n}{\partial u_1} & \dots & \frac{\partial g_n}{\partial u_n} \end{bmatrix}_{(\bar{X}, \bar{U})} \quad (\text{VI-43})$$

- **Choosing the operational point  $(\bar{X}, \bar{U})$**

First, the stability of the system is studied around one operational point. The DC Micro-grid is simulated using Simulink in order to get the point  $(\bar{X}, \bar{U})$  around which the state-space matrix is linearized. It corresponds to the steady-state after injecting 100 kW braking power to the system. The linearization is done around the following operational point:

$$\bar{X} = \begin{bmatrix} I_{Ld} \\ I_{Lq} \\ V_{dc} \\ X_{iq} \\ X_{id} \\ X_v \\ V_{sc} \\ I_{scL} \\ X_3 \\ I_{bat} \\ X_4 \\ I_{cat} \\ X_5 \\ V_{cat} \end{bmatrix} = \begin{bmatrix} -0.2529 \\ 0.0192 \\ 899.56 \\ -0.1407 \\ -0.2156 \\ -0.0333 \\ 578.991 \\ 226.548 \\ 0.4859 \\ 0.0058 \\ 4.39 \times 10^{-4} \\ 164.295 \\ 8.1497 \\ 818.883 \end{bmatrix}, \quad \text{and} \quad \bar{U} = \begin{bmatrix} I_{bat_{ref}} \\ E_{bat} \\ I_{Lq_{ref}} \\ V_{dc_{ref}} \\ V_{cat_{ref}} \\ P_{reg} \\ V_{Ld} \\ V_{Lq} \end{bmatrix} = \begin{bmatrix} 0 \\ 227.2 \\ 0 \\ 900 \\ 820 \\ 9.983 \times 10^4 \\ 320 \\ 0 \end{bmatrix} \quad (\text{VI-44})$$

As explained before, eigenvalues of matrix 'A' correspond to the system's closed-loop poles. The system is stable if its closed-loop poles are located in the left of the imaginary axes of the complex plane ( $\text{Real}(Z_n) < 0$ ). The matrix A has 14 eigenvalues, 12 reals and 2 complex conjugates:

$$eigv = \begin{bmatrix} -4.483 \times 10^8 \\ -1.161 \times 10^6 \\ -1.863 \times 10^4 \\ -1.617 \times 10^4 \\ -1.887 \times 10^4 \\ -238.72 \\ -115.59 \\ -0.0043 \\ -0.1 \\ -18.2 \\ -18.167 \\ -187.82 + 1.06 \times 10^5 i \\ -187.82 - 1.06 \times 10^5 i \\ -3.515 \end{bmatrix} \quad (VI-45)$$

The system's response is then the sum of 12 first-order systems' responses and one second-order system's response. Poles that are relatively far from the imaginary axes have the less impact on the system's transient state because their responses last a very short time. Thus, they can be eventually neglected in order to simplify the system's study. All poles are located on the left side of imaginary axe. The system is then stable. Yet, the pole  $z_8 = -0.0043$  is close to zero which may cause marginal stability. In addition, according to Figure 106, the second-order system is not well damped because a high value of angle ' $\beta$ ' entails low damping ratio ' $\zeta$ '. This may cause, in real conditions, instability risks.

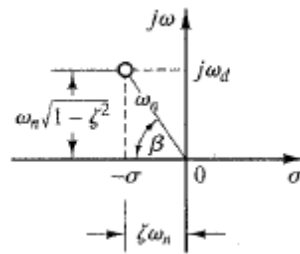


Figure 106. Damping ratio  $\xi$  of a second-order system's pole

- **Operational point variation**

The same analysis is repeated for different operational points in order to study the variation of system's eigenvalues. The following scenario in Figure 107 is simulated:

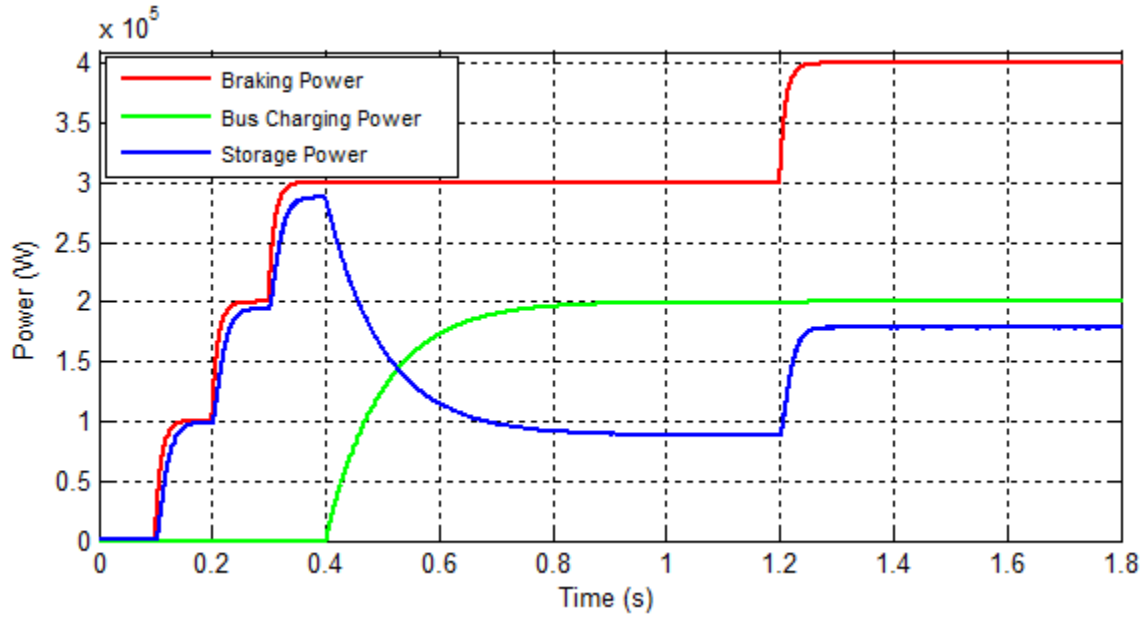


Figure 107. Simulated power flow scenario for operational points extraction

Four operational points are extracted corresponding to the static state of each power step:

	$\bar{X}_1$ (t=0.8 s)	$\bar{X}_2$ (t=0.28 s)	$\bar{X}_3$ (t=1 s)	$\bar{X}_4$ (t=1.6 s)
$I_{Ld}$	-0.2529	-0.5769	5.7243	-3.4797
$I_{Lq}$	0.0192	0.0212	0.0233	-0.0164
$V_{dc}$	899.56	899.12	897.962	896.564
$X_{iq}$	-0.1407	-1.6268	35.7472	-17.142
$X_{id}$	-0.2156	-0.2741	-1.4421	6.988
$X_v$	-0.0333	-0.1267	6.778	-1.876
$V_{sc}$	578.991	580.675	579.997	584.316
$I_{scL}$	226.548	333.253	156.461	305.087
$X_3$	0.4859	0.6458	0.6307	0.649
$I_{bat}$	0.0058	0.0058	0.0058	0.0058
$X_4$	$4.39 \times 10^{-4}$	$4.40 \times 10^{-4}$	$4.39 \times 10^{-4}$	$4.43 \times 10^{-4}$
$I_{cat}$	164.295	243.498	366.113	488.123
$X_5$	8.1497	7.8566	3.3985	3.3992
$V_{cat}$	818.883	818.894	819.532	819.461

Table 15. Selected operational points

The spate space matrixes are then linearized around each point of Table 15. Calculated eigenvalues in Table 16 are valid for linearization operational points and for small variations around them.

$eigv_1$	$eigv_2$	$eigv_3$	$eigv_4$
$-4.483 \times 10^8$	$-4.482 \times 10^8$	$-4.483 \times 10^8$	$-4.483 \times 10^8$
$-1.161 \times 10^6$	$-1.167 \times 10^6$	$-1.158 \times 10^6$	$-1.162 \times 10^6$
$-187.8 + 1.05 \times 10^5 i$	$-225.1 + 1.05 \times 10^5 i$	$-269.2 + 1.05 \times 10^5 i$	$-335.2 + 1.04 \times 10^5 i$
$-187.8 - 1.05 \times 10^5 i$	$-225.1 - 1.05 \times 10^5 i$	$-269.2 - 1.05 \times 10^5 i$	$-335.2 - 1.04 \times 10^5 i$
$-1.863 \times 10^4$	$-1.862 \times 10^4$	$-1.879 \times 10^4$	$-1.853 \times 10^4$
$-1.617 \times 10^4$	$-1.622 \times 10^4$	$-1.620 \times 10^4$	$-1.633 \times 10^4$
$-1.887 \times 10^4$	$-1.887 \times 10^4$	$-1.887 \times 10^4$	$-1.887 \times 10^4$
$-238.7$	$-243.2$	$-247.7$	$-246.6$
$-115.59$	$-115.6$	$-115.59$	$-115.59$
$-3.515$	$-3.451$	$-3.372$	$-3.463$
$-0.0043$	$-0.008$	$-0.0039$	$-0.0073$
$-0.1$	$-0.1$	$-0.1$	$-0.1$
$-18.20$	$-18.19$	$-18.198$	$-18.2$
$-18.17$	$-18.17$	$-18.167$	$-18.167$

**Table 16. System's eigenvalues around each operational point**

Table 16 shows that varying the operational point doesn't impact all eigenvalues. This depends on the state vector  $X$ 's values. Although the system is stable in all four cases, this doesn't ensure that it will remain stable when considerable signal variations are applied. In addition, different converters are connected to the DC busbar through filters. In the case where the latter is not well damped, to reduce energy losses, oscillations may occur between filters especially when their undamped natural frequencies  $w_n$  are close. Therefore, in the following subchapter, a stabilization control technique, backstepping, is introduced and tested on a low damped equivalent system.

## **VI.c. BACKSTEPPING APPROACH**

### **VI.c.1. Concept**

Backstepping is a technique developed by Petar V. Kokotovic and others in the 90s. It is a stabilizing control of non-linear dynamical systems that are built from subsystems evolving in a recursive structure. It is based on starting with stabilizing the known stable subsystem and "back-out" new controllers that progressively stabilize each following subsystem. Figure 108 shows the backstepping process for a system made up of six subsystems  $S_i$ . For each one, Lyapunov function is calculated in order to find the stabilizing command  $z_i$ . This will lead to the command  $u$  that will ensure all subsystems' stability and thus the global system's stability.

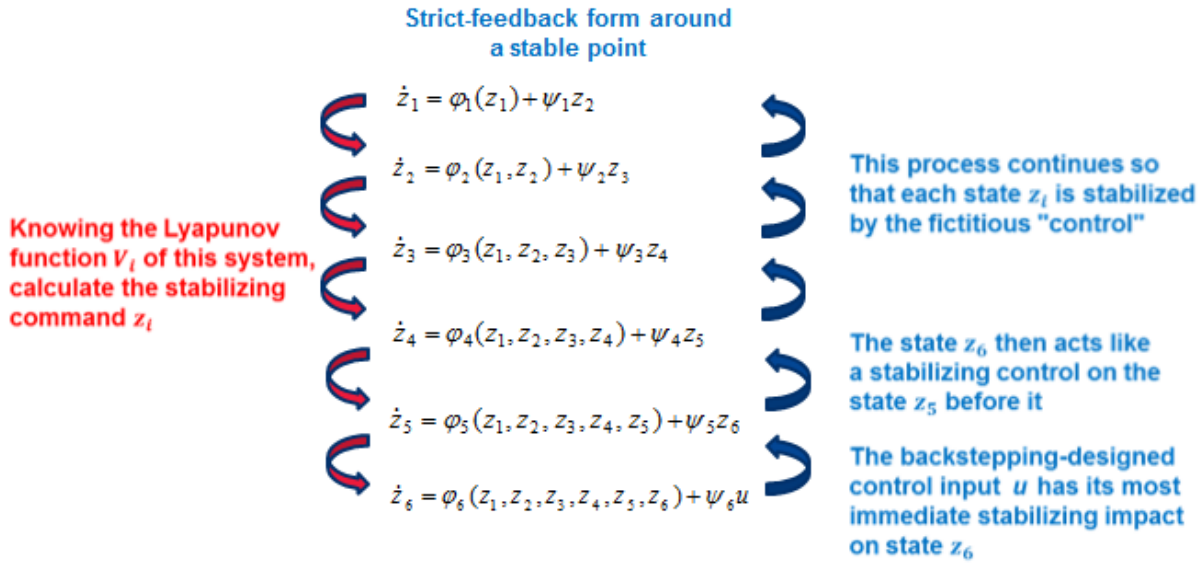


Figure 108. Backstepping stabilizing process

In this study, the backstepping approach will act on the control of the hybrid storage system and more precisely on the supercapacitor. It will stabilize the Micro-grid taking into consideration the dynamic evolution of the system.

#### VI.c.2. Application to Micro-grid simplified model

In order to simplify the problem, the converters are represented by current sources operating in consumption/generation modes. In figure 1.b, the studied system is presented where  $V_{inv}$  represents the inverter's output voltage ( $V_{inv}=900V$ ),  $P_{sc}$  the power absorbed by the hybrid storage system,  $P_t$  the braking power recovered by the trains and  $P_{bus}$  the constant power absorbed by the electric hybrid bus. The set of equations representing the system is given below. Note that  $V_{inv}$  and  $P_{bus}$  are constant,  $P_t$  is also considered as a constant because the system dynamics are much faster than the braking power variation.  $P_{sc}$  is the control input of the storage.

$$\left\{ \begin{array}{l} L_{inv} \frac{dI_{inv}}{dt} = V_{inv} - V_{dc} - R_{inv} \cdot I_{inv} \\ L_f \frac{dI_f}{dt} = V_{dc} - V_f - R_f \cdot I_f \\ L_{ft} \frac{dI_{ft}}{dt} = V_{dc} - V_{ft} - R_{ft} \cdot I_{ft} \end{array} \right. \quad \left\{ \begin{array}{l} C_{inv} \frac{dV_{dc}}{dt} = I_{inv} - I_f - I_{ft} - \frac{P_{bus}}{V_{dc}} \\ C_f \frac{dV_f}{dt} = I_f - \frac{P_{sc}}{V_f} \\ C_{ft} \frac{dV_{ft}}{dt} = I_{ft} + \frac{P_t}{V_{ft}} \end{array} \right. \quad (VI-46)$$

Considering the vector  $X_0 = [I_{inv0}, I_{f0}, I_{ft0}, V_{dc0}, V_{f0}, V_{ft0}]$  as an equilibrium point, equations (VI-46) can be centered round  $X_0$  with the following variable changes:

$$\left\{ \begin{array}{l} x_1 = I_{inv} - I_{inv0} \\ x_2 = I_f - I_{f0} \\ x_3 = I_{ft} - I_{ft0} \end{array} \right. \quad \left\{ \begin{array}{l} x_4 = V_{dc} - V_{dc0} \\ x_5 = V_f - V_{f0} \\ x_6 = V_{ft} - V_{ft0} \end{array} \right. \quad (VI-47)$$

After replacing (VI-47) in (VI-46), the new equivalent system is given in (VI-48) where the equilibrium point  $X_0$  is the system's origin:

$$\left\{ \begin{array}{l} L_{inv} \dot{x}_1 = -R_{inv} x_1 - x_4 \\ L_f \dot{x}_2 = -R_f x_2 + x_4 - x_5 \\ L_{ft} \dot{x}_3 = -R_{ft} x_3 + x_4 - x_6 \end{array} \right. \quad \left\{ \begin{array}{l} C_{inv} \dot{x}_4 = x_1 - x_2 - x_3 + \frac{P_{bus} \cdot x_4}{(x_4 + V_{dc0}) \cdot V_{dc0}} \\ C_f \dot{x}_5 = x_2 + \frac{P_{sc} \cdot x_5}{(x_5 + V_{f0}) \cdot V_{f0}} \\ C_{ft} \dot{x}_6 = x_3 - \frac{P_t \cdot x_6}{(x_6 + V_{ft0}) \cdot V_{ft0}} \end{array} \right. \quad (VI-48)$$

### 1.1. System stabilization

After modelling the DC Micro-grid and centring the equations round the equilibrium point  $X_0$ , the backstepping control technique requires equations describing the dynamics of system (VI-48) to be presented in cascaded form. To achieve that, a change of variables is done as follows:

$$\begin{bmatrix} z_1 \\ z_2 \\ z_3 \\ z_4 \\ z_5 \\ z_6 \end{bmatrix} = \begin{bmatrix} L_{inv} x_1 + L_{ft} x_3 \\ C_{ft} x_6 \\ L_{inv} x_1 - L_{ft} x_3 \\ C_{inv} x_4 \\ L_f x_2 \\ C_f x_5 \end{bmatrix} \quad \text{and} \quad \begin{bmatrix} z_{20} \\ z_{40} \\ z_{60} \end{bmatrix} = \begin{bmatrix} C_{ft} V_{ft0} \\ C_{inv} V_{dc0} \\ C_f V_{f0} \end{bmatrix}, \quad \text{with} \quad \frac{R_{ft}}{L_{ft}} = \frac{R_{inv}}{L_{inv}} \quad (VI-49)$$

After applying (VI-49), equations (VI-48) can be expressed in the following cascaded form presented in Figure 108 where 'u' is the backstepping command that will be added to the classic command  $P_{sc0}$  to ensure a global asymptotic stability (see VI.a):

$$\left\{ \begin{array}{l} \dot{z}_1 = \varphi_1(z_1) + \psi_1 z_2 \\ \dot{z}_2 = \varphi_2(z_1, z_2) + \psi_2 z_3 \\ \dot{z}_3 = \varphi_3(z_1, z_2, z_3) + \psi_3 z_4 \end{array} \right. \quad \left\{ \begin{array}{l} \dot{z}_4 = \varphi_4(z_1, z_2, z_3, z_4) + \psi_4 z_5 \\ \dot{z}_5 = \varphi_5(z_1, z_2, z_3, z_4, z_5) + \psi_5 z_6 \\ \dot{z}_6 = \varphi_6(z_1, z_2, z_3, z_4, z_5, z_6) + \psi_6 u \end{array} \right. \quad (VI-50)$$

with,

$$\begin{aligned} \varphi_1(z_1) &= -R_{inv} \cdot z_1 / L_{inv} & \psi_1 &= -\frac{1}{C_{ft}} \\ \varphi_2(z_1, z_2) &= \frac{z_1}{2L_{ft}} - \frac{C_{ft} P_t z_2}{z_{20}(z_{20} + z_2)} & \psi_2 &= -\frac{1}{2L_{ft}} \\ \varphi_3(z_1, z_2, z_3) &= -\frac{R_{inv}}{2L_{inv}}(z_3 + z_1) - \frac{R_{ft}}{2L_{ft}}(z_3 - z_1) + \frac{z_2}{C_{ft}} & \psi_3 &= -\frac{2}{C_{inv}} \\ \varphi_4(z_1, z_2, z_3, z_4) &= \frac{1}{2L_{inv}}(z_3 + z_1) + \frac{1}{2L_{ft}}(z_3 - z_1) + \frac{C_{inv} P_{bus} z_4}{z_{40}(z_{40} + z_4)} & \psi_4 &= -\frac{1}{L_f} \\ \varphi_5(z_1, z_2, z_3, z_4, z_5) &= -\frac{R_f}{L_f} z_5 + \frac{1}{C_{inv}} z_4 & \psi_5 &= -\frac{1}{C_f} \end{aligned}$$

$$\varphi_6(z_1, z_2, z_3, z_4, z_5, z_6) = \frac{1}{L_f} z_5 + \frac{C_f P_{sc0} z_6}{z_{60}(z_{60} + z_6)} \quad \psi_6 = -\frac{C_f}{(z_{60} + z_6)}$$

where  $R_{inv}, L_{inv}, R_f, L_f, R_{ft}, L_{ft}, C_{inv}, C_f$  and  $C_{ft}$  are constants characterizing the system;  $P_{bus}$  and  $P_t$  are measurable,  $P_{sc0}$  is the classic command of the storage system and it is equal to:  $P_{sc0} = P_t - P_{bus}$ .

The state vector presentation (VI-50) will allow calculating the command 'u' by dividing the system into six cascaded subsystems  $S_i$  defined by the state vector  $[z_1 \dots z_i]$ . The backstepping method consists of calculating a positive-definite Lyapunov function  $V_i$  for each subsystem  $S_i$ . The global stability is then achieved by stabilizing each subsystem. The subsystem  $S_6$  corresponds to the full system. Detailed calculus will be done for the first two subsystems; the rest can be done in the same manner. The command value of each  $S_i$  will be then directly given.

- **Stabilization of subsystem S1:  $\{\dot{z}_1\}$**

For  $S_1$ ,  $z_2$  represents the input command of the subsystem. The command value  $z_1^*$  of  $z_1$  is considered equal to zero. The state error  $\varepsilon_1$  is given by:

$$\varepsilon_1 = z_1 - z_1^* \Rightarrow \dot{\varepsilon}_1 = \dot{z}_1 - \dot{z}_1^* = \varphi_1(z_1) + \psi_1 z_2 - \dot{z}_1^* \quad (VI-51)$$

We consider the positive-definite Lyapunov function:

$$V_1 = \frac{1}{2L_{ft}} \varepsilon_1^2 \Rightarrow \dot{V}_1 = \frac{1}{L_{ft}} \dot{\varepsilon}_1 \varepsilon_1 = \frac{1}{L_{ft}} \varepsilon_1 (\varphi_1(z_1) + \psi_1 z_2 - \dot{z}_1^*) \quad (VI-52)$$

$S_1$  is asymptotically stable if the derivation of  $V_1$  is negative-definite. This condition is fulfilled by the following equation:

$$\varphi_1(z_1) + \psi_1 z_2 - \dot{z}_1^* = -k_1 e_1 \Rightarrow \dot{V}_1 = -k_1 e_1^2 < 0 \quad (VI-53)$$

where  $k_1 > 0$  is a parameter to be defined depending on the dynamic behaviour of  $S_1$ .

In order to insure convergence to  $X_0$ , the command value  $z_2^*$  of  $z_2$  should be equal to:

$$z_2^* = \frac{1}{\psi_1} (-\varphi_1(z_1) - k_1 e_1 + \dot{z}_1^*) \quad (VI-54)$$

- **Stabilization of subsystem S2:  $\{\dot{z}_1, \dot{z}_2\}$**

For  $S_2$ ,  $z_3$  is the input command that will let the output  $z_2$  equal to  $z_2^*$ . The state error vector is then:

$$\varepsilon_2 = z_2 - z_2^* \Rightarrow \dot{\varepsilon}_2 = \dot{z}_2 - \dot{z}_2^* = \varphi_2(z_1, z_2) + \psi_2 z_3 - \dot{z}_2^* \quad (VI-55)$$

We consider the positive-definite Lyapunov function:

$$V_2 = \frac{1}{2C_{ft}} \varepsilon_2^2 + V_1 \Rightarrow$$

$$\dot{V}_2 = \dot{V}_1 + \frac{1}{C_{ft}} \dot{\varepsilon}_2 \varepsilon_2 = \frac{1}{L_{ft}} \varepsilon_1 (\varphi_1(z_1) + \psi_1(\varepsilon_2 + \dot{z}_2^*) - \dot{z}_1^*) + \frac{1}{C_{ft}} \varepsilon_2 (\varphi_2(z_1, z_2) + \psi_2 z_3 - \dot{z}_2^*) \quad (\text{VI-56})$$

$S_2$  is asymptotically stable if the derivation of  $V_2$  is negative-definite. This condition is fulfilled by the following equation:

$$\frac{C_{ft}}{L_{ft}} \psi_1 \varepsilon_1 + \varphi_2(z_1, z_2) + \psi_2 z_3 - \dot{z}_2^* = -k_2 \varepsilon_2 \quad \text{with } k_2 > 0 \quad (\text{VI-57})$$

The input command of  $S_2$  is then:

$$z_3^* = \frac{1}{\psi_2} \left( -\frac{C_{ft}}{L_{ft}} \psi_1 \varepsilon_1 - \varphi_2(z_1, z_2) + \dot{z}_2^* - k_2 \varepsilon_2 \right) \quad (\text{VI-58})$$

- **Stabilization of subsystem S3:  $\{\dot{z}_1, \dot{z}_2, \dot{z}_3\}$**

As for the previous subsystems, the input command  $z_4^*$  that will insure stability of  $S_3$  is:

$$z_4^* = \frac{1}{\psi_3} \left( -\frac{L_{ft}}{C_{ft}} \psi_2 \varepsilon_2 - \varphi_3(z_1, z_2, z_3) + \dot{z}_3^* - k_3 \varepsilon_3 \right) \quad \text{with } k_3 > 0 \quad (\text{VI-59})$$

- **Stabilization of subsystem S4:  $\{\dot{z}_1, \dot{z}_2, \dot{z}_3, \dot{z}_4\}$**

The input command  $z_5^*$  that will insure stability of  $S_4$  is:

$$z_5^* = \frac{1}{\psi_4} \left( -\frac{C_{inv}}{L_{ft}} \psi_3 \varepsilon_3 - \varphi_4(z_1, z_2, z_3, z_4) + \dot{z}_4^* - k_4 \varepsilon_4 \right) \quad \text{with } k_4 > 0 \quad (\text{VI-60})$$

- **Stabilization of subsystem S5:  $\{\dot{z}_1, \dot{z}_2, \dot{z}_3, \dot{z}_4, \dot{z}_5\}$**

The input command  $z_6^*$  that will insure stability of  $S_4$  is:

$$z_6^* = \frac{1}{\psi_5} \left( -\frac{L_f}{C_{inv}} \psi_4 \varepsilon_4 - \varphi_5(z_1, z_2, z_3, z_4, z_5) + \dot{z}_5^* - k_5 \varepsilon_5 \right) \quad \text{with } k_5 > 0 \quad (\text{VI-61})$$

- **Stabilization of subsystem S6:  $\{\dot{z}_1, \dot{z}_2, \dot{z}_3, \dot{z}_4, \dot{z}_5, \dot{z}_6\}$**

$S_6$  represents the Micro-grid. The input command 'u' that will insure the global stability of the system is:

$$u = \frac{1}{\psi_6} \left( -\frac{C_f}{L_f} \psi_5 \varepsilon_5 - \varphi_6(z_1, z_2, z_3, z_4, z_5, z_6) + \dot{z}_6^* - k_6 \varepsilon_6 \right) \quad \text{with } k_6 > 0 \quad (\text{VI-62})$$

The Lyapunov function  $V$  of the system is:

$$V = \frac{1}{2L_{ft}} \varepsilon_1^2 + \frac{1}{2C_{ft}} \varepsilon_2^2 + \frac{1}{2L_{ft}} \varepsilon_3^2 + \frac{1}{2C_{inv}} \varepsilon_4^2 + \frac{1}{2L_f} \varepsilon_5^2 + \frac{1}{2C_f} \varepsilon_6^2 > 0 \quad (\text{VI-63})$$

The derivative of  $V$  is:



$$\dot{V} = -\frac{k_1}{L_{ft}} \varepsilon_1^2 - \frac{k_2}{C_{ft}} \varepsilon_2^2 - \frac{k_3}{L_{ft}} \varepsilon_3^2 - \frac{k_4}{C_{inv}} \varepsilon_4^2 - \frac{k_5}{L_f} \varepsilon_5^2 - \frac{k_6}{C_f} \varepsilon_6^2 < 0 \quad (\text{VI-64})$$

Equations (VI-63) and (VI-64) ensure asymptotic stability of the system around the origin  $X_0$  which is calculated dynamically using Newton-Raphson method.

### VI.c.3. Simulation of the simplified model

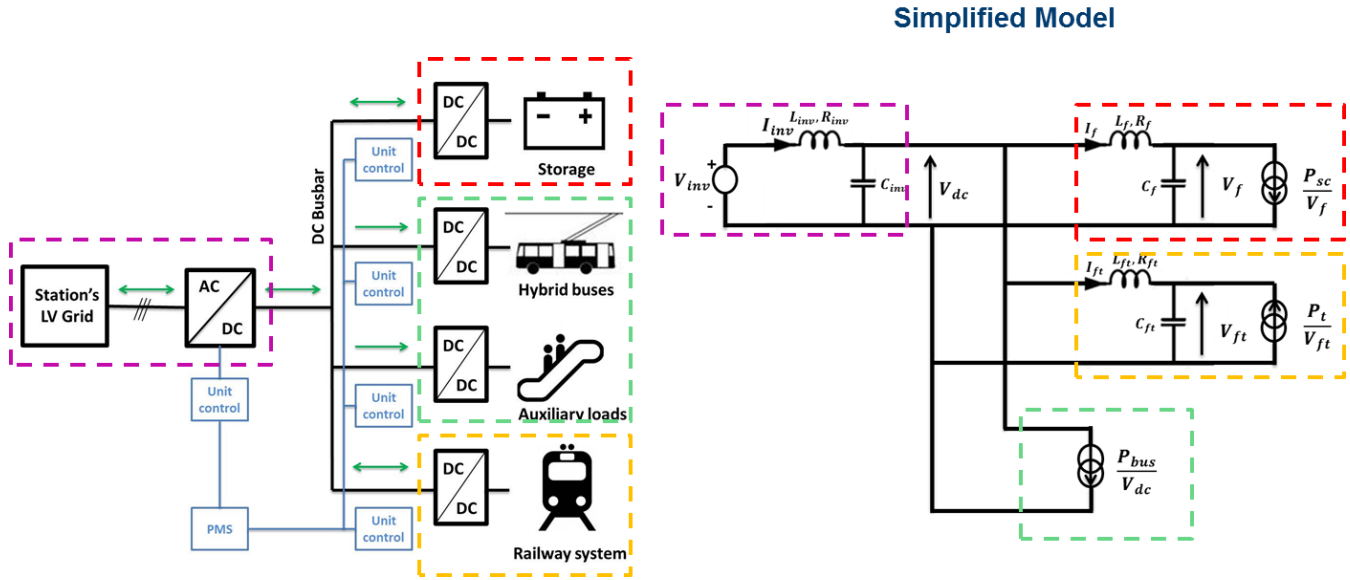


**Figure 109. Simplified model on which backstepping control is tested**

The simplified model of the DC Micro-grid shown in Figure 109 is simulated using Matlab-Simulink. The control command (VI-62) is applied to the storage system. The ki parameters used are:  $k_1=50$ ,  $k_2=30$ ,  $k_3=13$ ,  $k_4=8$ ,  $k_5=300$ ,  $k_6=10^{-5}$ . These values gave the better step response when simulating each subsystem using Matlab-Simulink. In fact, S1 is first simulated. Once finding a value for  $k_1$  giving a good step response, S2 is simulated to tune  $k_2$ . This process is repeated until we define all parameters  $k_i$  giving the global system a good step response (quick, stable, small overshoot...). The values of the electrical components of the DC Micro-grid are:  $C_f = 0,041$  F,  $C_{ft} = 0,011$  F,  $C_{inv} = 3.532 \cdot 10^{-4}$  F,  $L_f = 10.12$   $\mu$ H,  $L_{ft} = 9.45$   $\mu$ H,  $L_{inv} = 11.9$   $\mu$ H,  $R_f = 0.25$  m $\Omega$ ,  $R_{ft} = 0.23$  m $\Omega$ ,  $R_{inv} = 0.29$  m $\Omega$ . Figure 110 shows profiles of the recovered braking power and the electric hybrid bus charging power. The first one increases from zero up to 1MW. The second one is 200kW constant power.

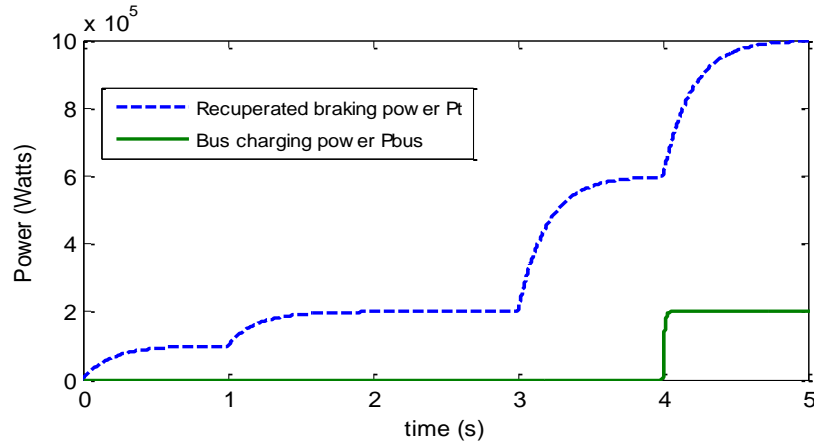


Figure 110. Recovered power and bus charging power simulated profile

Figure 111 compares between the classic storage reference power ( $P_{sc0} = P_t - P_{bus}$ ) and the one with backstepping control ( $P_{sc} = P_{sc0} + u$ ). Note that the simulation with the classic control stops at time=4,035s for divergence reason. The backstepping control allowed stabilizing the system and thus the DC busbar voltage ( $V_{dc} \cong 900V$ ).

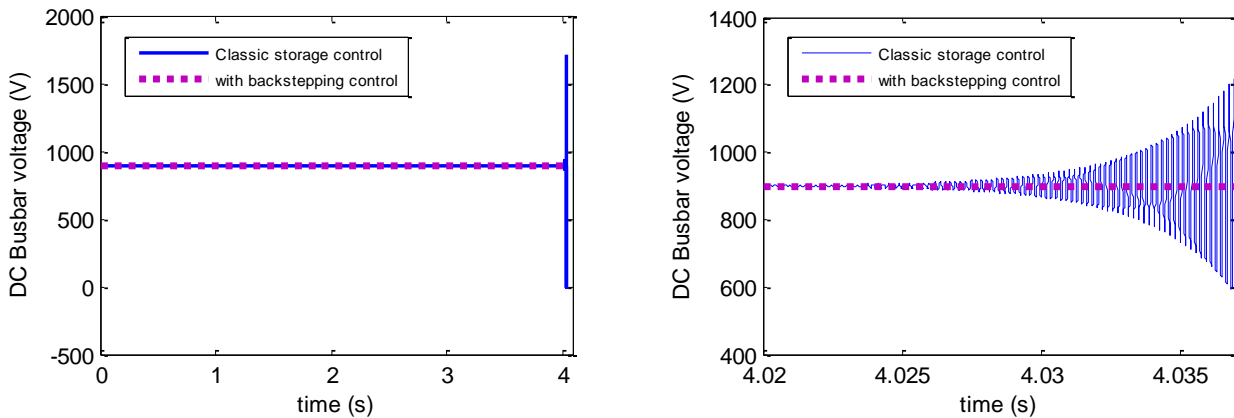


Figure 111. DC busbar voltages for classic and backstepping controls

#### VI.c.4. Conclusion

The problem of instability that can be caused by a constant power load was then explained. A solution called backstepping approach was detailed and a comparison of simulation results between classic and backstepping controls proved that the backstepping control is capable of converging and stabilizing a low-damped system. In the future, it would be interesting to simulate backstepping control on the complete DC Micro-grid with all the converters.

### VII.a. INVERTER'S SPECIFICATIONS

#### VII.a.1. Station's low voltage grid constraints

The voltage quality in railway stations is slightly different from the one in ordinary LV grids due to some specific railway equipment. Taking into consideration this particularity and based on EN 50160 and EN 61000-3-12 standards, the micro-grid should be able to operate properly in the following conditions:

- Voltage RMS value fluctuation reaching  $\pm 10\%$  of the nominal value 230/400 V
- Frequency equals to 50 Hz  $\pm 4\%$
- Voltage drops of:
  - 40% during 250 ms
  - 20% during 5 s
- Voltage interruption period less than 300 ms
- Transitional induced overvoltage in common or differential mode, with the following general characteristics:
  - Amplitude:  $\pm 1500$  V
  - Rise time: 2 to 3  $\mu$ s
  - Duration: 15 ms
- Voltage harmonics: THD  $< 8\%$
- Current harmonics: limits defined in EN 61000-3-12 (see Table 17)

In addition to the constraints listed above, the equipment should respect the electromagnetic compatibility standard EN 50121. In terms of environmental constraints and according to EN 50123-1 annex B, the air's maximum temperature in the electrical room is 40°C with a hygrometry that can reach 90% at 20°C and probably high dust levels due to natural non-filtered ventilation. Thus, converters should be able to operate normally in these particular conditions.

#### VII.a.2. Inverter's general characteristics

The 2-level AC/DC converter operates in two different modes:

- Rectifier mode: it consumes energy from the grid when the DC Busbar's voltage increases
- Inverter mode: it injects power into the grid when the DC Busbar's voltage decreases

In general, when the inverter consumes energy from the LV grid, its power is limited to the one allowed within the station. For example, if the station's transformer is 50% charged, the inverter can consume until 20% of the transformer's nominal power and let 30% of the transformer's power for future possible loads. In the other cases, when the inverter feeds back energy to the grid, the recuperated power will compensate the loads consumption in the station. The inverter's maximum allowed power is then equal to the transformer's permanent load. But, for cost reasons, this power

could be reduced and set to minimum power needed for stabilizing the DC busbar. The list below shows the inverter's main characteristics to be defined:

- Supply Frequency
- DC rated voltage
- AC rated voltage
- Rated Power (2h)
- Rated Power (1min)
- Rated Power (5s)
- Power Factor
- Voltage THD: < 8%
- THC, PWHC: Respecting EN 61000-3-12 (see Table 17)

The Total Harmonic Current (THC) is the RMS value of the current harmonics from order 2 to 40. It is calculated as follow:

$$THC = \sqrt{\sum_{h=2}^{40} I_h^2}$$

The Partial Weighted Harmonic Current (PWHC) is the total RMS value of the current harmonics, from order 14 to 40 according to the EN 61000-3-12, weighted by the harmonic order  $h$ . it is calculated as follow:

$$PWHC = \sqrt{\sum_{h=14}^{40} h \cdot I_h^2}$$

Minimum $R_{SCE}^*$	Individual harmonic current accepted ( $I_h / I_{ref}$ )** %				Harmonic parameters accepted %	
	$I_5$	$I_7$	$I_{11}$	$I_{13}$	$THC / I_{REF}$	$PWHC / I_{REF}$
33	10,7	7,2	3,1	2	13	22
66	14	9	5	3	16	25
120	19	12	7	4	22	28
250	31	20	12	7	37	38
$\geq 350$	40	25	15	10	48	46
<p>The relative values of the even harmonics which order (<math>h</math>) is lower or equal to 12 should not exceed 16/h %.</p> <p>The even harmonics which order is higher than 12 are considered in the <math>THC</math> and the <math>PWHC</math> in the same manner as the odd orders.</p> <p>The linear interpolation between successive values of <math>R_{SCE}</math> is authorized.</p>						
<p>* Short Circuit Ratio: <math>R_{sce} = S_{sc} / S_{equ}</math>, with <math>S_{sc}</math> = Short Circuit Power at connection point, <math>S_{equ}</math> = equipment nominal power</p> <p>** <math>I_{ref}</math>=reference current; <math>I_h</math> = Current's harmonic component of order (<math>h</math>)</p>						

**Table 17. Current emission limits for a three phase balanced equipment [EN61000-3-12]**

### VII.a.3. Paris Metro line 13 application

After simulating RATP's Metro line 13 in Paris with the Smart DC Micro-grid connected at "Porte de Saint-Ouen" station, the following characteristics have been specified for the AC/DC inverter:

Supply Frequency	50 Hz
DC rated voltage	900 V
AC rated voltage	230 V / 400 V
Rated Power (1h)*	3 kW
Rated Power (1min)*	7 kW
Rated Power (5s)*	10 kW
Power Factor	> 0.98

**Table 18. Electrical characteristics of the AC/DC Converter**

### VII.b. **STORAGE CONVERTER'S SPECIFICATIONS**

There are different kinds of SCs modules in the market. The following main characteristics should be specified:

- Rated capacitance (F)
- Rated voltage (V)
- Maximum voltage (V)
- Maximum repetitive dv/dt (V/ $\mu$ s)
- Usable power (W)
- Absolute maximum current (A)
- Max current ripple (A peak to peak)
- Internal series resistance ESR ( $\Omega$ )
- Thermal resistance Rth depending of the cooling air speed.
- Thermal stresses, the maximum absolute hot spot temperature (THS) to not exceed
- Lifetime: at least 10 years at 25°C

After simulating RATP's Metro line 13, the following characteristics have been specified for the SC module, based on Maxwell's 125V ultracapacitors module, such as it is able to absorb maximum power peak measured for 290s headway:

Rated voltage	750 V
Maximum voltage	816 V

Absolute maximum current	13 300 A
Maximum ESR	15.4 mΩ
Usable specific power	4.35 MW

**Table 19. Electrical characteristics for supercapacitors modules**

The DC/DC converter connecting the SC to the DC Busbar is dimensioned based on the electrical characteristics of the SC indicated in the table above.

Concerning battery storage, Li-ion technology is quite promising and its price is decreasing with the emergence of electric vehicles and electric hybrid vehicles. The DC/DC converter is sized to support the permanent charging power of one hybrid bus (200kW).

### VII.c. RAILWAY CONVERTER SPECIFICATION

The railway DC/DC converter connects railway electrical grid to the DC busbar of the micro-grid. Its basic function is to recuperate trains' braking energy. Therefore, its dimensioning depends directly on the studied railway line. Based on Metro line 13 simulations in ELBAS, the converter's maximum RMS power on increasing time window is shown in Figure 112. It represents, for each headway, maximum RMS power of the converter over 1 second, 2 seconds till all simulations' duration. We can see that the highest power is for 175s headway (blue curve). Thus, it will be considered for dimensioning the converter.

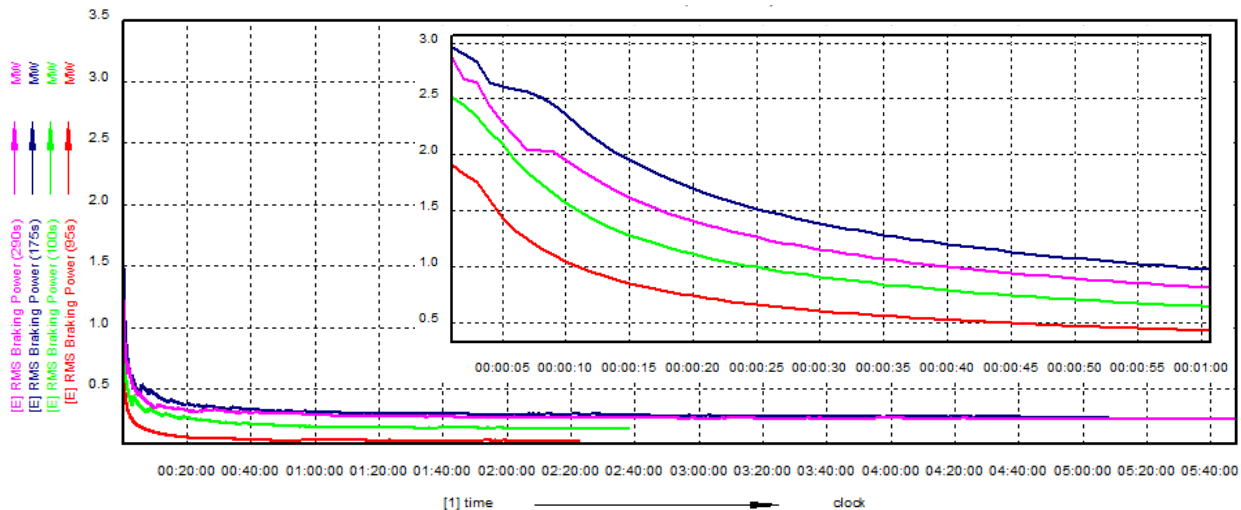


**Figure 112. Railway converter maximum RMS power over increasing time window**

EN 50328-2003 requires values over 2 hours (permanent), 1 minute and 15 seconds. We choose to add a fourth value, over 5s, because it is much higher than the value over 15s which can be constraining especially from thermal point of view. It should be dimensioned for headway 175s where maximum power is absorbed:

DC Busbar rated voltage	900 V
DC 3 <sup>rd</sup> rail rated voltage	750 V
Rated Power (2h)	300 kW
Rated Power (1min)	1 MW
Rated Power (15s)	2 MW
Rated Power (5s)	3 MW

**Table 20. Electrical characteristics of the railway DC/DC Converter**

The DC/DC converter could be partially compliant with the standard EN 50328 2003 related to “Railway applications — Fixed installations — Electronic power convertors for substations”. However, the high power capability required for a short time exceeds that of usual duty cycles for railway applications. For example, the Class VII specified in EN 50328-table 5 indicates a current capability of 4.5 p.u. during 15 s. The table above shows a ratio is higher between 2h power and 15s power (6.67 p.u.). Therefore, the converter’s power could be limited in order to correspond to common existing products.

Note that this dimensioning is for recuperating all braking power’s excess. From economical point of view, reducing converter’s maximum power may be interesting if the amount of lost energy is not considerable while the price of the converter is lower. A simple test was done using Matlab’s simplified model (see V.f.3) in order to study the impact of limiting the converter’s power. We considered headway 290s where recuperated energy over one hour is the highest. When limiting the power to 2MW, 333 kWh are saved instead of 336 kWh. For 1.5 MW, the energy is 317 kWh but limiting the power to 1 MW is less interesting because in this case, only 279 kWh are recuperated. This can be explained by the fact that high power peaks exceeding 1.5 MW are short and thus do not impact the total energy assessment.

To conclude, Section B presented an urban solution that increased a line's efficiency by recuperating trains' braking energy when no exchange was possible. It is a new concept based on DC micro-grids that allowed a passengers' station to become an intelligent actor in its energy environment. Recuperated braking energy was stored in a hybrid storage system and then used in "non-railway" applications, for example, charging electrical hybrid buses. The energy simulation of Paris metro line 13 showed that there was enough energy to charge more than one bus per hour. The stability of the micro-grid was also studied. A stabilization control was proposed based on Backstepping approach. Unfortunately, this solution cannot be applied on high speed lines where braking energy can be sent back to the upper grid through substations. In addition, these lines cover long distances which require using a global optimization approach instead of a local one. The following section will propose a 'software' solution for optimizing both energy and power consumption of HSL's timetable.



## **SECTION C: ENERGY OPTIMIZATION FOR SUBURBAN AND HIGH SPEED LINES**

As shown in section A, High Speed Lines (HSL) are AC powered systems. Thus, contrarily to urban DC railways, regenerated braking energy can be directly fed back into the grid through substations (SST). The DC Micro-grid solution for reducing braking energy losses is no longer applicable. Nevertheless, HSL have other particularities. Long distances between stations give more driving flexibility. In addition, High Speed Trains (HST) consume high powers compared to urban trains. Consequently, if many trains accelerate simultaneously in the same electric zone, power peaks can be observed at SSTs level. When exceeding maximum subscribed power, penalties should be paid. Based on that, another solution is more appropriate for HSL: optimizing the traffic in order to reduce total energy and power consumptions.

In high speed lines, a theoretical timetable contains all planned journeys consisting of departure and arrival times, served stations, etc. Operators try to respect it by adjusting manually trains' run in order to reduce the gap (delays / advances) between theoretical and real timetables. Thus, it is important to have a Traffic Management System (TMS) because real timetables reflect what's really happening on the ground. It allows forecasting future timetable (next trains movements, resources to be used...), helps the operator taking appropriate decisions and avoiding conflicts. Nowadays, TMS priority is to ensure security and fluidity by avoiding future perturbations. The proposed solutions don't necessarily take into consideration the energy consumption or possible power optimization. A traffic solution can then cause energetic conflicts. Hence, energy savings can be achieved with traffic operation strategies such as eco-driving, timetable optimization, etc. In literature, energy efficiency optimization has been widely studied in the last decade. The main contributions were for urban and suburban railways. Indeed, these lines operate today with a high degree of automation which allows better operational control and implementation of energy-efficient driving strategies. In [DOM12], automatic train operation (ATO) system is used for applying optimal speed profiles to metro trains taking into account the energy recovered from regenerative brake. In [MIY10], predefined speed profiles are uploaded and then selected according to the departure and running time. Railway simulations tools were also integrated in optimization procedure. They allowed a parallel computing approach in the optimization loop and thus reducing considerably computing time [QUA11]. Concerning interaction between the driver and the train, [ALB10] proposed to apply an energy-optimal train control to driver's advisory system using the minimum necessary number of regime changes. In [SIC10], eco-driving was designed for high speed lines in partnership with RENFE, Spanish national railway operator. It was tested in collaboration with ADIF, Spanish national infrastructure manager, in commercial high speed trains and it showed that it is possible to reach an average energy saving of 20 %.

Train commercial timetables consist of inter-stations running time and commercial dwell times (station's parking time). A slack time is also added to the flat-out time  $T_{flat\ out}$  (minimum running time corresponding to a tight run). According to the UIC Code 451-1, the slack time is expressed with a percentage of the flat-out time [CUC12]. When a delay arises, it will serve to recover this delay and will allow arriving on time to the next station. When a train is on time, the slack time can be used for coasting and reducing a run's total energy consumption. if a conflict is detected by the TMS, the DSS (Decision Support System) will try to solve it in different ways (train retention, changing speed limits, changing slack time distribution, etc.) depending on its cause. The selection is made by affecting to each solution an index that takes into consideration systems' priorities, delays, new generated conflicts and other pre-configured constraints. Each proposed solution will have an energetic impact and may cause undesired power peaks if the energetic criteria was not taken into consideration. Therefore, regulation process should integrate an energy evaluation that helps taking more efficient decisions as shown in

Figure 113:

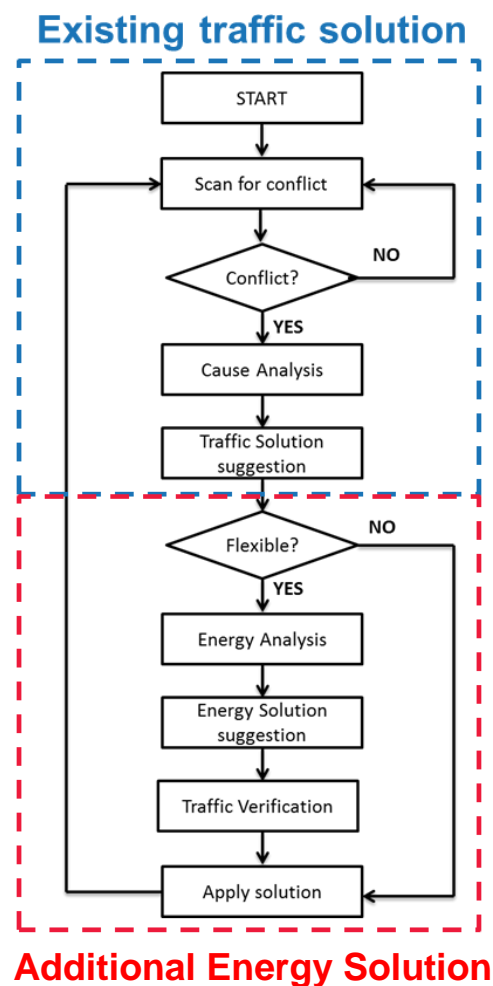


Figure 113. Energy and traffic regulation flow chart

Inspired from previous works found in literature, this Section will present cascaded energy and power optimizations. High speed lines' particularities will be taken into consideration to ensure respecting their operational constraints. The Section is then divided into two main parts. First, an algorithm for optimizing a train's speed profile is presented. It is a single train optimization that will calculate a less energy consuming speed profile. The second part is dedicated to trains synchronization; Substations power peaks will be reduced by acting on dwell time, in order to avoid exceeding maximum subscribed power. Finally, simulations will be done for both optimization steps based on a real high speed line case.

## IX - Speed profile and energy optimization

### IX.a. INTRODUCTION

For the same slack time, there is large variety of speed profiles. Some are more energy efficient than others. In order to evaluate their consumption and make the right choice, these profiles are compared to the Pareto curve defined for each interstation. Figure 114 shows an example for a run time-consumption graph where each point represents a specific driving in a given inter-station [CUC12]. For each interstation's runtime, the Pareto curve represents speed profiles with minimum energy consumption. If the line contains  $X$  stations, then  $(X-1)$  interstation, there will be  $(X-1)$  Pareto curves to consider when proposing new slack time distribution. They will serve as an input to the DSS which will evaluate the energetic impact of proposed traffic solutions. Pareto curve can be calculated using a train motion simulator and an iterative process called Differential Evolution Algorithm (DEA) [CUC12]. The train motion simulator will generate different speed profiles, simulate them in railway conditions and give the associated energy consumption. The DEA will then help selecting the optimal driving style.

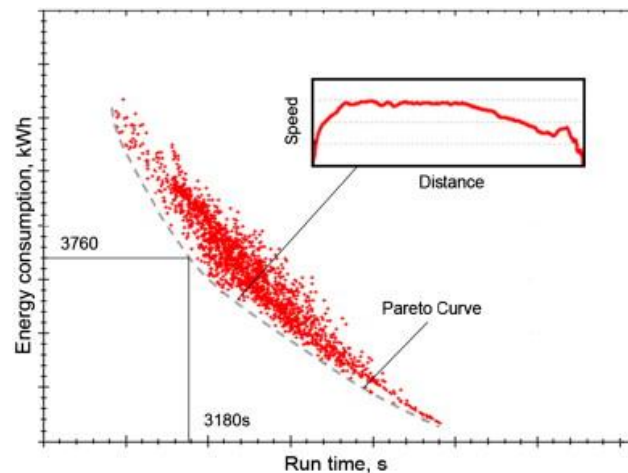


Figure 114: Run time-energy consumption and Pareto curve [CUC12]

For a given run trip time, the train motion simulator used in our study, developed internally within Alstom, can generate speed profiles with:

- Coasting zones before each station arrival.
- Economical speeds for each section, the first to trigger coasting and the other to resume traction (speed regulation without braking).
- Speed holding below the maximum speed limits for each section.

- Coasting before each braking maintain at maximum speed to avoid this maintain to happen.

The efficiency of each solution depends strongly of the line's topology. When a coasting could be the best way to save energy in a line, speed limitations could be better in another. Once speed curves are generated, they constitute a "random population" of driving profiles that will be analysed by the DEA. In a given iteration, each profile is considered as an "individual" belonging to a "generation" of population. In each generation, the fitness of every individual is evaluated. The fitness "f" is the objective function to optimize. In this case, it should evaluate the energy consumption and the running time of each speed profile. It is considered as the cost of the solution and thus it should be minimized. In [CUC12], the following fitness function was considered:

$$f = w_E \frac{E}{E_{flat_{out}}} + w_t \frac{T_{target}}{T_{flat_{out}}} \quad \text{if } T \leq T_{target} \quad (IX-1)$$

$$f = w_E \frac{E}{E_{flat_{out}}} + w_t \frac{T^2}{T_{flat_{out}} \times T_{target}} \quad \text{if } T > T_{target} \quad (IX-2)$$

where  $w_E$  and  $w_t$  are weighting factors and  $E_{flat_{out}}$  consumed energy during a flat-out run.

Equation (IX-2) penalizes the speed curves whose runtime exceeds the target time ( $T_{target}$ ) by a factor equal to the run time (T) divided by  $T_{target}$ . This fitness doesn't include any penalty for trains arriving in advance. The new generation in the next iteration consists of the elite group, individuals with minimum fitness. Combinations and crossovers and mutations are done to complete the size of the generation. The size of the elite group and the number of iterations are configurable. Note that the consumption of different speed profiles can be analysed offline in order to have a database that can accelerate real-time decision making process.

#### **IX.b. METHODOLOGY GENERAL SPECIFICATIONS**

There are 4 different modes to run a train:

- Traction : consuming energy to accelerate the train
- Cruising: running at a constant speed
- Coasting: cutting off engines to run only on train's inertia. In the case of a positive slope, the train will slow down without braking
- Braking: the train decelerates using mechanical or electrical brakes

Figure 115 shows a simplified representation of different modes. It is important to remind that these curves depend directly on line's profile and can be much more variating. This figure is presented only to help readers understand.

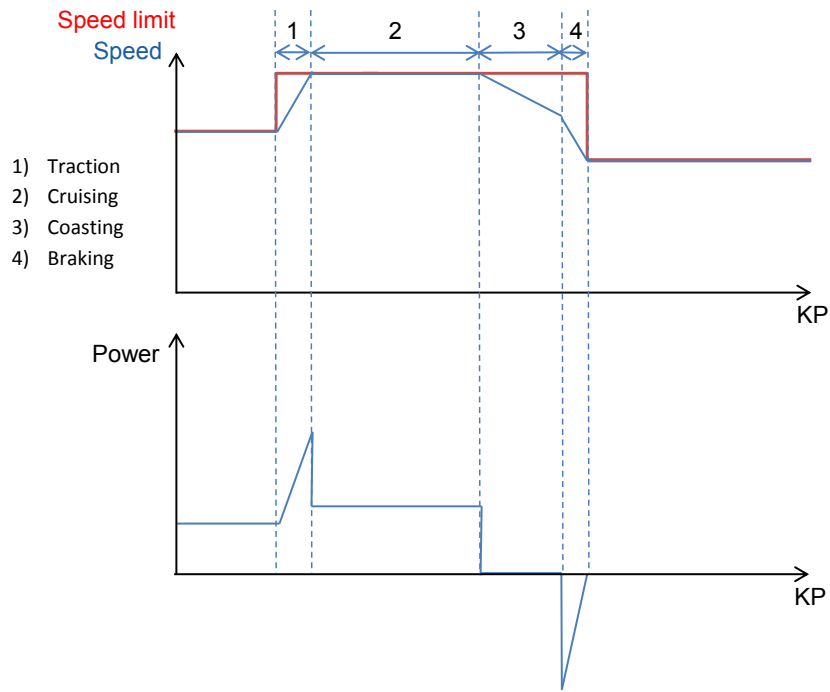


Figure 115: The four different modes for a train's run

Between two stops with a constant speed limitation, the minimum travelling time is obtained by the following pattern: first the train will accelerate until it reaches the maximum speed. Then, it will maintain its speed and finally brake as late as possible. This driving method is called a flat-out run and requires the minimum running time (the flat-out time). However, a flat-out run is not energy-friendly. Moreover, in a theoretical timetable, the drivers always have a margin on the flat-out time (the slack-time). It is the difference between the running time of the timetable and the flat-out time and is expressed as a percentage of the flat-out time.

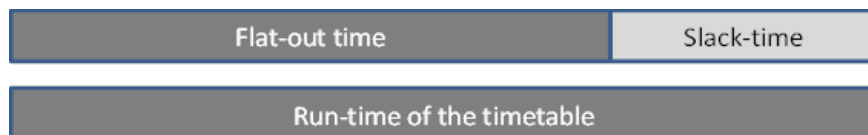


Figure 116. Slack-time representation

For urban and suburban trains, literature can be found on optimizing the speed profile between two stops by taking the slack-time as an input and applying coasting only at the end of the journey. However, in the case of mainlines between cities, there are few stops and some intermediary constraints: the train must pass through some points at a given time to avoid delays and possible conflicts with other trains. These points will be named “operational points” and often correspond to unmarked stations (where the train doesn't necessary stop) and junctions. Therefore, the slack-time will be considered between each two successive operational points because coasting will be applied many times between two stops and not only at the end before stopping.

In order to optimize the energy consumption, metaheuristic stochastic processes is used such as differential evolution algorithm [PRI00]. It generates an initial random population that will be improved generation after generation.

#### IX.b.1. Initialization:

The first step computes a random population of individuals. The size of the population generated, NP, is an input parameter to the algorithm. Therefore, we end up with a matrix  $X(NP, D)$  where D represents the number of parameters used to characterize an individual. The matrix will be named  $X_0$  as it represents the initial population (generation 0).

$$X_0 = (x_{i,j})_{i \in [1; NP], j \in [1; D]} = \begin{pmatrix} x_{1,1} & \cdots & x_{1,D} \\ \vdots & \ddots & \vdots \\ x_{NP,1} & \cdots & x_{NP,D} \end{pmatrix} \quad (IX-3)$$

$x_i$  represents the individual 'i' and  $x_{i,j}$  the parameter 'j' of the individual 'i'. Each parameter  $x_{i,j}$  is subject to boundary constraints that depend of the parameter 'j':

$$b_{lower}(j) \leq x_{i,j} \leq b_{upper}(j) \quad \text{for } i = 1..NP, \quad j = 1..D \quad (IX-4)$$

Therefore, the initial population  $X_0$  is generated by the following expression:

$$x_{i,j} = b_{lower}(j) + \text{rand}([0,1]) * (b_{upper}(j) - b_{lower}(j)) \quad (IX-5)$$

#### IX.b.2. Heredity:

From the population of generation 'g', the differential evolution algorithm will produce a new generation 'g+1' using successively the following processes:

- **Mutation**

The mutation consists in modifying randomly some parameters of a selected individual in order to form a new one as shown in Figure 116.

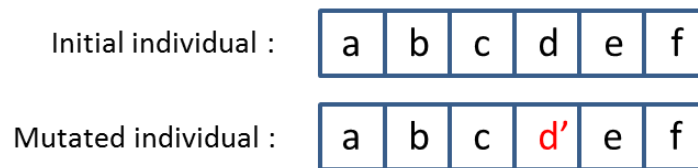


**Figure 117. Description of mutation. Parameters are changed randomly**

Usually, the mutation is done by modifying the value of parameters randomly as done in the "initialization" step in equation (IX-5). The specificity of the DEA algorithm is to mutate the parameter of an individual according to a differential scheme. The mutated individual  $v_i$  is generated by randomly



selecting three other individuals different from one another and from  $x_i$  named  $x_{r0}$ ,  $x_{r1}$  and  $x_{r2}$  as it is shown in Figure 118.

$$v_i = x_{r0} + F_{scaling}(x_{r1} - x_{r2}) \quad (IX-6)$$

$v_i$  corresponds to the mutated individual  $i$ .  $F_{scaling}$  is an input parameter of the DE algorithm. The scale factor,  $F_{scaling} \in (0,1+)$ , is a positive real number that controls the rate at which the population evolves. While there is no upper limit on  $F$ , effective values are seldom greater than 1.0. This parameter impacts directly the search area of the solution and the convergence of the algorithm.

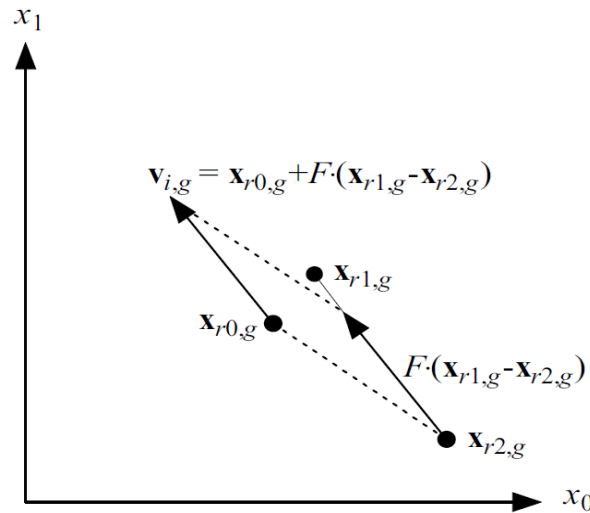


Figure 118. Differential mutation: the weighted differential,  $F_{scaling}(x_{r1} - x_{r2})$ , is added to the base vector  $x_{r0}$  to create the mutant  $v_i$  [PRI00]

- **Crossover**

The crossover process crosses randomly parameters of the original individual  $x_i$  and the ones of the mutated individual  $v_i$  with a probability of  $C_r \in [0; 1]$ . Two types of crossovers are possible: block and uniform crossovers (see Figure 119). In the first type, the new individual is composed by two parts: the first one corresponds to either the initial or the mutated individual and the second part by the other. In uniform crossover, also known as discrete recombination and used by DEA algorithm, each parameter is chosen independently from the initial individual or the mutated one.

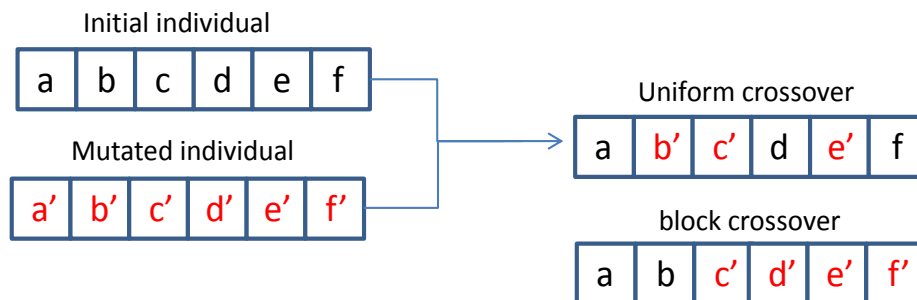


Figure 119. Crossover of two individuals

To ensure at least one crossover per individual,  $j_{rand}$  is added. It is generated randomly for each individual: the trial parameter ' $j_{rand}$ ' is taken from the mutant to ensure that the trial vector does not duplicate  $x_{i,j}$ . Because of this additional demand,  $C_r$  only approximates the true probability,  $P_{Cr}$ , that a trial parameter will be inherited from the mutant. The scheme of the crossover in the differential evolution algorithm is the following:

$$u_{i,j} = \begin{cases} v_{i,j} & \text{if } (rand_j(0,1) \leq C_r \text{ or } j = j_{rand}) \\ x_{i,j} & \end{cases} \quad (IX-7)$$

with  $u_i$  is the trial individual ' $i$ '. A specificity of the DEA algorithm compared to the genetic algorithm (GE) is that mutation and crossover operation are not separate: crossovers are made between the mutated individual and the original one, whereas in genetic algorithm they are done between different individuals of the original population. In addition, DEA is often used when parameters are scalar and not Boolean as in GE.

### IX.b.3. Selection:

To each individual  $x_{i,j}$ , a fitness value  $f(x_i)$  is associated. This fitness value contains the information about the criterion to optimize. Therefore, we are going to select the individuals with the best fitness values (the lowest one). The selection operation compares for each individual the fitness value of the original  $x_i$  and the trial one  $u_i$  as shown in the following expression:

$$x_{i,g+1} = \begin{cases} u_{i,g} & \text{if } f(u_{i,g}) \leq f(x_{i,g}) \\ x_{i,g} & \text{otherwise} \end{cases} \quad (IX-8)$$

$x_{i,g}$  represents the individual ' $i$ ' of the generation ' $g$ ';  $u_{i,g}$  represents the trial individual ' $i$ ' of  $x_{i,g}$  generated thanks to mutation and crossover processes.  $x_{i,g+1}$  represents the new individual ' $i$ ' of the next generation. Mutation, crossover and selection processes are done on the new generation and so on until the stop criterion is reached: for example attending maximum number of generation or a convergence criterion. A pseudo C-code of the algorithm is given as an illustration in Figure 120 and a flow-chart describing different steps of the DEA can be found in Figure 121.

The following Table 21 represents an application of differential evolution algorithm to our case:

Notations	Description
Individual $x_i$	Vector of driving instruction defining a train's profile
Parameter $x_{i,j}$	Driving instruction
Fitness $f$	Function of energy consumption and time constraints
Selection criteria	lowest value of $f$

**Table 21: Connection between the differential evolution algorithm and the optimization of high-speed lines**

```

// initialize...

do // generate a trial population
{
    for (i=0; i<Np; i++) // r0!=r1!=r2!=i
    {
        do r0=floor(rand(0,1)*Np); while (r0==i);
        do r1=floor(rand(0,1)*Np); while (r1==r0 or r1==i);
        do r2=floor(rand(0,1)*Np); while (r2==r1 or r2==r0 or r2==i);
        jrand=floor(D*rand(0,1));

        for (j=0; j<D; j++) // generate a trial vector
        {
            if (rand(0,1)<=Cr or j==jrand)
            {
                 $u_{j,i} = x_{j,r0} + F * (x_{j,r1} - x_{j,r2});$  //check for out-of-bounds ?
            }
            else
            {
                 $u_{j,i} = x_{j,i};$ 
            }
        }
    }

    // select the next generation

    for (i=0; i<Np; i++)
    {
        if ( f( $u_i$ ) <= f( $x_i$ ) )  $x_i = u_i$ ;
    }
} while (termination criterion not met);

```

Figure 120: Pseudo C-code of the differential evolution algorithm [PRI00]

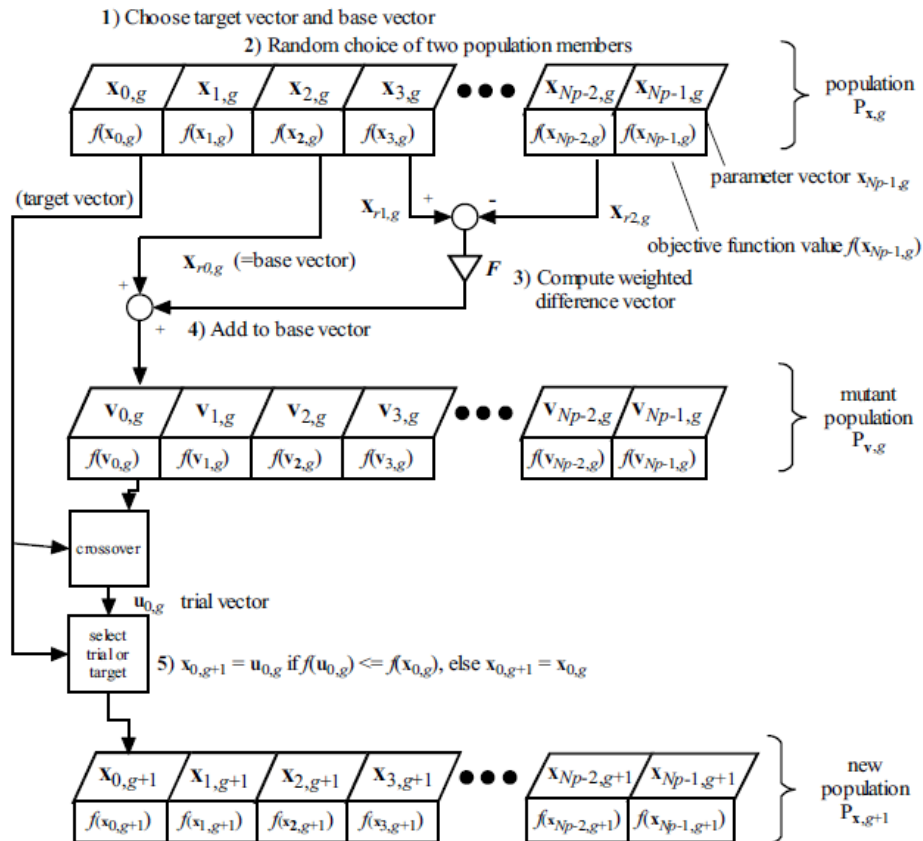


Figure 121: Flow chart of the differential evolution algorithm [PRI00]

### IX.c. DEFINITION OF THE ALGORITHM

In order to implement the differential evolution algorithm in high speed line application, a speed profile should be defined by the few parameters (in genetic algorithm these parameters are referred as “genes”). Taking into consideration the long distance of a high speed line and its varying profile, the journey can be cut into  $N_z$  zones. Each zone is characterized by a number of parameters. Therefore, the problem consists in choosing the criteria for cutting the line into zones and defining the characteristics of each zone. In our study, each zone is characterized with the following three parameters:

- $V_{max}$  : speed at which coasting is applied when reached
- $V_{min}$  : speed at which traction is applied again after coasting
- $Coef$  : maximum traction coefficient applied in the selected zone. Motors full power is applied when  $Coef=1$ . Else it will be limited.

The total number of parameters per individual ‘D’, mentioned in (IX-3), will be then:  $3 \times N_z$ . In the following, these three parameters will represent the driving instructions in each zone. For the geographic division, we can choose inter-operational zones, speed zones, or a combination of both. An inter-operational zone is a zone between two operational points; a speed zone corresponds to one speed limit. In this study, a combination of both zones is applied.

#### IX.c.1. Constraints handling:

- **Time constraints**

As explained previously, for HSL, there are strong constraints related to passage times at each operational point (OP). They should be respected by each train in order to avoid collisions or traffic perturbations. Any delay or advance may cause troubles to the traffic. An operational point is typically a train station or a junction. To take into account those constraints, a penalty is added in the fitness function depending if the train is late or ahead. This will bias the fitness function in favour of the solutions that respect the constraints. The fitness function (IX-1,2) used in [CUC12] penalizes explicitly the arrival time constraint. We observe that the more the train is late, the more it is penalized. However, if the train is ahead, the penalty does not depend on the time of advance as  $\frac{T_{target}}{T_{flat-out}}$  does not depend of the running time ‘T’. In fact, the penalty is implicit: the more the train is ahead, the more energy it will consume. Thus, it is penalized by the energy factor. However, in our case, we have several time constraints along the journey. When taking the same fitness function, we observed that the train was always ahead, for the first operational points of the journey. Thus, the energy does not cover effectively this case and this function does not completely fit our problem: we need to have an explicit time penalty for trains in advance. The choice of a new function will be done later in the chapter.

- **Boundary constraints**

When generating a new individual, boundary tests should be done on each parameter. Parameters ‘Coef’, ‘Vmax’ and ‘Vmin’ should belong to a pre-defined interval (IX-9) or to an evolutionary changing interval (IX-10) (IX-11) that depends of the selected zone. In (IX-9), ‘Coef’ can evolve between 0.5 and 1. At its lower bound, the train will accelerate with half of its maximum effort. A lower value will be too much penalizing and may cause severe impact on the traffic. Thus, an individual with a ‘Coef’ less than 0.5 or more than 1 will be automatically corrected using (IX-16).

$$0.5 \leq \text{Coef} \leq 1 \quad (\text{IX-9})$$

$$0 \leq V_{\min} \leq V_{\max} \leq V_{\text{limit}} \quad (\text{IX-10})$$

In order to avoid that the trains run too slowly, more restrictive constraints were made on Vmax and Vmin. In (IX-11), a train’s maximum speed should not exceed the speed limitation in the selected zone. It should neither go under  $V_{\text{limit}}/2$  else the train will run too slowly and the solution won’t be interesting because of its big delay. In (IX-12),  $V_{\min}$  should not exceed the maximum speed. As in (IX-11), the lower bound is set to half of the upper bound, i.e.  $V_{\max}/2$ , to avoid long coasting range causing high delays.

$$\frac{V_{\text{limit}}}{2} \leq V_{\max} \leq V_{\text{limit}} \quad (\text{IX-11})$$

$$\frac{V_{\max}}{2} \leq V_{\min} \leq V_{\max} \quad (\text{IX-12})$$

As  $V_{\text{limit}}$  depends on the considered zone “z”,  $V_{\max}$  and  $V_{\min}$  also depends on the zone. Hence:

$$\frac{V_{\text{limit}}(z)}{2} \leq V_{\max}(z) \leq V_{\text{limit}}(z) \quad (\text{IX-14})$$

$$\frac{V_{\max}(z)}{2} \leq V_{\min}(z) \leq V_{\max}(z) \quad (\text{IX-15})$$

The problem with differential mutation is that the new values of  $v_{i,j}$  can be out of bounds. Therefore, the bounced-back method described in [PRI00] is used to handle those cases.

For the parameter Coef, this method is rather simple as the upper and the lower bounds are constants:

$$\text{If } v_{i,j} < b_{\text{lower}} = 0.5, \quad v_{i,j} = \frac{(b_{\text{lower}} + x_{i,j})}{2} \quad (\text{IX-16})$$

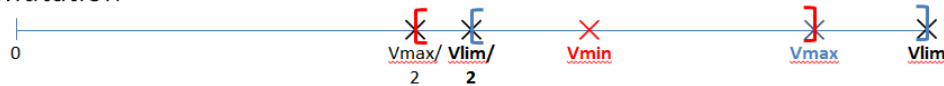
$$\text{If } v_{i,j} > b_{\text{upper}} = 0.5, \quad v_{i,j} = \frac{(b_{\text{upper}} + x_{i,j})}{2}$$

where  $x_{i,j}$  is the parameter's value before the mutation which already respects the constraints.

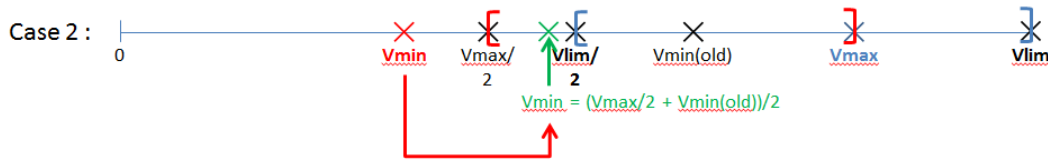
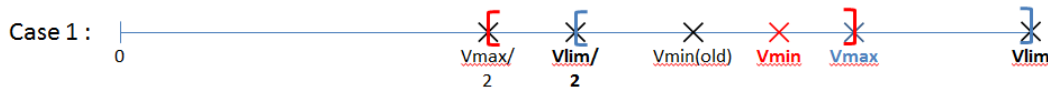
For  $V_{\text{max}}$ , the situation is the same except that  $b_{\text{lower}}$  and  $b_{\text{upper}}$  depend on the zone  $z$  but they remain constant between two generations. However, for  $V_{\text{min}}$ , the situation is much more complex as  $b_{\text{lower}}$  and  $b_{\text{upper}}$  depend on the zone and the generation: the value before mutation  $x_{i,j}$  might not respect the new boundaries  $b_{\text{lower}}$  and  $b_{\text{upper}}$  as they both depends on  $V_{\text{max}}$  which changes between two generations. Two situations are possible; each one present many eventual evolution cases (Figure 122) that were detected and solved while developing the algorithm.

### Situation 1: $V_{\text{min}}(\text{old})$ belongs to the new interval allowed for $V_{\text{min}}$

Before mutation

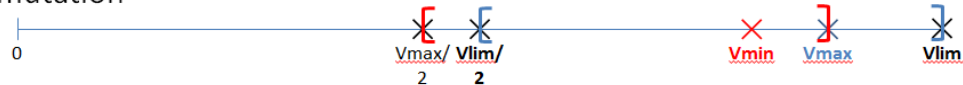


After mutation



### Situation 2: $V_{\text{min}}(\text{old})$ does not belong to the new interval allowed for $V_{\text{min}}$

Before mutation



After mutation

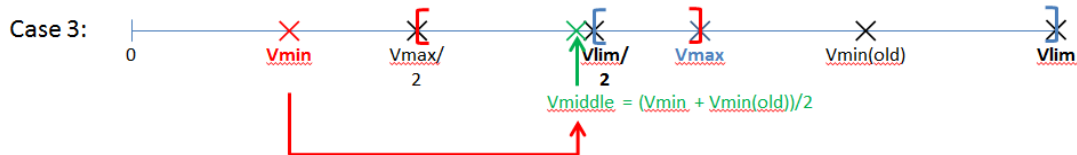
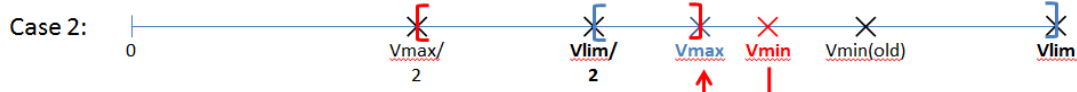
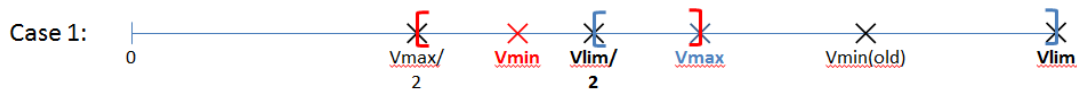


Figure 122: Flow chart of the handling of the constraints for  $V_{\text{min}}$

In situation 1, we cope with the same situation as for  $V_{max}$  and the classic bounced-back method is applied when  $V_{min}$  is below  $V_{max}/2$ . The new value is set midway between the old  $V_{min}$  (value of  $V_{min}$  at the previous generation), and the closest bound ( $V_{max}/2$ ).

In situation 2, the problem is more complicated as  $V_{min}(old)$  does not belong to the new interval allowed. Therefore, three cases emerge depending on the value of the new  $V_{min}$ . If  $V_{min}$  belongs to the new interval, nothing is done as it respects the constraints (Case 1). If  $V_{min}$  is out of bounds on the same side as  $V_{min}(old)$ , we set  $V_{min}$  to be equal to the closest limit of the interval (Case 2). If  $V_{min}$  and  $V_{min}(old)$  are both outside the interval on opposite side, we calculate the value of  $V_{middle}$ . If it is within the bounds, then the new  $V_{min}$  is equal to  $V_{middle}$ . Otherwise, we set  $V_{min}$  equal to the closest boundary of the interval to  $V_{middle}$  (Case 3).

#### IX.c.2. Fitness function definition

We are looking for a fitness function expression that ensures that the time constraints are respected with a margin of +/- 30 seconds while selecting the less consuming solutions. All the target times are given in seconds and correspond to the time elapsed since the starting point of the section of study. An individual's energy consumption should be evaluated based on a reference value. Therefore, for a given journey, we consider as reference energy consumption the flat-out run's energy. In the following, we will start by studying the fitness function defined in equations (IX-1, 2), then, it will be improved to meet our application's specificity.

- **Parametric study of convergence parameters**

Before starting to study the fitness function, initial parameters  $F_{scaling}$ ,  $Cr$  and  $NP$  should be defined.

According to [PRI00], the stated range for  $F_{scaling}$  is  $[0,1]$ . On one hand, 1 is an empirically derived upper limit because no function successfully optimized has required  $F_{scaling} > 1$ . This is not to say that solutions are not possible when  $F_{scaling} > 1$ , but only that they tend to be both more time consuming and less reliable than if  $F_{scaling} < 1$ . On the other hand, a small value of  $F_{scaling}$  causes premature convergence (toward a local minimum) due to crucial selection process and limited population diversity. Therefore, and based on examples presented in [PRI00],  $F_{scaling}$  is set to 0.9 in order to explore a large searching area.

Concerning  $Cr$ , the crossover rate, it can be considered "approximately" equal to the probability that a parameter is inherited from a mutated individual. When it's near  $Cr=1$ , exploration is favoured and algorithms take longer time to converge due to high diversity. For this study, we set  $Cr=0.7$ .

The choice of the population size ( $NP$ ) is very strategic as the computation time is linearly dependent of this parameter. Therefore, by doubling the value of  $NP$ , the computation time is twice longer. However, it is also important not to choose this input data too small as the research area of the optimal solution will be more restricted. Moreover, knowing that for each individual, three other

individuals (r0, r1 and r2) are chosen randomly for the mutation, a minimum of 4 individuals is required. For this study, we set NP=8 that seems to be an acceptable compromise.

- **Ponderation**

For the ponderation, the number of weights depends on the number of operational points (NbOp). There is always one weight for the energy and (NbOp -1) weights for the time (as the first operational point corresponds to the beginning of the section where there is no time constraints). Moreover, the sum of the weights must be equal to one. Therefore:

$$w_e + \sum_{op=1}^{NbOp-1} w_t(op) = 1 \quad (IX-17)$$

The convergence is observed on a simple case: 1 speed zone and 2 operational points which is the minimum required with a slack-time of 5%. Therefore, there are only two weights, one for the energy and one for the time. Setting  $w_t = w_e = \frac{1}{2}$ , the time was not sufficiently penalized. Then setting  $w_t = \frac{2}{3}$  ;  $w_e = \frac{1}{3}$ , this restriction was a little too strict. Therefore, by dichotomy,  $w_t = \frac{7}{12}$ ;  $w_e = \frac{5}{12}$  are set. The results are shown in the Table 22.

	Ponderation		Delay (s)		Energy savings (%)	
	$w_e$	$w_t$	average	std dev	average	std dev
Case 1	1/2	1/2	170	2	93	0.6
Case 2	1/3	2/3	0	0	46	0.0
Case 3	5/12	7/12	12	4	49	1.2

**Table 22: Average delay and average energy savings on 1 speed zone and 2 operational points for the final population and for different ponderations**

In this simple case, the optimal weight factor between time and energy ponderation is:

$$WF = \frac{w_t}{w_e} = \frac{7}{5} \quad (IX-18)$$

This ponderation is tested first on a case with two speed zones and then on a case with several operational points and thus several time constraints. We consider that all time weights ( $w_t(op)$ ) are equal and the weight factor (WF) of each one is kept to 7/5. Therefore:

$$w_t(op) = \frac{7}{5} w_e, \quad op \in \llbracket 1; NbOp - 1 \rrbracket$$

$$w_e = \frac{1}{1 + \frac{7}{5}(NbOp - 1)} \quad (IX-19)$$

The results can be found in Table 23. We observe that they confirm our preliminary ponderation system.



speed zones	operational pts	Time 1 (s)		Time 2 (s)		Energy savings (%)	
		average	std dev	average	std dev	average	std dev
2	2	9.0	4.7	-	-	30	1.1
2	3	1.0	1.4	-1.7	2.9	42	0.6

**Table 23: Average delay and average energy savings on 2 speed zones and many operational points for the final population and for selected ponderations**

A comparison is done between two runs, between station A and station B, with a 5% slack-time and containing many OP; in the first case, the train stops at station A then at station B, in the second, the train passes without stopping at both stations. Even though in both cases the train always finishes its journey around the given target time (see column “Time 3” in Table 24), it tends to be early at the first operational point (see column “Time 1” in Table 24). This phenomenon can be explained by the fact that the fitness penalizes implicitly ahead trains through consumed energy. Indeed, this works when the train has only one time constraint (case of urban systems) and thus, when it is ahead, the train has certainly consumed more energy when running faster. However, in the case of several time constraints, if the fitness does not depend explicitly of the ahead duration ( $T(op)$ ), the train tends to run faster in the beginning of its journey and will coast and cut power in the end. Then, all of the slack-time is kept for the end of the trip to avoid braking and the energy consumption is then considerably reduced. For example, the energy saved by coasting when going from 300 km/h to 150 km/h corresponds to the three quarter of the kinetic energy of the train  $\left(\frac{1}{2} m \frac{(300^2 - (300/2)^2)}{3.6^2} = \frac{3}{4} \cdot \frac{1}{2} m \frac{(300)^2}{3.6^2}\right)$ . Thus, the consumption does not anymore penalize sufficiently trains ahead and the expression of the fitness function has to be changed in order to avoid this kind of situations (HSL and suburban applications).

Stations		Time 1 (s)		Time 2 (s)		Time 3 (s)		Energy Savings (%)	
A	B	average	std dev	average	std dev	average	std dev	average	std dev
Stop	Stop	-28.4	8.3	-8.7	9.7	3.7	6.5	20.7	0.5
Pass	Pass	-32.4	4.8	-3.3	2.8	2.7	4.9	22.5	0.3

**Table 24: Average delay and average energy savings of the final population for different runs showing that trains are ahead in the 1<sup>st</sup> OP and keep coasting for the end**

○ Time penalty expression

As mentioned before, the fitness expression (IX-1, 2) does not penalize sufficiently trains passing ahead. To find a new efficient expression of the time penalty, the previous weight distribution described in Equation (IX-19) is kept. The following solutions in Table 25 will be studied, first on simple

cases then on more complex ones and finally on real scenarios (note that solution n°1 corresponds to the expression used so far):

Time Penalty	$T \leq T_{target}$	$T > T_{target}$
1	$\frac{T_{target}}{T_{flat\_out}}$	$\frac{T^2}{T_{target} T_{flat\_out}}$
2	$\frac{T_{target} T_{flat\_out}}{T^2}$	$\frac{T^2}{T_{target} T_{flat\_out}}$
3	$\frac{T_{target}}{T}$	$\frac{T^2}{T_{target} T_{flat\_out}}$
4	$\frac{T_{target}}{T}$	$\frac{T}{T_{target}}$
5	$\frac{T_{target}^2}{T^2}$	$\frac{T^2}{T_{target}^2}$

Table 25. Different time penalties tested for the fitness expressions

First, different time penalty expressions (Table 25) are tested on a simple section with two operational points, one speed zone and 5% slack-time. Results immediately show that time penalty N°4 is not adequate because the train is too delayed (see Table 26).

Time Penalty	Time (s)		Energy savings (%)	
	average	std dev	average	std dev
1	0.5	0.6	26	0.2
2	-0.8	0.8	25	0.7
3	-1.7	1.2	25	0.7
4	73.5	10.3	41	1.5
5	1.5	0.0	26	0.0

Table 26: Average time and energy savings of the final population for different time penalties

In the case of three operational points, simulation results are given in Table 27. For time penalty N°2, the train is always ahead everywhere. Moreover, the results show that it takes less into account energy savings. Therefore, this solution can also be eliminated.

Time Penalty	Time 1 (s)		Time 2 (s)		Energy savings (%)	
	average	std dev	average	std dev	average	std dev
1	5	16	28	20	27	2
2	-2	1	-10	5	22	1
3	19	8	15	22	24	3
5	-9	12	16	11	26	1

Table 27: Average time and energy savings of the final population for different time penalties applied on a run with 3 OPs

Finally, the study is done for four operational points, first with 5% slack-time, then with 2% slack-time. The results are given respectively in Table 28 and Table 29. The first table confirms the fact that penalty N°2 is not good. The train arrives at the end point with 87 seconds average delay, exceeding the 30 seconds allowed.

Time Penalty	Time 1 (s)		Time 2 (s)		Time 3 (s)		Energy savings (%)	
	average	std dev	average	std dev	average	std dev	average	std dev
1	-39	15	-12	16	16	18	20	1
2	-36	13	-6	15	87	76	22	3
3	-16	14	-8	5	-6	7	18	1
5	-4	6	17	8	12	10	19	1

**Table 28: Average time and energy savings of the final population for different time penalties**

(NP = 8 ; Gen = 50 ; slack-time: 5%)

The 2% slack-time is a very constraining case as the flexibility is very limited. The penalty N°1 is also eliminated because the train is always ahead in the beginning of the run and late at the end. Therefore, the convergence time is longer (Gen=100 generations). The two solutions that remain possible are N°3 and N°5. The latter is chosen because time penalty's expressions between advance and delay are "symmetric". To validate this choice, three different real trains' scenarios are tested. The three of them with respectively one, two and three operational points, converged to a final population respecting punctuality within  $\pm 30$ s and good energy savings.

Scenario 1		Scenario 2			Scenario 3			
Energy savings (%)	$\Delta T1$	Energy savings (%)	$\Delta T1$	$\Delta T2$	Energy savings (%)	$\Delta T1$	$\Delta T2$	$\Delta T3$
34	27	26	-1	10	35	-1	-6	-15
31	5	27	1	23	35	-6	2	1
32	2	26	0	12	36	4	-4	18
33	15	25	0	5	36	-5	4	32
32	11	25	1	9	34	12	-5	-5
32	2	26	0	12	35	-4	-10	0
31	-1	27	2	22	36	0	6	-4
31	4	27	-2	25	35	-7	-19	14

**Table 29. Time differences with target times and energy savings for three real scenarios using penalty N°5**

The results of the simulations for function fitness n°5 on four different real trains are shown in Table 29. Solution N°5 is finally retained. The fitness function is then:

$$f(x) = w_e \frac{E(x)}{E_{flat-out}} + \sum_{\substack{op=1 \\ T_{réel} \leq T_{target}}}^{NbOP-1} w_t(op) \left( \frac{T_{target}(op)}{T(x, op)} \right)^2 + \sum_{\substack{op=1 \\ T_{réel} \geq T_{target}}}^{NbOP-1} w_t(op) \left( \frac{T(x, op)}{T_{target}(op)} \right)^2$$

With:

$$\begin{cases} w_t(op) = \frac{7}{5} w_e, & op \in \llbracket 1; Nbre_{pts_{op}} - 1 \rrbracket \\ w_e = \frac{1}{1 + \frac{7}{5} (Nbre_{pts_{op}} - 1)} \end{cases} \quad (IX-20)$$

- **Energy penalty expression**

In the case where the speed profile of a service begins and/or ends with speeds different than zero (for example a train disappearing from a timetable due to bifurcation), the difference of kinetic energy between reference speeds and actual ones should be considered. Thus, in order to compare the energy consumption of two individuals belonging to a same service, we need to take into account this kinetic energy. In most cases, the entry speed is fixed in simulations and therefore, there are no differences between both individuals at the entry of the service. However, the exit speed can be quite different and it is clear that a train that exits at a lower speed has normally consumed less energy than the one who exits with a higher speed. Nevertheless, the latter has a higher kinetic energy and will thus consume less on the next section. This is the case of trains disappearing from timetable at bifurcations.

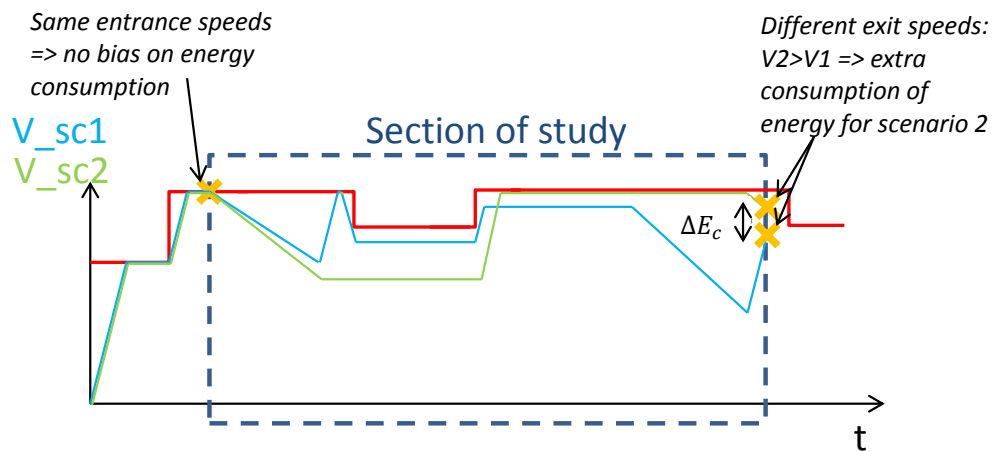


Figure 123. Comparison between two solutions with different exit speeds

Therefore, we correct the energy consumption with the difference of kinetic energy between the target exit speed and the actual one obtained by simulation for each individual  $x$ . The fitness function chosen for our study is:

$$f(x) = w_e \frac{E(x) + \Delta E_{kinetic}}{E_{flat-out}} + \sum_{\substack{op=1 \\ T \leq T_{target}}}^{Nb\_OP-1} w_t(op) \left( \frac{T_{target}(op)}{T(x, op)} \right)^2 + \sum_{\substack{op=1 \\ T \geq T_{target}}}^{Nb\_OP-1} w_t(op) \left( \frac{T(x, op)}{T_{target}(op)} \right)^2 \quad (IX-21)$$

With:

- $w_e$ : ponderation of the energy expression in fitness function
- $E(x)$ : traction energy consumed by the individual  $x$
- $\Delta E_{kinetic}$ : difference of kinetic energy between the reference exit speed and the actual exit speed of individual  $x$
- $E_{flat-out}$ : traction energy consumed by a flat-out run
- $w_t(op)$ : ponderation of the time penalty expression in fitness function at operational point  $n^\circ(op+1)$
- $T_{target}(op)$ : target time given by the timetable that the train must respect at operational point  $n^\circ(op+1)$
- $T(x, op)$ : Time when the individual  $x$  reaches the operational point  $n^\circ(op+1)$
- $NbOP$ : number of operational points

- **Initial parameters backward validation**

In order to study the fitness function, some assumptions were considered concerning algorithm's parameters ( $F_{scaling}$ ,  $NP$ ,  $Cr$ ,  $w_t/w_e$ ). Therefore, after defining the fitness to be used (IX-21), a test is done to validate or modify these values.

A small correction has been made to the ponderation system after some trials on real timetables with the new fitness function. Therefore, the new ponderation system described in Equation (IX-22) will be used.

$$w_t(op) = \frac{8}{5} * w_e, \quad op = 1 \dots Nb\_OP - 1$$

$$w_e = \frac{1}{1 + \frac{8}{5} * (Nb\_OP - 1)} \quad (IX-22)$$

In addition,  $F_{scaling}=0.7$  gave better results as the algorithm converged faster to a satisfying solution while  $NP=8$  and  $Cr=0.7$ .

#### **IX.d. CONCLUSION**

In conclusion, speed profile optimization is applied to each train service separately. Its aim is to find a solution that consumes the less energy while respecting time passage at each operational point within a margin of  $\pm 30s$ . For HSL use case, an algorithm is proposed based on differential evolution algorithm. Solutions were compiled using a mono-train simulator developed internally in ALSTOM. The algorithm associated for each individual a vector of input parameters that were injected into the

simulator. The latter calculated energy and speed profile taking into account trains and line's characteristics. A new fitness function specific for HSL and suburban lines was also defined and tested. Different railway constraints were also handled.

Now that trains are optimized from energy point of view, power peaks that may occur due to unfavourable timetable synchronisation should be avoided. Therefore, a second optimization step will be detailed in the following chapter.

Electrical bills are calculated based on the energy consumed by a system while its average power over 'T' minutes (T depends on each country: in France T=10 min while in Belgium T=15 min) doesn't exceed the maximum subscribed power. In the opposite case, an additional cost is added because the consumer didn't respect his contract and perturbed grid's equilibrium. Railways are no exception. Operators try to reduce their energy consumption while ensuring the respect of maximum substations' power. As explained in section A, HSL are AC powered system. Substations are simply composed of transformers which allow re-injecting braking power into the upper grid. However, today, the average power over 'T' minutes is calculated only from the consumed power value at substation's level and doesn't take into consideration later braking power peaks. Therefore, trains synchronization objective is to coincide braking and accelerating powers in order to reduce the consumed average power at SST's level.

In general, Traffic Management System (TMS) is centralized. The control center receives data on a wide predefined territory. Trains' run within this zone are supervised and controlled by the TMS through the associated train dispatcher. The objective of a TMS is not only to solve traffic problems and avoid conflicts; a main task is to restore the stopped traffic operations as soon as possible. Therefore, when retention solution is selected by TMS to solve a detected problem, a power constraint should be added to avoid simultaneous trains' acceleration in the same electric zone. This will prevent power peaks and voltage drops in this zone. Trains synchronization's objective is to optimize the energetic interaction between trains in order to favour braking power exchange and avoid power peaks at substations. It should also respect fundamental constraints such as security, punctuality and fluidity. Global energy consumption optimization should not oppose to the traffic regulation's rules.

The previous sub-paragraph presented energy optimization solution for trains driving profile. The output is then a timetable with defined departure times, dwell times and running time. Each train's journey is energetically optimised by selecting the most efficient speed profile. Nevertheless, it does not mean that the timetable is optimised. A first step, dwells time modification, will be done offline. It acts on dwell times in order to increase the amount of braking power exchanged between trains and eliminate simultaneous accelerations. This will reduce power peaks and the total energy consumption. The second step "delay compensation" will be rather done online. It takes into consideration the time delays encountered when the trains are in service. In real operation conditions, there are a variety of random disturbances that will keep trains off the pre-calculated energy-efficient timetable such as doors reopen/reclose for safety issues. Only short disturbances that can be fixed automatically are taken into consideration. The flowchart below summarises the methodology:

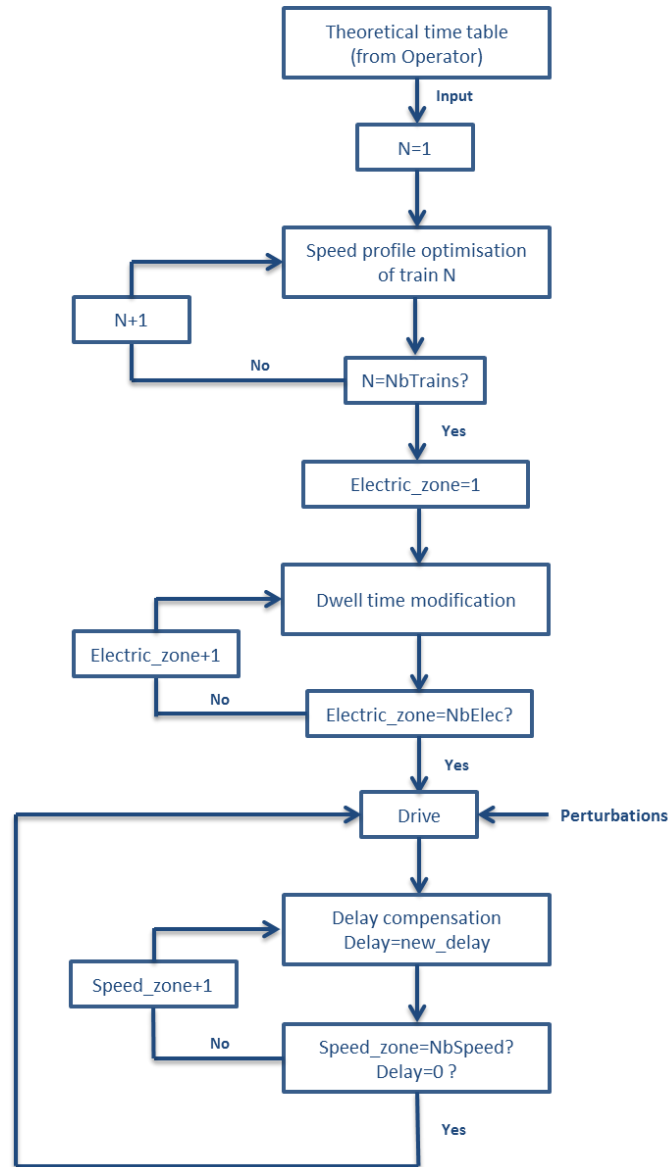


Figure 124: Energy optimization flowchart

In the following paragraphs, both steps, dwell time modification and delay compensation, will be detailed.

#### X.a. DWELL TIMES MODIFICATION

In high speed AC networks, the track is divided into electric zones in order to alternate the connection of railway grid to the AC 3-phase grid (connection A-B, B-C and C-A), and thus to ensure a better load balancing. Therefore, the study can be split geographically into zones given the fact that two trains in different electric zones cannot interact energetically. In addition, in most cases, each zone is fed by one substation. Thus, by extracting trains' power curve in this area and after time rescaling, SST's power consumption is simply equal to the sum of these curves. This optimization step can be resumed as following:



- Objective : minimize the maximal average power calculated with 'T' minutes sliding window at each substation
- Variables : dwell-time at each station for each train
- Constraints :
  - ✓ Trains can only be delayed (without exceeding the maximum limit allowed)
  - ✓ Dwell-time increase must be an integer and bigger than 5 (even a multiple of 5)
  - ✓ If a train's service is delayed, all the following services belonging to the same train must be also delayed

This can be expressed mathematically as follows: 
$$P_t(t) = \underbrace{\sum_i P_i(t)}_{P1} + \underbrace{\sum_j P_j(t + T_j)}_{P2} \quad (X-1)$$

P1 represents the total power of trains that are not shifted. P2 represents the total power of shifted trains.  $T_j$  is the integer parameter to optimize while respecting the following constraints:

- $P_t < P_{max}$  ; with  $P_{max}$  the maximum allowed power defined in the contract between the operator and the energy provider
- $T_j \geq 0$

The objective function is then:  $\min_{T_j}(P_t)$ . The optimization process is then repeated for the other selected electric zones.

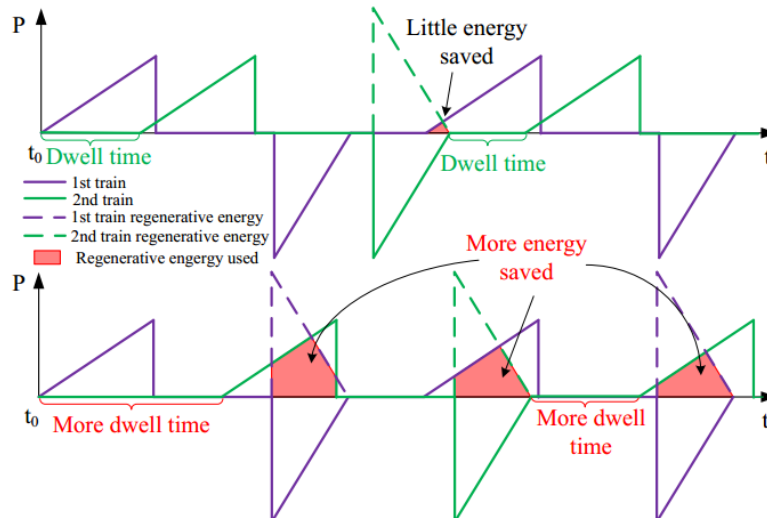


Figure 125: Dwell time modification and braking energy exchange [CHE14]

Figure 125 shows two trains' power profiles. Positive values correspond to acceleration mode and negative values represent braking mode. Extending second train's dwell time allows increasing power exchange between trains and reducing by that the total consumed power.

From operational point of view and to be more realistic, the time step of a train's shift should be higher than 5 seconds because high speed lines are not automatic. Thus, we included the response time of the driver. The shift should also be limited as a train too much delayed is unacceptable. Therefore, we chose a maximal 30 seconds value for a train's total shift. This time shift limitation

should include previous delays already introduced by the speed profile optimization (eco-driving module). Even though these constraints are very important, they are also quite severe and reduce the algorithm's flexibility. The latter can be increased by increasing time delay tolerance.

#### X.a.1. Algorithm definition

In order to solve optimization problem, Mixed Integer Programming (MIP) is suggested by [KYU10]. It is a heuristic method consisting in choosing the substation to optimize and the train to delay and try if shift this train increases or decreases the power peak. The user enters the following information in the algorithm:

- $Shift_{Max}$ : corresponds to the maximum train's shifting time
- $T$ : time over which the average power is computed (*In our case:  $T=10\text{ min}$* )
- $MaxIteration$ : maximal number of train shifts allowed by the user

The main steps of the algorithm are:

- Select the non-optimized substation (SST) with the highest 10 minutes average power
- Select the train with the highest instantaneous power at the end of the corresponding 10 minutes window
- Shift the train with 5s time step while: the average powers of the selected SST and the ones already optimized do not increase; the maximum time shift is not exceeded. Once finished, it is not allowed to re-shift the train.

The algorithm stops when:

- maximum time shifts is reached
- all SSTs were optimized
- no train can be shifted anymore

In order to calculate the remaining maximum time shift after speed profile optimization for a service  $n^o$ , the following system of inequalities (X-2) should be solved where  $\delta_j$  represents the algebraic value of the delay introduced in the eco-driving step applied on service  $n^o$ ,  $T_j$  represents the new shift added before service  $n^o$  ( $\forall j, T_j \geq 0$ ),  $Shift_{Max}$  the total maximal delay allowed for each service and  $N$  the number of services for a given run:

$$\left\{ \begin{array}{l} T_1 + \delta_1 \leq Shift_{Max} \\ \vdots \\ T_1 + \delta_1 + \dots + T_i + \delta_i \leq Shift_{Max} \\ \vdots \\ T_1 + \delta_1 + \dots + T_N + \delta_N \leq Shift_{Max} \end{array} \right. \quad (X-2)$$

Figure 126 shows the different time shifts introduced by both optimizations. Grey lines indicate the reference time at which the train should stop.

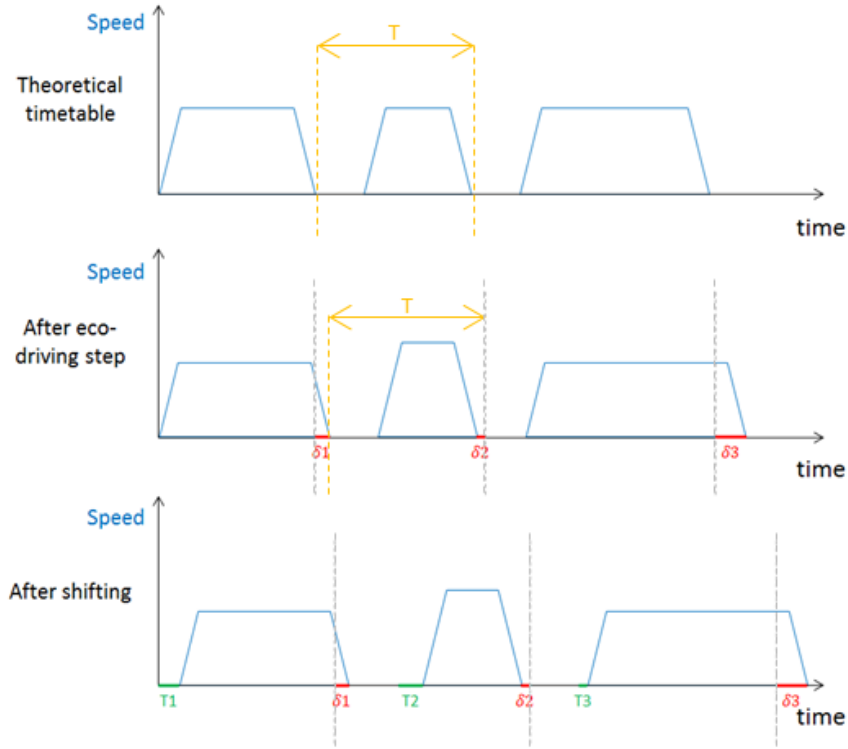


Figure 126. Different delays introduced by the two-step optimization

The total dwell time shift of service n°l is:

$$Shift_{S_i} = \sum_{j=1}^i T_j \quad (X-3)$$

Hence, the system of inequalities (X-2) can be written as follows:

$$\left\{ \begin{array}{l} Shift_{S_1} + \delta_1 \leq Shift_{Max} \\ \vdots \\ Shift_{S_i} + \sum_{j=1}^i \delta_j \leq Shift_{Max} \\ \vdots \\ Shift_{S_N} + \sum_{j=1}^N \delta_j \leq Shift_{Max} \end{array} \right. \quad (X-4)$$

with  $0 \leq Shift_{S_i} \leq Shift_{S_{i+1}} \leq \dots \leq Shift_{S_N}$  and  $\delta_j \geq 0$

Finally, we obtain:

$$Shift_{S_i} = Shift_{Max} - \max_{p \in \llbracket i:N \rrbracket} \left( \sum_{j=1}^p \delta_j - \sum_{k=i+1}^p T_k \right) \quad (X-5)$$

## X.b. DELAY COMPENSATION

Now that the first step is executed, a theoretical energy-efficient timetable is calculated. When trains are in operation, different perturbations can cause unexpected time delays. The new delayed

timetable is not necessarily energy efficient because of the reduction of braking energy exchange. In this step, delay compensation will be executed on the speed zone following the detected time delay. If the delay is completely caught up, the timetable will re-match the pre-calculated energy-efficient timetable. In the opposite case, remaining time delay will be treated in the next speed zone. A speed zone is defined for every speed limitation. In a given speed zone, four types of possible driving phases can be considered: acceleration, speed maintain, coasting, braking. Depending on speed limitations before and after the selected zone, it is not mandatory to have the 4 types in a same zone. In Figure 127, different speed profile possibilities depending on speed limitations are presented.

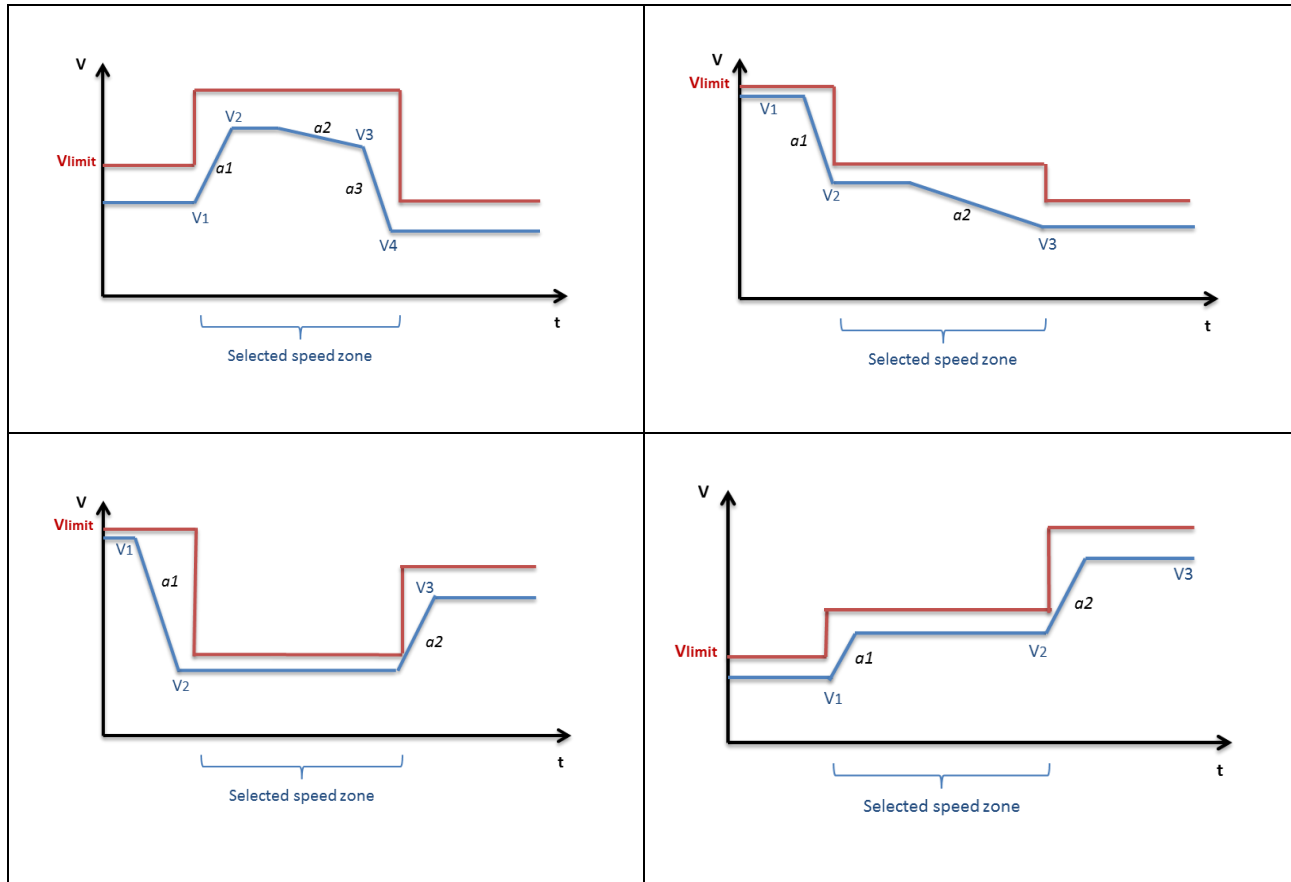


**Figure 127. Different speed profile variations depending on speed limitations**

We consider the case where the limit speed in the selected zone is higher than the surrounding speed zones (Figure 128). Only this case, which is the most complicated one, will be detailed. The rest can be done in the same manner. The speed profile consists of the 4 driving phases. The target is to calculate the new value of  $V_2$  that will allow compensating the detected time delay.

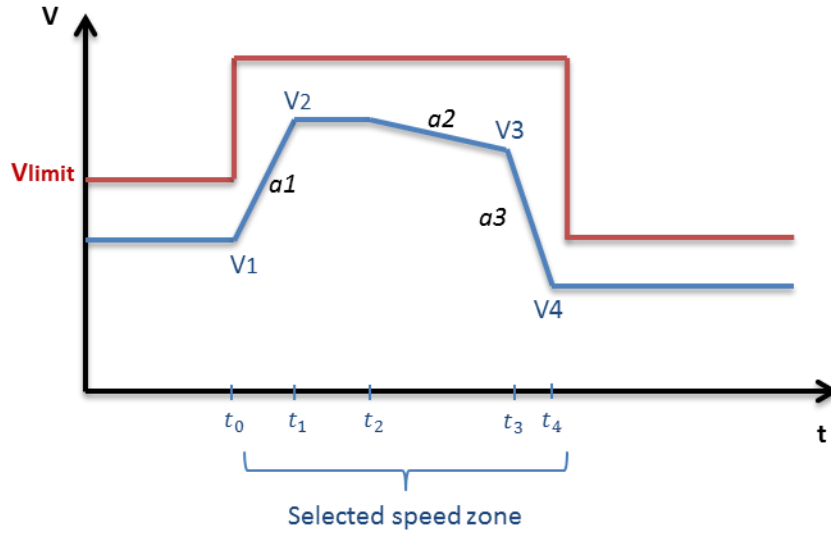


Figure 128: Speed profile containing the 4 driving phases

In the selected zone, the distance “L” crossed by the train is:

$$L = \int_{t_0}^{t_0+t_1} (a_1 t + V_1).dt + \int_{t_0+t_1}^{t_0+t_1+t_2} V_2 .dt + \int_{t_0+t_1+t_2}^{t_0+t_1+t_2+t_3} (a_2(t - t_0 - t_1 - t_2) + V_2).dt \\ + \int_{t_0+t_1+t_2+t_3}^{t_0+t_1+t_2+t_3+t_4} (a_3(t - t_0 - t_1 - t_2 - t_3) + V_3).dt$$

In addition:

- $V_2 = a_1 t_1 + V_1$
- $V_3 = a_2 t_3 + V_2$
- $V_4 = a_3 t_4 + V_3$

Replacing  $V_2$ ,  $V_3$  and  $V_4$  in L:

$$L = \left( \frac{a_3 - a_1}{2a_3a_1} \right) V_2^2 + \left( t_2 - \frac{a_3 - a_2}{a_3} t_3 \right) V_2 + \frac{1}{2} a_2 \frac{a_3 - a_2}{a_3} t_3^2 + \frac{1}{2a_3} V_4^2 - \frac{1}{2a_1} V_1^2$$

As mentioned earlier, the target is the new value of  $V_2$  that will compensate the delay. Therefore, all parameters except  $V_2$  and  $t_3$  are considered as a constant. In order to calculate the new  $V_2'$  we need to calculate the new  $t_3'$ . If we consider “T” the new time needed to cross the speed zone, it is calculated as follows:

$$T = t_1 + t_2 + t_3 + t_4 - t_{delay}$$

$$T = \frac{V_2}{a_1} - \frac{V_2}{a_3} + t_2 - t_{delay} + \left( \frac{a_3 - a_2}{a_3} \right) t_3 + \frac{V_4}{a_3} - \frac{V_1}{a_1}$$

$$T = \frac{V_2'}{a_1} - \frac{V_2'}{a_3} + t_2 + \left( \frac{a_3 - a_2}{a_3} \right) t_3' + \frac{V_4}{a_3} - \frac{V_1}{a_1}$$

$$t_3' = \left( \frac{(V_2 - V_2')}{a_1} - \frac{(V_2 - V_2')}{a_3} - t_{delay} + \left( \frac{a_3 - a_2}{a_3} \right) t_3 \right) \times \left( \frac{a_3}{a_3 - a_2} \right)$$

By replacing  $t_3$  by  $t_3'$  in L and solving the new equation of second order, the new value  $V_2'$  is obtained. It is important to note that the maximum delay that can be compensated correspond to the flat\_out speed profile. If  $t_{delay} > t_{max}$ , the delay left ( $t_l = t_{delay} - t_{max}$ ) will be reported to the next speed zone.

The delay compensation methodology is summarized in the following flow chart:

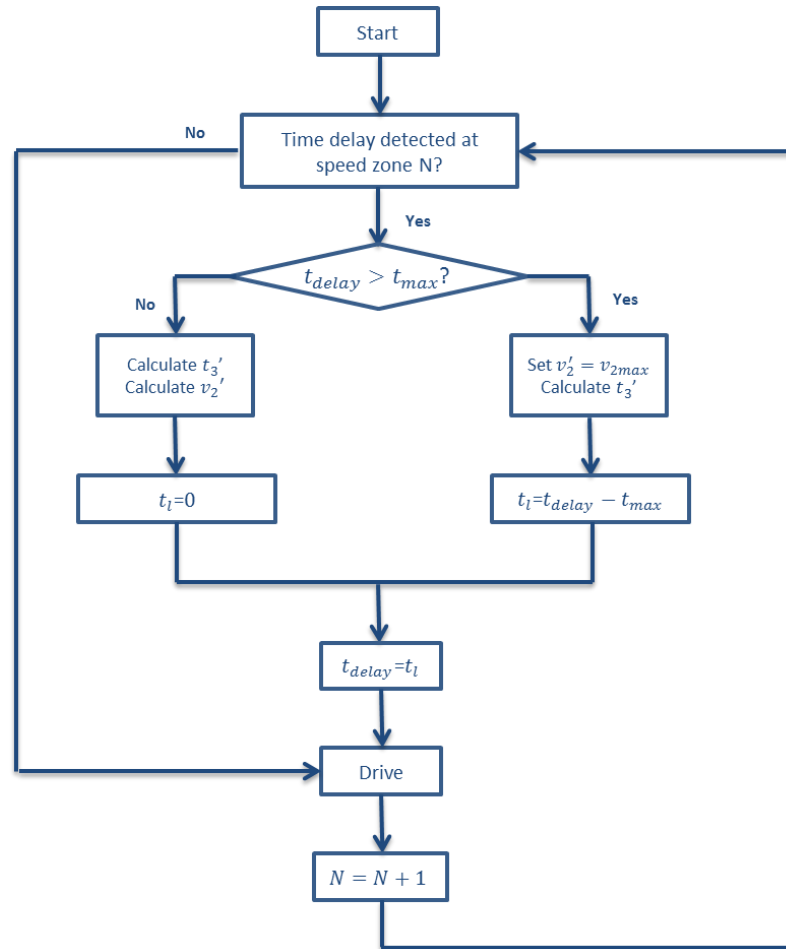


Figure 129: Delay compensation flow chart

## XI - Simulations: Application on Paris-Lyon high speed line

This study is done in the frame of the European collaborative project Merlin [MER00]. Alstom is the leader of task 4.1 where new smart technologies are studied in collaboration with SNCF and ADIF. Thus, in order to test the both optimization algorithms, it is applied on SNCF's 25 kV French High Speed line LGV1 connecting Paris to Lyon. It was inaugurated in 1981 and marked the beginning of French passenger high-speed rail service. Currently, a maximum of 13 trains per hour and per direction are running at peak hours on this line. Trains are coming from Paris, Massy, Marne-la-Vallée and Lille on one side and from Lyon, Dijon, Geneva and Milano among others on the other side. SNCF is planning to have up to 16 trains running per hour and per direction by 2025. However, this traffic increase would entail new costly investments (increasing substation power, adding a new substation...) due to expensive connection costs to the grid as the upstream electrical network around the Morvan is weak (see Figure 130). The problem gets also more complicated by the increasing traffic density and thus perturbations frequency. Therefore, there is overload risk at the two substations located near this area, Commune and Sarrey (Figure 131). This would entail a voltage drop on the line, decreasing the traction efficiency of the trains, and power penalties due to consumption higher than the subscribed one. Thus, an intelligent traffic management solution taking into account the energy consumption could reduce these investments.

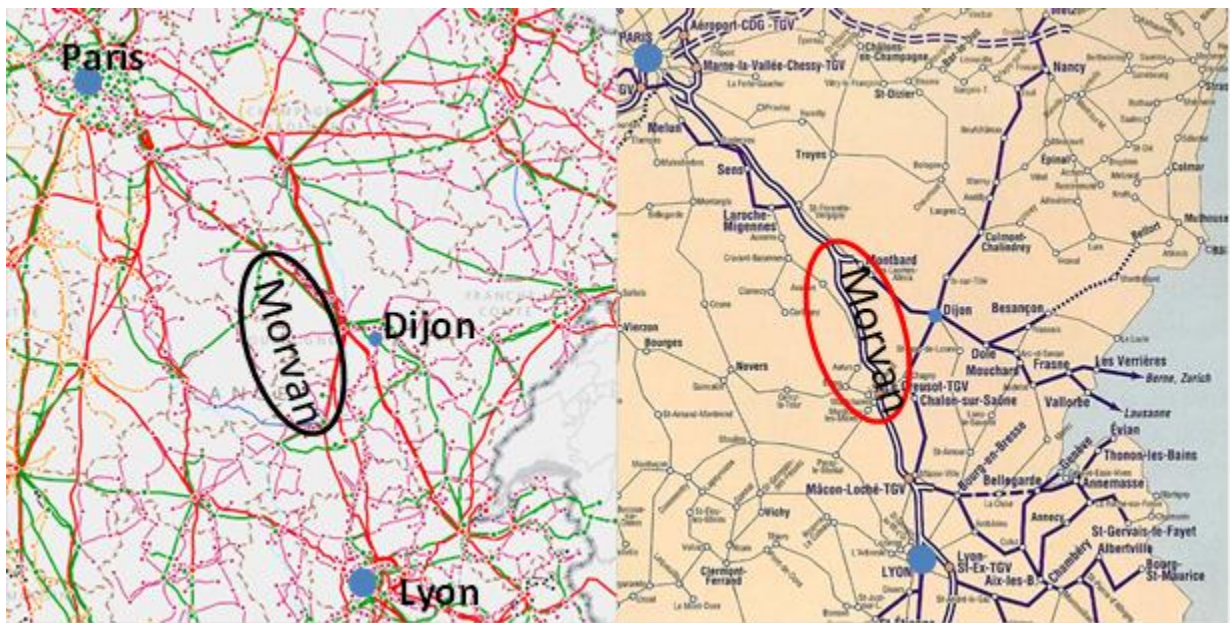


Figure 130. Map of RTE power grid on the left (400kV in red, 250kV in green) and map of the high-speed line between Paris and Lyon on the right (line in white and blue) [RTE00][TGV00]

The line is modelled in a train simulator, used internally in Alstom, that is configured with the characteristics of the line and trains (slopes, stations, train mechanical parameters, speed limits...). A theoretical timetable for the line during rush hours is also provided by SNCF (see appendix A1). To

achieve the traffic and energy studies and simulations, Alstom has received from SNCF necessary input data. LGV1 modelling allows traffic and energy optimization simulation in order to see the influence of the speed profile on the energy consumption especially when a conflict is foreseen and avoided.

#### **XI.a. CONTEXT**

In 2014, the LGV1 Paris-Lyon line allows maximum 13 trains per hour and per direction. From Paris to Lyon, 11 trains comes from Paris downtown “Paris Gare de Lyon” station and 2 trains come from Paris suburb “Massy TGV” station and join the LGV by the junction of Yerres (bifurcation). An operational objective is to increase the line capacity to 16 trains per hour by 2025. It is necessary to optimize both traffic and power consumption in order to allow such high capacity.

##### XI.a.1. Topology

The line includes several junctions with conventional lines (not high speed) between Paris and Lyon, according to the following:

- Pompadour at the beginning of the LGV at an equivalent LGV1 KP -23.000, where there is a possible deviation to conventional line Paris-Lyon (South).
- Yerres at equivalent LGV1 KP -18.881, where there is the junction to Massy.
- Triangle of Coubert at equivalent LGV1 KP 4.085.
- Crisenoy at LGV1 KP 16.982, where there is the junction to the conventional line Paris-Lyon (North).
- Pasilly at LGV1 KP 162.108, where there is trains from/to Dijon.
- Mâcon at LGV1 KP 337.888, where there is trains from/to Bourg-en-Bresse.
- Montanay at LGV1 KP 380.500, where there is the junction to Lyon Part-Dieu station and to Lyon Saint-Exupéry station.

Junctions are speed limited according to the following:

- Pompadour: 160 km/h.
- Yerres: 160 km/h.
- Triangle of Coubert, Crisenoy, Pasilly, Mâcon and Montanay: 300 km/h.

Trains coming from other lines and entering to the LGV1 are speed limited according to the following:

- Yerres: 90 km/h.
- Triangle of Coubert, Crisenoy, Pasilly and Montanay: 220 km/h.
- Mâcon: 160 km/h.

In Paris region, power supply is 1500 VDC. In the South of Yerres junction, at equivalent LGV1 KP - 19,000, the power supply changes to 25 kVAC. The power supply in Lyon downtown (Lyon Part-Dieu station) is also 1500 VDC.



The following figure shows the line with all useful details considered in the study.

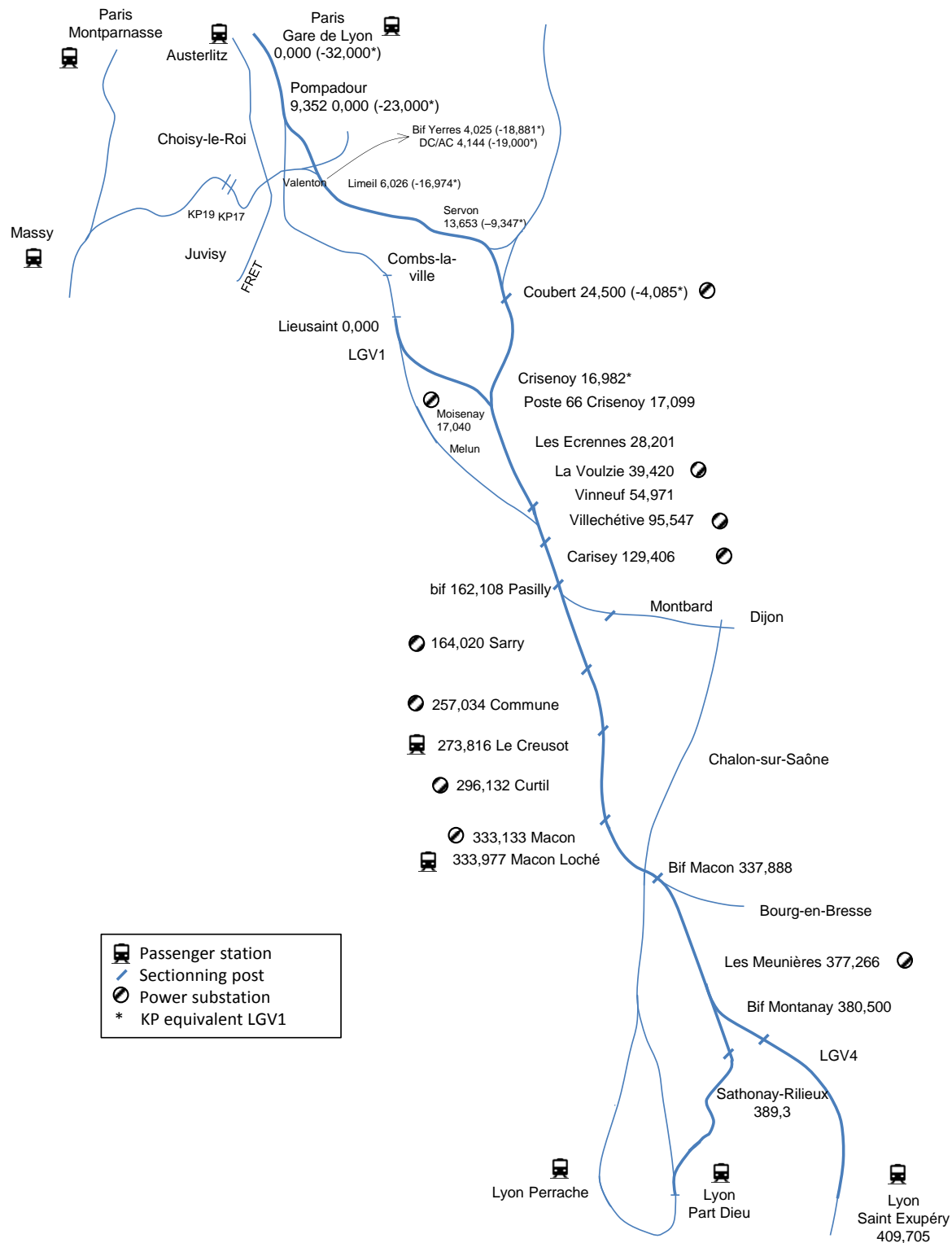


Figure 131: Topology of the LGV1 line Paris-Lyon

## XI.b. RESULTS OF SPEED PROFILE OPTMIZATION

As an application of the algorithm, simulations are run for every train within a 2 hours timeslot of a timetable that is given by SNCF (see Appendices-D). The chosen date and timeslot was Friday February 21<sup>st</sup> 2014 between 4pm and 6pm as it is a very critical case: it corresponds to a peak period due to departure on ski holidays. First, only the outward journeys have been simulated which correspond to 34 trains (all trains running between Crisenoy and Montanay between 4pm and 6pm are taken into account). These trains can be classified into 10 services corresponding to a run between 2 stops. The different services are listed below (“P” corresponds to a train that “passes” at the given operational point, “S” to a train that “stops”).

- Crisenoy (P) – Pasilly (P)
- Crisenoy (P) – Le Creusot (S)
- Le Creusot (S) – Montanay (P)
- Crisenoy (P) – Mâcon (S)
- Mâcon (S) – Mâcon2 (P) (Mâcon corresponds to the train station, Mâcon2 to the junction)
- Mâcon (S) – Cesseins
- Mâcon (S) – Montanay (P)
- Crisenoy (P) – Mâcon2 (P)
- Crisenoy (P) – Cesseins (P)
- Crisenoy (P) – Montanay (P)

### XI.b.1. Example 1 : Train A5135 Crisenoy (P) – Montanay (P)

After 110 generations, the differential evolution algorithm has converged. The final population is shown in Figure 132.

Vmax1	Vmin1	Coef1	Vmax2	Vmin2	Coef2	...	Conso	E_kinetic	Tps1	Tps2	Tps3	Tps4	Tps5	Tps6	Fitness	E / E_flat_out	Exit speed
254	138	1.0	279	276	0.6	...	6418	0	0	44	-9	-12	7	21	0.97082055	0.61652257	160
247	152	0.9	283	279	0.5	...	6536	0	-3	13	-3	-7	16	34	0.97020185	0.62785783	160
269	166	0.9	277	277	0.6	...	6631	0	3	25	3	-1	4	13	0.969733	0.63698367	160
268	174	1.0	278	276	0.6	...	6614	0	3	15	1	-2	14	24	0.96989852	0.63535062	160
270	145	1.0	281	278	0.5	...	6488	0	5	27	-4	-8	7	23	0.97024912	0.62324688	160
221	148	0.9	282	277	0.5	...	6535	0	5	18	-10	-14	-2	15	0.96990001	0.62776177	160
173	164	1.0	285	278	0.5	...	6521	0	-5	12	-13	-17	4	32	0.97077948	0.62641691	160
250	158	1.0	285	277	0.5	...	6495	0	-3	27	3	-1	19	37	0.97103816	0.62391931	160

Final population X
Energy consumption + passage times

Figure 132. Final population and associated values after 580 generations for the train A5135

The target times given on the timetable are:

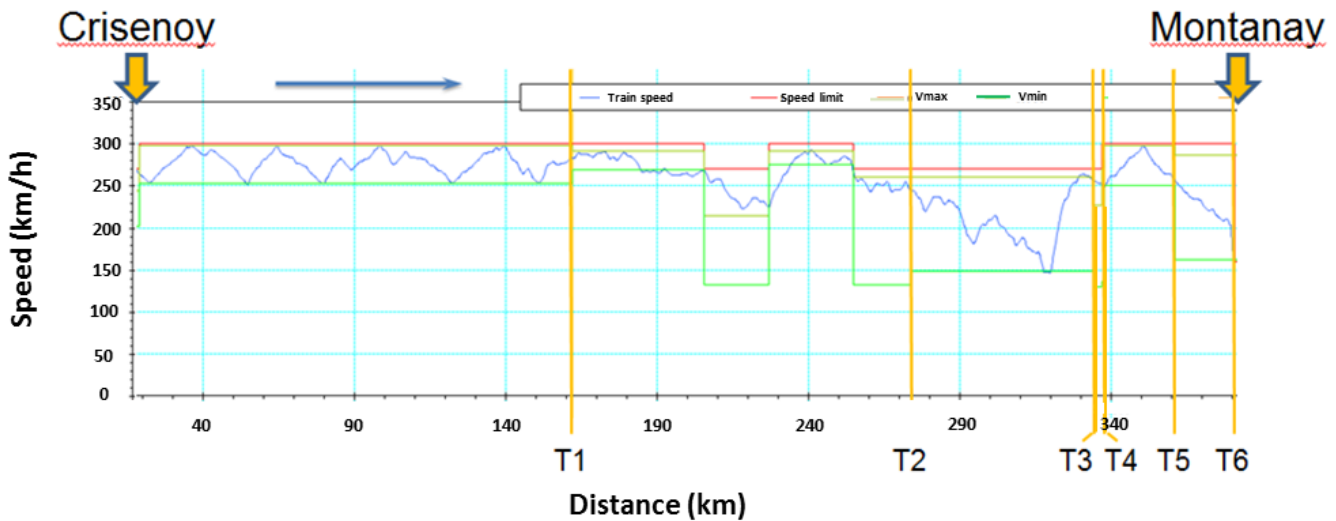
- $T_{target}(1) = 1890s$
- $T_{target}(2) = 3420s$
- $T_{target}(3) = 4470s$
- $T_{target}(4) = 4530s$
- $T_{target}(5) = 4830s$
- $T_{target}(6) = 5130s$

Table 30 shows that almost all time constraints are respected for each operational point and the average energy savings in regard to a flat-out run is about 37%.

Energy savings (%)	$\Delta T 1$	$\Delta T 2$	$\Delta T 3$	$\Delta T 4$	$\Delta T 5$	$\Delta T 6$
38	0	44	-9	-12	7	21
37	-3	13	-3	-7	16	34
36	3	25	3	-1	4	13
36	3	15	1	-2	14	24
38	5	27	-4	-8	7	23
37	5	18	-10	-14	-2	15
37	-5	12	-13	-17	4	32
38	-3	27	3	-1	19	37

**Table 30.** Time difference in seconds between the target time and the time observed for each individual of the final population at each operational point and their associated energy savings

The best fitness value 0.969733 corresponds to the individual  $i = 3$ . Its speed profile is shown in Figure 133. According to Table 30, the train arrives with 3 sec delay at T1 and T3, 25 sec at T2, 1 sec early at T4, 4 sec delay at T5 and 13 sec at T6. The train consumes then 6631 kWh which corresponds to an energy saving of 36% in comparison to a flat-out run. The average slack-time of the run is 12.9%.



**Figure 133.** Speed profile of the optimal solution

#### XI.b.2. Example 2 : Train A6759 Crisenoy (P) – Pasilly (P)

In this case, the convergence is much quicker as the running distance is shorter, thus leading to fewer zones: there are only two operational points, Crisenoy and Pasilly which correspond to the beginning and the end of the section, and one shift in the speed limit. Therefore, only 30 generations are needed to converge. Again, all the time constraints are respected as shown in Table 31. The

optimal solution correspond to individual  $i = 5$ . The associated speed profile is shown on Figure 134. The 16.4% slack-time enables us to save 27% of energy compared to a flat-out run.

Energy savings (%)	$\Delta T 1$
27	-4
27	2
27	4
27	7
27	-1
27	10
26	-6
27	-3

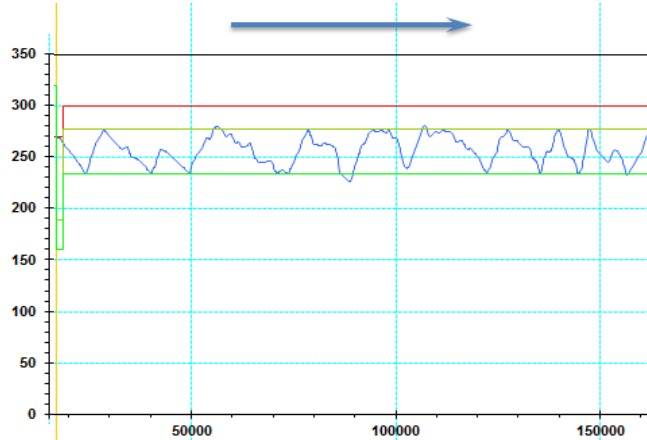


Table 31 : Time difference in seconds between the target time and the time observed for each individual of the final population and their associated energy savings

Figure 134: speed profile of the optimal solution for train A6759

#### XI.b.3. Example 3 : Train A6621 Crisenoy (P) – Le Creusot (S)

This example differs from the previous ones as the end of the service is marked by a stop “S”. The algorithm converged in 30 generations. All the solutions respect the time constraints with a precision of  $\pm 10$  seconds except individual 3 (see Table 32). The optimal speed profile is shown in Figure 135 and corresponds to the individual  $i = 6$ . Even if the average slack-time is smaller than in the previous cases with only 8.4%, the energy savings compared to a flat-out run are 28%.

Energy savings (%)	$\Delta T 1$	$\Delta T 2$
27	9	-1
27	-7	9
29	17	21
26	0	-9
26	4	-4
28	-6	-9
25	1	2
26	-3	-7

Table 32. Time difference between the target time and the time observed for each individual of the final population and their associated energy savings

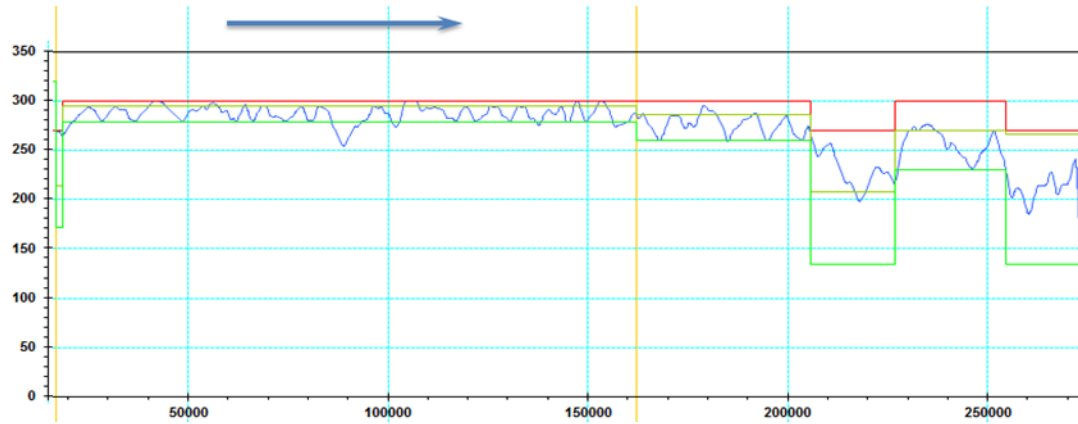


Figure 135. Speed profile of the optimal solution for A6621

#### XI.b.4. Pareto curves

All the energy savings previously mentioned are given in comparison to the flat-out run. However, as drivers must respect the timetable, he will never run a flat-out run; thus, he will consume less energy and the energy savings computed by the algorithm might be much smaller. To answer to this question, a comparison is done between the energy consumptions of random speed profiles respecting same constraints. The driver's real behaviour should be close to one of them and then can be compared to the optimal computed solution. Figure 136 represents all the individuals that were simulated during the whole calculation of the algorithm for A6215 from Crisenoy (P) to Cesseins (P). The number of generations required was 90. Therefore,  $90 \times 8$  individuals (generation  $\times$  NP) are represented. For the same final running time, the energy consumption can vary by 6% between an eco-friendly and a non-eco-friendly drive. Then the Pareto curve can be plotted (red curve in Figure 136) which is a curve that passes by all the optimal couples (energy consumption, running time). Afterwards, we are able for a new slack-time to compute the optimal energy consumption thanks to this curve.

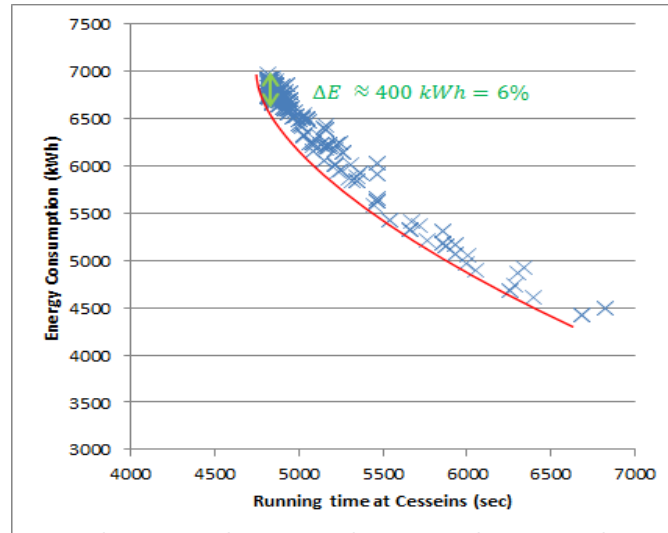


Figure 136. Energy consumption vs final running time for all the individuals simulated by the algorithm and Pareto curve

Another example corresponds to the train A6759 shown in Figure 137 (generation =20; NP = 8; total of individuals = 20x8). This train runs between Crisenoy (P) and Pasilly (P). Again, we observe a big dispersion of energy consumption for the same running time, enabling to save 9% between an eco-friendly and a non-eco-friendly drive. We observe that the algorithm converge to the most eco-friendly solutions as wanted.

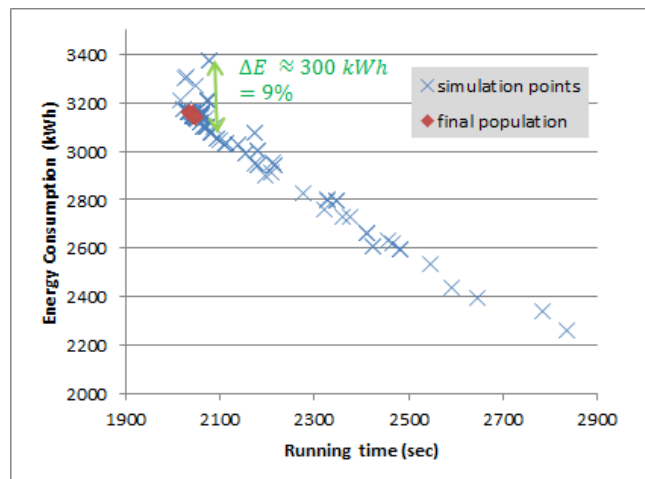


Figure 137. Energy consumption vs final running time for all the individuals simulated by the algorithm (blue) and solutions of the final population (in red) for the train A6759

Finally, in Figure 138, points represent all simulated trains running between Crisenoy (P) and Pasilly (P): A6755, A6741, A9273, A9219, A6759 and A9589. The associated slack-times are respectively 18%, 13%, 16%, 13%, 16% and 10%. We observe that in each case, the algorithm converges towards the Pareto curve (red triangles). For a given slack-time, a great disparity of energy consumption can again be observed, emphasizing the savings that can be made thanks to eco-driving.

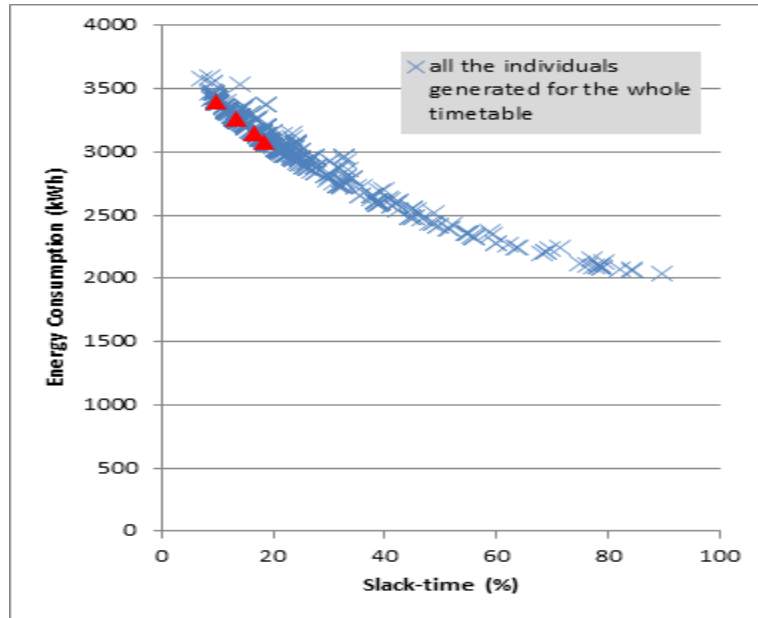


Figure 138. Energy consumption vs final running time for all the individuals simulated by the algorithm (blue) and solutions of the final population (in red) for all the trains going from Crisenoy (P) to Pasilly (P)

#### XI.c. RESULTS OF SUBSTATIONS POWER OPTIMIZATION

Optimizations are done for  $Shift_{Max} = 30$  seconds and  $Shift_{Max} = 45$  seconds, for an average period  $T=10$  minutes for computing the power. The shift's step is 5 seconds in both cases. Results are given in Table 33 where the three most loaded power substations are highlighted in grey. We observe that we can reduce of around 2 % the power peak on the three power substations if we take  $Shift_{Max} = 45$  seconds. However, for  $Shift_{Max} = 30$  seconds, the improvement made on SARRY leads to worsen the situation of COMMUNE, thus the optimization is less interesting. However, in this case, the shift is very limited for each train as most of them have more than 10 seconds delay after the eco-driving step.

Maximal Average Power (MW)					
SST Name	Before optimisation	ShiftMax=30		ShiftMax=45	
MOISENAY	8.047	7.81	-2.9%	7.81	-2.9%
LA VOULZIE	26.205	26.175	-0.1%	26.145	-0.2%
VILLECHETIVE	31.4	31.059	-1.1%	30.843	-1.8%
CARISEY	23.93	23.001	-3.9%	22.521	-5.9%
SARRY	35.952	35.155	-2.2%	35.128	-2.3%
COMMUNE	35.593	35.77	0.5%	34.929	-1.9%
CURTIL	21.057	21.053	0.0%	20.855	-1.0%
MACON	12.851	12.605	-1.9%	11.935	-7.1%
LES MEUNIERES	11.111	11.199	0.8%	11.199	0.8%

Table 33. Comparison before and after optimization for ShiftMax = 30 sec and ShiftMax = 45 sec

To summarize, eco-driving showed that it is possible to make significant energy savings by acting on coasting speed ( $V_{max}$ ,  $V_{min}$ ) and the traction coefficient. Solutions were evaluated using a

fitness function that included energy and time constraints. Three examples were presented and confirmed the algorithm's convergence. Pareto curve was drawn for different services. It highlighted the impact of the driver's random behavior on the energy consumption. Therefore, giving speed indications can help improving the driving's efficiency while respecting time constraints. The second power optimization step was more constraining because it takes into consideration the delays already introduced in the first step. Results were not too much promising but this can be improved by increasing time tolerance.

Note that these optimizations were done off-line. In real-time operation, a third step, delay compensation, should be developed to readjust dynamically trains hence they respect the optimized theoretical timetable and speed profiles. This online step was not tested because it needs to be implemented in a traffic simulator. In addition, it is important to remind that this energy module should work in coordination with traffic optimization modules already existing. These two points would be subject of a future study.



## **C**ONCLUSION AND **P**ERSPECTIVES

To resume, electric railways are more and more expanding all around countries. In big cities, they are presented as a green solution for reducing pollution because of zero gas emission. However, other road transportations are becoming electrical such as buses and cars. These new technologies are presented today as railway's competitors especially in urban areas where no dedicated infrastructure is possible. However, railways, electric cars and electric buses are also complementary in a multi-modality approach. Increasing energy efficiency of urban, suburban and high speed lines will reduce energy cost and improve competitiveness. In addition, European Commission is giving a lot of attention for climate. In particular, the 20-20-20 plan declared in 2007 set three targets: reducing by 20% greenhouse gas emissions from 1990 levels, increasing by 20% renewables energy share and improving by 20% EU's energy efficiency. This thesis tried to find solutions for increasing railways' efficiency in the framework of two collaborative European projects, OSIRIS and MERLIN, which consist one of many steps towards meeting the 3<sup>rd</sup> target. Yet, railways are very various depending on their location (urban or not) and used technologies. In order to understand this diversity, an overview on railway systems was first done. It explained this sector's evolution through last two centuries starting from steam engines till electric motorized trains we see today. It shows how technologies varied from one country to another and even in the same one. Some were eliminated shortly after employment; others are still being used today. Many past choices were taken after experiences; some were also political and strategic, but all of them led to the system we have today. Effort is now being done to unify and standardize railway solutions. This is very important in a world where globalization affects almost all sectors: energy connections between countries (cables, pipes), road connections...etc. Railway sector should be a link between different regions and cultures especially for freights exchanges where it is still very competitive.

After this overview, a focus was done on the existing types of electrification. The difference between AC and DC modes was highlighted showing the particularity of each one. It showed that in DC railways (urban and suburban applications), classic substations consist of diode rectifiers allowing unidirectional power flow (from the AC grid to the catenary/3<sup>rd</sup> rail). Thus, when a train brakes, if no other one is accelerating nearby, braking energy is burned in resistors onboard the train because it cannot be reinjected into the upper AC grid. On the other hand, in AC mode, substations are mainly consisted of a transformer allowing reinjection of the excess of braking power into the main grid. No energy is then burned. Different braking systems were detailed in chapter III and the environmental impact of railways was presented. Existing solutions, same as the ones under development, were also listed in this chapter such as onboard and wayside storage systems, reversible substations, etc. The difference between AC and DC modes showed that it was not possible to propose one common solution for both and that each one should be studied alone. Section B was dedicated for DC urban lines while Section C is more adapted to suburban and high speed lines.

For urban lines where main losses were measured in braking resistors, the “Smart DC station” was proposed as a solution for recuperating trains braking energy when no exchange is possible. It is a new concept based on DC micro-grids that made, for the first time, a bridge between railways and their energy environment. Instead of reusing this energy internally, this solution suggested to use it for non-railway loads that need specific power supply. In our use case, we considered recuperating the excess of braking energy from railway side through a DC/DC converter that respects energy exchange between trains, storing the energy in a hybrid storage system and reusing it to charge electric hybrid buses parked next to a metro station. Power flew through a DC busbar. A low power AC/DC converter was also connected to the latter to avoid over and under voltages. First, each component was studied separately. In order to choose which storage technology is the most adapted to this application, an overview on storage systems was done. It distinguished two categories: energy storage and power storage. After listing advantages and drawbacks of different technologies, the better choice seemed supercapacitors and Li-ion batteries. Then, power converters were studied. For storage, a cascaded architecture was proposed and current regulations were used. Limitations were also introduced to protect the supercapacitor from charging and discharging excess. Concerning the AC/DC converter, a 2-level architecture was proposed. It was controlled by two cascaded loops: the outer loop regulated DC busbar voltage. Its output gave the reference value to the inner loop regulating the direct current at AC grid's side. For railway DC/DC converter, a bidirectional converter was studied with a voltage regulation where the reference voltage varies to ensure giving priority to power exchange between trains. All these converters were managed by a “power management system” that optimized power flow within the micro-grid according to pre-defined scenarios. Each subsystem was first simulated separately then the whole system was simulated using Simulink.

As RATP was ALSTOM's partner in Task 4.1 of OSIRIS, Paris metro line 13 was chosen as an application. But given the fact that Simulink simulations were too long due to small time step, a simplified model was developed using Matlab allowing energy evaluation for different scenarios corresponding to 95s, 100s, 175s and 290s headways. This model used the braking power profile, calculated in the multi-train simulator ELBAS, to estimate the amount of recovered energy to store and the one sent to the AC grid. Results were satisfying and showed that there was more than enough energy for charging one electrical hybrid bus per hour. To study the competitiveness of this solution compared to the alternative one (fast charging station), an economic evaluation was done to evaluate the cost. It showed that both solutions require investment, but the advantage of the Smart DC station is that no electric contract is needed and thus, no energy bill.

In chapter VI, the stability of the DC micro-grid was studied. First, instability risks that may cause low damped systems were explained. Then state-space representation of the whole system was done. It showed that it was a non-linear system because the state matrix contained state variables. Therefore, in order to calculate system's poles, a small signal stability study was done. It

consisted in linearizing the system around an operational point. The calculated poles, showing whether it is stable or not, were valid only for small variations around the selected point. The four different points that were studied have shown that the system is stable. Unfortunately, this does not guarantee that it will remain stable for large variations. To avoid this risk, the next subchapter VI.c introduced a stabilizing control, backstepping, acting on the SC module's command to avoid oscillations in the case of low damped systems. It consisted on dividing the system into cascaded subsystems so that stabilizing one will ensure the stability of the ones beneath.

To conclude, Section B studied a new concept that allows increasing energy efficiency of urban railway systems by saving braking energy before it burns in trains' resistors. We tried to cover different aspects: power electronics, control, stability...etc. Technical recommendations were also given at the end for pre-dimensioning different converters and integrating the micro-grid into the SGAM defined by CENELEC. This solution is quite interesting for future stations especially when the price of batteries same as DC/DC converters is expected to drop due increasing demand especially in transport sector.

After presenting a hardware solution for urban DC railways, Section C proposed for high speed lines (HSL) a software solution that intends to optimize HSL's timetable. As explained through this document, AC electrified mainlines are quite different from DC urban systems. While the latter arises braking energy saving problems, AC mainlines are more impacted by timetable synchronization. In fact, high speed trains are much more powerful than metros and thus, when many trains are accelerating in a same electric zone, power peaks can be caused at SST's level. From protection point of view, this is not a problem because the system is dimensioned for worst cases. The question that should arise is whether this power peak exceeds the maximum subscribed power. In this case, penalties are paid to energy provider. Therefore, we decided to study this problem from two different angles: energy and power.

The first part of this solution was to optimize trains' energy consumption while respecting time constraints. Thus, an algorithm based on differential evolution algorithm was developed. It started with an initial population generated randomly. Every iteration, new individuals were generated from previous ones using mutation and crossing processes. Then, a selection was done based on a fitness function that is directly related to both energy and time. In a first step, we considered a fitness found in literature that was more dedicated to metro application. Given the fact that speed profiles in HSL are quite different from urbans, the fitness was adapted to our application by improving time penalties so the train respects time passage at operational points. An additional term was also added to the energy which is the difference of kinetic energy compared to the reference exit speed. This term was important in cases where train went out of the timetable (bifurcation) at none-zero speed. On the other hand, mutations may give out of boundary values. Therefore, this was handled using bounce-back method where these values were brought back into each parameter's interval. The algorithm was

tested and results were satisfying: up to 30% energy reduction, compared to a flat-out run, and trains passing at time with  $\pm 30$ s variance.

The second step was to reduce power peaks at SST's level by shifting trains. Another algorithm was then developed. It selected the SST with highest power peak and detected trains present on its electric zone during the measured peak. While taking into account delays/advance already introduced by the first optimization, we tried to shift trains consuming the most within acceptable total time margin (first 30s then 45s). This process is repeated until no trains can be shifted.

After both steps were developed, they had to be tested on a real HSL. In MERLIN, SNCF was ALSTOM's partner in this task. Therefore, HSL Paris-Lyon was chosen as application. A theoretical timetable was introduced in the algorithms. They proved that it is possible to make significant energy savings on this line without bringing big changes to the timetable applied today.

To resume, this thesis intended to propose energy solutions for DC and AC railways. Urban lines were seen as a new component of future smart grids or smart neighborhoods. Instead of solving the problem locally, a more global approach was proposed. A hardware solution was proposed locally at passengers' station that seemed to be the best location to make an electric bridge from railways to surrounding environment. While HSL cover long distances and generally non-urban areas, it was more reasonable to propose an "internal" optimization for these systems where time flexibility is a main advantage. Thus, timetable was optimized so that trains consume less energy while respecting punctuality.

Maybe we will need to wait a while before seeing solutions as the Smart DC station emerging in railway because it remains a very conservative sector. This is due to security and safety reasons because any mistake, even small ones, may put a person's life into danger. A progressive implementation can be done starting with simple storage until we get a true DC grid within the station. This work was based on integrating one DC smart station in a metro line while it would be interesting, in future studies, to evaluate the interest of multiplying this solution along the line. This would allow saving all braking energy lost in trains' resistors. In addition, prices of DC/DC converters and Li-ion batteries are expected to drop due to increasing demand in different applications such as photovoltaic micro-grids, electric cars and electric buses. This will reduce the cost of the DC smart station in case of future implementation. An energy strategy for electric buses' charging should also be studied especially in big cities like Paris if all diesel buses will be replaced by electric ones. A possible solution is to make a full principal charge during night (off-peak hours) and only complete with short charges along the day. In the latter case, recuperated braking energy will allow more frequent bus charging.

Concerning the second solution, we can expect a fast development because many efforts are being done on this subject. It is a software solution that costs less than hardware components (storage, converters...) and is capable of reducing considerably energy consumption. But we have to

remind that today HSL are not driverless trains. Thus, an eco-speed instruction will be communicated to the driver who will try to follow it. Note that no energy module can be applied alone. It should be coupled by a traffic management module to ensure the feasibility of the solution and that it does not generate traffic perturbations because in railways, punctuality and fluidity remain the main objectives.

Finally, today, even sectors as conservative as railways are starting to open their doors to new ideas and new technologies. Economic and climate crises should push them towards accepting changes. We are now living in a more connected world where information is everywhere: in our laptops, smartphones and even watches. This is finally starting to change minds towards a better thinking ready to communicate with other domains and from my point of view, the only way to improve our world today is by working together, people from different competences, regions... because diversity is source of strength...

## References

---

- [ABB00] [new.abb.com/power-electronics/home/dc-wayside-power-solutions/energy-management/enviline-ers](http://new.abb.com/power-electronics/home/dc-wayside-power-solutions/energy-management/enviline-ers)
- [ACI00] S. Acikbas, M. T. Soylemez, 2008. Coasting point 182ptimization for mass rail transit lines using artificial neural networks and genetic algorithms. IET Electr.Power Appl. 2 (3), 172-182
- [ADF00] [http://www.adif.es/en\\_US/compromisos/doc/PT\\_11-SubestRev\\_Eng.pdf](http://www.adif.es/en_US/compromisos/doc/PT_11-SubestRev_Eng.pdf)
- [ALB10] T. Albrecht, C. Gassel, A. Binder and J. van Luipen, "Dealing with operational constraints in energy efficient driving," Railway Traction Systems (RTS 2010), IET Conference on, Birmingham, 2010, pp. 1-7
- [ALS00] [www.alstom.com/Templates/Corporate/Pages/ContentHub.aspx?id=17457](http://www.alstom.com/Templates/Corporate/Pages/ContentHub.aspx?id=17457)
- [ALS01] <http://www.alstom.com/products-services/product-catalogue/rail-systems/Infrastructures/products/hesop/>
- [ALS02] <http://www.alstom.com/press-centre/2013/1/williams-hybrid-power-and-alstom-cooperate-to-develop-flywheel-energy-storage-technology-for-citadis/>
- [ALS03] Citadis Ecopack, On-board autonomy for tramways, Urban Transit Catenary-free Solutions, Alstom Transport, 2014
- [AMP00] "Battery Pack Design, Validation, and Assembly Guide unsing A123 Systems AMP20m1HD-A Nanophosphate Cells", User Documentation, A123 Energy Solutions, February 7, 2014
- [APC65] APC Schneider Electric – White Paper #65
- [BAR05] F. Barruel, N. Retiere, J.-L. Schanen, and A. Caisley, Stability approach for vehicles dc power network: Application to aircraft on-board system. In Power Electronics Specialists Conference, PESC '05, IEEE 36<sup>th</sup>, June 2005, pp. 1163–1169.
- [BAR08] Ch. Barjracharya, "Control of VSC-HVDC for wind power", Master of Science in Energy and Environment Report, June 2008
- [BBC15] <http://www.bbc.com/news/world-asia-32391020>

- [CEN00] “Smart Grid Reference Architecture”, CEN-CENELEC-ETSI Smart Grid Coordination Group, November 2012
- [CHE14] An Integrated Energy-Efficient Operation Methodology for Metro Systems Based on a Real Case of Shanghai Metro Line One. Cheng Gong, Shiwen Zhang, Feng Zhang, Jianguo Jiang, Xinheng Wang. S.l. : [www.mdpi.com/journal/energies](http://www.mdpi.com/journal/energies), 2014.
- [CIT01] <http://www.citedutrain.com/fr/collections/locomotive-electrique-cc-7107-record-monde-vitesse-331-kmh>
- [CIT00] <http://www.citedutrain.com/fr/collections/locomotive-electrique-e1-boite-sel>
- [COM91] Jean-Marc Combe, Bernard Escudié, Jacques Payen , *Vapeurs sur le Rhône : histoire scientifique et technique de la navigation à vapeur de Lyon à la mer*, Presses Universitaires de Lyon, 1991, p. 60.
- [CON00] [www.conifer.fr](http://www.conifer.fr)
- [CUC12] A.P. Cucala, A. Fernandez, C. Sicre, M. Dominguez, 2012. Fuzzy optimal schedule of high speed train operation to minimize energy consumption with uncertain delays and driver's behavioral response, *Eng. Appl. Artif. Intell.*, 1548-1557.
- [DOM12] M. Domínguez, A. Fernández-Cardador, A. P. Cucala and R. R. Pecharromán, "Energy Savings in Metropolitan Railway Substations Through Regenerative Energy Recovery and Optimal Design of ATO Speed Profiles," in *IEEE Transactions on Automation Science and Engineering*, vol. 9, no. 3, pp. 496-504, July 2012.
- [ELC11] International Electrotechnical Commission , “Electrical Energy Storage White paper”, 2011
- [ENS00] <http://energystorage.org/compressed-air-energy-storage-caes>
- [ENS01] <http://energystorage.org/energy-storage/storage-technology-comparisons/thermal2>
- [ENS02] <http://energystorage.org/energy-storage/facts-figures>
- [ERI99] R. Erickson, Optimal single resistors damping of input filters. In: *Applied Power*



Electronics Conference and Exposition, 1999. APEC '99. Fourteenth Annual, vol. 2, Mar 1999, pp. 1073–1079.

- [EUR09] High-speed Europe, European Commission, Europa 2009
- [EUR00] [ec.europa.eu/energy/en/topics/renewable-energy/biofuels](http://ec.europa.eu/energy/en/topics/renewable-energy/biofuels)
- [EUR01] <http://ec.europa.eu/programmes/horizon2020/en/what-horizon-2020>
- [EUR01] <http://eurailmag.com/of-trains-and-brakes/>
- [FRA00] [www.france.fr/en/paris-and-its-surroundings/brief-history-paris-metro.html](http://www.france.fr/en/paris-and-its-surroundings/brief-history-paris-metro.html)
- [FRE00] <http://www.efreightproject.eu/default.aspx>
- [HAM00] Hamache D, Fayaz A, Godoy E, Karimi Ch, Stabilization of a DC electrical network via backstepping approach. Presented at: Industrial Electronics (ISIE), 2014 IEEE 23<sup>rd</sup> International Symposium on industrial electronics, 2014.
- [HOL75] J.H. Holland, Adaptation In Natural And Artificial Systems s.l.: University of Michigan Press, 1975.
- [IEA14] IEA-UIC railway handbook 2014
- [IEA13] IEA-UIC railway handbook 2013
- [IZT00] IZT, “Evaluation of Energy Efficiency Technologies for Rolling Stock and Train Operation of Railways”, final report, Berlin, March 2003
- [KYU10] A Mathematical Approach for Reducing the Maximum Traction Energy: The Case of Korean MRT Trains. Kyung min Kim, Suk-mun Oh, Moonseob Han. Hong-Kong : s.n., 2010. IMECS 2010.
- [LEJ12] A. Lejeune, R. Chevrier, J. Rodriguez. 2012. Improving an evolutionary multi-objective approach for optimizing railway energy consumption.
- [LIM00] L.R. Limongi, R. Bojoi, C. Pica, F. Profumo and A. Tenconi, “Analysis and comparison of Phase Locked Loop Techniques for Grid Utility Applications”, Politecnico di Torino, Department of Electrical Engineering, Torino-Italy.
- [MAX00] Maxwell ultracapacitors; [www.maxwell.com](http://www.maxwell.com)
- [MAX01] <http://www.maxwell.com/products/ultracapacitors/125v-tran-modules>
- [MID00] R. D. Middlebrook, Input filter considerations in design and application of

switching regulators. In Proc. IAS'76, pp. 366–382, 1976

- [MIY10] Miyatake, M. and Ko, H. (2010), Optimization of Train Speed Profile for Minimum Energy Consumption. IEEJ Trans Elec Electron Eng, 5: 263–269. doi: 10.1002/tee.20528
- [NET00] <http://www.railway-technical.com/etracp.shtml>
- [NET01] <http://www.railway-technical.com/brake1.shtml>
- [OGA00] Katsuhiko Ogata, “Modern control engineering”, Aeeizh 2002, P220
- [PAR00] [www.paris1900.fr](http://www.paris1900.fr)
- [PRI00] K. V. Price, R. M. Storn, J. A. Lampinen. Differential Evolution, a Practical Approach to Global Optimization.
- [QUA11] E. Quaglietta, L. D'Acierno, V. Punzo, R. Nardone and N. Mazzocca, "A simulation framework for supporting design and real-time decisional phases in railway systems," Intelligent Transportation Systems (ITSC), 2011 14th International IEEE Conference on, Washington, DC, 2011, pp. 846-851.
- [RAI00] [http://www.railway-energy.org/static/Regenerative braking in DC systems 103.php](http://www.railway-energy.org/static/Regenerative_braking_in_DC_systems_103.php)
- [RAT04] Rattenbury, Gordon; Lewis, M. J. T. (2004). *Merthyr Tydfil Tramroads and their Locomotives*. Oxford: Railway & Canal Historical Society. [ISBN 0-901461-52-0](https://www.isbn-international.org/number/0-901461-52-0).
- [RHP29] R.H. Park *Two Reaction Theory of Synchronous Machines* AIEE Transactions 48:716-730 (1929)
- [REG00] E. Godoy and Coll, Regulation Industrielle. Paris: Dunod, 2007.
- [RTE00] <http://www.rte-france.com/fr/la-carte-du-reseau>.
- [RTP00] [http://www.ratp.fr/fr/ratp/r\\_111743/bus-hybrides-la-revolution-en-marche/](http://www.ratp.fr/fr/ratp/r_111743/bus-hybrides-la-revolution-en-marche/)
- [SIC10] C. Sicre, A.P. Cucala, A. Fernandez-Cardador, J.A. Jiménez, I. Ribera, A. Serrano, 2010. A method to optimize train energy consumption combining manual energy efficient driving and scheduling. WIT Trans. Built Environ. 114, 549-560.
- [SIE00] <http://www.mobility.siemens.com/mobility/global/en/rail-solutions/rail-electrification/dc-traction-power-supply/energy-storage->

- [SUS11] Susdef based on IEA (2013a), IEA (2013b), IPCC (2006) and IEA (2008)
- [TAR01] J. M. Tarascon and M. Armand, “Issues and challenges facing rechargeable lithium batteries”, *Nature*, vol. 414, no. 6861, pp. 359–67, Nov. 2001.
- [TAR02] <http://www.tarifsreglementes.com/tarifs-reglementes/electricite/vert>
- [TGV00] [http://cheminet.free.fr/tgv\\_pse\\_carte.php](http://cheminet.free.fr/tgv_pse_carte.php).
- [TUY12] D. Tuytens, H. Fei, M. Mezma, J. Jalwan. Simulation-Based Genetic Algorithm towards an Energy-Efficient Railway Traffic Control, 2012.
- [UIC12] UIC, *Research on Optimum Speed for High Speed Lines*, Volume II, appendix 3, railway speed historical evolution, October 2012
- [UNE00] <https://www.unesco-ihe.org/node/5659>
- .

## **APPENDICES**

## A- OSIRIS Project

---

*Reference: FP7 Nr. 284868 "OSIRIS" Description of work*

Title: Optimal Strategy to Innovate and Reduce energy consumption In urban rail Systems

OSIRIS project is a way to innovate and achieve the 20-20-20 plan. It is a 3-year European project started on the 1st of January 2012 and it will finish in December 2014. It aims at enabling a reduction of the overall energy consumption within Europe's urban rail systems of 10% compared to current levels by 2020.

Seventeen partners are taking part in the project: public transport operators, railway manufacturers and universities work together in order to improve railways with a global vision including the infrastructure to the trains. This global vision is necessary in railways because urban rail systems are complex environments and their energy consumption is characterized by a wide range of inter-dependent factors. That's why the development of energy reduction can't be studied only at the level of the train. In fact, the vehicle has to be integrated into the infrastructure and improvements on the vehicle can create decrease of the infrastructure's performance. Finally the global performance won't be as well as planned.

Benefits which are expected from OSIRIS are:

- For the community:
  - Energy and CO2 savings thanks to progress in real tested technologies and solutions.
- For operators:
  - Common understanding with the manufacturers on energy savings and related innovative technologies (Key Performance Indicators, duty cycles, Technical Recommendations)
  - Decision Support Tool methodology: selecting optimum combinations of technical and operational solutions
  - Real experimental results from the field of innovative technologies to save energy (RS, Infrastructure & operational measures / thermal & electric energy)
- For manufacturers:
  - Clearly defined and harmonized requirements by operators
  - Extended electrical system simulations tools to integrate the new smart grid concept and new thermal simulation tool

The realization of OSIRIS is divided into 8 work packages:

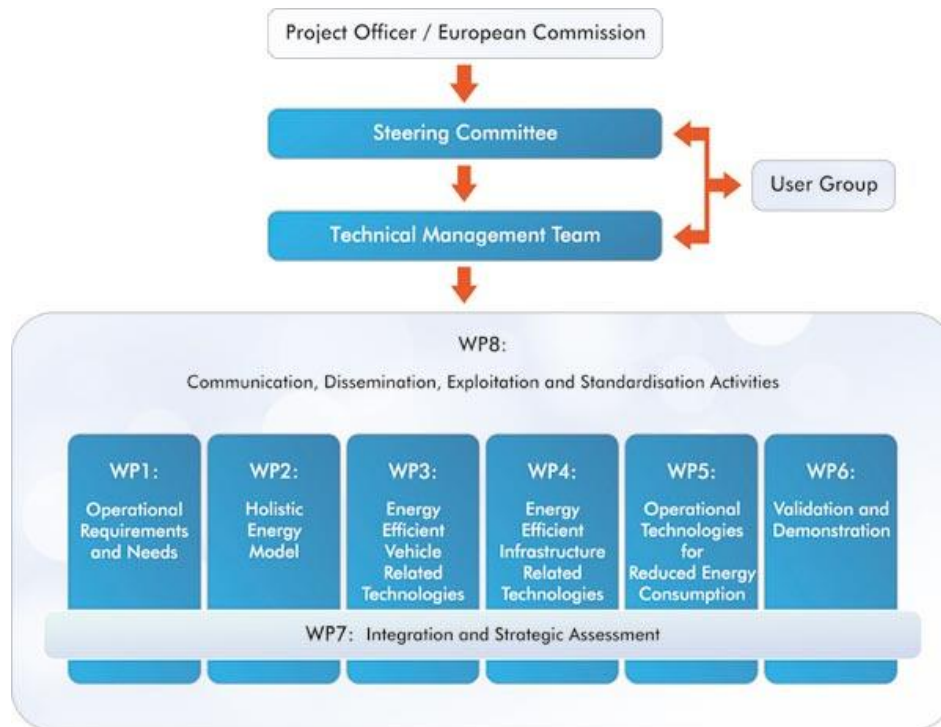


Figure 139. OSIRIS Organization

WP4 studies the impact on energy saving and CO2 emission of infrastructure recovery technologies in mass transit systems (i.e. LRV, Subway, Suburban systems). The above defined objectives will be reached realizing different technical solutions. The technical objectives will be in the electrical and thermal domains and will include an eco-design approach in the whole system lifecycle. It is divided into 3 tasks:

- Task 4.1 : “Smart grid solutions study and related simulations”
- Task 4.2 : “Heat gaps evaluation and heat pump solutions to reduce the energy consumption of station and tunnel auxiliaries”
- Task 4.3 : “Thermal simulation and thermal management of infrastructure”

Section B is related to task 1 of work package 4. Its objectives are the following:

- Defining a smart grid management will allow to optimize the energy management of plants (including traction supply system, on ground auxiliaries and energy storage equipment) defining an optimized power supply architecture. In particular, ground plants, seen as intelligent nodes, will dynamically be considered to optimize the energy flow among loads and generators, such as several energy storage systems and renewable energy generators installed along a railway line. A smart management approach will consider plant operational cycles. Smart grid includes an intelligent monitoring system (including different types of sensors) to real-time monitor and manages the different intelligent nodes of the grid. The smart grid energy architecture will be used to manage the energy flow among upstream network, line feeders, storage systems, substations and auxiliaries to reach energy saving goals.

- Pushing the recovery of braking energy to its maximum potential (potentially 100% of receptivity of the line for DC systems) by recovery of energy braking on trackside for subway and suburban trains, running in what's called "close systems". Different technologies will be evaluated: line side energy storage systems such as batteries, super capacitors, fuel cells, etc. and DC reversible substations. A comparison among different technologies to recover and re-use braking energy will be done through the holistic model developed in WP2.

The final goal is to apply the concept of smart grid for electrical networks in the suburban and tramway network and to give a vision of what a smart grid should be. The improvements that a smart grid should achieve will be defined in terms of quality (perturbation or failure recovery, flexibility and interconnection) and quantity (energy savings, intelligent load sharing, lower impact on environment in terms of CO2 emissions).

It should treat of the following questions:

- Gap analysis: what are the goals to be achieved by a smart grid in the future compared to the current technologies, processes, regulations? The desired future state is compared to the current one and gap statements will be identified. Specific solutions that integrate new technologies and applications are identified
- Mass transit energy configuration and load profiles: The mass transit system engineering evaluation will be set up in order to give the appropriate energetic profile specific to different transportation systems (tramway/metro, etc.)
- Smart grid available technologies evaluation and component studies.

Simulations of urban rail systems based on different operational conditions and a sensitive analysis, concerning electrical characteristics, will be carried out to evaluate a preferred topology of a future smart grid for the different transportation systems. Electrical transportation systems are enabling the use of regenerative energy sources as a substitution of fossil energy use. Every measure increasing the acceptance of public transport is therefore welcome in order to reduce GHG emissions and other disadvantages of individual transport like noise space and dust. The acceptance can be increased by providing fast and comfortable transport. All measures to improve the reliability of traction networks and increase the speed and the comfort are welcome. The power supply has to serve these requirements beneath the need for permanent increase of efficiency. Better ambient conditions, faster transportation and higher reliability with same energy consumption are also welcome. Efficiency is only one point.

## B- MERLIN Project

---

*Reference: FP7 Nr.314125 “MERLIN” Description of work*

Title: sustainable and intelligent management of energy for smarter railway systems in Europe: an integrated optimization approach

MERLIN's main aim and purpose is to investigate and demonstrate the viability of an integrated management system to achieve a more sustainable and optimized energy usage in European electric mainline railway systems. MERLIN provides an integrated optimization approach that includes multiple elements, dynamic forecasting supply-demand scenarios and cost considerations to support operational decisions leading to a cost-effective intelligent management of energy and resources through:

- Improved design of existing and new railway distribution networks and electrical systems as well as their interfaces with the public grid and considering network interconnections
- Better understanding of the influence on energy demand of operations and operational procedures of the different elements of the railway system
- Identification of technologies and solutions able to further contribute to the optimization of energy usage
- More efficient traction energy supply based on optimized use of resources
- Understanding of the cross-dependency between these different technological solutions to define optimum combinations for optimized energy usage
- Improving cost effectiveness of the overall railway system
- Contribution to European standardization (TecRec)

MERLIN also delivers the interface protocol and the architecture for energy management systems in the railway domain, combining the technical development with new business model that would enable and foster their application.

The overall approach of this project is based on the definition, understanding, assessment and optimization of the interfaces and relations between the railway network, the vehicles, the public grid and rail operations. Market constraints and dynamic forecast of immediate supply-demand operational conditions over a period of time are essential unique characteristics of this approach. The work begins with the identification and definition of the sub-systems and elements of the railway networks, the analysis of the requirements coming from the operators and infrastructure managers and the elaboration of a global consumption map in order to realize where the critical problems are (WP1). The sub-systems and elements identified are then used to define the modules required for the global energy model (railway smart grid) as well as specifying and developing its architecture and interfaces (WP2).



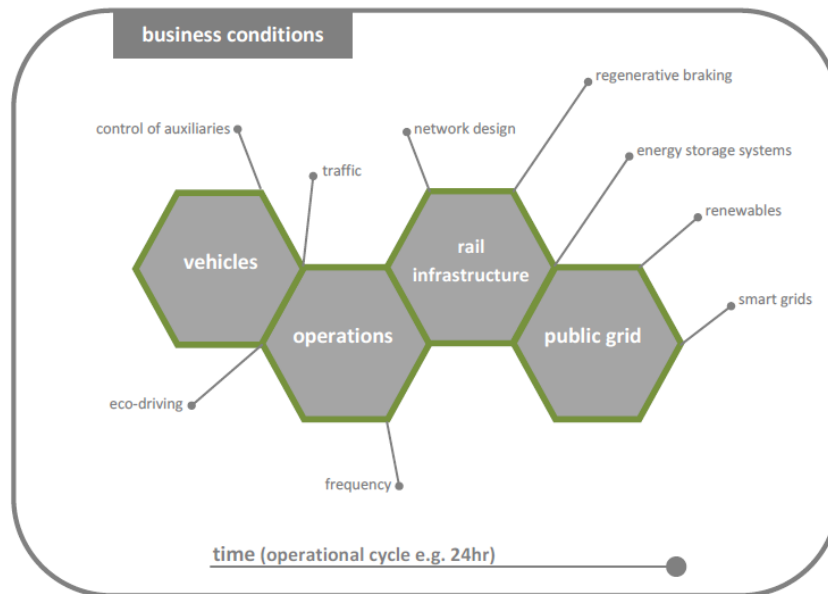


**Figure 140. Interface diagram**

The most suitable real scenarios (high-speed, mainline, mixed passenger & freight lines) are defined (WP3) by train operating companies and infrastructure managers, supported by UIC and the Rail Reference Group organized by the latter. Technological developments are divided into strategic and operational. From the strategic point of view specific optimization tools (decision making oriented) are created (WP5) based on the results of the previously defined architecture in WP2 (modules and interfaces). These tools and models aim the strategic investment in new energy saving technologies for new lines or retrofitting of existing ones. From the operational side studies target the development of new controllable components, modules and applications and protocols of the railway smart grid (WP4) as defined in the global architecture in WP2. An evaluation exercise of the strategic tool is carried out in WP6, amongst other several simulations of the predefined scenarios in WP3, leading to recommendations for implementation (WP7). In addition, some new components of the Railway Energy Management (i.e. the railway smart grid) will be deployed in a real environment to evaluate the feasibility and performance of the concept.

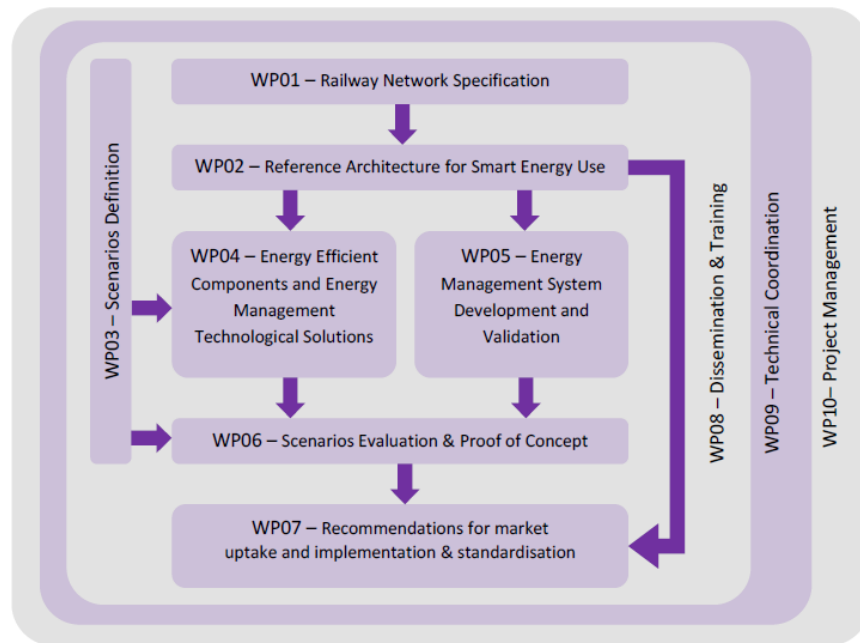


Figure 141. Project Structure

## **C- ELBAS software used for energy simulations**

---

### Areas of application

The program system ELBAS-Webanet® is a simulation system for simulating the running of AC operated short-distance and long-distance railways. Furthermore, the system makes it possible to simulate the running of tractive units that are independent of a contact wire. The system allows the simulation of one or several routes and their meshing to build line networks. The program system has been designed to handle the following problems:

- New development of railway power supply equipment.
- Optimization of existing railway power supply equipment.
- Determining optimum and alternative power supply concepts.
- Calculation of short-circuits currents.
- Stray current corrosion and track-to-earth voltage.
- Vehicle design, vehicle component design.
- Calculation and optimization of timetables.

### Program structure

The following initial data are used for calculations in the program system:

- Line data (kilometer stationing, maximum speed, low-speed sections, operating control points, conditional stops, gradients, curve radii, single-track sections, tunnel sections).
- Timetable data.
- Vehicle data.
- Network data (substations, feeder cables, contact wires, tracks, connectors, sectioning points).
- On-board and wayside energy storage system Data (Power, charge/discharge curves, capacity, efficiency...).

The initial data are stored and edited in a database. For calculation the data are checked and made available by the database system.

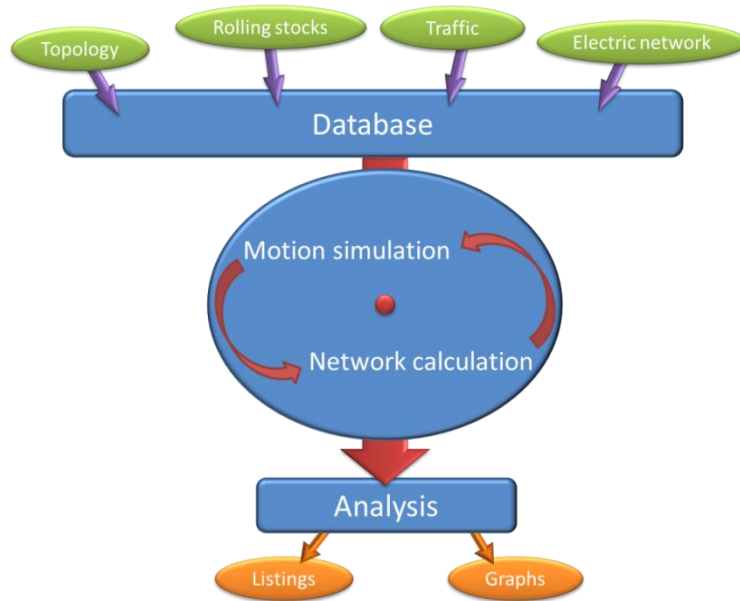


Figure 142: ELBAS Program Structure

Below some results given by ELBAS:

- Energy balance in substations.
- Energy losses.
- Results of train running simulation (timetable, train running chart, tractive effort, transport work, vehicle-specific results).
- Results of network calculation (power levels, currents, voltages in substations, feeder cables, contact wires, connectors, stray current, track-to-earth voltage, energy storage system voltage, current, energy content...).

### Interfaces

Results can be displayed using ELBAS graphic tool. All results can be extracted in Excel files.

### Special features

In addition to the dimensioning, ELBAS allows to:

- Achieve energy balances: for each scenario it is possible to assess criteria such as energy consumptions, receptivity and losses on a given line, which allows calculating the system's efficiency.
- Evaluate the impact of integrating new technologies: It is possible to simulate new technologies such as on-board and wayside energy storage systems, reversible substation, etc.

## D- Timetable of Paris-Lyon High Speed Line

